University of Nevada, Reno

Improving Decision Support During High Impact Weather Through Data Analysis and Visual Communication

A dissertation
submitted in partial fulfillment of the
requirements for the degree of Doctor of Philosophy in
Atmospheric Science

by

Anne Heggli

Benjamin Hatchett, Ph.D./Dissertation Advisor

August, 2023

THE GRADUATE SCHOOL

We recommend that the dissertation
prepared under our supervision by

Anne Heggli

entitled

Improving Decision Support During High Impact Weather Through Data Analysis and Visual Communication

be accepted in partial fulfillment of the
requirements for the degree of

Doctor of Philosophy

Benjamin Hatchett
Advisor

Dan McEvoy
Committee Member

Neil Lareau
Committee Member

Emily Hand
Committee Member

Andrew Schwartz
Committee Member

Lynda Olman
Graduate School Representative

Markus Kemmelmeier, Ph.D., Dean
Graduate School

August, 2023

ABSTRACT

Title:

Improving Decision Support During High Impact Weather Through Data Analysis and Visual Communication

Author:

Anne Heggli

Major Advisor:

Benjamin Hatchett, Ph.D.

Rain-on-snow is linked to many of the largest floods in the Western United States. Forecasting runoff in snow-covered areas prone to flooding is complicated due to the difficult nature of predicting and observing the rain-snow transition elevation and the variation in runoff efficiency and magnitude when snow is present. Looking at forecasts, reservoir operators must constantly weigh decisions to store water for economic and ecological benefits (managing water as a resource) or to release water to mitigate downstream flooding potential (managing water as a hazard). Rain-on-snow events will continue to increase in frequency and magnitude as the climate warms. This change will multiply uncertainties and risks in operational decision-making related to extreme weather. To meet these mounting challenges, this dissertation explores the feasibility for an empirically-based Snowpack Runoff Decision Support system, which considers the likelihood of snowmelt runoff through risk quantification. The research is coupled with a literature review to identify and apply the best practices for visual communication of weather hazards. The dissertation aims to develop a conceptual snowpack runoff decision support framework tested at a regional scale in collaboration with relevant decision-makers over the period 2006-2023. To facilitate broad and efficient communication, this approach also incorporates the guiding principles from graphic design and social science for visual communication of the snowpack's potential to modulate rain-on-snow events.

Craig,

Your unwavering support and patience reminded me to persist with strength and softness. Amidst doubts and uncertainties, your steadfast presence empowered me, and your lighthearted playfulness nourished and renewed my passion for knowledge. Thank you for being a constant source of encouragement throughout my journey.

Acknowledgements

This dissertation would not have been possible without the unwavering support and guidance of numerous individuals, whose contributions and encouragement have been invaluable. Above all, I would like to express my deepest gratitude to my advisor, Benjamin Hatchett, who encouraged me to pursue ideas, learn from mistakes, refine approaches, and ultimately discover effective solutions through experimentation. This experience has exceeded my expectation because of him.

I would like to acknowledge each of the following individuals for their unique contribution to my learning and successes over the years:

The Western Snow Conference community for always making me feel at home and like I truly belong in this field. Each year and so many people have all contributed to my experience and knowledge and especially my passion for more operationally driven research.

The Central Sierra Snow Laboratory including Randall Osterhuber and now Andrew Schwartz for allowing me to test sensors, explore data, and dig snow pits. The things I learned over the years in the snow at the CSSL has been some of the most valuable.

The unparalleled community in the Sierra Nevada for field days and their time teaching me a little about what it takes to run an operational network.

Jeff Anderson for his swift replies regarding my questions about SNOTEL stations and sensors that were fundamental in understanding the data.

Jordan Clayton & Kent Sutcliffe for taking the time to clean hourly soil moisture data and particularly to Jordan for answering all of my soil moisture data questions.

Tim Bardsley for acting as my NWS champion for the COMET Outreach Grants and taking hours out of his day to help improve the SR-DSS.

Alan Haynes & Pete Fickenshire at the CNRFC for their interest and support in my research ideas since day one.

Brian Matthews and Jim Moore at the Nevada Department of Transportation for their interest in my work and support to help connect this research to operations.

Team Meander - To Kat, Lynda and Meghan for being so open to having me jump in on the project and learn about rhetoric and communication, and to Zach Tolby for his steadfast support and willingness to do the most to help me learn more about the NWS communications.

Bruce McGurck for the years of encouragement and guidance on all things snow, but most of all for helping to create a community.

Paul Kucera & Martin Stienson for their support of my passion for observational data and helping me keep one foot at the CSSL for me during my PhD.

Greg McCurdy for his help deciphering anomalous data and teaching me more about sensor behavior.

Scotty Strachan for sharing the same passion for long-term observational data and opening doors to work across Nevada.

Gary Estes for the opportunity to connect in a more meaningful way by becoming a part of the California Extreme Precipitation Symposium community.

My Family & friends especially my endlessly supportive mother and my father who taught me that water is soluble in blood. Each of you gave me a little something different that I needed to find sucess.

This work was funded by:

DRI Internal Project Assignment, COMET Outreach Program, Nevada NASA Space Grant, NOAA Weather Prediction Office, and the Nevada Department of Transportation.

Table of Contents

List of Tables

List of Figures

List of Acronyms

CNRFC	California Nevada River Forecast Center
DSS	Decision Support System
NDOT	Nevada Department of Transportation
NRCS	Natural Resource Conservation Service
NWS	National Weather Service
ROS	Rain-on-Snow
SNOTEL	Snow Telemetry Network
TWI	Terrestrial Water Input
W/SDM	Warm/Sunny Day Melt

Chapter 1

Introduction

End-to-end solutions for hydrometeorological data represent comprehensive and integrated approaches that encompass the entire data lifecycle. This lifecycle extends from data collection to analysis necessary to develop decision support systems (DSS) for stakeholder engagement. The four chapters (Chapters 2-5) presented in this dissertation serve to build the foundation for an integrated end-to-end solution to address the lack of operational guidance on midwinter rain-on-snow runoff events in the Sierra Nevada through the development of a Snowpack Runoff Decision Support System (SR-DSS). Looking beyond the current development of the SR-DSS, this research also identifies the guiding principles for the visual communication of probabilistic forecast information. Probabilistic forecast information not only will be beneficial to integrate into the SR-DSS in future phases of development but are useful for current communication of probabilistic forecast data within stakeholder groups and from trusted sources such as the National Weather Service. Each dissertation chapter takes the form of a standard peer academic journal article.

Chapter 2, "Towards Snowpack Runoff Decision Support", presents a preliminary framework for SR-DSS developed at the University of California, Berkeley Central Sierra Snow Laboratory (CSSL) and was published in *iScience* (Heggli et al., 2022). The objective of this chapter is to identify thresholds for present weather (precipitation and air temperature) and antecedent snowpack conditions (snowpack density) conducive to producing TWI. This paper leverages hourly data for water years 2006–2019 from the U.S. Department of Agriculture (USDA) Natural Resource Conservation Service (NRCS) SNOw TELemetry (SNOTEL) station at the CSSL. The thresholds for six-hour precipitation, six-hour maximum air temperature, and the snowpack density one hour prior to TWI are developed with

data from water years 2008–2019 and are then tested on two case studies in water year 2006 to assess the viability of the preliminary SR-DSS. This paper was published in *iScience*.

In the third chapter, "Visual Communication of Probabilistic Hazard Information", we synthesized guidelines for visualizing PI from literature aimed specifically at visual communication for weather-related hazards and general effective graphic design conventions and summarize the findings in a one-page printout. To showcase how forecasters can incorporate guiding principles in the local context, we provide examples built from readily usable templates to demonstrate how probabilistic forecast information can be used to enhance the visual communication of PI to support more informed decision-making. This paper was published by the *Bulletin of the American Meteorological Society*.

The fourth chapter, "The Value of Sub-daily Observational Data: An approach to improve hourly SNOTEL data and the potential benefits", presents a novel semi-automated quality control workflow for hourly SNOTEL data. Not only are these methods necessary for the development of the SR-DSS, but they can move the entire snow research community beyond daily data to better understand sub-daily processes, like rain-on-snow runoff or other natural hazards, across the western US. With 16 years and counting of hourly data collected at SNOTEL stations across the Western U.S., the addition of quality-controlled hourly data can be used to further develop models and identify climatological behaviors and trends in extreme precipitation and snowmelt rates. These methods were presented at the 90th annual Western Snow Conference and a summarized write-up was submitted to the proceedings.

Chapter 5 integrates the conceptual snowpack runoff decision support system (SR-DSS) developed in Chapter 2 with the quality-controlled data set from Chapter 4 and applies the guiding principles for visual communication of probabilistic hazard information identified in Chapter 3. The principal objective of this paper is to test whether the approach developed in Chapter 2 can be applied at a basin scale in order to provide valuable and timely information to decision-makers. We performed an operational test case where only data that was subject to the automated quality control procedures were applied to the RS-DSS to assess the reliability of the tool.

These four chapters contribute to the understanding of snowpack runoff in mountain regions through the novel integration of observational data, which underwent a newly-developed quality-control approach, into a first-of-its-kind decision support system. Creating decision support systems requires end-to-end solutions that start with reliable data and follow through to effective visual communication through collaborative efforts between research and operations to enhance the capabilities of decision-making processes.

Chapter 2

Towards Snowpack Runoff Decision Support

This chapter is an adapted version of the following publication:
Heggli, A., Hatchett, B., Schwartz, A., Bardsley, T., & Hand, E., (2022) Toward snowpack runoff decision support, *iScience*, Volume 25, Issue 5, 104240, ISSN 2589-0042, `https://doi.org/10.1016/j.isci.2022.104240`.

2.1 Introduction

Reliable hydrometeorological data in mountain regions benefits society when applied to decision support tools at relevant scales, helping decision makers allocate valuable and limited resources to better prepare for potential flooding in order to protect life and property (White et al., 2013; Ralph et al., 2014; Uccellini and Ten Hoeve, 2019; Siirila-Woodburn et al., 2021). Agencies such as the National Weather Service (NWS) (Uccellini and Ten Hoeve, 2019; National Weather Service, 2019a), National Oceanic and Atmospheric Administration (NOAA) (NOAA, 2020), and World Meteorological Organization (WMO) (WMO, 2021) are transitioning from deterministic forecasts towards probabilistic forecasts with risk thresholds that communicate uncertainty to enable targeted messaging for their partners through impact-based decision support services. The National Weather Service provides forecasts, briefings, and watches, warnings and advisories to inform decision-makers and the public of potential weather- and water-related hazards. Essential elements of information and impacts for probabilistic hazard information decision support services consider specific hazards, timing, peak conditions, as well as compounding and/or cascading impacts.

Currently, there is no decision support service to provide situational awareness regarding the timing and peak conditions of changes in the snowpack during warm, windy, and wet winter storms. To address the lack of operational guidance on whether mountain snowpack will reduce runoff, act to enhance it, or have no effect (Brandt et al., 2022b), we propose the development of a Snowpack Runoff Decision Support System (SR-DSS), which aims to add another link in the chain of essential information for agencies like the NWS to examine the likelihood and impact of midwinter rain-on-snow (ROS) runoff.

The snow-dominated Sierra Nevada is a major water source for California and western Nevada (He et al., 2016; Sterle et al., 2019). Forming part of the western margin of the North American Cordillera, the Sierra Nevada trends north-northwest to south-southeast and is approximately 640 km long and 110 km wide. It receives about half of its annual 1,580 mm precipitation in the core Northern Hemisphere winter months (December-February) (Chang et al., 2015) with over 70% falling as snow in the upper elevations (Lynn et al., 2020). Spring snowmelt from snow accumulated during winter provides approximately one-third of California's water supply (He et al., 2016) and is responsible for refilling reservoirs for domestic water supply (Dettinger et al., 2015), hydropower generation (Vicuna et al., 2008), irrigation (Godsey et al., 2014), groundwater recharge (Jasechko et al., 2014), and recreation (Ligare et al., 2011).

The Sierra Nevada, like other maritime mountain ranges worldwide, is prone to ROS. ROS is an efficient generator of runoff that can produce 50-80% higher peak flows than spring snowmelt (Kattlemann, 1997; Kattelmann and Dozier, 1999; Hatchett and McEvoy, 2018). As a consequence, rainfall and snowmelt together can produce greater floods than either rainfall or snowmelt alone (Harr, 1981; Kattlemann, 1997; Singh et al., 1997; Marks et al., 1998). However, skillfully forecasting ROS events remains a significant challenge (Musselman et al., 2018; Henn et al., 2020). The lack of operational guidance creates a need for tools to provide situational awareness and decision support in both transitional (ephemeral) and snow-dominated regions (Siirila-Woodburn et al., 2021; Hatchett et al., 2020; Uccellini and Ten Hoeve, 2019).

This long-standing historic decision support need is accelerating with recent research

suggesting ROS-prone regions, including the Sierra Nevada, are approaching a period of "peak ROS". Peak ROS results from the juxtaposition of a warming climate experiencing more precipitation falling as rain but before warming induces a persistent decline in snowpack volumes (Siirila-Woodburn et al., 2021). More frequent rainfall is projected to increase the magnitude and frequency of ROS events during the 21st century resulting in 20% to >100% increase in runoff with the greatest ROS flood risk impacting the Sierra Nevada (Musselman et al., 2018). The second signal is a continuation of a historical trend in declining snow volumes with projected losses of 30-85% by 2100 (Siirila-Woodburn et al., 2021). These warming-induced changes are compounded by natural interannual snowpack variability (Dettinger and Cayan, 1995; Cayan and Georgakakos, 1995). Despite inter-annual changes, there is a trend across the western US of increased midwinter snow melt (before peak SWE), but the role of ROS in midwinter snowmelt has not yet been analyzed (Musselman et al., 2021). The numerous challenges facing water resource managers as the region approaches "peak ROS" will be further exacerbated by increasing demand for consumptive water uses (OECD, 2012), emphasizing the timely need for midwinter snowpack runoff decision support to optimize water resource management.

Effective flood forecasting benefits from accurate meteorological predictions but potential hazard also depends on antecedent basin conditions (Georgakakos, 2006; Norbiato et al., 2008; Ralph et al., 2013; Oakley et al., 2017). Observational networks are key components in providing antecedent basin information for extreme event analysis to improve the understanding of physical processes linking hydrometeorological forecasts to impacts as well as real-time information for decision support (Ralph et al., 2013; Sumargo et al., 2020; Sterle et al., 2019; White et al., 2019; Hatchett et al., 2020). High temporal frequency resolution data from these networks are particularly valuable in providing event-based information. For example, hourly data from the US Department of Agriculture Natural Resource Conservation Service (NRCS) SNOw TELemetry (SNOTEL) network provides critical event-based information such as terrestrial water input (TWI) from the snowpack (Julander and Holcombe, 2005; Flint et al., 2008; Sutcliffe, 2014; Koskinas et al., 2023), snowmelt (Jennings and Jones, 2015), and density changes (Avanzi et al., 2014). At the University of Califor-

nia, Berkeley's Central Sierra Snow Laboratory (CSSL) SNOTEL station, midwinter TWI from the snowpack corresponds not only with landfalling atmospheric rivers but also with increasing streamflow in nearby basins (Figure 2.2) on both the windward and the leeward sides of the Sierra Nevada (Figure 2.1; (Hatchett et al., 2016; Sterle et al., 2019)). The visible correlation between soil moisture and streamflow response is the motivation for our primary research question: can we use hourly data from existing snow monitoring networks to develop a decision support tool to aid in high-impact ROS events?

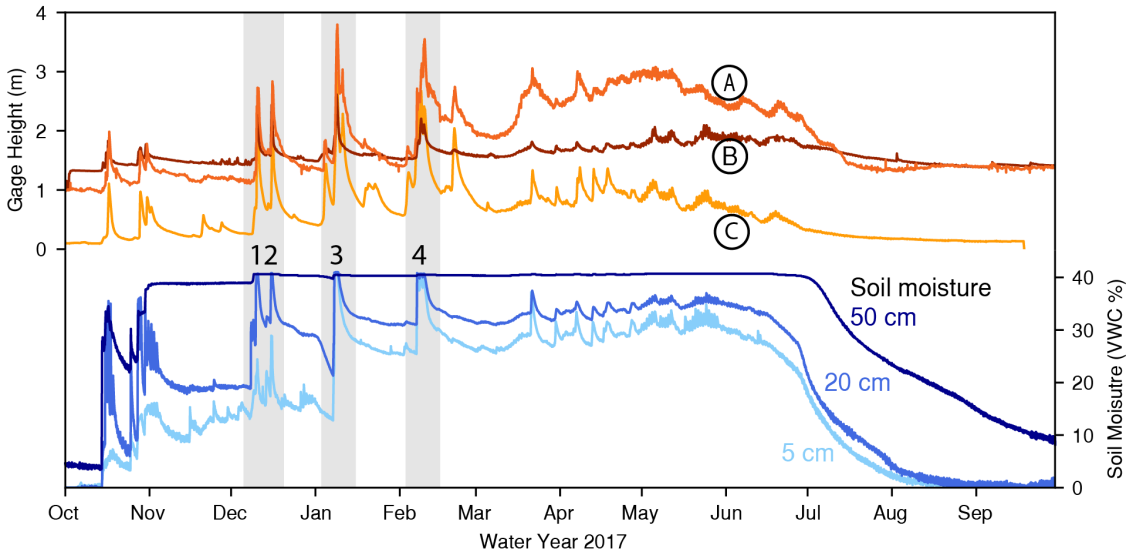

Figure 2.1: Correspondence between soil moisture change and streamflow response in nearby watersheds during four ROS events. 0Hourly soil moisture data (VWC %) at the Central Sierra Snow Laboratory for water year (WY) 2017 at 5 cm (light blue), 20 cm (medium blue), 50 cm (dark blue) corresponds with stream flow response at three US Geological Survey gages: A) Truckee River at Reno, B) Ward Creek, C) North Fork of the American at North Fork Dam.

A knowledge gap in snow hydrology stems from a limited understanding of runoff timing and generation, specifically during ROS events (Colbeck, 1972; Kattelmann, 1985; Schneebeli, 1995; Kattelmann and Dozier, 1999; McCabe et al., 2007; Mazurkiewicz et al., 2008; Rössler et al., 2014). Midwinter ROS causes rapid grain growth due to capillary action concentrating the flow of water at the flow finger, aiding in the formation of preferential flow paths ahead of the leading edge of the newly wetted snow (wetting front) (Church, 1948; Colbeck, 1976; Marsh and Woo, 1984a; Kattelmann, 1985; Marsh, 1987; McGurk et al., 1988;

Marsh, 1999; Kattelmann and Dozier, 1999; Hirashima et al., 2010; Katsushima et al., 2013). Once formed, the size and spatial extent of preferential flow paths vary depending on antecedent snowpack conditions and prior wetting events, which makes ROS runoff generation difficult to model (Marsh and Woo, 1984a; Wever et al., 2014b). Current snowmelt models use a degree day algorithm (e.g. SNOW-17, (Anderson, 2006)), temperature index (e.g. HEC-HMS, (Bartles et al., 2021), or more complex mass and energy balance equations (e.g. ISNOBAL, (Marks et al., 2001); SNOWPACK, (Wever et al., 2014b,a); SNODAS, (Cho and Jacobs, 2020)) to calculate snowmelt. These models assume a uniform wetting front, do not account for preferential flow, and require snowmelt to occur to calculate TWI as a product of snowmelt. Cold content is a key parameter used in energy balance models to calculate the energy required to raise the temperature of the snowpack to 0°C and transition to latent heat exchange in order to melt snow. However, the snowpack does not need to become isothermal (0°C throughout) to transmit water during ROS (Marsh and Woo, 1984a; McGurk et al., 1988). The dependency to satisfy cold-content requirements could, in part, explain why snowmelt models struggle to reliably estimate event-based TWI during ROS (McCabe et al., 2007; Hirashima et al., 2010; Rössler et al., 2014; Clark et al., 2017).

To address the knowledge gap associated with TWI during ROS events and support the generation of an empirically-based snowpack runoff decision support framework, three fundamental methods were applied consecutively to build the snowpack runoff decision support framework. First, we developed a TWI identification algorithm, which uses SNOTEL soil moisture data to classify periods of midwinter TWI (Section 2.2.3 and 2.3.3). Second, we developed Quality Assurance (QA) and Quality Control (QC) methods (discussed in detail in Chapter 4) to prepare hourly data for event-based learning as a key component of our exploration. Hourly SNOTEL data is not subject to the same quality control procedures as daily data and a skillful tool requires quality input data. The third method used decision tree classification (Section 2.3) to simultaneously test the feasibility of automated classification of TWI drivers as ROS or warm day melt and measure the value of the QA/QC process by testing clean and raw data. Since we accurately classified TWI drivers, we then performed a frequency analysis of present weather and antecedent snowpack conditions for

each TWI driver. This process aimed to demonstrate what can be learned about midwinter runoff generation from hourly data and develop the initial framework for a more broadly applicable SR-DSS.

Using data from CSSL spanning water years (WY) 2006-2019 (Figure 2.2), our paper aims to demonstrate how hourly data aids understanding of event-based changes and helps to improve decision support through (1) the dissemination of runoff-relevant changes in the snowpack in real-time, (2) pattern recognition of present weather and antecedent snowpack conditions that contribute to midwinter TWI, and (3) the provision of higher confidence validation data to advance the development of operational snowpack or hydrologic models. We demonstrate the feasibility of SR-DSS by developing methods for QA/QC (Chaper 4), pattern recognition, and threshold identification at a single station as a testable framework for regional development. We anticipate this framework could be applied beyond the ROS problem and adapted for other environmental monitoring networks to aid the development of new or improved decision support for other natural hazards.

2.2 Methods

2.2.1 Study Location

Our study location is the University of California, Berkeley Central Sierra Snow Laboratory (CSSL; 2.2). The CSSL was established in 1946 and is currently co-located with a SNOTEL station at 2,100 m elevation approximately 2 km west of the Sierra Nevada crest in Soda Springs, California (Figure 2.2). The CSSL SNOTEL station (#428) began collecting data in 1982 with a precipitation gauge, a snow pillow to monitor snow water equivalent (SWE), and an air temperature sensor. In 2005, the station was upgraded with an ultrasonic snow depth sensor and soil moisture and temperature sensors at 5, 20, and 50 cm depths (`https://wcc.sc.egov.usda.gov/nwcc/site?sitenum=428`). The CSSL provides a unique opportunity to inform conditions in three highly managed watersheds in California and Nevada. While it sits in the headwaters of the westward-draining South Fork of the Yuba River, it is 3 km north of the westward-draining North Fork of the American River and

2 km east of the headwaters of the eastward-draining Truckee River watershed. The terrain surrounding the CSSL is predominantly exposed Jurassic to Cretaceous granitic bedrock overlaid with tertiary volcanic deposits. The surrounding forest is comprised of Lodge Pole Pine *(Pinus murrayana)*, Red Fir (*Abies magnifica*), and Whitebark Pine (*Pinus albicaulis*) with timberline occurring at approximately 2,500 meters (Osterhuber, 2009). Using the Köppen climate classification system, the CSSL experiences a Humid Continental Climate with a Dry Cool Summer (Dsb). The region west of the crest is characterized by a Warm Summer Mediterranean climate (Csb) while the region to the east is characterized by a Cold Desert Climate (BWk).

Data for this study was selected for WY2006, when the SNOTEL station was upgraded, through WY2019. WY2011 and WY2012 were not included in the analysis because the 20 cm soil moisture sensor stopped reporting. The median annual precipitation for the period of study was 1576 mm and the median maximum SWE was 946 mm. The period of study captures the highest (WY2017) and second lowest (WY2014) precipitation totals as well as the second largest (WY2017) and lowest SWE totals since WY1983 when the SNOTEL record began. Additionally, there were several significant ROS events within this period that produced floods in the region (Hatchett et al., 2016). The most notable of these were January 2006 and February 2017 (Underwood et al., 2009; Henn et al., 2020).

2.2.2 Quality Control (QC) and Quality Assurance (QA) Methods

This paper used STAR Methods published by Heggli et al. (2022) which have since been improved upon. Chapter 4 provides a fully revised version of the hourly QA/QC methods that build upon the initial approach by enhancing the automated portion and streamlining the workflow.

2.2.3 Terrestrial Water Input (TWI) Identification Algorithm

Terrestrial water input (TWI) is water input to the land surface from either precipitation or melting snow. TWI can be identified from shallow soil moisture observations (Flint et al., 2008; Sutcliffe and Clayton, 2021). TWI was identified when soil moisture increased 0.5%

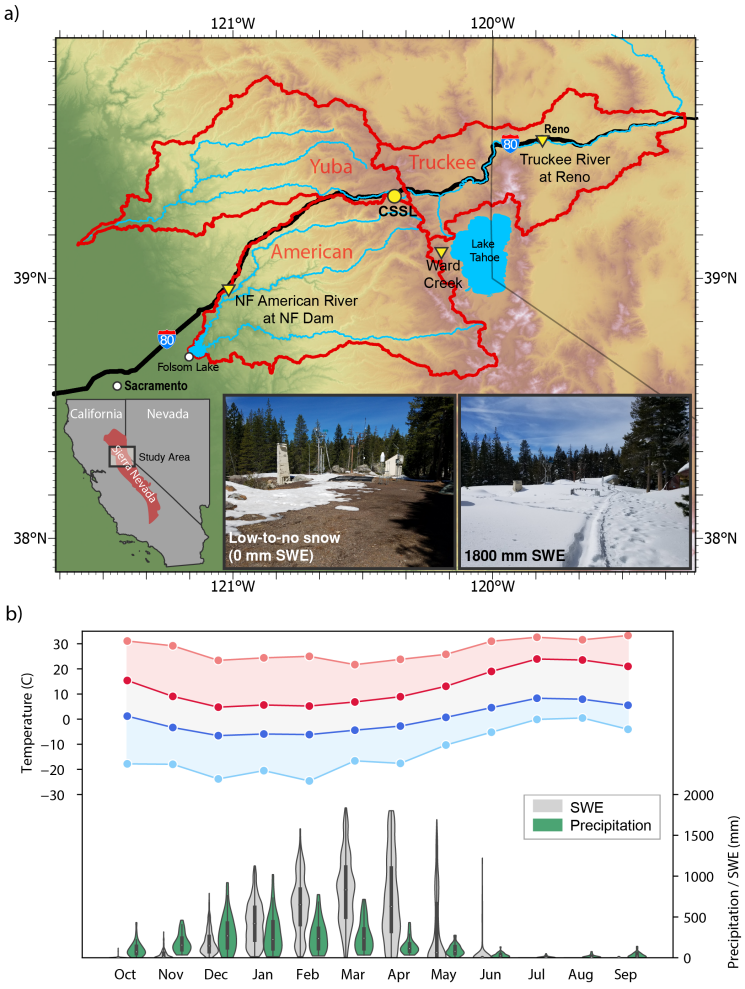

Figure 2.2: Study area location and climatological characteristics. (A) Map of the Central Sierra Snow Lab. (B) climograph based on water years 1988 through 2019 showing average (dark) and all-time (light) maximum (red) and minimum temperature (blue) on the left y-axis. The right y-axis shows the distribution of monthly accumulated precipitation (green) and snow water equivalent (grey).

in one hour or 1.0% in two hours at 5 cm and 20 cm depths. The soil moisture data has a resolution of 0.1%; a threshold of 0.4% identified 200 additional TWI events as a result of normal variation in the sensor. A 0.6% increase over one hour identified 30 less TWI events, so the 0.5% threshold was selected to capture the majority of events while reducing misidentified TWI events triggered by noise. A threshold of 1.0% aided in identifying events that had a slower initial increase while maintaining the same rate of change. Saturation was identified through observations of soil moisture values during spring snowmelt where

each sensor asymptotes at a value of 39%. TWI was classified using the rate of change identification parameters or when all three sensors were saturated. The soil at the 5 cm and 20 cm depths at the CSSL is well-draining and soil moisture begins to recede when TWI ceases. The TWI identification algorithm will likely require calibration for other locations due to site specifics like soil properties.

2.3 Quantification and Statistical Analysis

2.3.1 Decision Tree Classification

The Decision Tree Classifier is a supervised machine learning algorithm selected to aid in pattern recognition of midwinter snowpack TWI drivers (Pedregosa et al., 2011). The decision tree can handle continuous and categorical data, does not require the normalization or scaling of data, and can automatically handle missing values. Decision trees present a series of questions that split data into branches using the Gini Impurity where a value of 0 is a pure classification split and 0.5 is an impure split that incorrectly classified half of the samples.

The decision process begins by identifying the initial root node by calculating the weighted sum of the Gini Impurity from all the possible sub-nodes. This is repeated on each impure internal node creating branches until the tree is complete with only pure leaf nodes. Growing the tree until all pure leaf nodes are achieved often causes over-fitting of the model. Decision trees are sensitive to noise in the data (Pedregosa et al., 2011) meaning small changes to the data can result in large changes to the structure of the tree. The learning process of the Decision Tree Classifier was designed with these limitations in mind. The maximum depth of the tree is limited to reduce over-fitting, data was hand-cleaned to reduced noise and increase stability, and the application of the tree as an aid in pattern recognition allows flexibility to address any changes in the tree structure. The Python code for the clean and raw data can be found in the repository information in Section 1.3.

2.3.2 Feature Engineering

There are a total of four native features in the hand-cleaned data: precipitation, SWE, snow depth, and air temperature. Soil moisture at all three depths was used to develop the TWI target variable and therefore not included in feature engineering or feature selection. Machine learning algorithms compare data from a single point in time. However, the evolution and state of the snowpack is dependent on weather, which is transient by nature. Features were engineered to include information from the current time for up to 12 hours before TWI was identified. To identify TWI related to present weather, the following features were engineered: 1–6 hour precipitation totals, 12 hour precipitation total, and 6 hour maximum temperature.

2.3.3 Filtering Data for Midwinter Snow-cover

Midwinter is defined in this paper to include snow cover when SWE was greater than 100 mm before the ablation period melt begins following peak SWE (median date 24 March). Shallow snow, defined in this study when SWE is less than 100 mm, requires less energy input than deeper snow to melt and initiate runoff and is therefore considered to be perpetually at higher risk of melting (Colbeck, 1976; Harr, 1981; Berris and Harr, 1987; Marks et al., 1998, 2001).

SWE at the CSSL does not always follow a typical SWE accumulation pattern with a defined peak leading into the ablation period. Some water years, such as WY2013, present a plateau before the initiation of the spring ablation period while other years, such as WY2014, display two peaks (Figure 2.3). Midwinter ablation periods identified in 2014 and 2015 were filtered out of the training data for this study. Data qualified as suspect during the QC process were also filtered out of the training data.

2.3.4 Target Variable: ROS or Warm Day Melt TWI

The TWI driver was manually identified at each data point through inter-sensor comparison and human expert judgment (Kondragunta and Shrestha, 2006) and is available in the

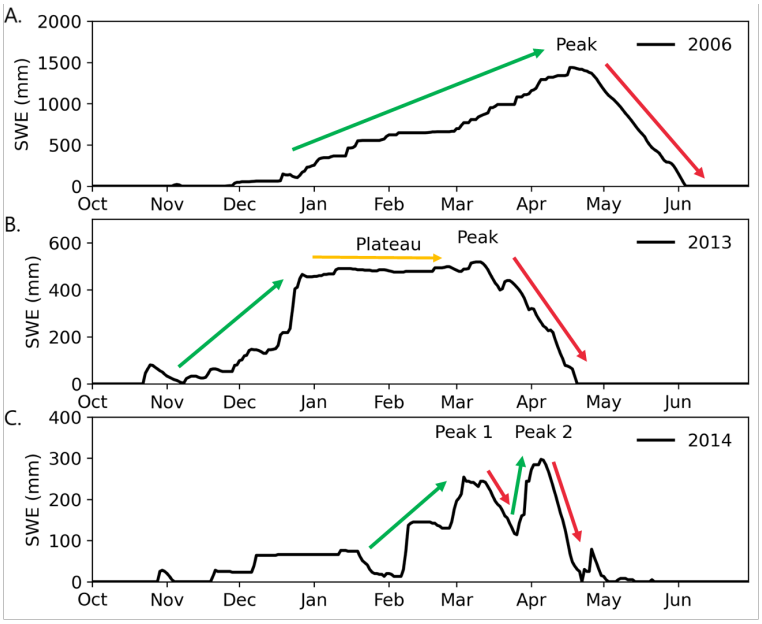

Figure 2.3: Example of the types of SWE accumulation patterns. Possible SWE accumulation (green) and ablation (red) scenarios. (A) steady accumulation leading to a defined peak prior to ablation period, (B) accumulation with prominent plateau (yellow) prior to ablation, and (C) two peaks with two ablation period melts.

repository information in Section 1.3. Warm day melt was assigned a value of 0. Warm day melt was manually identified when there was no recent precipitation, a maximum daily temperature that peaked above at least 5 °C with TWI typically initiating in the late afternoon (around 13:00 local time) and stopping in the evening (around 17:00 local time). This TWI cycle follows the lag of diurnal temperature and is consistent with expected the outcome of warm day melt. ROS was assigned a value of 1 if there was active or recent precipitation that corresponded with above-freezing temperatures. It is not yet possible to identify TWI drivers with numeric thresholds as changes in snowpack depth, density, and prior wetting can inhibit TWI under some meteorological conditions but not others; identifying these patterns is one of the objectives of this study.

2.3.5 Decision Tree Classifier Criteria

The decision tree classifier was trained on data from WYs 2008–2019 and tested against WYs 2006 (wet year; four events) and 2007 (dry year; two events). WY2011 and WY2012

were missing soil moisture data and were not included in the training data. The manually identified TWI driver was used as the target variable. The maximum depth of the decision tree was set to four to assure the model did not overfit and provide a comprehensible tree. The model was run using the clean data and the raw data to measure the model improvement achieved with cleaned data. A cross-validation of model performance was also performed for each set of two consecutive years (eg. 2008 & 2009, 2009 & 2010, 2010 & 2013, etc.) for both clean and raw data.

2.4 Results

Our results are the outcome of cascading methods. The TWI identification algorithm (Section 2.2.3), QA/QC of hourly SNOTEL data (Chapter 4), and manual identification of TWI drivers as ROS or warm day melt (Section 2.3.4) were used in conjunction to test the feasibility of automated decision tree classification of TWI driver and measure the value of data QA/QC (Section 2.3). The decision tree classification model proved accurate and a frequency analysis was performed for the midwinter training data (WYs 2008–2019; Section 2.3.3) to aid in pattern recognition of present weather and snowpack conditions for ROS and warm day melt TWI. Access to clean hourly data and the results from these methods demonstrate what can be learned to minimize the ROS runoff knowledge gap. Finally, the results from the frequency analysis were translated into the preliminary conceptual snowpack runoff decision support framework. The successive results are described in detail in subsequent sections.

2.4.1 Soil Moisture Data Can be Applied to Identify Terrestrial Water Input (TWI)

The TWI identification algorithm developed with SNOTEL soil moisture data to identify periods of TWI (Section 2.2.3) resulted in a total of 782 hours of TWI with maximum soil moisture increases of up to 21% in one hour (13 February 2019). During one exceptional ROS event, TWI occurred for 48 consecutive hours and soil was saturated at all three depths

for 24 consecutive hours (7–9 January 2017). At least six hours of continuous TWI occurred on 25 days, all associated with ROS events. In contrast to ROS, warm day melt-driven TWI lasted less than three hours on average but not more than five hours.

Periods of TWI identified by the algorithm were manually classified as ROS or warm day melt (Section 2.3.4). Of the 782 hours of TWI, 499 hours coincided with ROS, 264 hours coincided with warm day melt, and 19 hours could not be explained by ROS or warm day melt. Of the anomalous 19 hours, 16 hours were misidentified by the algorithm and the remaining three instances could not be explained by precipitation or temperature data. The 19 unidentifiable data points were excluded from the study to address the principal drivers of TWI from ROS and warm day melt. From the remaining 763 data points, ROS TWI accounted for 65.4% of all TWI events and warm day melt accounted for the remaining 34.6%.

2.4.2 Automated Classification of TWI Driver

2.4.2.1 Clean Data Improved Model Accuracy by up to 25.7% When Classifying TWI Drivers

The decision tree classification performed with raw and clean data quantified the added value the QA/QC method had in classifying TWI drivers (Section 2.3). The cross-validation of the model tested on each set of two consecutive water years and trained on remaining years for clean and raw data (Section 2.3.5) demonstrates the value of the QA/QC methods (Chapter 4) applied to the hourly data (Table 2.1). The model performance was measured with accuracy (number of correct classifications) and F1 score (harmonic mean of the precision and recall)(Pedregosa et al., 2011). On average, clean data was 95.5% accurate (standard deviation of 4.4%) with an average F1 score of 0.96 (standard deviation of 0.03). Raw data performed consistently worse with an average accuracy of 84.0% (standard deviation of 5.3%) and an average F1 score of 0.859 (standard deviation of 0.08). 2009 and 2010 performed the same because the data during TWI events did not need significant correction and had a very small data set to test on. On the other hand, WY 2018 and 2019 required

extensive quality control during periods of TWI that improved the model accuracy by 25.7%. On average for the study period, the clean data was 13.7% more accurate.

Test Data Parameters				Clean Data		Raw Data	
Water Years	**Data Points**	**Data Size**	**ROS Data**	**Accuracy**	**F1**	**Accuracy**	**F1**
2006-2007	212	27.8%	62.3%	0.977	0.981	0.825	0.871
2007-2008	125	16.4%	36.8%	0.992	0.989	0.816	0.875
2008-2009	64	8.4%	40.6%	1.000	1.000	0.891	0.868
2009-2010	82	10.7%	40.2%	0.951	0.943	0.951	0.943
2010-2013	124	16.3%	26.6%	0.960	0.928	0.823	0.667
2013-2014	134	17.6%	45.5%	0.948	0.942	0.821	0.774
2014-2015	73	9.6%	80.8%	0.863	0.911	0.836	0.891
2015-2016	46	6.0%	91.3%	0.891	0.943	0.804	0.883
2016-2017	191	25.0%	88.5%	0.979	0.988	0.853	0.913
2017-2018	184	24.1%	90.2%	1.000	1.000	0.875	0.927
2018-2019	99	13.0%	80.8%	0.939	0.962	0.747	0.839

Table 2.1: Decision Tree Classification Model Cross Validation Results. A model was built and tested on two consecutive water years, the total test data side in number of points and percent of data are detailed along with the percentage of TWI events that were classified as ROS. Accuracy (number of correct classifications) and F1 score (harmonic mean of the precision and recall) are provided as a measure of model improvement for clean versus raw data.

Our results demonstrate that randomized selection of test and training data for unbalanced data like is collected at CSSL will not necessarily build the best model. The size of the test data is not consistent between water years because the snow cover season is not consistent. Similarly, the results between water years is variable because the number of ROS or warm day melt events is not consistent. Criteria for the test and training data split benefit from a comprehensive understanding of the data set (e.g. length of the snow-covered season, number of TWI events, number of ROS events or warm day melt events).

2.4.2.2 Model Results

The decision tree classification trained on WYs 2008–2019 and tested against WYs 2006 (wet year; four events) and 2007 (dry year; two events) was selected to develop the framework model. The 2006 and 2007 test parameters had the highest number of test data points and the most representative distribution of ROS and warm day melt events compared to the entire data set; 62.3% (132 data points) were associated with ROS and 37.7% (80 data

points) were associated with warm day melt. The clean data model accurately classified 97.6% of TWI drivers with an F1 score of 0.981 while the raw data model was 82.5% accurate with F1 score of 0.871 (Table 2.1).

The classification model developed with clean data has four impure leaf nodes where a total of six warm day melt events and three ROS events were incorrectly classified (Figure 2.4). The confusion matrix shows the number of true positives (TP), true negatives (TN), false positives (FP), and false negatives (FN) of the predicted values against the actual values with true identifying ROS and false identifying warm day melt TWI for the model results and test data. The root node split identifies the variable that best splits the data and the model identified 12 hour precipitation totals less than or equal to 0.75 mm for the root node. Following the false classifications down the right-most side of the tree, the decision tree correctly classified 335 out of 338 samples as ROS by looking for and 6 hour precipitation totals over 1.75 mm. The first internal node to the left of the root node correctly identified all 172 samples as warm day melt when 6 hour maximum temperatures greater than 0.45 °C. The five samples classified as ROS when 12 hour precipitation was less than 0.75 and temperatures less than 0.45 °C, the samples were manually identified as a lagged ROS release from the 13–14 February 2019 ROS event.

2.4.2.3 Raw Data is Less Reliable

The decision tree classification model was also built with raw data under the same criteria. The raw decision tree model has five impure nodes where 20 warm day melt samples and 10 ROS samples were incorrectly classified (Figure 2.5). There are three examples of data issues impacting the model. Three leaves with negative precipitation values demonstrate the impact of diurnal flutter causing false decreases in precipitation. The classification of 12 hour precipitation less than -67.5 mm was the result of the 7–9 January 2017 ROS event that flooded the station and damaged the pressure transducer. Events with 6 hour maximum temperatures greater than 6.5 °C and more than 7.5 mm of precipitation in the last two hours were classified as ROS, but this is an example of warm day melt that caused a snow plug release (see Chapter 4) for information about snow plug releases).

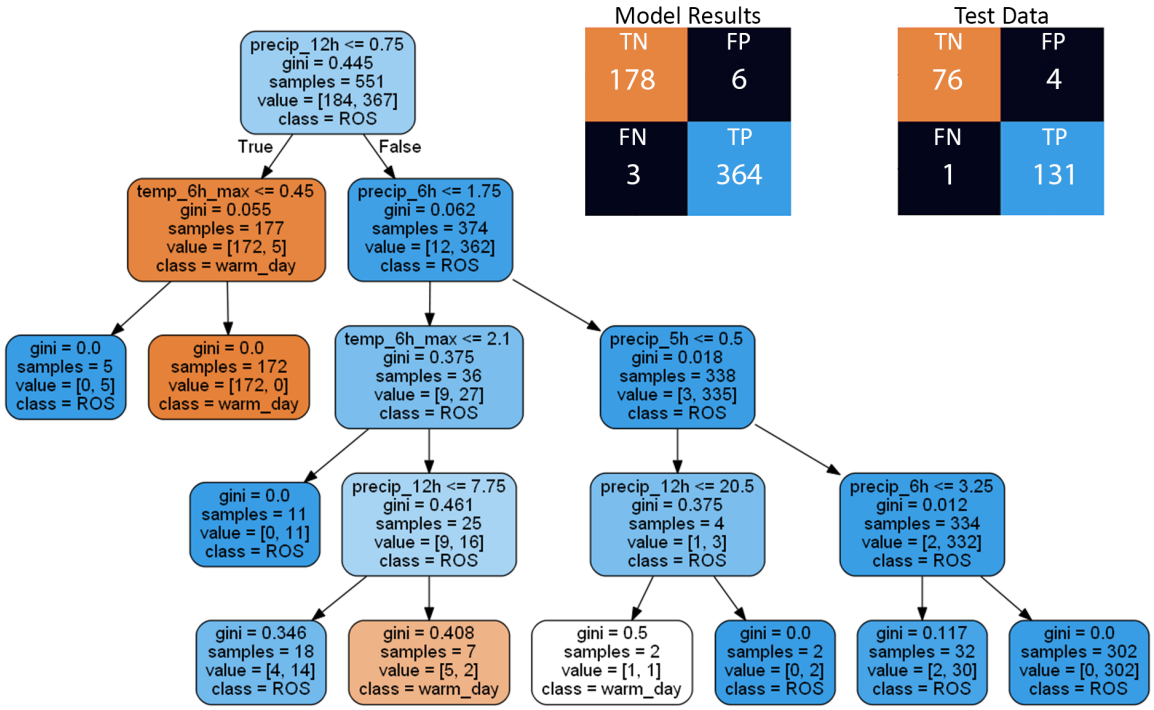

Figure 2.4: Decision Tree Classification of ROS and warm day melt events from the cleaned data. Decision tree classification model (2.3.1) for the cleaned data and confusion matrix for the results of the model and test data illustrating the number of true positives (TP), true negatives (TN), false positives (FP), and false negatives (FN) of the predicted values against the actual values with true identifying ROS and false identifying warm day melt TWI. See Section 2.3.1 and 2.3.5 for further detail.

2.4.3 Present Weather and Antecedent Snowpack

2.4.3.1 Frequency Analysis

The automated classification of TWI drivers as ROS or warm day melt (Section 2.3.5) derived from the TWI identification algorithm (Section 2.2.3), QA/QC of hourly SNOTEL data (Chapter 4), and manual identification of TWI drivers as ROS or warm day melt (Section 2.3.4) proved both feasible and reliable. Identifying TWI and classifying the driver as ROS or warm day melt facilitates pattern recognition of present weather and antecedent snowpack conditions with the potential to generate runoff for each TWI driver. To build the SR-DSS framework, the frequency of present weather and antecedent snowpack conditions were examined for the training data (WYs 2008–2019) using the manually classified TWI

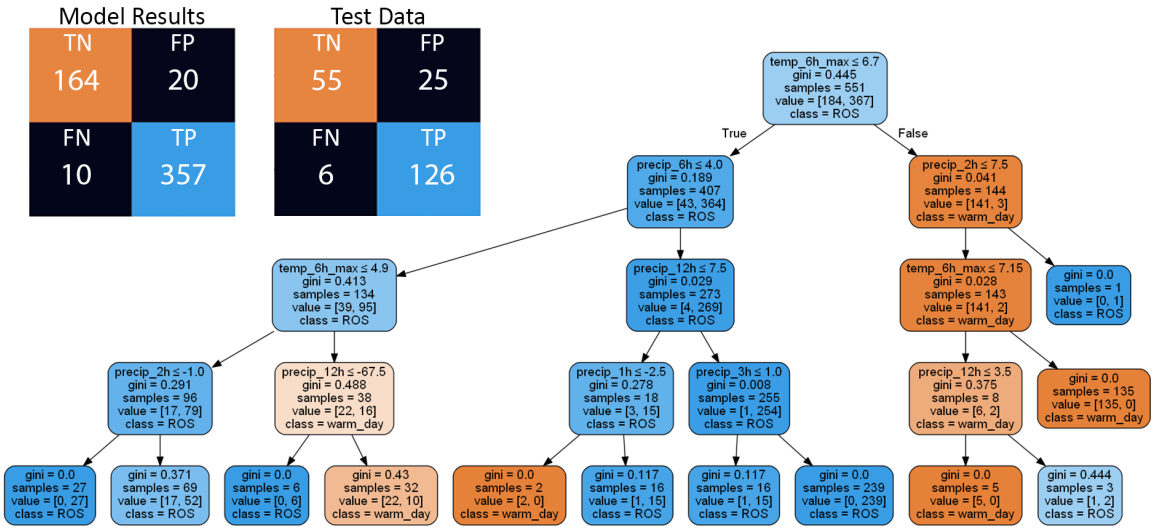

Figure 2.5: Decision Tree Classification of ROS and warm day melt events from the raw data. Decision tree classification model (Section 2.3.1) for the raw data and confusion matrix for the results of the model and test data illustrating the number to true positives (TP), true negatives (TN), false positives (FP), and false negatives (FN) of the predicted values against the actual values with true identifying ROS and false identifying warm day melt TWI. See Section 2.3.1 and 2.3.5 for further detail.

driver. The 6 hour maximum temperature and 6 hour precipitation totals provides the distribution and frequency of present weather conditions while snowpack density as a percent (NRCS, 2014) shows the distribution and frequency of antecedent snowpack conditions during periods of TWI. It is worth noting that warm day melt is correlated with incoming solar radiation, which is the primary driver of snowmelt, however as solar radiation is not commonly measured at SNOTEL stations, temperature is used as a proxy (Painter et al., 2012). The ROS classification was subset to include ROS + melt/drainage defined as all ROS events with at least a 2 mm loss of SWE in the last one hour. Of the 454 hours of ROS TWI, only 45 hours were coupled with SWE loss, accounting for 9.9% of ROS TWI and 5.8% of all TWI identified in this study. These results provide the first indication that snowmelt is not a primary source of midwinter runoff.

ROS-driven TWI events during the training data period had 6 hour maximum temperatures ranging from -3.6 °C to 6.3 °C with an interquartile range of 1.6 °C to 3.89 °C (Figure 2.6 A & B). The maximum 6 hour temperature for ROS + melt/drainage ranged from 2.0

°C to 6.0 °C with interquartile values of 3.4 °C and 5.2 °C. Warm day melt had 6 hour maximum temperatures range of 0.8 °C to 14.8 °C and interquartile range of 6.3 °C to 11.0 °C.

ROS events produced TWI when snowpack densities were as low as 13.3% and up to 51.1% with an interquartile range of 26.4% to 35.2% (Figure 2.6 C & D). Snowpack density was also higher for ROS + melt/drainage events, ranging from 23.5% to 50.0% with an interquartile range of 28.3% to 40.5%. Density values 1 hour prior to warm day melt-driven TWI ranged from 17.3% to 45.9% with an interquartile range of 27.6% to 37.5%.

ROS TWI only occurred with measurable precipitation when temperatures were greater than 0 °C (Figure 2.6 E). 6 hour precipitation totals during ROS TWI ranged from 0-65 mm with an interquartile range of 5–24 mm (Figure 2.6 F). When 6 hour precipitation totals were 0 mm, TWI observations were associated with lagged ROS TWI (14 February 14 2019). During ROS + melt/drainage, 6 hour precipitation totals ranged from 9 to 44 mm with an interquartile range of 23 to 38 mm.

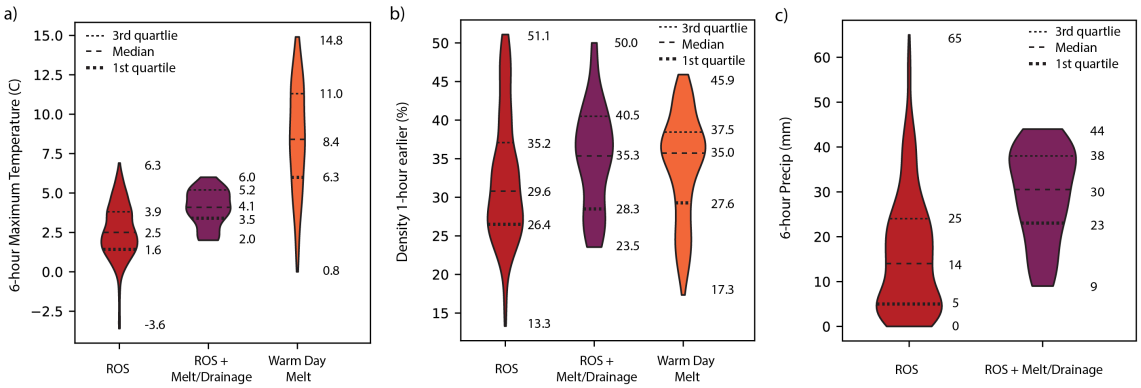

Figure 2.6: Distributions of present weather and snowpack conditions for rain-on-snow (ROS), rain-on-snow plus snow water equivalent loss (ROS + melt/drainage), and warm day melt. (A) Histogram showing the distribution of 6 hour maximum temperature (°C) for ROS (orange), ROS + melt/drainage (red), and warm day melt (purple) events. (B) Box-percentile plots showing the distribution of ROS, ROS + melt/drainage, and warm day melt events for varying temperatures. Dashed lines represent first quartile, median and third quartile values with first quartile in bold to draw the connection to the development of the framework in Section 2.4.4. (C) and (D) As in panels (A) and (B), but for density (%). (E) and (F) As in panels (A) and (B), but for 6 hour precipitation (mm).

2.4.3.2 Snowmelt is Not a Primary Source of Runoff in Deeper Snowpacks

Our findings are consistent with previous findings that snowmelt is not a primary source of runoff during ROS events in deeper snowpacks (Singh et al., 1997; Whitaker and Sugiyama, 2005; Mazurkiewicz et al., 2008). At least 75% of 1 hour, 3 hour, 6 hour, 12 hour, and 24 hour SWE changes resulted in an increase in SWE during ROS TWI (Figure 2.7 A). Therefore, the snowpack can accumulate SWE while simultaneously producing runoff. Notably, only 16% (80 of 499 hours) of ROS TWI occurred with 24 hour SWE loss. 38.7% (31 of 80 hours) of 24 hour SWE loss occurred during the January 2017 and February 2017 ROS events (Figure 2.7 B). These events require additional analysis to differentiate the draining of liquid water following snowpack charging-where water is transiently stored in the snow matrix (Marsh and Woo, 1984a; Brandt et al., 2022a)-from actual snowmelt.

2.4.3.3 Daily Rainfall Thresholds That Produce TWI

There is a general relationship between the precipitation phase and intensity with TWI. The CSSL manual observations include daily precipitation phase values as percent rain and percent snow. The percent rain values were used to analyze hours of TWI as a function of daily total rainfall (precipitation and percent rain; Figure 2.8). TWI occurred if at least 22 mm of precipitation fell as rain. This relationship was not observed when less than 25% of precipitation falls as rain. However, 24 hour precipitation totals of at least 56 mm with at least 25% rain produced a TWI signal in the soil moisture response. As storms include a greater fraction of precipitation falling as rain, less total precipitation was required to produce TWI. Days with 50% rain required at least 38 mm to fall as rain whereas on days with 100% rain only 22 mm of precipitation was necessary.

2.4.4 Snowpack Runoff Decision Support Framework

2.4.4.1 Preliminary Snowpack Runoff Decision Support Framework

We present a first-step, conceptual snowpack runoff decision support framework guided by the knowledge acquired through the development of a TWI identification algorithm,

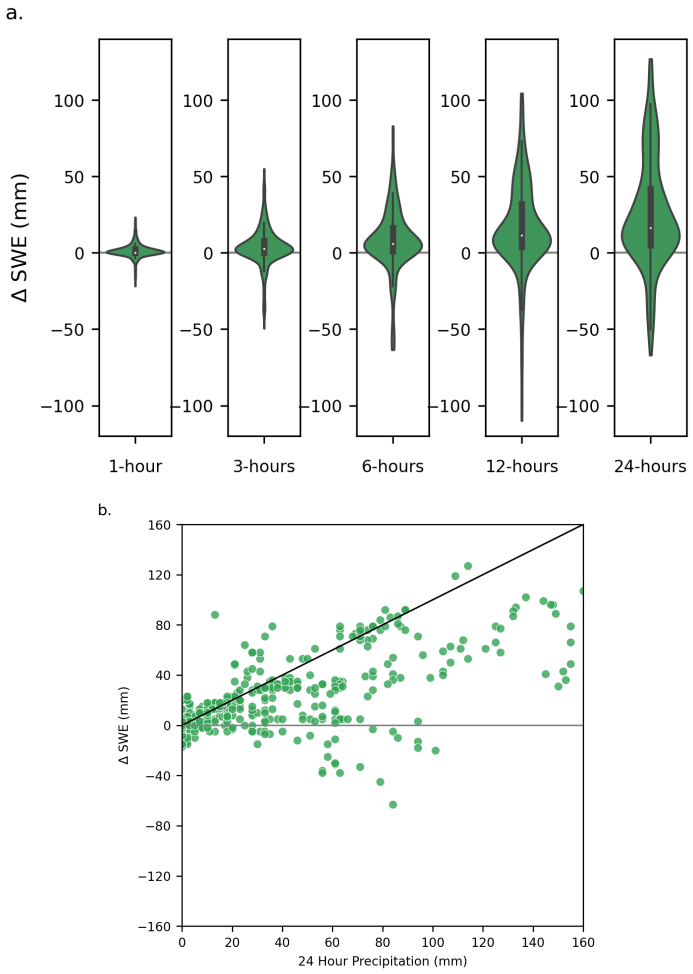

Figure 2.7: Change in SWE from one to 24 hours during ROS. (A) 1 hour, 3 hour, 6 hour, 12 hour, and 24 hour total change in SWE (mm) during ROS events. (B) 24 hour change in SWE (mm) versus 24 hour precipitation totals (mm) with the black 1:1 line indicating periods when the snowpack accumulated all of the precipitation and a grey line when SWE was lost over 24 hours.

high confidence hourly data via QA/QC procedures, decision tree classification of ROS and warm day melt driven TWI, and frequency analysis of present weather and antecedent snowpack conditions. TWI is the first indication of snowpack runoff. Identifying and classifying periods of TWI lays the foundation for snowpack runoff decision support. To build upon this, we selected first quartile values for 6 hour maximum temperature (Figure 2.6 B), 6 hour precipitation (Figure 2.6 F), and snow density 1 hour prior to TWI (Figure 2.6 D) as preliminary indicators of potential TWI. These indicators were integrated into

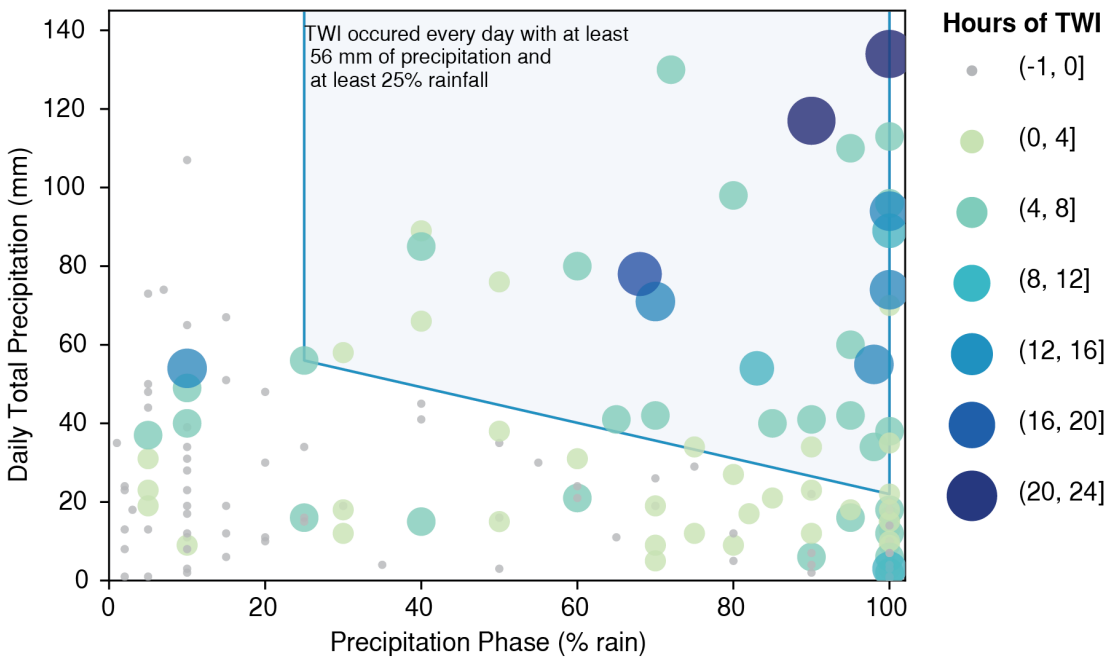

Figure 2.8: Duration of TWI as a function of total daily precipitation and percent rain. Daily total precipitation and precipitation phase as percent (%) rain from manual observations from the Central Sierra Snow Laboratory and SNOTEL-derived cumulative hours of TWI per day and total precipitation.

the conceptual three-dimensional snowpack runoff decision support framework (Figure 2.9). "Low Potential" refers to values when TWI potential was below first quartile values. Warm day melt was defined by non-ROS TWI as a result of 6 hour maximum temperatures of at least 6.3 °C and density of at least 27.6%. The potential for ROS-induced TWI was established with as little as 5 mm of precipitation, maximum temperatures greater than 1.6 °C, and density of at least 26.4%. The potential for TWI during ROS events increases when SWE loss can occur as a result of either snowmelt or drainage of transiently stored rainwater. The potential for ROS + melt/drainage was defined when 6 hour precipitation totals exceed 23 mm, 6 hour maximum temperatures are greater than 2.0 °C, and the snowpack density is at least 28.3%.

There was no evidence of midwinter precipitation occurring above 7.0 °C during the period of study. A midwinter ROS event when temperatures are greater than 7.0 °C would be unprecedented in recent history as the 1997 New Years event had daily maximum tem-

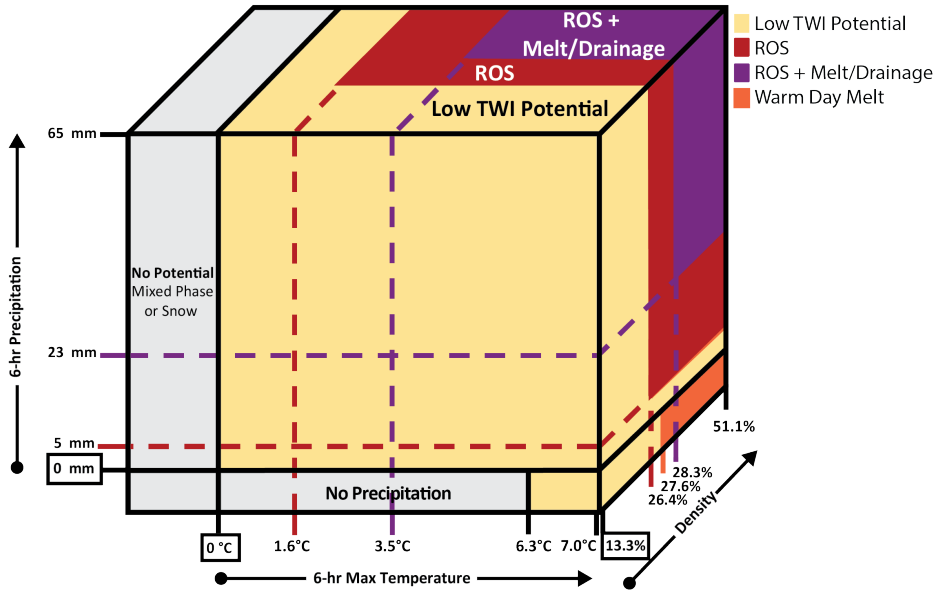

Figure 2.9: Conceptual snowpack runoff decision support framework. Snowpack runoff decision support conceptual framework developed through the application of first-quartile 6 hour precipitation, 6 hour maximum temperature, and density 1 hour earlier as indicators of low, ROS, ROS + melt/drainage, or warm day melt TWI potential.

peratures at or below 7.0 °C (Osterhuber and Schwartz, 2021). Though it is plausible for threshold to be crossed some day since the CSSL does experience rainfall in the fall months above 7.0 °C, identifying the current precipitation ceiling is an important metric. Crossing this threshold could produce greater runoff as the rainfall would carry more energy to melt snow. This further emphasizes the value of reliable hourly data, which would make it possible to analyze larger scale changes like an increase in the midwinter precipitation temperature ceiling.

We translated the conceptual snowpack runoff decision support framework into a decision tree with an index to simplify the identification of snowpack runoff potential for decision makers (Figure 2.10). This initial step towards snowpack runoff decision support demonstrates how hourly data can be fed into a system to improve multidimensional situational awareness. Impactful decision support tools like the Air Quality Index (Environmental Protection Agency, 1999) include a quantitative color scale but only provide one-dimensional information (particulate matter). Multidimensional advisories like the National Weather Service Heat Index (Hawkins et al., 2017) and Avalanche Danger Scale (Statham et al.,

2010) provide a cohesive measure of danger through qualitative color scales. We applied qualitative and quantitative communication methods by including a color scale for the TWI potential and values for each TWI indicator.

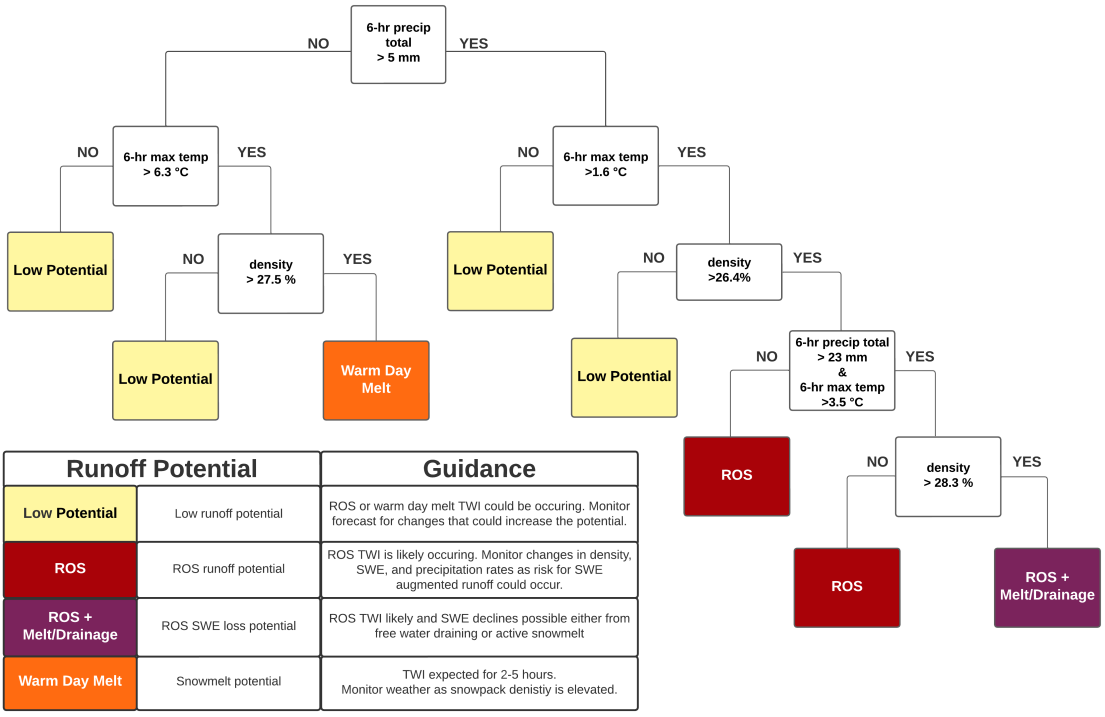

Runoff Potential		Guidance
Low Potential	Low runoff potential	ROS or warm day melt TWI could be occuring. Monitor forecast for changes that could increase the potential.
ROS	ROS runoff potential	ROS TWI is likely occuring. Monitor changes in density, SWE, and precipitation rates as risk for SWE augmented runoff could occur.
ROS + Melt/Drainage	ROS SWE loss potential	ROS TWI likely and SWE declines possible either from free water draining or active snowmelt
Warm Day Melt	Snowmelt potential	TWI expected for 2-5 hours. Monitor weather as snowpack denistiy is elevated.

Figure 2.10: Decision tree visualization of the snowpack runoff decision support framework developed at the Central Sierra Snow Laboratory.

2.4.4.2 Example Application of Preliminary Framework

As an example of the application of the preliminary snowpack runoff decision support framework, we applied the decision tree thresholds to two periods with three ROS events from WY2006 of the test data set (Figure 2.11). From 26 December 2005–3 January 2006, two ROS events both produced TWI resulting in increases in soil moisture (Figure 2.11 A). However, the ROS TWI potential was low because snowpack density values were below 26.4% and therefore did not qualify as ROS potential. The presence of ROS TWI when the snowpack density is low could be an indication of the formation or preferential flow paths as a uniform wetting front would increase the liquid water content to capacity prior to TWI

(Marsh and Woo, 1984a; Colbeck, 1976; McGurk et al., 1988). This highlights an area to improve the framework since density may not be as critical in dictating TWI potential as rainfall intensity and totals due to the formation of preferential flow paths. The 2006 New Year's Day ROS event had widespread impacts in the American, Yuba, and Truckee watersheds (CNRFC, 2006). The snowpack runoff decision support framework correctly indicated the potential to produce ROS TWI and later ROS + melt/drainage TWI. The second analysis period (20 February–2 March 2006) had a ROS event proceeded by five days with no precipitation and maximum temperatures over 6.3 °C with the potential for warm day melt (Figure 2.11 B). By the second day of warm day melt potential conditions being met, the 5 cm soil moisture sensor registers diurnal melt from the snowpack. Knowing that the snowpack is in a state of active melt ahead of a potentially warm storm would indicate that the snowpack is ready to transmit water and potentially contribute to TWI. On 27 February 2006, a ROS event began at the CSSL, and with two hours of precipitation initiating the soil moisture sensors registered increases. TWI potential increases to ROS + melt/drainage and all three soil moisture sensors measure a period of saturation when the TWI input rate is greater than the soil infiltration rate. While this example demonstrates the utility of the approach to identify present weather and antecedent snowpack conditions that could produce TWI, it also highlights the thresholds that miss TWI and can be used as guidance for further calibration of the framework.

2.5 Discussion

2.5.1 Development of a Cascading Workflow: Data QA/QC, TWI Identification Algorithm, and Pattern Recognition

Readily available, high confidence and comprehensive hourly data helps streamline research efforts, allowing investigators to focus on results and analysis to close the ROS runoff knowledge gap (McCabe et al., 2007; Rössler et al., 2014; Brandt et al., 2022b). The semi-automated QA/QC approach discussed in detail in Chapter 4 represents a step forward in achieving this goal by reducing the time required to clean data by leveraging automated

processes during more predictable periods, allowing the data reviewer to focus on events and flagged data anomalies.

Our research found soil moisture data to be useful for identifying the timing of TWI (Cardell-Oliver et al., 2005; Julander and Holcombe, 2005; Flint et al., 2008; Bales et al., 2011; Sutcliffe, 2014). Since hourly soil moisture data has already been reviewed by NRCS staff, expanding the application of the TWI identification algorithm to other SNOTEL stations could be implemented immediately. TWI identification could be beneficial for NWS hydrologists and decision makers by notifying them of active TWI in near-real time, especially when interpreted in tandem with data from other hydrometeorological networks (Hatchett et al., 2020). With the addition of quality controlled hourly data for the remaining parameters from other stations (precipitation, snow depth, and snow water equivalent), applying the remaining methods could improve the pattern recognition of antecedent snowpack conditions and present weather that produces TWI regionally rather than at a single location.

Augmenting surface station-based data with information regarding present atmospheric conditions is an important component of early warning or real-time information systems by providing situational awareness (Hatchett et al., 2020) and contributing to impact-based decision support (Uccellini and Ten Hoeve, 2019) ahead of forecast extreme events. To show our identified ROS-induced TWI events have common ingredients with ROS events, we created synoptic composites using daily averages from the National Center for Environmental Prediction's 36 km horizontal resolution North American Regional Reanalysis (Mesinger et al., 2006). We selected 17 unique storm events (for multi-day events, the first day was used) with at least six hours of continuous TWI. Anomalies were calculated by differencing each identified TWI day from the average of the same calendar days calculated between 1981-2010.

The presence of an offshore trough at 500 hPa and a broad plume of precipitable water (integrated water vapor) oriented in a southwest-northeast direction (Figure 2.12 A) in conjunction with strong moisture flux (Figure 2.12 B) and anomalously warm mountain-top (700 hPa temperatures; (Figure 2.12 C)) are key components of storms producing heavy pre-

cipitation and high elevation snow levels in the Sierra Nevada (O'Hara et al., 2009; Kaplan et al., 2009; Hatchett et al., 2017a). The broad plume of precipitable water (Figure 2.12 A) and integrated vapor transport in exceedance of 250 kg m^{-1} s^{-1} (Figure 2.12 B) originating from the subtropics and extending northeastwards into California are consistent with the typical genesis location of costly flood-producing atmospheric rivers (Prince et al., 2021). The dual composite moisture plumes indicate two primary corridors along which moisture export from the midlatitude cycle occurs leaving behind the footprint of concentrated water vapor (Dacre et al., 2015). The sustained liquid precipitation at CSSL needed to generate TWI is consistent with the strong moisture transport created by a baroclinic environment with anomalously cold air to the north and anomalously warm air to the south (Figure 2.12 C). The sea level pressure gradient between lower pressure in the Gulf of Alaska and higher pressure off the coast of Baja California (Figure 2.12 D) favors southwesterly winds blowing perpendicular to the Sierra Nevada and enhancing orographic uplift. The sustained precipitation at CSSL is further enhanced by quasigeostrophic ascent occurring in the exit region of the broader 500 hPa trough (Figure 2.12A). The 0 °C isotherm at 700 hPa is located just south of CSSL (Figure 2.12 C), suggesting mountain-top temperatures during TWI events on average are near- to slightly-above freezing, leading to greater fractions of precipitation falling as rain. Favored by a poleward shifted and anticyclonically curved upper level jet (Figure 2.12 D), the anomalously warm temperatures (Figure 2.12 C) indicates strong warm air advection and downstream geopotential height building as latent heat is advected into the region via transport of moist subtropical air (Figures 2.12 A-B). These conditions are all broadly consistent with established synoptic patterns favoring heavy and sustained precipitation with elevated rain-snow transition elevations producing ROS and subsequent flooding (Kaplan et al., 2009; O'Hara et al., 2009; Hatchett et al., 2016, 2017a, 2020). This information provides additional insight to the snowpack runoff decision support in two ways. First, a forecast storm with some or all of these characteristics could prime the existing snowpack to actively produce runoff in a subsequent event by establishing preferential flow paths or reducing cold content (Brandt et al., 2022b). Second, regardless of the initial state of the snowpack, a forecast storm with these characteristics should elevate

situational awareness for the potential to produce typical winter storm impacts in addition to TWI and subsequent runoff.

Our findings from the CSSL analysis suggest concerns about potential flooding should grow if more than 22 mm of precipitation as rain at the CSSL elevation is forecast for a 24 hour period. By using higher confidence data via the quality-controlled hourly data and the TWI identification algorithm from more stations to identify historic circulation patterns to assess the potential for TWI, we both enhance confidence in our ability to capture impactful storms but also move further towards integrating an ingredients-based forecasting approach (e.g., (Doswell et al., 1996)) into the snowpack runoff decision support framework.

2.5.2 Snowpack Response to ROS

Our results, which show that midwinter storms can produce TWI from the snowpack while SWE increases (Figure 2.7), contradict the previously-held assumption that the snowpack has three separate time periods for warming (must become isothermal), ripening (maximum liquid water retention), and output (liquid water release) (Kinar and Pomeroy, 2015). Studies have documented that liquid water can move through the snowpack through the formation of preferential flow paths ahead of the wetting front though the dynamic feedback between present weather and snowpack conditions is not well-understood (Marsh, 1999; Kattelmann and Dozier, 1999; Eiriksson et al., 2013; Jennings and Jones, 2015; Brandt et al., 2022b). For example, Berman et al. (2009) found isotope signatures transitioned from rain to snow, demonstrating the different time travel for rainwater that only needed to remain warm enough to progress as liquid water. In contrast, snowmelt requires sufficient warming for the latent heat exchange within the snowpack. Consistent with these findings, hourly observations made at the CSSL SNOTEL provide evidence that the snowpack can release water while simultaneously accumulating SWE and increasing in density during ROS events. This implies that ROS does not always lead to a decrease in SWE (Guan et al., 2016). Furthermore, the hourly data demonstrated that liquid water content could increase as the snowpack charged with water and subsequently drains from the snowpack, similar to a rising and falling limb of a hydrograph, but with a positive net change in SWE. Therefore,

decreases in SWE are not always synonymous with snowmelt during ROS events (Fassnacht and Records, 2015; Musselman et al., 2017; Yan et al., 2018; Henn et al., 2020; Musselman et al., 2021; Brandt et al., 2022a). This highlights the value of using soil moisture as an indicator of TWI and that TWI should be used in tandem with other parameters to improve the definition of snowmelt in research, especially in ROS-prone regions.

2.5.3 Value of the Snowpack Runoff Decision Support

With additional confidence in hourly data, we extracted information about present weather and antecedent snowpack conditions that coincided with midwinter TWI. This facilitated the development of the first iteration of a decision support framework indicating favorable snowpack runoff conditions for producing TWI (Figure 2.9). Leveraging observations to identify potential hazards is the first step to build reliance through impact-based decision support for a Weather Ready Nation (Uccellini and Ten Hoeve, 2019). Advisories and early-warning systems represent a proven technique for communicating hazards to user communities. Operational examples in the United States are commonly provided by Federal agencies intending to provide decision support to regional user groups. Some examples include United States Forest Service avalanche forecasts (Statham et al., 2010), Environmental Protection Agency air quality index forecasts (Environmental Protection Agency, 1999), U.S. Geological Survey post-fire debris flows assessments (Force, 2005), and the National Weather Service heat risk tool (Hawkins et al., 2017). Inspired by these advisory systems, and notably by the current lack of such a framework (to our knowledge) despite the known challenges and impacts for water management created by ROS in the western United States (e.g., McCabe et al. (2007); Musselman et al. (2018); Siirila-Woodburn et al. (2021)), we created this initial iteration of snowpack runoff decision support. We employed similar visualization strategies (e.g., color-coding following an ordinal scale) for communicating levels of runoff hazard. Similar to decision support developed to track the location of landfall and intensity of atmospheric rivers (Ralph et al., 2019), identifying regions with varying levels of risk for runoff based on antecedent snowpack conditions could increase the lead time for decision-making and confidence in choices made. Coupling observations

that provide information about the current state of the snowpack with an improved understanding of ROS processes (e.g. 22 mm of rainfall in 24 hours at the CSSL always resulted in TWI) could provide more nuance to meteorological forecasts by better understanding the range of potential hydrological impacts ahead of the event. Another example includes forecast-informed reservoir operations, which are demonstrating the value of shifting from fixed flood control schedules towards risk-based ensemble forecasting to plan water releases (Delaney et al., 2020). A risk-based approach to SR-DSS could be a valuable tool integrated into next-generation water resource management in transitional and snow-dominated regions. The use of hourly data highlights this advisory is possible and ongoing research aims to continue to develop the concept and address limitations as they are exposed through soliciting stakeholder feedback.

2.6 Limitations of Study

While we have provided the initial steps towards operational SR-DSS, this study is limited in scope by only investigating one station, resulting in thresholds specific to the CSSL that have not yet been tested regionally. Caution should be exercised before the model and conceptual framework established at the CSSL is applied to other stations. However, the methods developed in this study can be applied to other SNOTEL stations and provides a testable framework to continue the research toward SR-DSS. Our approach would benefit greatly from subsequent engagement and iterative development activities in tandem with water management or other natural hazard-focused stakeholders as well as the incorporation of additional stations and data including, but not limited to streamflow, wind speed, solar radiation, and relative humidity for validation or to refine thresholds. Lessons learned and useful strategies from the development of forecast-informed reservoir operations may facilitate this threshold-refining process.

The TWI identification algorithm will likely require calibration at other stations and will not work at stations without well-draining soil where soil is saturated throughout the winter. The algorithm developed for this study was intended to identify prominent periods

of TWI but could not capture small increases in soil moisture without also capturing normal fluctuations during other periods not related to TWI.

Identifying each hour of TWI during ROS shows 6 hour precipitation and temperature values that can be misleading. Once a precipitation event ends, the rolling 6 hour precipitation total slowly decreases, but the snowpack could still release water. Some rainfall events turn to snow with the cold frontal passage and erroneously associate the TWI with precipitation falling as snow (e.g. 13–14 February 2019). Precipitation phase classification from either in-situ instrumentation such as disdrometers (Sumargo et al., 2020) or citizen science (Arienzo et al., 2021), would help further constrain ROS magnitude, TWI classification, and indicators of potential TWI.

2.7 Conclusions

The motivation for our work was to investigate the potential value that hourly data has to (1) improve process-based understanding of midwinter runoff generation and (2) provide real-time information to decision-makers when rapid changes in the snowpack overcome the capability of the model. The SNOTEL network provides near real-time information valuable to the analysis of midwinter runoff and exceptional events, like the initiation and duration of ROS TWI from soil moisture sensors. These observations can be leveraged to develop a snowpack runoff decision support system by connecting observations to potential outcomes in order to mitigate risk (Uccellini and Ten Hoeve, 2019). We found value in the QA/QC hourly observations from a SNOTEL station, as these data can be used as input to decision support tools for pattern recognition and improve model accuracy by up to 25.7%. We then showed how this data can be applied to ingredients-based forecasting (Doswell et al., 1996) and could help to establish the framework for a regionally-specific snowpack runoff decision support. In addition, our approach provided quantitative values of liquid precipitation required to produce a soil moisture response. Without a soil moisture response, runoff and subsequent flooding is unlikely. We also showed consistency between atmospheric conditions and identified ROS events using our framework, which provides additional confidence in the

skill of the approach at correctly identifying physically consistent events.

Our efforts here represent a first step towards operational snowpack runoff decision support that is applicable across management scales and adjustable depending on flood management infrastructure. With increasingly frequent ROS and decreasing water availability projected in a warming climate (Musselman et al., 2018; Siirila-Woodburn et al., 2021), runoff advisories may become valuable tools to inform decision support for adaptive water management strategies such as forecast-informed reservoir operations (Delaney et al., 2020) or managed aquifer recharge (Steinschneider and Brown, 2012) intended to better capture and retain water to meet consumptive and ecosystem demands. In Chapter 4 I incorporate additional SNOTEL stations to test the robustness of these methods at a regional scale and incorporate feedback from forecasters, decision-makers, and water managers.

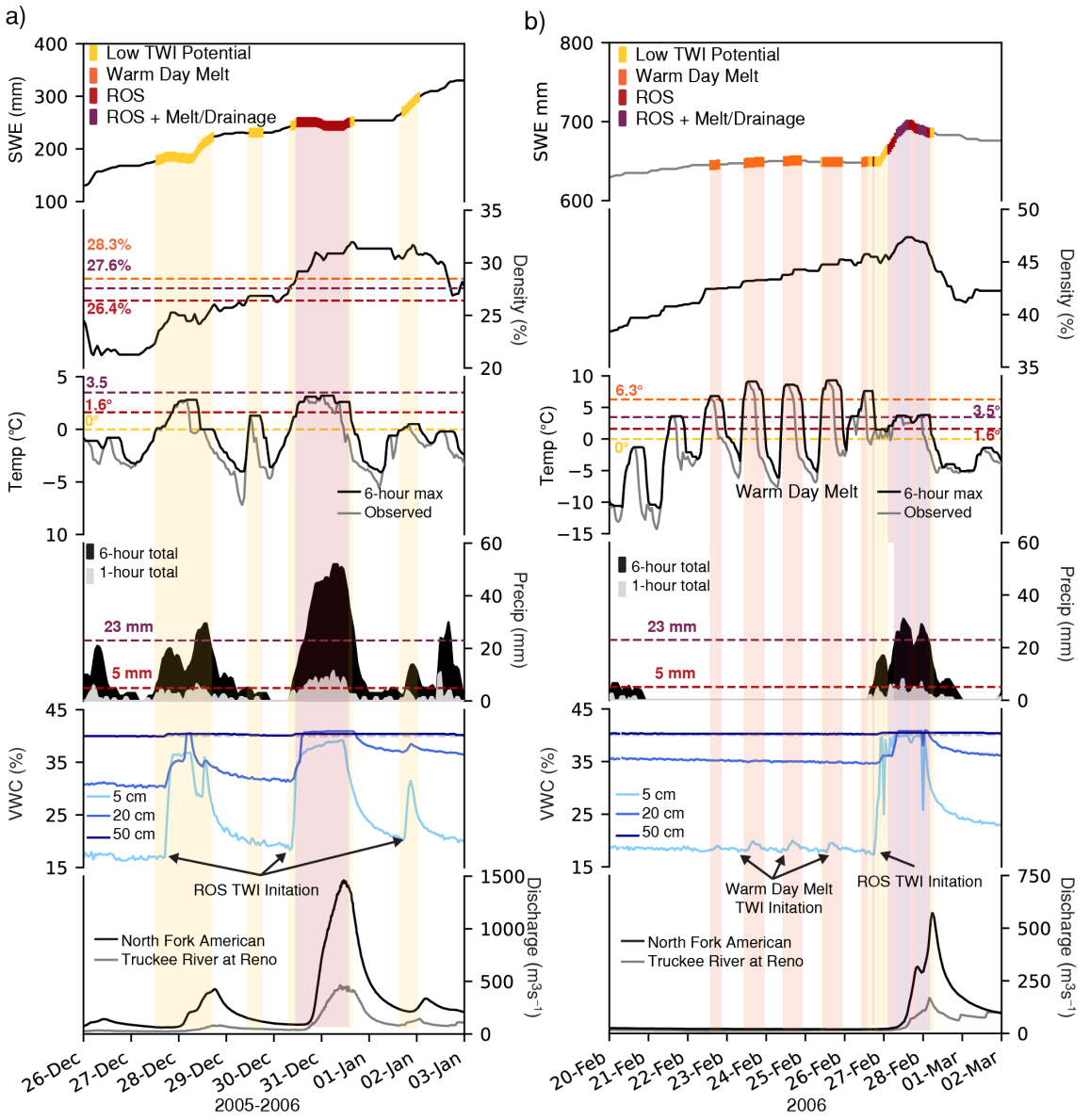

Figure 2.11: Example applications of the preliminary snowpack runoff decision support framework. The decision tree TWI potential thresholds applied to (a) 26 December 2005–3 January 2006 and (b) 20 February–2 March 2006. The first subpanel of each plot shows SWE (mm) colored by TWI potential as low potential (yellow), ROS (orange), ROS + melt/drainage (red), and warm day melt (purple). The second subpanel shows the snowpack density (%) with corresponding TWI potential thresholds with representative colors. The third subpanel shows observed (grey) and 6 hour maximum (black) air temperatures (°C) with corresponding thresholds and the fourth panel shows 1 hour (filled grey) and 6 hour (filled black) precipitations totals (mm) with the 6 hour precipitation corresponding TWI potential thresholds. The fifth subpanel shows volumetric water content (%) from the soil moisture sensors at 5 cm (light blue), 20 cm (medium blue), and 50 cm (dark blue) depths. The sixth subpanel shows streamflow (m^3s^{-1}) at two US Geological Survey gages: North Fork of the American at North Fork Dam (black) and Truckee River at Reno (grey).

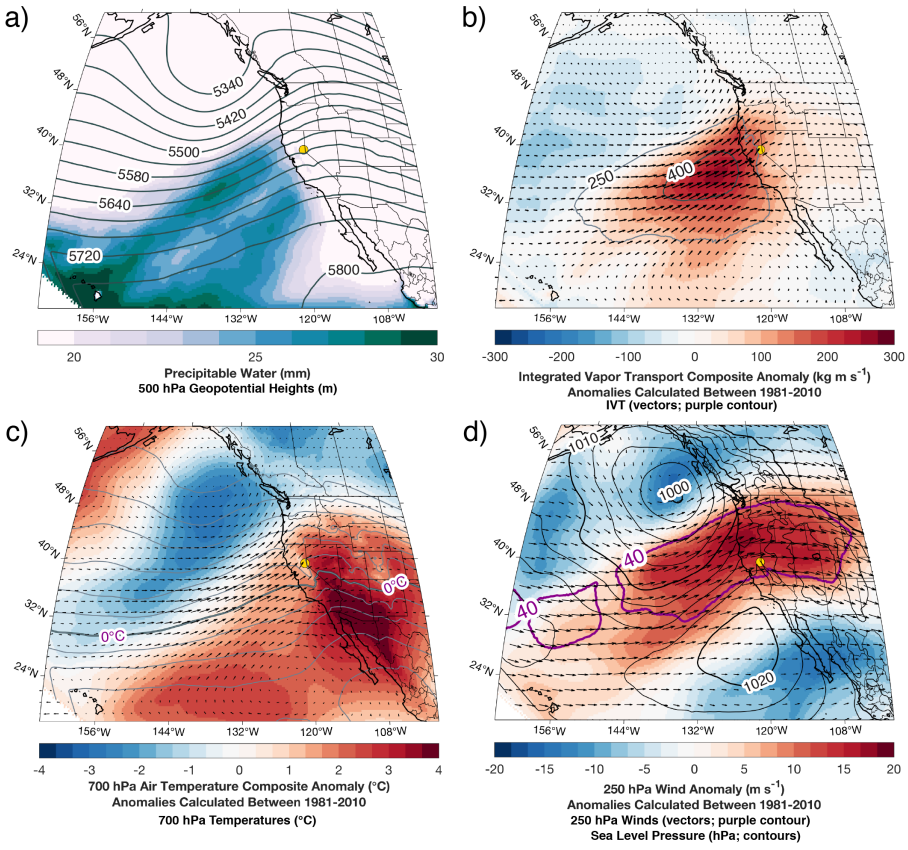

Figure 2.12: Composite synoptic conditions for events with at least six hours of TWI from ROS. Composite synoptic conditions from the North American Regional Reanalysis (Mesinger et al., 2006) for 17 unique events that produced at least six hours of TWI. (A) Composite precipitable water (mm) and 500 hPa geopotential heights (m; contours). (B) Integrated vapor transport (IVT; kg m^{-1} s^{-1}; relative vectors); IVT anomalies (colored); and regions indicating atmospheric river conditions (>250 kg m^{-1} s^{-1}) or elevated moisture transport (>400 kg m^{-1} s^{-1}). (C) 700 hPa air temperatures (contours) and 700 hPa air temperature anomalies (^{c}ircC; filled contours) with IVT vectors overlaid (kg m^{-1} s^{-1}). (D) 250 hPa winds (vectors; m s^{-1}); 250 hPa wind anomalies (m s^{-1}; filled contours); 250 hPa winds exceeding 40 m s^{-1} (purple contours); sea level pressure (hPa; black contours).

Chapter 3

Visual Communication of Probabilistic Information to Enhance Decision Support

This chapter is an adapted version of the following publication:
Heggli, A., Hatchett, B., Tolby, Z., Lambrecht, K., Collins, M., Olman, L., & Jeglum, M. (2023). Visual Communication of Probabilistic Information to Enhance Decision Support. *Bulletin of the American Meteorological Society.* https://doi.org/10.1175/BAMS-D-22-0220.1

3.1 Introduction

Consistent with the World Meteorological Organization's (WMO) recommendations (WMO, 2021; Zhongming et al., 2021), the United States National Weather Service (NWS) and its parent organization, the National Oceanic and Atmospheric Administration (NOAA), are transitioning towards probabilistic forecasts as a way to modernize forecast operations to maximize the decision-making value of Impact-based Decision Support Systems (IDSS) (National Weather Service, 2019a; National Weather Service, 2022; Uccellini and Ten Hoeve, 2019). However, effectively communicating probabilistic information (PI) visually to emergency managers and general audiences alike remains a challenge (Joslyn and LeClerc, 2013; Grounds et al., 2017; Juanchich and Sirota, 2018). In a review of 327 studies, Ripberger et al. (2022) established the numerous benefits associated with PI but concluded these ben-

efits hinge on the visuals being well-designed (Franconeri et al., 2021; Padilla et al., 2021). Creating effective PI visualizations requires an interdisciplinary approach that respects the importance of scientific accuracy and leverages visual communication practices that have been proven to be effective.

Visual communication scholars have established that visualization is the best approach to communicate complex information like PI (Lipkus and Hollands, 1999; Ash et al., 2014; Carr et al., 2016; Dallo et al., 2020; Murchie and Diomede, 2020; Carr et al., 2021; Franconeri et al., 2021; Kuller et al., 2021). Visuals capitalize on the brain's visual system to extract complex information rapidly and accurately (Essen et al., 1992; Zacks and Franconeri, 2020). At the same time, visuals such as graphs, charts, and maps enhance the comprehension of complex information by breaking down the information into smaller, more meaningful units (Malamed, 2015). Visuals are essential aids to communicate PI to both core partners (e.g. emergency managers, school districts, government agencies) and public audiences.

With more accessible probabilistic forecast information, the NWS is transitioning towards improved PI visualizations to maximize the decision-making value in order to build a Weather-Ready Nation (Schumacher et al., 2021; National Weather Service, 2022; Harrison et al., 2022; Schumacher et al., 2022; Novak et al., 2023; Tripp et al., 2023). However, there remains a gap in the application of best practices from visual communication research to PI forecasting in the NWS. Tools like the public-facing experimental 1D Viewer or internal Whole Story Uncertainty & Probabilities (WSUP) Viewer and Probabilistic Graphics Generator are designed to visually convey probabilistic forecasts and thereby increase the capacity for agencies to disseminate PI when appropriate. However, these tools still require effective visual communication strategies to help improve the user's understanding of the forecast.

To support ongoing efforts of the NWS to communicate more PI to core partners and public audiences alike, we synthesize guidelines for visualizing PI from literature aimed specifically at visual communication for weather-related hazards and general effective graphic design conventions and summarize the findings in a one-page printout (Figure 3.1). We then apply these guidelines to create "plug-and-play" templates (Heggli et al., 2023) to develop

PI graphics in Excel and "plug" them into a PowerPoint template to "play" with colors and update text and icons accordingly. The templates incorporate the guiding principles identified in the literature as a way to demonstrate how PI extracted from probabilistic forecast tools can be visualized to support decision-making. To incorporate these methods into practice, we provide examples for primary weather conditions that commonly pose widespread and localized hazards in the Western United States: snowfall, wind, temperature, and thunderstorms developed in collaboration with the NWS Reno. These tools are designed with an emphasis on PI visualization for the NWS Western Region (WR). Nonetheless, they are designed to be adaptable for other public-facing hazard communications in other NWS regions as well as by other government agencies and emergency managers for other hazards requiring early warning systems to encourage communities to prepare and/or take protective action (e.g. hurricanes, smoke, heat, and debris flows) (Hatchett et al., 2021; Lambrecht et al., 2021; VanderMolen et al., 2022; Oakley et al., 2023; Rosen et al., 2023).

Guidelines for Visual Communication of Probabilistic Information (PI)

ACCESSIBILITY

Follow 508 Compliance Guidelines[1] but use this as first step to improve accessibility

LAYOUT

Use the template* to ensure content uniformity. New templates should respect familiar design conventions (e.g. title at the top and supplemental information at the bottom). Organize thoughts with color blocking using a grid space approach like the example provided. Do not overcrowd the visual.

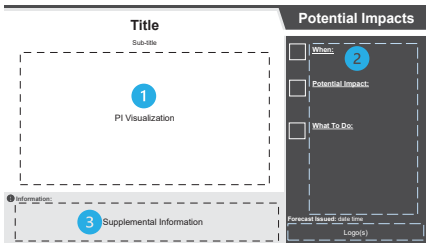

CONTENT

Title:	Explain the weather
Subtitle:	Set up Probabilistic Information (PI) visualization
PI Visualization:	Insert the PI visualization
Supplemental Info:	Explain the graphic and/or direct users to information about the source of the data or more specific forecast information. Keep it short!
Impact Statement:	When – Communicate the timing Potential Impacts – Briefly describe the potential impacts What To Do – Provide preventative guidance or action items aimed at reducing exposure to the potential impacts

COLOR

- ✓ Use a single hue that varies in lightness to communicate uncertainty (darker = more certain)
- ✓ Check colors with an online colorblindness simulator[2]
- ⊘ Do not use red-green or orange-green color maps
- ⊘ Do not use rainbow color maps
- ⊘ Do not use colors that conflict with risk or hazard color scales

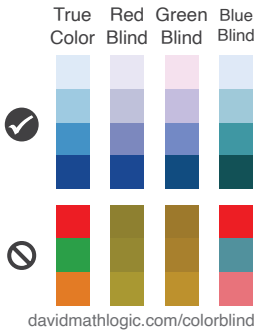

FONT

Arial, Univers, Helvetica

Title 32 pt, subtitle 18 pt, body 16 pt, minimum size 14 pt

Use **boldface** to draw attention and avoid italics

EMBELLISHMENT

Communicate - don't decorate! Icons and photos should directly aid the message.

*Download the template: bit.ly/visualize_PI

1. section508.gov
2. color-blindness.com/coblis-color-blindness-simulator

Figure 3.1: A one-page printout of key visual communication guiding principles intended for forecasters tasked with disseminating PI visualizations.

3.2 Why Communicate Probabilistic Forecast Information

Though deterministic forecasts remain important to some users and are adequate for some situations (Carr et al., 2021; National Weather Service, 2022), communicating the full range of possibilities and their associated uncertainties becomes invaluable when a hazardous event is forecast (Hirschberg et al., 2011; Joslyn and LeClerc, 2012; Miran et al., 2019). When a deterministic forecast is given, the uncertainty information is omitted thus obscuring the complete forecast (National Research Council et al., 2006). A single-valued deterministic forecast without a measure of uncertainty can be acceptable when the uncertainty in the forecast is very narrow or the weather will not impact routine operations or require any action (National Weather Service, 2022; National Weather Service Western Regional Headquarters, 2022). For example, if the weather is expected to be 71.6 °F (22 °C) with a 10% chance of being 77.0 °F (25 °C), the addition of PI increases the cognitive load (the amount of visual information that can be processed mentally) to interpret the forecast with minimal additional benefit.

Though deterministic forecasts do not include uncertainty information, research indicates that people do infer some uncertainty from them (Morss et al., 2008; Joslyn and Savelli, 2010; Morss et al., 2010; Savelli and Joslyn, 2012; Zabini et al., 2014). However, during high-uncertainty and high-risk events, deterministic forecasts are problematic (Hirschberg et al., 2011; Todhunter, 2011). People often incorrectly estimate the level of uncertainty in deterministic forecasts, resulting in the perception of too much uncertainty when it is not warranted or not enough certainty when the forecast is highly uncertain (Fleischhut et al., 2020). Furthermore, when a hazard is presented in the deterministic forecast but the hazard does not occur, it results in a false alarm. Continued exposure to false alarms can lead to poor decision-making from the messaging fatigue effect ("crying wolf") when people no longer trust the forecast (Breznitz, 2013; LeClerc and Joslyn, 2015; Oakley et al., 2023). On the other hand, weather resulting in a greater impact due to an under-prediction from the deterministic forecast can be more costly than false alarms since protective action may not have been taken to reduce losses to life and property. Balancing the cost-benefit between

false alarms and costly misses can make it difficult to trust a forecast, and trust is a strong predictor of the likelihood of people taking preparatory action (Losee and Joslyn, 2018). Visually communicating PI offers a more effective way to improve compliance with preventative guidance and decision quality than efforts to improve deterministic forecast accuracy aimed at reducing false alarms and costly misses alone (LeClerc and Joslyn, 2015).

Research shows PI is valuable in building trust, increasing confidence and understanding of the forecast, and improving decision-making (Morss et al., 2008; Joslyn and LeClerc, 2012; Joslyn and Grounds, 2015; Grounds and Joslyn, 2018; Howe et al., 2019; Joslyn and Demnitz, 2019; Carr et al., 2021; Ripberger et al., 2022). Communicating uncertainty demonstrates a commitment to transparency that increases credibility and trust (Joslyn and LeClerc, 2012, 2013; van der Bles et al., 2020). When users trust the forecast they are more motivated to take preventative action, thereby decreasing the impact of the hazard (LeClerc and Joslyn, 2012, 2015; Grounds et al., 2017; Miran et al., 2019). However, making the forecast is only beneficial if it motivates action (Murphy, 1993).

3.3 Guidelines for Visual Communication of Probabilistic Weather Information

Through an interdisciplinary review of visual communication research, we identify common guidelines that improve infographic-style PI visuals. Our review attempts to cover the spectrum of literature from graphic design to social science as they relate to the visual communication of public messaging using an infographic format for hazard communication. This spectrum includes many topics ranging from the visual aesthetic to scientifically-proven communication methods building off of the work done by Ripberger et al. (2022). We focus on six components of effective visual communication: (1) accessibility, (2) layout, (3) content, (4) color, (5) font, and (6) embellishments to apply to probabilistic weather information (Samara, 2020). These key findings are summarized in a one-page printout (Figure 3.1).

3.3.1 Accessibility

Inclusivity through accessibility is an important aspect of communication to increase the reach of information and improve user experience. Accessibility compliance is legally required by federal agencies in the United States (Congress, 1973). Making documents accessible for disabled populations is an important consideration for anyone who creates or publishes documents; this is especially true for PI visualizations. For example, it is important to consider color vision deficiencies. Red-green color blindness (protanopia and deuteranopia) is the most common, occurring in around 8% of males though less frequently in females (0.5%) (Sharpe et al., 1999; Deeb, 2005; Motulsky and Deeb, 2001). Beyond color vision deficiencies, the use of alternative text ("alt text"), promotes inclusivity for people who are visually impaired or have difficulty seeing images by providing equal access to information. Alt text ensures individuals using screen readers or assistive technologies can understand the context and content of images shared on social media platforms (Chiarella et al., 2020; Huntsman, 2022). It is also important to consider neurodivergent characteristics (e.g. dyslexia, ADHD, autism, etc.) (Mcgee, 2012). Between 10-15% of the U.S. population is estimated to have symptoms of dyslexia and simple design changes (e.g. font selection) can improve readability for some individuals (Eden and Moats, 2002; Fletcher et al., 2018).

Accessibility standards help ensure the information and resources are available and usable for as many people as possible, especially those with disabilities. Since this is an overarching consideration, we provide specific examples throughout the following sections. We integrate considerations for colorblind safe color palettes (Section 3.3.4), design the layout to guide the viewer's focus (Section 3.3.2), and select fonts with sufficient contrast between font color and background to improve readability (Section 3.3.5) into the guiding principles. Each of these is an important visualization consideration. While alt text is not a part of the visual communication design, we urge anyone posting images to social media to include a summary as the alt text when posting the image.

3.3.2 Layout

The term "layout" encompasses the organization and placement of text, color, and images. Layout influences how readers navigate the visualization by implementing effective use of (1) hierarchy to highlight the most important message, (2) alignment to create a visual connection between elements, (3) repetition to build familiarity, and (4) negative space to help create a sense of simplicity to reduce cognitive load (Poulin, 2018; Tondreau, 2019; Samara, 2020). Reducing cognitive load is especially important for probabilistic weather information, and arguably even more important for public audiences that may not have the motivation to look further into the forecast (Palmer, 2002). The layout for PI visualizations should respect familiar design conventions, like titles at the top of the layout with supplemental information at the bottom, as this reduces cognitive load (Andry et al., 2021; Franconeri et al., 2021; Gordon et al., 2022). This top-down approach is further advantageous as visualizations are read cyclically between the title, legend, and the data before reasoning (Andry et al., 2021).

Lowering cognitive load is especially helpful for neurodivergent audiences such as individuals with autism or dyslexia (Eraslan et al., 2020). A simple and effective layout technique is to apply a grid system to organize visual content (Hilligoss and Howard, 2002; Poulin, 2018; Ambrose et al., 2019; Samara, 2020). Within each grid, there should be sufficient negative (empty) space to frame active spaces and call attention to content (Hilligoss and Howard, 2002; Samara, 2020). Color-blocking major grid sections can also be an effective tool to separate thoughts within the visualizations (Poulin, 2018).

3.3.3 Content

PI visuals should include a combination of graphics and writing: graphics provide the visual overview and the text provides the key details since the ability to understand graphics alone is related to numeracy levels (having the ability to understand numbers and do math) (Dallo et al., 2020). Effective visual communication benefits from content uniformity (Gordon et al., 2022). PI visualizations should include three core components: (1) the PI visualization

of where and what the weather is forecast to be with an expression of likelihood, (2) an impact statement, and (3) supplementary information as we demonstrate in Figure 3.2, which is consistent with the findings and work of Bean et al. (2015); Grounds and Joslyn (2018); Sutton and Kuligowski (2019); Gordon et al. (2022); Kuller et al. (2021).

It is beneficial to build on what is familiar, especially if the intended audience has limited exposure to PI (Fundel et al., 2019). Familiar graphs to populate with PI include axis-aligned bar charts, data-filled tables, and maps (Fundel et al., 2019; Dallo et al., 2020; Franconeri et al., 2021; Andry et al., 2021). However, less familiar designs like box-plots, which communicate the full range of scenarios and most likely scenario in a single figure for a location, may be more useful to communicate PI though they can hinder comprehension if not properly introduced (Authority et al., 2019; Carr et al., 2021). Therefore, when introducing graphics, we suggest the addition of a supplemental information section (Figure 3.2) to build familiarity through repetition for those who are less familiar with the visualization. Over time, increased familiarity helps users interpret the graphic quickly and provides space to seek more information, a common request from users analyzing PI (Fundel et al., 2019; Carr et al., 2021; Flynn and Lide, 2022).

In any PI visualization, it is recommended to provide numerical and verbal expressions of uncertainty (e.g. 40% moderate chance) and if only one must be selected, numerical expressions of uncertainty are more effective than verbal expressions in reducing subjective interpretations (Nadav-Greenberg and Joslyn, 2009; Joslyn and LeClerc, 2012; Windschitl et al., 2017; Jenkins et al., 2018, 2019; Lenhardt et al., 2020; Rosen et al., 2021; Koskinas et al., 2023). Finally, the PI visualization should include a standard impact statement summarizing when the weather is expected, the potential impacts, and preventative guidance to reduce exposure (Bean et al., 2015; Grounds and Joslyn, 2018; Sutton and Kuligowski, 2019; Kuller et al., 2021; Gordon et al., 2022; Koskinas et al., 2023).

3.3.4 Color

Color is more than a decorative choice. Color is one of the most important and powerful selections in visual communication (Stone et al., 2008). Color attracts attention, conveys

meaning, and visually organizes information (Stone et al., 2008; van Gorp and Adams, 2012). There is a growing consensus regarding the rank order of colors to communicate impact or hazard: green, yellow, orange, red, and violet (Gordon et al., 2022; National Weather Service Western Regional Headquarters, 2022). However, any color-coded uncertainty should not conflict with the hazard level since the probability is not necessarily proportional to the impact. If color is required to communicate uncertainty, the color values should be assigned on a continuum of lightness, hue, or both, if the data benefits from a diverging palette (Wong, 2010, 2011; Crameri et al., 2020; Dasgupta et al., 2020; Franconeri et al., 2021). It is also best for the highest saturated hue to communicate the greatest certainty with the lightest hues representing lower certainty since saturation levels have an effect on cognitive arousal (van Gorp and Adams, 2012; Wilms and Oberfeld, 2017). If data is best represented with multiple hues, they must be visible to those with color vision deficiencies. Red-green color combinations are the most problematic, but any colors with red or green components (e.g. brown and green) can make it difficult to decipher (Wong, 2011; Crameri et al., 2020; Basak and Roy, 2022). We suggest using red-blue in lieu of red-green and verifying any color selection with an online color-blindness simulator (e.g., `www.color-blindness.com/coblis-color-blindness-simulator/` or `davidmathlogic.com/colorblind/`). An example of effective color mapping of probabilities is the NOAA Climate Prediction Center's Temperature and Precipitation Outlooks, which communicate the probability of temperature above normal or below normal (red to blue) (`https://www.cpc.ncep.noaa.gov/`).

Weather forecasts and hazard maps are repeat offenders of the misuse of color (e.g. commonly applied NWS weather radar, temperature, and wind speed graphics). This is due in part to the precedence of such color scales in early versions of weather products likely due to ease of access to flawed color scales (e.g. rainbow) from visualization programs (Borland and Ii, 2007; Dasgupta et al., 2020). Using color scales that vary indiscriminately in hue and brightness, such as rainbow-type color scales, are well-known to poorly represent data and should be avoided at all costs (Rogowitz and Treinish, 1998; Borland and Ii, 2007; Stauffer et al., 2015; Crameri et al., 2020; Dasgupta et al., 2020). Since PI visualizations lie

at the intersection between science and society with a potentially large impact on decision-making, they should specifically address effective color use. This includes avoiding red-green color palettes and rainbow-type color maps (Morss et al., 2008; Carr et al., 2021). In general, it is advised to use two or three colors and apply a contrasting color sparingly if the graphic needs something extra to "pop" (Samara, 2020).

3.3.5 Font

Fonts frame the tone of what is being communicated. Selecting the proper font creates trust and confidence as well as improves the overall perception of a visualization's impact (Hyndman, 2016; Nersesian et al., 2020). When selecting a typeface, readability and legibility are critical considerations. Sans serif fonts such as Helvetica, Arial, and Verdana are more effective than serif (embellished) fonts not only for people with dyslexia (Rello and Baeza-Yates, 2013) but all populations (Bernard et al., 2001; Chaparro et al., 2010). Later, Rello et al. (2016) found an increase in font size above 14 pt, but no larger than 22 pt, improves readability. When communicating hazard information, selecting familiar fonts is especially important since the message needs to be trusted (Hyndman, 2016). Familiar sans serif fonts (without embellishment), such as Helvetica, Arial, and Univers, are preferred for warning messages and scientific illustrations over serif fonts like Times New Roman, Garamond, and Courier New (Sattler et al., 1997; Nersesian et al., 2020).

Though most readers can engage with two or three fonts, these should be selected as an organizational aid to establish hierarchy if needed (Poulin, 2017). Variation in contrast (boldface) and font size also effectively establish hierarchy, indicating where the attention of the reader should go first, second, and third (i.e., heading, subheading, informational body) (Poulin, 2017). We recommend avoiding italics to improve readability for all populations (Rello and Baeza-Yates, 2013).

3.3.6 Embellishments

Embellishments such as icons, color gradients, shadows, shapes, and background images (sometimes referred to as "chart junk") decrease clarity as they are not essential to under-

standing the data (Tufte, 1997). It is a good practice to remove non-critical design elements as this reduces the cognitive load requirement for visualizations that are necessary for more complex PI visualizations (Tufte, 1997; Sweller, 2011; Franconeri et al., 2021). However, relevant embellishments can be effective for catching the attention of busy viewers, help readers distinguish the purpose of one visualization, and anchor the detail in the viewer's memory (Bateman et al., 2010; Andry et al., 2021). An effective rule for developing visualizations is "communicate, don't decorate" (Samara, 2020). For example, the use of snowflakes for snow-related PI quickly signals the reader what the graphic is about, potentially increasing engagement (Andry et al., 2021).

3.4 Examples

To show what these principles look like in practice, we provide examples of PI visualization by coupling PI with the previously-discussed guiding principles from graphic design and social science-informed visual communication. Grounding these examples in the WR, which covers Arizona, California, Colorado, Nevada, Idaho, Montana, Oregon, Utah, and Washington, we focus on primary weather conditions that pose widespread and localized hazards including snowfall, temperature, wind, and thunderstorms. Each example has unique probabilistic visualization requirements.

3.4.1 Data and Methods

Following the graphic design of weather impact and hazard statements by Gordon et al. (2022), we developed a template (Heggli et al., 2023) to facilitate consistent formatting to promote familiarity through repetition. Repetition indirectly reduces the cognitive load to interpret the data each time it is provided (Franconeri et al., 2021; Fundel et al., 2019).

Figure 3.2 employs the best practices identified in Section 3.3:

- A grid system approach to create three color-blocked sections to distinguish each core content components: (1) PI visualization, (2) impact statement, and (3) supplemental information (Hilligoss and Howard, 2002; Poulin, 2018; Ambrose et al., 2019; Samara,

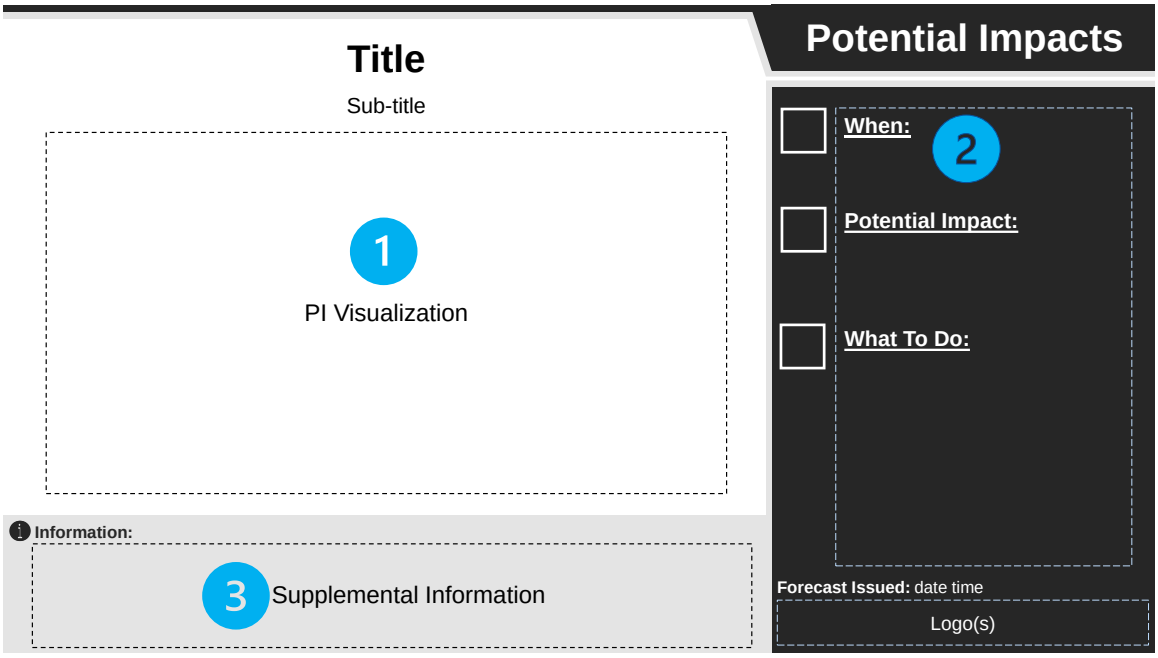

Figure 3.2: Example layout for PI visualizations following recommended guiding principles with three areas for key content: (1) the PI graphic, (2) an impact statement, and (3) supplementary information.

2020)

- Gridded layout with color blocking to create a visual connection between elements (Hilligoss and Howard, 2002; Poulin, 2018; Ambrose et al., 2019; Samara, 2020)
- Appropriate negative space to aid in simplicity (Hilligoss and Howard, 2002; Samara, 2020)
- Variation in font size and weight changed to establish a hierarchy of information (Poulin, 2017)
- Arial font (a minimum font size of 14 pt) for readability (Sattler et al., 1997; Bernard et al., 2001; Chaparro et al., 2010; Nersesian et al., 2020; Rello et al., 2016)
- Space for communication-driven embellishments to act as topical cues (Samara, 2020)

The template provided is designed with a color theme based on `http://www.ColorBrewer.org` (Harrower and Brewer, 2003). The deepest single hue color (with five data classes)

was used as the base color option providing five template colors (blue, green, orange, red, and purple) in addition to standard black and white colors. Each color should be established to represent one weather parameter to (1) build familiarity of that color to the weather being communicated (Dasgupta et al., 2020) and (2) limit the graphic use to just two or three hues (Samara, 2020). We selected a blue template for precipitation/snowfall due to blue being a cool color and the association with water, green for thunderstorms to build on the familiarity of existing thunderstorm potential products issued by the NWS Reno office, orange for wind as a warmer color often associated with drying vegetation, and the black/white template that can be used for ad-hoc weather concerns like a hard freeze (Stone et al., 2008).

The templates were designed to establish content uniformity while providing options and space to customize the PI visualization for the community. Our approach allows forecasters to "color within the lines", i.e., to add content that connects with their communities but is restricted by visual communication guidelines aimed to communicate the message effectively. The dashed boxes within each section delineate the area reserved for content and demonstrate the use of negative space (Hilligoss and Howard, 2002; Samara, 2020). The icons for the impact statement can be customized; we selected a clock icon to communicate the "When" section and a light bulb icon for the "What To Do" section. An appropriate icon should be selected to visually represent the potential impact. Each template uses an information icon to cue the supplemental information section where forecasters can provide instructions to familiarize users with new graphics or provide links to additional resources Carr et al. (2021). Finally, there is a space for the forecast issue time stamp and a logo.

Our template uses Arial font throughout the entire visualization. The title is 32 pt, the subtitle is 18 pt, and the other body text is 16 pt with boldface to distinguish the headers. The minimum font size is 14 pt, used in the forecast date and on some labels given space limitations. These templates assume the platforms have zooming capabilities. All of the graphics were verified for readability and display with cellphone use.

We used the NBM to extract probabilistic forecast information. The NBM is a blend of NWS and non-NWS models that creates probabilistic gridded forecast guidance (Craven

et al., 2020; National Weather Service, 2022). Following the recommendation of NWS forecasters, the PI graphics were developed in PowerPoint and Excel since these tools are readily available in NWS offices. The PI visualization PowerPoint and Excel templates are available online (Heggli et al., 2023). Data extracted from the NBM 1D Viewer and WSUP Viewer were used to develop graphics in Excel. The map is exported directly from GraphiDSS, an internal NWS program, to create public-facing weather map graphics.

3.4.2 Snowfall

Snowfall does not have a universal impact threshold; a dusting of snow on cold roads before rush hour may be more impactful than heavy snow on a holiday. For decision-making, the regional Department of Transportation traction (chain) control threshold is typically different from school districts' snow day policies. A range of risk tolerances likely exists for community members driving in the snow. Some will have more experience and snow-capable vehicles while others avoid driving if any snow accumulates on roads. The objective of the snowfall example (Figure 3.3) is to communicate a range of potential scenarios so users can make a decision based on their personal risk threshold.

A box plot is a data visualization tool currently used in NWS visual communications to express a range of possible outcomes with an associated expression of likelihood. Since users may not be familiar with how box plots are constructed Frigge et al. (1989) and because box plots can be challenging to correctly interpret Bakker et al. (2004); Edwards et al. (2017), we utilize the supplementary information section to teach users how to interpret a box plot. We recommend box plots to present information that needs to communicate the high- and low-end scenarios for parameters like snowfall or rainfall. Box plots are not recommended for temperature, as showing a range of potential temperatures can cause deterministic construal error where a user misinterprets the probabilistic forecast as being deterministic (Joslyn and Savelli, 2021). We also give both numerical and simple verbal expressions of uncertainty (Nadav-Greenberg and Joslyn, 2009; Lenhardt et al., 2020; Rosen et al., 2021). The impact statement communicates timing, potential impacts, and preventative guidance. To emphasize the potential for traction control, a car and chain icons illustrates the im-

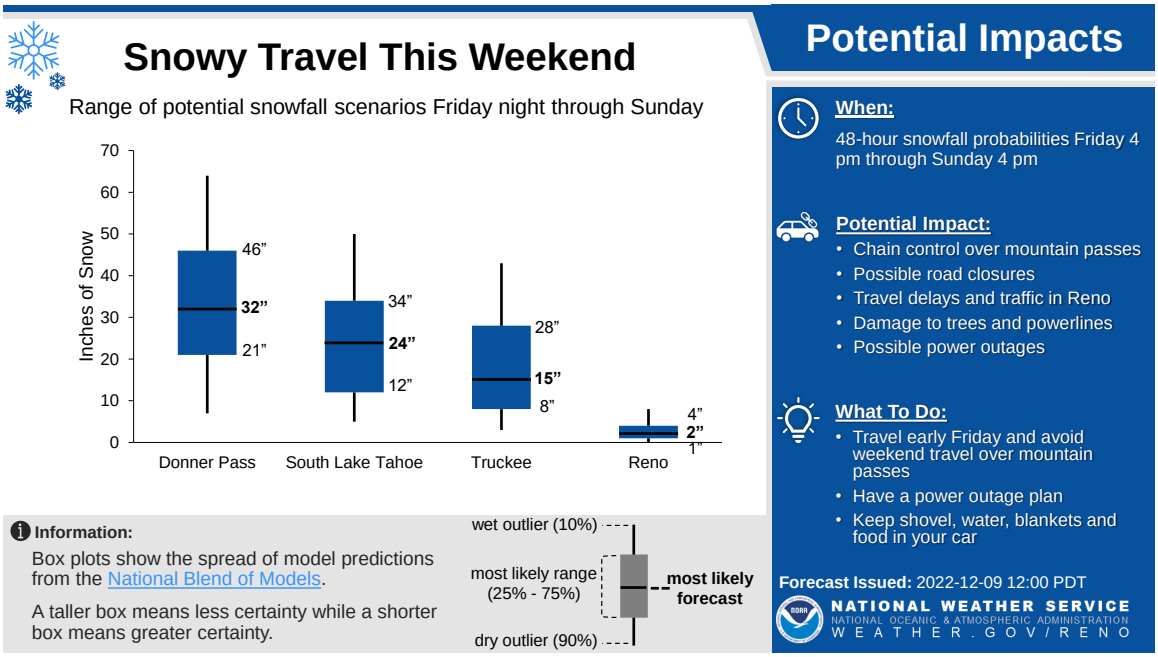

Figure 3.3: An example PI visual of using a box plot to communicate a range of possible snowfall scenarios.

pact. Last, the statement includes guidance to reduce exposure or impacts by suggesting protective actions. The blue color theme is a “cool” color often associated with cold and water. Embellishments were limited to snowflake icons to reinforce the graphic’s focus on snowfall.

3.4.3 Hard Freeze

A hard freeze, unlike snowfall, has a defined risk threshold of 28 °F (-2 °C) (National Weather Service, 2019b). Temperatures dropping below this threshold for multiple hours present a hazard for ornamental and agricultural vegetation, exposed or poorly-insulated water pipes or irrigation systems, and drivers. The example in Figure 3.4 demonstrates how PI can be applied to show the chance of a hard freeze threshold being exceeded.

We selected a familiar axis-aligned bar chart (Andry et al., 2021) and labeled the y-axis with the percent chance of exceeding the threshold to communicate the uncertainty numerically with an adjacent verbal expression of uncertainty. This chart style could also be

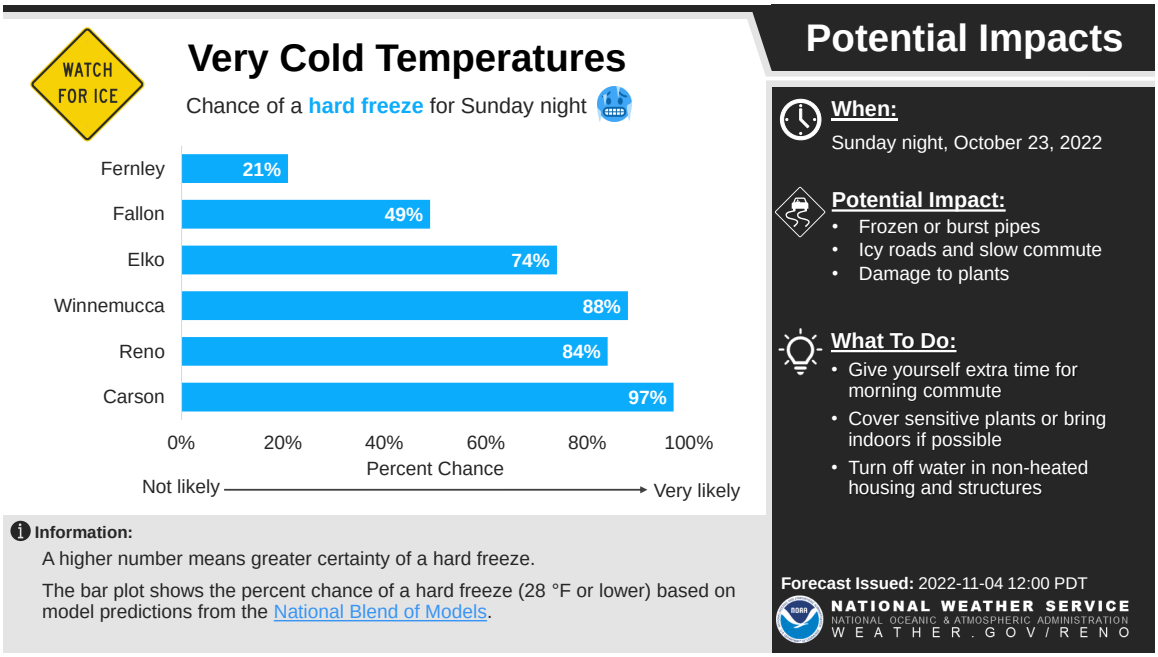

Figure 3.4: Example of a horizontal bar chart to communicate the probability of exceeding the hard freeze threshold of 28 °C.

employed to communicate record-breaking or critical thresholds of temperatures, snowfall, or rainfall totals. The supplementary information section provides information section and a link to learn more about the NBM, a common request from users (Carr et al., 2021; Kuller et al., 2021). It also includes a sentence to help users understand the numerical information. The impact statement gives consistently formatted information about when the hard freeze is expected to occur, the potential impacts of a hard freeze with a frozen pipe icon, and provides preventative guidance to minimize these impacts. A black and white theme was selected as we consider this type of PI visualization to be an ad-hoc advisory and not a standard event like precipitation, wind, or thunderstorm that benefits from a consistent color theme. We used a cooler blue tone to illustrate the chart and a contrasting color embellishment in yellow to attract the viewer's attention and communicate that the visualization is about the potential for ice (Samara, 2020). Emojis can have a positive impact on interpersonal communication (Elder, 2018) and can be useful for non-verbal communication (Bai et al., 2019). In this PI visualization, we included a cold face emoji.

3.4.4 Damaging Wind

Similar to a hard freeze, wind speed has a specific hazard threshold for damaging winds, classified when sustained winds exceed 40 mph (≈64 kmh) for at least one hour or gusts greater than 58 mph for any duration (≈ 93 kmh) (National Weather Service, 2019b). However, wind speed impacts can vary depending on timing and duration. The wind example aims to communicate the likelihood of damaging winds in different regions and the expected timing and duration by using a table.

We extracted the exceedance probability of wind gusts greater than 58 mph and color-coded the probability of damaging winds over a 72-hour period. Since color-coded PI can improve the understanding of likelihood (Ash et al., 2014; Miran et al., 2019), we use a single hue of orange that increases in lightness as the probability of damaging winds decreases (van Gorp and Adams, 2012; Wilms and Oberfeld, 2017). The color-coded uncertainty is labeled using a numerical expression of uncertainty. A legend with color-coded verbal and numerical expressions is provided (Nadav-Greenberg and Joslyn, 2009; Lenhardt et al., 2020). In this example, we use the supplementary information section to develop weather literacy by explaining the impact of 58 mph winds and coupling this with a fallen tree icon (Fleischhut et al., 2020). Embellishments to communicate a warning about wind were included adding a warning icon coupled with a wind icon. A dark theme background was selected to add contrast and intensity to the orange theme color. A similar design approach could communicate the timing and probability of precipitation or snowfall.

3.4.5 Thunderstorm

Thunderstorms in the Western U.S. are often isolated and have different likelihoods of occurring regionally and locally. Thunderstorms produce lightning hazards for life and property Holle (2014), wildfire ignitions from dry lighting Nauslar and Hatchett (2018), gusty outflow and downdraft winds Peterson (2000), and localized rainfall and flooding Changnon (2001). This example aims to demonstrate how PI can be communicated spatially with a map to show the probability of occurrence both regionally and locally.

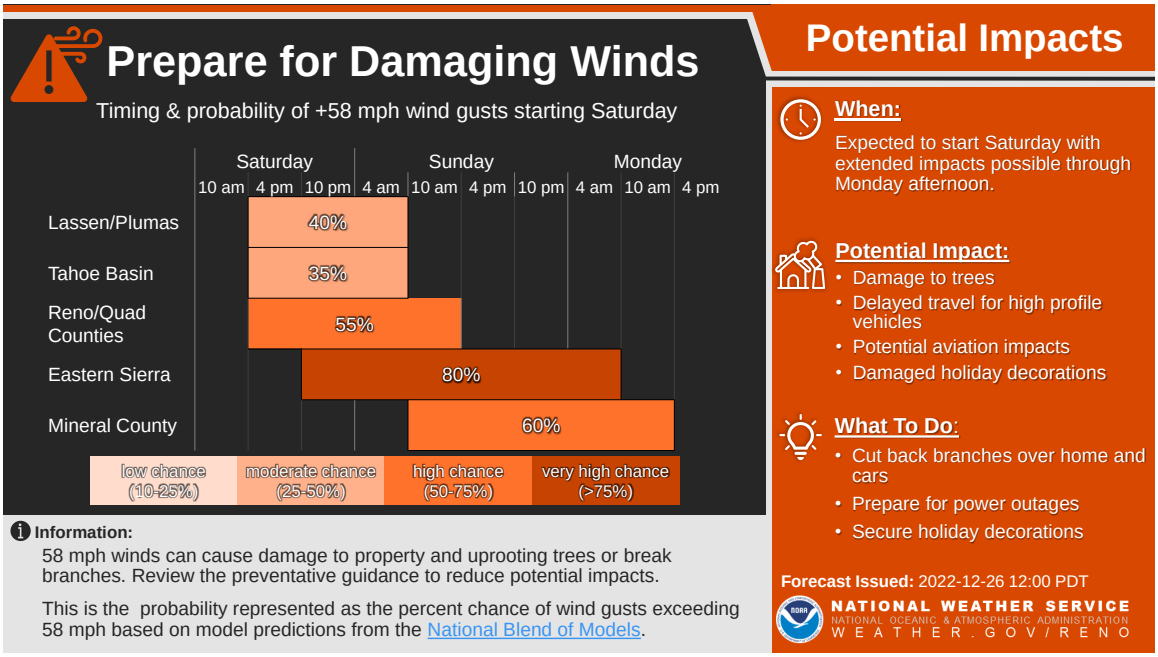

Figure 3.5: Example using a table to communicate timing and probability of damaging winds.

Since current thunderstorm probability graphics already use a green color scale, we chose to use green for this example to retain a sense of familiarity while improving accessibility by having categorical colors rather than a gradient scale. Similar to the damaging wind example, we used a single hue that varies in lightness with the uncertainty level (van Gorp and Adams, 2012; Wilms and Oberfeld, 2017). The color-coded legend provides both numerical and verbal expressions of uncertainty. If terms such as "slight", "moderate", or "high" are used in PI communications as expressions of uncertainty, but do not correspond to the Storm Prediction Center's (SPC; `https://www.spc.noaa.gov/`) Severe Thunderstorm Outlook Categories or other products, it is necessary to explicitly define these terms (i.e., "high *chances*") and provide the quantitative ranges associated with them ("50-75%") used in the PI graphic to avoid any confusion with SPC products or definitions. For forecast maps with areas of less than low chances (i.e., 0-10%), we recommend defining the basemap color in the legend if a monochromic color is used to avoid potential confusion about an undefined color on the map. We leverage the supplementary information section

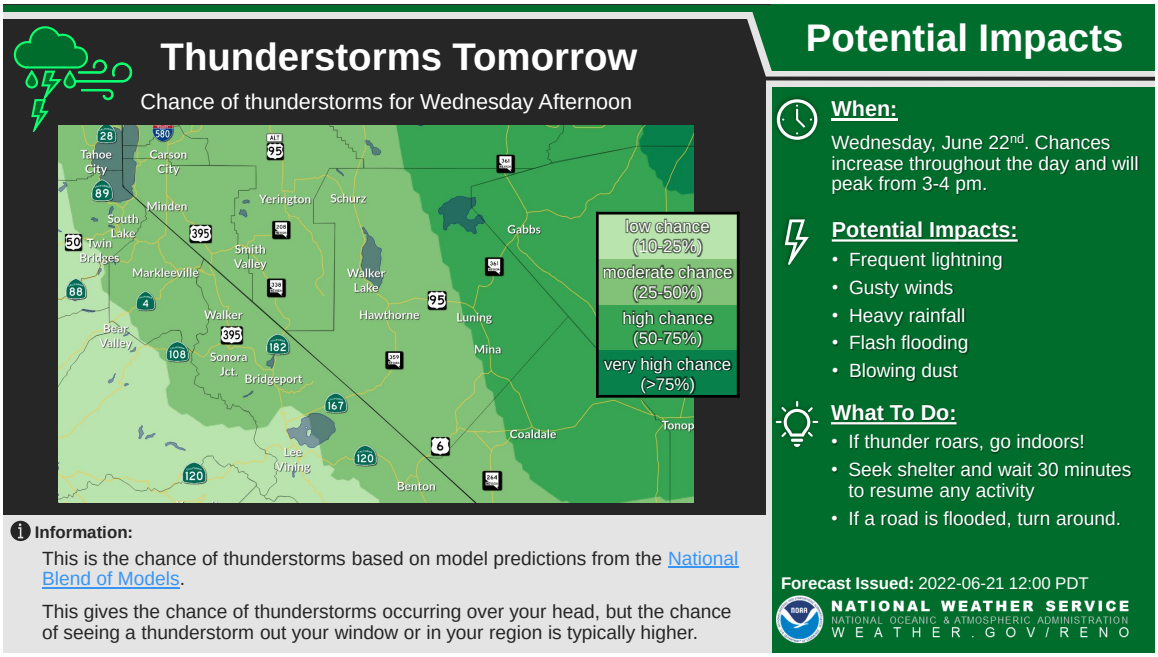

Figure 3.6: Example of a map to communicate the probability of thunderstorms in a region. If less than low chances (0-10%) are required, a lighter green can be used. For areas of no chances (0%) we recommend defining the basemap color in the legend if a monochromic basemap is used.

to clarify that this graphic only provides the probability of a thunderstorm occurring "over your head" but regionally the chances of seeing a thunderstorm is typically higher. In this impact statement, we issue the standard information to communicate when, the possible impacts, and preventative guidance if a thunderstorm does occur. To make the graphic "pop" we selected a dark background with a green theme using thunderstorm and wind icons with a bright green outline to improve the aesthetic (Samara, 2020).

3.5 Discussion

Building a Weather-Ready Nation benefits from a customer-centric approach to forecasting for core partners and general audiences that does not sacrifice the scientific accuracy of a product (Uccellini and Ten Hoeve, 2019). To support a customer-centric approach, we provided an adaptable tool with a "plug-and-play" approach by developing Excel and PowerPoint templates (Heggli et al., 2023) through an iterative design process with NWS

forecasters. These templates incorporate guiding principles based on a review of graphic design and social science literature as a step toward producing more effective and accessible PI visualizations. We designed these templates to facilitate consistent messaging between NWS offices and to reduce the time required to develop PI visualizations. Reducing time investments could allow forecasters to focus time on creating multiple visualizations targeted at individual regions within their forecast area of responsibility. Many NWS forecast offices have found daily weather briefing packages effective tools for providing context about upcoming weather events to core partners (Carr et al., 2021). However, social media remains a common place for NWS offices to disseminate forecast information (National Weather Service, 2017). Carefully designed visual explanations will likely improve regional weather literacy among both core partners and the general public. This will help users leverage the power of probabilistic weather forecasts to improve decision-making (Fundel et al., 2019; Fleischhut et al., 2020).

Successful efforts to visualize probabilistic weather information have focused on the probability of precipitation (PoP) (Lowry and Glahn, 1976), hurricane forecasts (Broad et al., 2007; Rosen et al., 2021), and severe weather (Rothfusz et al., 2014). Currently, other efforts are being carried out across the NWS with the Central Region Probabilistic Messaging Testbed (Schumacher et al., 2021, 2022), High-Resolution Ensemble Forecast system (HREF) for thunderstorm guidance (Harrison et al., 2022), and probabilistic hazard information and decision support services for winter storms Novak et al. (2023); Tripp et al. (2023). Continued engagement and co-production are critical to improving the utility of PI tools through transparency and communication, which further develops trust between forecasters, core partners, and the general public (Pappenberger et al., 2012; Sivle et al., 2014; Fundel et al., 2019; Carr et al., 2021). However, it is important to reiterate that the numerous benefits associated with PI hinge on the visuals being well-designed (Franconeri et al., 2021; Padilla et al., 2021). Layout, color selection, font, and embellishments are more than a decorative choice with PI visualization as they impact the users' ability to efficiently and accurately extract information.

There are limitations associated with the use of PI that can be counterproductive, but

identifying these limitations can lead to solutions that can improve user understanding. Unfamiliar visualizations can cause deterministic construal error when users do not understand forecast information is probabilistic, so the visualization must expressly communicate that the information is probabilistic. (Grounds et al., 2017; Joslyn and LeClerc, 2013; Fleischhut et al., 2020; Joslyn and Savelli, 2021; Savelli and Joslyn, 2013). To reduce the chances of deterministic construal error, we attempt to cue the users to the presence of uncertain information by using words like "could", "chance", and "probability" as well as expressing the impact statement as "potential impacts". PI can also lead to biased or subjective decision-making (Wernstedt et al., 2018). However, bias in decision-making is hard to quantify as it relates to people's past experiences, predisposition to certainty, and avoiding loss (Grounds and Joslyn, 2018). Even when considering the limitations, probabilistic forecasts are generally considered to be better than deterministic forecasts because they provide a more accurate and realistic representation of uncertainty, and can help to reduce the risk of overconfidence and bias (Ripberger et al., 2022). Our work attempts to address these limitations by encouraging consistent messaging, transparency of information, and familiarity with PI.

In parallel with ongoing development of technical products (Schumacher et al., 2021; Harrison et al., 2022; Novak et al., 2023; Tripp et al., 2023), the communication and perception of these products by users should be systematically examined (Lambrecht et al., 2019; Dallo et al., 2020). While our visualization examples were developed collaboratively with NWS forecasters, further research should analyze the impact and perception of probabilistic visualizations more broadly with emergency managers and the general public across a diversity of environments, demographics, and hazards.

3.6 Summary

PI can improve credibility, understanding of the forecast, support decision-making, and help build trust by enabling targeted messaging and demonstrating a commitment to transparency by communicating forecast uncertainty (Morss et al., 2008; Joslyn and LeClerc,

2012; Grounds and Joslyn, 2018; National Weather Service, 2022; Ripberger et al., 2022). Our work leverages social science and graphic communication literature to develop a ready-to-use template (Heggli et al., 2023) aimed at improving the usability and comprehension of probabilistic forecast information. The templates provide a "plug-and-play" tool to develop PI visualizations to reduce the forecaster's time, increase consistency, and ensure design principles are followed when developing graphics. While these templates were designed with a focus on advancing the NWS with improved PI visualizations, the principles can be applied to other weather information graphic designs. The value of PI is not that it provides the decision. Rather, PI provides information useful for the binary decision-making process for user-specific thresholds (Pappenberger et al., 2012). PI can inform any weather-related decision, but single-value deterministic information with no expression of uncertainty leaves decision-makers less well-equipped to make the best possible decision(s). The continued integration and improved visual communication of PI into NWS forecasts will help NOAA reach its goal: to continuously transform weather, water, and climate information service delivery to better support evolving societal needs (National Oceanic and Atmospheric Administration, 2022).

Chapter 4

The Value of Sub-daily Observational Data: An approach to improve hourly SNOTEL data and the potential benefits

4.1 Introduction

The mountain snowpack serves as a natural reservoir for communities and industry across the western US. Knowing the volume of water in the mountain and being able to predict the timing of runoff in the western US has been the focus of snow hydrologists since the beginning of the 1900's (Church, 1933). In the early 1900's in the Lake Tahoe region, a conflict over the impact of forest thinning on the conservation of snow was amplified by flooding on Lake Tahoe, epitomizing the struggle of western water as either not having enough or having too much (Church, 1933). The Sierra Nevada became a laboratory to study the relationship between the snowpack and spring runoff, which of course required data to be collected. Through the invention of the Mt. Rose sampler, the first snow surveys were performed in Nevada's Carson Range 1909 by Dr. James E. Church. Through collaboration with Dr. Horace P. Boardman they established a method to identify the relationship between the snow water equivalent (SWE) and the spring stream flow. The observations proved to be so valuable that collaborative snow survey programs started across the Western US. By the 1930's the value of the monthly snow surveys for water

supply forecasting was clear and the cooperation of the states had grown through the success of the Western Interstate Snow Survey Conference, now known as the Western Snow Conference. In 1935, the US Department of Agriculture (USDA) assumed the responsibility to coordinate the snow survey and water supply forecasting programs in every Western US state except for California (which is state-run). By the 1960's, the pursuit of more SWE data led to the development of the snow pillow. The automation of SWE measurements gave the USDA a way to obtain the data collected during the monthly snow survey program multiple times a day. Throughout the 1970's and 1980's, the USDA installed over half of the existing SNOw TELemetry (SNOTEL) network which deployed precipitation gauges, air temperature sensors, and snow pillows as a means to improve the forecast of seasonal water supply from the snow-covered mountain systems. Now the USDA Natural Resource Conservation Service (NRCS) has installed a total of 895 SNOTEL stations (NRCS, 2023).

The daily SNOTEL data product is one of the most reliable observational data sets used to calibrate snow models, verify atmospheric models, and is a key component of efforts to forecast water supply for the Western US. Though the SNOTEL network was initially designed for seasonal water supply forecasting, the high-quality daily data has opened up opportunities for the research community to improve our collective understanding of the valuable snow-covered mountain systems in the western US. Beyond the immediate operational benefit, daily SNOTEL data has been used for research to evaluate remote sensing products and ground truth spatially distributed snowpack models (Fleming et al., 2023).

In the late 1990's the time and technology had advanced enough to further enhance the SNOTEL network and the 5 daily observations increased to 24 hourly data points. Again in the mid-2000s, the network was upgraded to include snow depth, soil moisture, and soil temperature in addition to SWE, precipitation, and air temperature. For over 15 years, approximately half of the SNOTEL period of record, hourly data has been collected but it is not subject to the same rigorous quality control procedures as the high-confidence daily data product. To maximize the investment made by the NRCS, this work focuses on a semi-automated approach to improve the quality of hourly data as another step to advance the SNOTEL monitoring applications.

This paper provides a semi-automated QA/QC workflow for hourly SWE, snow depth, and precipitation SNOTEL data. The proposed QC procedure consists of four levels:

Level 0 (L0): Remove the midnight stamp daily edit

Level 1 (L1): Range and rate of change check

Level 2 (L2): Dynamic smoothing

Level 3 (L3): Human expert judgment (Heggli et al., 2022; Kondragunta and Shrestha, 2006; Oakley et al., 2018)

We also published the Level 0, Level 1, and Level 2 data products for every SNOTEL station in California and Nevada in addition to Level 3 hand-cleaned products for three stations: Central Sierra Snow Lab (SNOTEL #428), Blue Lakes (SNOTEL #356), and Spratt Creek (SNOTEL #778) (Heggli, 2023). To demonstrate the added value of sub-daily data compared to daily data, we provide a set of examples demonstrating what can be learned about rain-on-snow events and diurnal snowmelt using this data.

4.2 Study Area

The automated portion of the methods (Level 0 through Level 2) was performed on 81 SNOTEL stations in California and Nevada spanning a total elevation range of 1,649 meters (1575 to 3224 meters above sea level). At these stations, peak SWE ranges from 124 mm (4.9 in) in northwesternmost portion of Nevada to 3001 mm (122.1 in) at Leavitt Lake in the central Sierra Nevada in California (NRCS, 2023). ReferencesappendixA provides climographs for the SNOTEL stations selected for the study as a reference for the regional climatology spanning WY1992–2022.

4.3 Data and Instrumentation

Hourly and daily SNOTEL data were extracted from the NRCS report generator using the Download_SNOTEL.py script for SWE, snow depth, precipitation, air temperature, soil

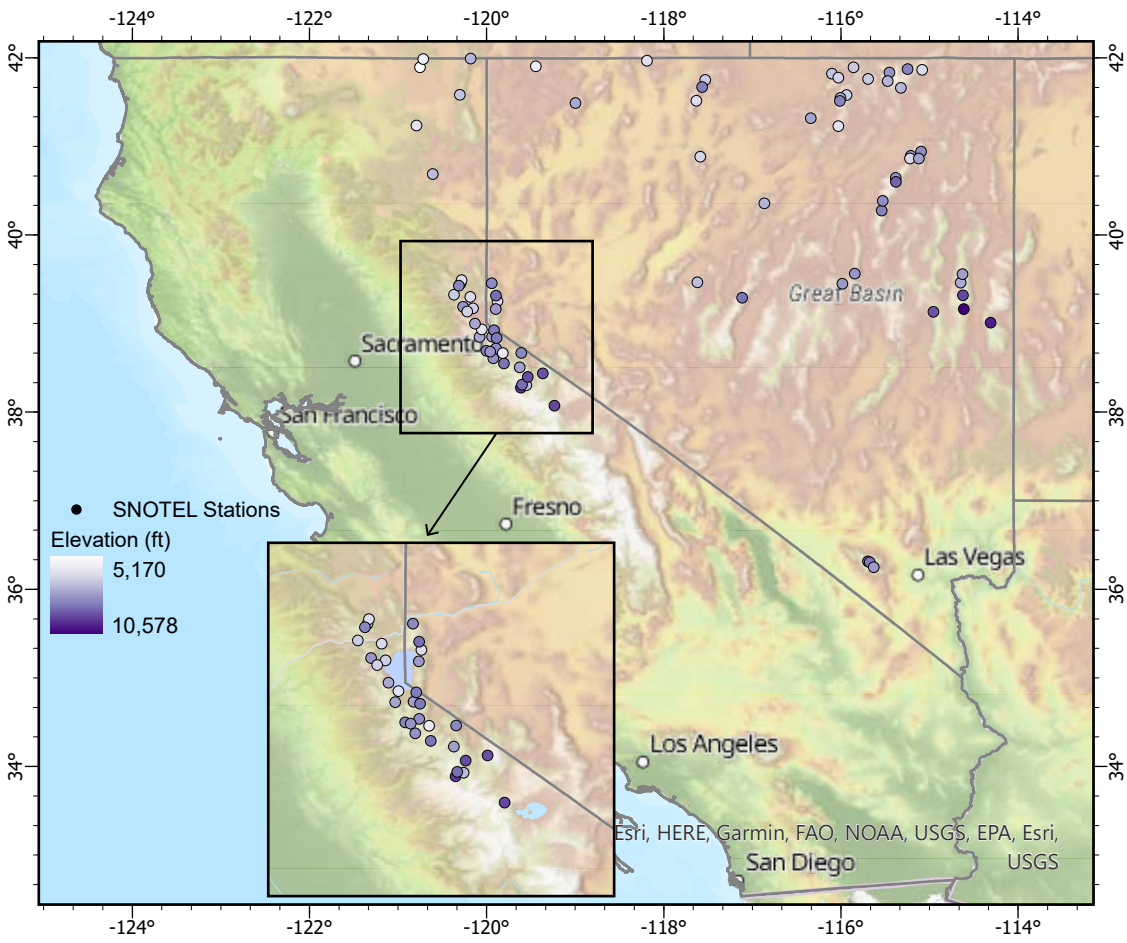

Figure 4.1: Map of the SNOTEL stations processed with the automated QA/QC methods.

moisture, and snow depth for water years (WY) 2006 through 2022. A full report of the SNOTEL data parameters and quality control methods can be found in Chapter 2 of Part 622 Snow Survey and Water Supply Forecasting National Engineering Handbook (NRCS, 2014).

An important aspect of quality control procedures is understanding the limitations and functionality of the sensor. No sensor works indefinitely without error, especially in harsh mountain environments subject to meters of snow, water, wind, intense radiation, and widely ranging temperatures. The following sections are intended to provide the reader with a basic understanding of the instrumentation used to collect data and the limitations of each.

4.3.0.1 Snow Water Equivalent

Every SNOTEL station is instrumented with a snow pillow. In California and Nevada, the snow pillows are made from hypalon or polypropylene with a 3.05 m (10 ft) diameter or an array of four 1.2 m x 1.5 m (4 ft x 5 ft) bladders made from stainless steel. The snow pillow is filled with a non-toxic antifreeze solution and plumbed into a pressure transducer. As snow accumulates on the bladder, pressure is applied and the pressure transducer is used to equate the weight of the snow to the height of the snow to SWE. However, it is essential to remember that snow pillows only measure the applied weight; complex snowpack structures including crust layers and changes in applied weight caused by snow creep and thermal differences at the snow-sensor-soil interface can cause over and under-reading (Serreze et al., 1999; Johnson and Schaefer, 2002; Johnson, 2004; Johnson and Marks, 2004; Julander, 2007). Snow pillow data errors include over- and under-reading, diurnal flutter (temperature-impacted increases and decreases on a diurnal cycle), and steady decreases to zero due to bladder leaks. Some over- and under-reading of data happens when a snow bridge forms. A snow bridge occurs when weather conditions cause the formation of a solid crust layer or ice lens, which acts to impede the even distribution of weight onto the snow pillow. However, bridging of the pillow does not necessarily present itself as a plateau in the data and can cause erratic fluctuations in the SWE data (example provided in Section 4.6).

4.3.0.2 Precipitation

The SNOTEL automated all-season storage gauge records the volume of water via a pressure transducer that measures the change in hydrostatic pressure in the column of the collector. The gauge has a 730 cm^2 orifice and has an Alter shield. The height of the orifice varies so that it does not get buried by snow in the deepest snowpack years. During snowfall events, snow can collect on the inside of the standpipe causing a "plug" in the gauge (McGurk, 1986; Goodison et al., 1998). This plug inhibits the recording of any snowfall until the snow plug is released by melting from warmer temperatures, solar radiation, or rainfall.

The precipitation gauges are also subject to diurnal flutter. Temperature swings can

cause the fluid and the SNOTEL gauge itself to expand and contract, resulting in a change in hydro-static pressure applied to the pressure transducer that can produce negative precipitation values that interfere with data analysis (NRCS, 2014).

4.3.0.3 Snow Depth

SNOTEL stations utilize an ultrasonic snow depth sensor, which is an acoustic sensor that emit a sound wave and measures the travel time with an integrated retry algorithm as an attempt to minimize the data issues during precipitation events (Anderson and Wirt, 2008). When heavy precipitation prevents a sensor from making a measurement, the sensor retries 10 times before outputting a full-scale value. Snowpack observations with ultrasonic sensors suffer from two main issues: (1) diurnal flutter due to the difference of the air temperature at the sensor and throughout the column of air to the snow surface and (2) inaccurate readings during precipitation events from the reflection from falling hydrometeors rather than the snowpack surface (Hauptmann et al., 2002). However, once the snow accumulation season starts and between snow storms, the ultrasonic snow depth sensors reliably obtain high quality measurements when properly maintained (NRCS, 2014).

4.3.0.4 Air Temperature

The SNOTEL network upgraded the temperature sensors across the network in the 1990's with the YSI extended range temperature sensor. A bias was documented by Brown et al. (2019) and since then the NRCS has refined the bias correction algorithm (Joel Atwood et al., 2023). The most up-to-date information can be found through the following link: `https://nrcs.usda.gov/resources/guides-and-instructions/air-temperature-bias-correction`. The air temperature data has been corrected with the NOAA9 CONUS equation. Upon reviewing the data, we determined that no further quality control procedures were required.

4.3.0.5 Soil Moisture

The NRCS monitors soil moisture and temperature at 5, 20, and 50 cm depths with a Steven's HydroProbe. Soil moisture data for this period of study was independently quality controlled at the hourly time-step by the NRCS (Sutcliffe and Clayton, 2021). Therefore, soil moisture data did not require additional quality control procedures or editing for this study.

4.4 Quality Assurance (QA) and Quality Control (QC) Methods

There is a trade-off between time invested and the accuracy of data when cleaning data. Overly automating the QC process could compromise data accuracy to a degree where the data is no longer reliable or representative of hydrometeorological processes. On the other hand, spending human time reviewing each data point by hand makes the tasks too time-consuming (and ultimately too expensive) to overcome.

The intention of our semi-automated QA/QC process is to find an optimum balance between automation and human review. Our methods leverage automated routines for predictable data errors and reserve valuable and limited time for human review to perform the necessary analysis to develop a high-confidence hourly data set. When applying quality control methods to improve the quality of data for multipurpose use, it is important to "do no harm" (Sutcliffe and Clayton, 2021). If the data cannot be reliably corrected with a high degree of confidence then the data should not be edited and marked as suspect. These methods are designed to improve the quality of hourly SNOTEL data while flagging data that could not be confidently corrected. The proposed QC procedure for SWE, precipitation, and snow depth consists of four levels: Level 0: removing the midnight stamp daily edit; Level 1: range and rate of change check; Level 2: an inter-sensor comparison and dynamic smoothing; and Level 3: human expert judgment (Kondragunta and Shrestha, 2006; Oakley et al., 2018; Heggli et al., 2022; Koskinas et al., 2023).

The NRCS QA and QC flagging system was adapted for the development of these

methods (Table 4.1). QA flags designate the level of review that the data has passed following the level of QC: L0 for Level 0, L1, for Level 1, L2 for Level 2, L3P for provisional Level 3 data, and L3 once finalized to be archived. QC flags denote the measures taken to improve the quality of the data. Three of the NRCS QC flags were applied to these methods: Valid (V) for data that has not required any changes, Edited (E) for data that was edited, and Suspect (S) for data that does not pass QC checks.

Quality Assurance (QA) Flags		
L0	Raw	Downloaded and midnight stamps removed
L1	Level 1 QC	Range and Rate of Change Check
L2	Level 2 QC	Range and Rate of Change Check
L3P	Level 3 QC Provisional	Preliminary Human Review
L3	Final Data Product	Processing and Final Review Completed
Quality Control (QC) Flags		
Flag	Name	Description
V	Valid	Valid observed value
E	Edit	Edit existing value
S	Suspect	Suspect value

Table 4.1: QA/QC flagging system adapted from NRCS Snow Survey and Water Supply Forecasting National Engineering Handbook.

Data were corrected with a semi-automated approach developed by A. Heggli (Python code available from `https://zenodo.org/record/7820055`) to limit subjective editing and encourage a more repeatable workflow that directs the data reviewer to the sensor or time periods that require human review. Level 0, Level 1, and Level 2 data for all SNOTEL stations in California and Nevada in addition to Level 3 data for CSSL, Blue Lakes, and Spratt Creek can be found in the same Zenodo repository (Heggli, 2023). These methods are a revised and extended version of the methods published by Heggli et al. (2022).

4.4.1 Level 0

After data is downloaded, it is first run through a Level 0 process (SNOTEL_L0.py) that removes the midnight stamp edits as daily data edits are made on the midnight stamp of hourly data. The data value is then replaced with an interpolated value only if there is data the hour before and after the midnight stamp, otherwise, it remains null. The QC flag is

not changed but the QA flag is set to "L0" to indicate that it has passed Level 0.

4.4.2 Level 1: Range and Rate of Change Check

Level 1 is a first-order process to improve hourly SNOTEL data by using range and rate of change checks to eliminate major data errors like spikes and flag data that deviate from the daily data. The Level 1 automated QA/QC process (SNOTEL_L1.py) performs a range check based on the period of record values extracted from the NRCS (NRCS, 2023) and rate of change checks using hourly thresholds in Table 4.2. Negative values are replaced with a zero and flagged as edited (E) and values that exceed the thresholds are set to null and flagged as suspect (S) to be reviewed against the original data and edited as necessary in subsequent processing. We also apply linear interpolation with a 24-hour limit to fill in short-term data gaps. This is intended to fill in data spikes, but this is most valuable for ultrasonic snow depth sensors, which have an inherent limitation in collecting data during snowfall as discussed in Section 4.3.0.3. At this stage (L1), all data is assumed to have been edited and then null values are set to suspect (S). Additional QC is performed on the data by comparing it to a linear interpolation of the high-quality daily data with tolerance variables that flag data outside an acceptable degree of variability from the daily data. This range for filtering suspect data can be modified based on the data question to capture more data or lower it to capture observed hourly data that is within a tighter range of agreement. In our data set SWE and precipitation must be within ± 25.4 mm (1") and snow depth must be within ± 15.24 cm (6") of the linear interpolation of daily data (Table 4.2). This does not edit the data, but flags it as a way to quickly identify potentially problematic data that will require further review. The QA Flag is set to "L1" to indicate that the data has passed the Level 1 QC process.

4.4.3 Level 2: Dynamic Smoothing

The level 2 automated process (SNOTEL_L2.py) is the novel approach to correcting hourly SNOTEL data. In the pursuit of improving the majority of data, Level 2 applies methods that may sacrifice some valid observed values by altering them minimally with the

Parameter	Tolerance	Level 1		Level 2	
		Min Rate	Max Rate	Min Rate	Max Rate
SWE	25.4 mm	25.4 mm/hr-	25.4 mm/he	-10.0 mm/hr	25.4 mm/hr
Snow Depth	15.2 cm	-20.0 cm/hr	20.0 cm/hr	-10.0 cm/hr	10.0 cm/hr
Precipitation	25.4 mm	-5 mm/hr	25.4 mm/hr	0 mm/hr	25.4 mm/hr

Table 4.2: User defined tolerance for deviation of automated QC from the linear interpolation of daily data and minimum and maximum rate of change thresholds for Level 1 and Level 2 QC for SWE, snow depth, and precipitation.

application of rolling medians. However, the improvement of erroneous data outweighs the minimal changes of observed data. We use the high-quality SNOTEL daily data in the Level 2 QC process, which is subject to rigorous quality control procedures outlined in detail in the National Engineering Handbook Part 622: Snow Survey and Water Supply Forecasting (NRCS, 2014). In addition to the daily NRCS data product, we perform an intersensor comparison to correct predictable data issues like diurnal flutter. By automating predictable data errors, we are able to reserve human time to focus on anomalous data. These methods implement either 6-hr, 12-hr or 24-hr rolling median that were applied dynamically to the data based on the values of other parameters. When and how the dynamic smoothing was applied varies since each sensor experiences unique limitations (see Section 4.3). In the following sections, we explain the specific Level 2 QC method for each parameter.

4.4.3.1 SWE and Snow Depth

First, a 6-hr and a 24-hr rolling median guides are created. Level 2 is set to the 6-hr rolling median as this was beneficial for smoothing slight noise in the SWE and snow depth data though it did mute snow depth peaks that need to be retained during Level 3 QC. We found it beneficial to apply the 24-hr rolling median if the 24-hr change in SWE or snow depth was negative and when the daily maximum air temperature was above 7 °C as both of these typically caused diurnal flutter. In order to differentiate snowmelt from ROS-induced decreases in SWE, we only applied the 24-hour rolling median to decreases in SWE when the maximum air temperature was above 7 °C. If the daily data product equals zero, then the hourly data will also read zero.

For the QC flag, all data is considered edited and the flag is set to "E". Any null values are flagged as suspect along with any data that is outside of the rate of change and tolerance thresholds listed in Table 4.2. The QA Flag is set to "L2" to indicate Level 2 automated QC. Upon exporting the Level 2 data, the observations are compared to the original Level 0 data. If the value matches, then the Level 0 QC flag is applied to retain any QC flag adjustments made by NRCS staff. A Level2.csv is output with QA and QC flags for each data point. A second .csv is output (Level2_QC.csv) that includes the hourly change in SWE and snow depth for each guide with the addition of a 12-hr rolling median guide for snow depth to be used for the iterative Level 3 QC process discussed further in Section 4.5.

4.4.3.2 Precipitation

The formation of unpredictable snow plugs complicates the QC as some snow plugs can persist for weeks or even months and miss numerous events that cannot be corrected with snow pillow data alone. The inherent limitations of the precipitation gauge result in a Level 2 precipitation product that is not as reliable as it is for SWE and snow depth. The intention of the Level 2 QC for precipitation is to improve individual events and flag suspect data to inform users of issues in the record that require human review prior to use.

To address the impact of temperature that can even cause event data to have errors, we start by applying a 12-hr rolling median to all data. Diurnal flutter in precipitation data can cause artificial data swings of 5-40 mm in a single day, so we then use the same methods as SWE and snow depth by applying the 24-hr rolling median if the 24-hr change in SWE or snow depth is negative or if the daily maximum air temperature is above 7 °C. If the daily data is zero, then the Level 2 data is also set to zero. The accumulated data is then treated as hourly incremental data. The following methods are not conclusively the best, but they were the approach that appeared to improve the quality of data across multiple stations and water years. We then look at daily changes in precipitation over a 3-day (72-hr) period and if there has been no change, all hourly data is set to 0 mm/hr. The 3-day threshold was beneficial because it identified breaks between systems and not just breaks between a series of storms that were part of the same system.

Any hourly decreases of at least -5 mm/hr and increases over 150 mm/hr were also set to 0. Removing decreases below 0 was too strict as the diurnal flutter is a decrease followed by an increase (or vice versa) and removing the decreases without addressing the increases caused accumulated precipitation values to deviate too far from the daily data record. It also created problems for the Level 3 QC process where it is best to identify the decrease and use those to remove that and the nearby artificial increase. Removing data increases greater than 150 mm/hr eliminated the majority of spikes that occurred during summer maintenance but did not eliminate snow plug releases. Through the development of the Level 2 QC, we established that it was better to keep the snow plug releases and use the QC flagging system to identify anomalous increases in precipitation that are typically associated with snow plugs as a means to highlight these events for quicker identification during Level 3.

Finally, we performed a cumulative sum of the precipitation and once more set any negative values to zero. The QC flag methods are the same as SWE and snow depth. All data is considered edited and the QC flag is set to "E". Any null values are flagged as suspect along with any data that is outside of the rate of change and tolerance thresholds listed in Table 4.2. Then the data is compared to the Level 0 data and any matching values retain the Level 0 QC flag. The QA Flag is set to "L2" to indicate Level 2 automated QC. Finally, the hourly change in precipitation for each guide is calculated for Level 3 QC discussed further in 4.5.

4.5 Level 3 Human Review

This section describes the methods for the manual QC and specific examples of the application of these methods are provided in Section4.6. Preliminary data was manually reviewed using SNOTEL_L3.py, which provides interactive visualization to aid in the manual editing of .xlsx (Excel) files that retain references to other cells or calculations but also saved as a .csv format file. This code utilizes the Level2 QC data frame that has all of the previously generated columns including the rolling median guides. An additional "_L3" column with

QA and QC flag columns is created which is filled with the Level 2 data to be edited as necessary.

Each parameter has unique data anomalies as a result of the sensor limitation or the environment it is measuring in, so it is important to QC one parameter at a time. We chose to process one water year at a time in order to build in breaks in the workflow. We found it helpful not only to work through the water years one by one but also to quickly make additional adjustments at a later point in time if an error was overlooked during the initial Level 3 review. When addressing each parameter, SWE must be done before precipitation because SWE data is used to fill missing data after a snow plug forms. During Level 2, the formation of snow plugs, decreases in precipitation, or deviation from the daily SNOTEL product is flagged as suspect. Each of the suspect data points must be manually reviewed and corrected. The rolling medians are designed to be used as guides to clean diurnal flutter or apply more robust smoothing to data for designated periods of time. However, smoothing data with rolling medians can mute real peaks and delay the signal response. Therefore event peaks were manually retained and the rolling median calculations were applied so the automated guide was centered on the observation and closed right (the first point in the window is excluded from calculations) thereby reducing the delay in response. This is a trade-off for absolute accuracy in order to save time, but the slight delay is considered negligible for the hourly data.

When reviewing the data, it is important to look at the behavior of other sensors and consider the environmental conditions. Take for example a decrease in SWE, which indicates that snow is melting, sublimating, or draining transiently stored water after a rain-on-snow event. If the snowpack is melting on a dry day, then daily temperatures should be above freezing with a temperature increase indicative of a full sunny day, snow depth will also likely be also decreasing, soil moisture could be increasing due to water input from the snowpack, and no precipitation should be occurring. If temperatures are well below zero, sublimation and/or wind transport may be the cause of SWE decreases. For a decrease in SWE during a precipitation event, there should be precipitation occurring at temperatures above 0 °C (indicating rain-on-snow), a decrease in snow depth, and soil moisture will likely

increase. However, in both cases of melting snow, soil moisture responses may be muted or non-existent if lateral flow is occurring, if dry soils are draining water at the same rate as water is input, or if saturated soils are producing overland flow.

Bridging of the snow pillow was identified through inter-sensor comparison of precipitation and temperature data. Rain-on-snow as well as warm and sunny days with below-freezing temperatures during the night or following the passage of a cold front often cause the formation of a crust layer prior to the erratic data from the pillow. Erratic data that indicated the formation of a bridge was flagged as suspect. Soil moisture was used also used to validate suspect SWE data. Specific examples of data anomalies caused by rain-on-snow or the onset of the ablation period are provided in Section 4.6.

We identified the release of snow plugs when there was an abnormal increase in the hourly precipitation data. These rates likely vary based on location, but for the SNOTEL stations in our study, we found precipitation rates greater than 10 mm/hr, were most often associated with snow plug releases during mid-winter. Therefore, we chose to review hourly precipitation above 10 mm/hr to validate the precipitation event or correct for a snow plug. After snow plug releases were identified, hourly SWE data were used to identify the initiation of the event. Since snow pillows can provide accurate surrogates of precipitation data during snowfall, hourly increases of SWE were added to the precipitation values until the snow plug released and precipitation measurements resumed accurately from the SNOTEL station. It is important to note that the catch efficiency of the snow pillow with a much larger surface area is different from the smaller catch of the precipitation gauge and a coefficient should be applied to correct for this. These relationships are understood by NRCS staff who QC the daily data. We found and applied a coefficient that would correct the SWE data to match the daily precipitation data.

If data quality could not be verified, the data was flagged as suspect. Once all parameters had gone through full preliminary review, the QA flags were changed to L3P (provisional). The QA flag can be updated to L3 once the reviewer is confident that the data has attained the highest accuracy possible.

4.6 Results

Each level of QC improves the quality of the hourly data. A review of each level of QC compared to the Level 3 data for each parameter at each station for each water year is provided in ReferencesappendixB. The automated flagging in Level 1 and Level 2 is designed to draw attention to data that needs to be reviewed. Figure 4.2 illustrates the automated Level 2 flagging in the top panels for SWE (A), snow depth (B), and precipitation (C) as compared to the Level 3 result in the lower panel. We discuss each of these examples and how the data was corrected next.

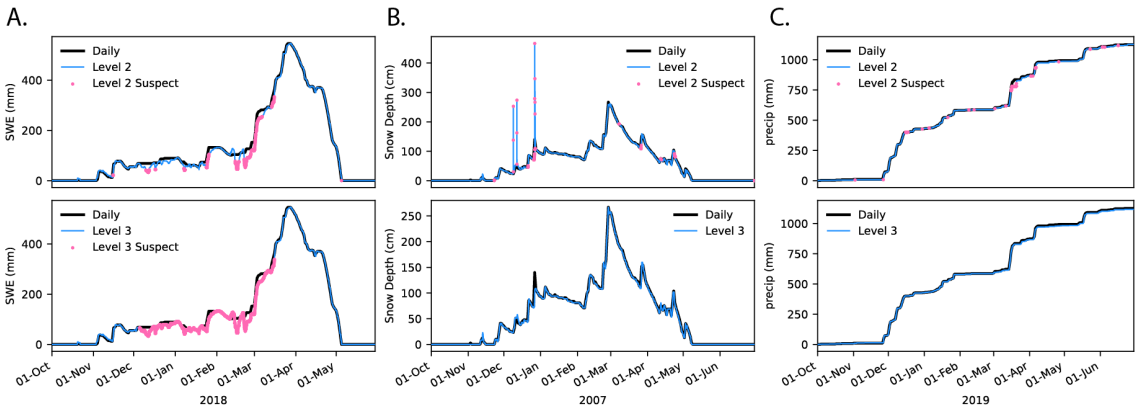

Figure 4.2: Comparison of daily data (black line) to automated QC output data (blue) with level 2 data (top panel) and Level 3 data (bottom panel) highlighting data automatically flagged as suspect (pink dots) for SWE (A), snow depth (B), and precipitation (C).

The erratic behavior of the SWE data triggered the code to flag numerous data points between December and April WY2018 (Figure 4.2.A). Upon further review of the days leading to this erratic behavior, there is evidence of the formation of a bridge or crust layer. Figure 4.3 illustrates the weather prior to the onset of the erratic data. There was a week of warm days that did not drop below freezing followed by a cold front where the daytime high did not exceed freezing. The series of warm days allowing surface melt followed by the freeze can cause a bridge to form. Following the cold snap, a snowfall event occurred and the pillow is not able to register the change in the snowpack weight. Though the pillow eventually does start to regain some of the load of the snowpack, it does not fully receive the entire weight of the snowpack until a rainfall event and warmer days help to break up

the bridge.

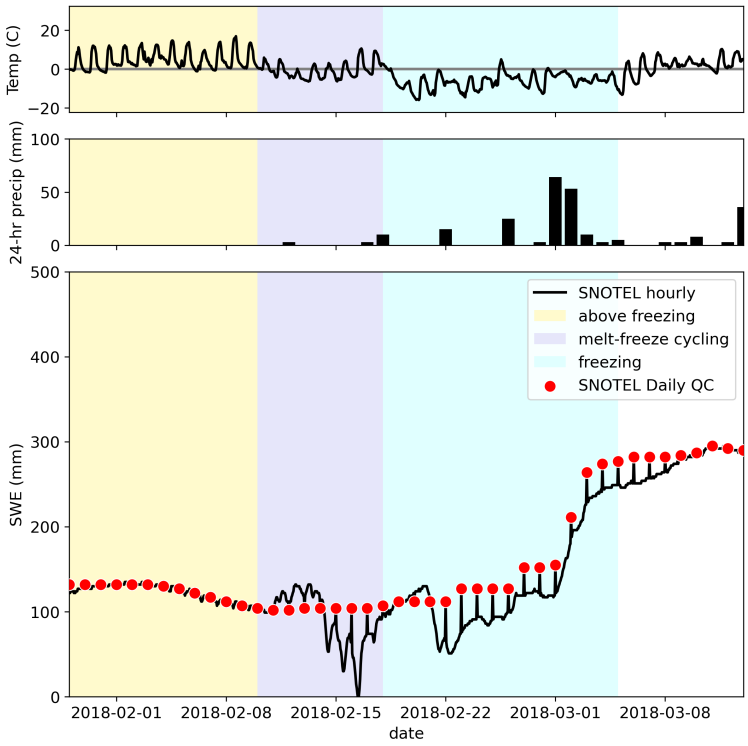

Figure 4.3: An example of bridging over a snow pillow. An extended period of above-freezing days (yellow) followed by melt-freeze cycles (purple) and sub-freezing temperatures (blue) can cause the formation of complex crust layers that inhibit the transfer of weight to the pillow. The erratic readings from the pillow occur during the melt-freeze cycle and persist through persistent sub-freezing. There is no significant precipitation to justify the change in SWE and therefore this data should be classified as poor quality. Related to STAR Methods

The manual review of snow depth data is relatively straightforward though it heavily relies on the rolling medians. Figure 4.4 provides an example of how the rolling median was dynamically applied. After the full-scale measurements that are produced when a valid measurement cannot be made are removed in Level 1 and dynamic smoothing is applied during Level 2, the human reviewer will compare the automated data product to the raw hourly data, rolling median guides, and daily data product. A different reference guide can be selected if more robust smoothing is necessary to reduce the diurnal changes in the data. During snowfall events, the raw hourly data can be retained to capture the most representative increases and the absolute peak snow depth.

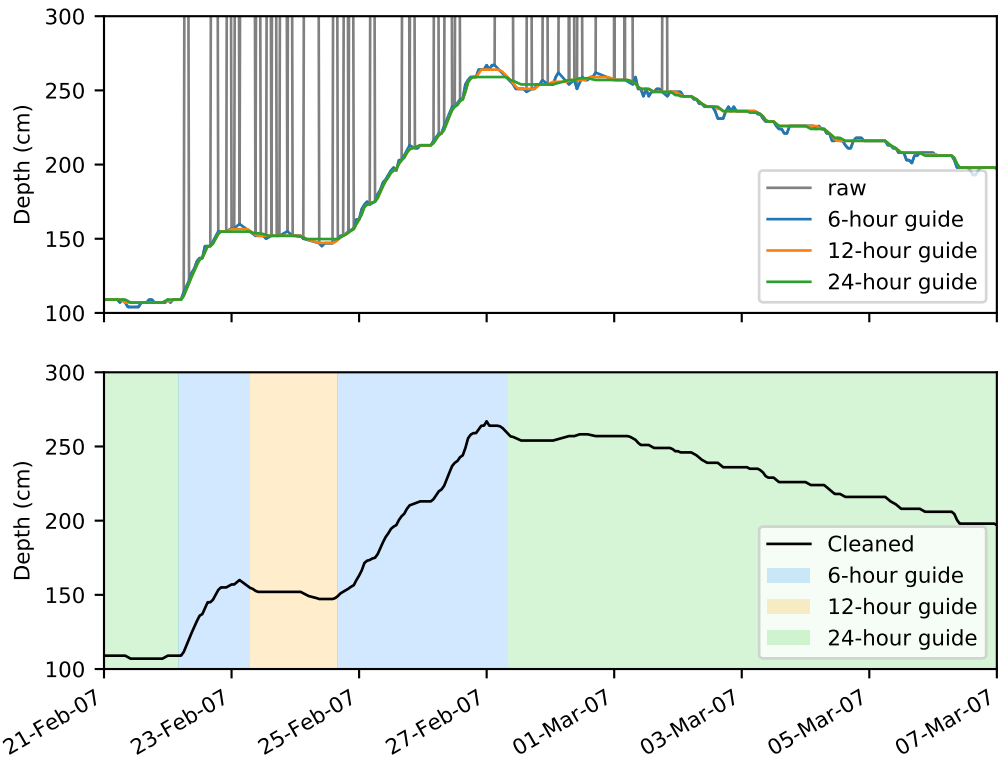

Figure 4.4: An example of semi-automated cleaning process and results. Raw data represented with grey shows the full-scale readings that occur during snowfall events. The 6-hr guide (blue) removes full-scale readings but experiences diurnal flutter, the 12-hr guide (orange) and the 24-hr guide help reduce diurnal flutter or other sensor noise.

Snow plugs should be automatically flagged as a result of the Level 2 QC. However, all precipitation rates greater than 10 mm/hr should be reviewed for evidence of snow plug release. When the hourly precipitation data deviates from the daily SNOTEL data, it can indicate the formation of a snow plug. This can be verified by looking for increases in SWE and snow depth. Once the precipitation begins to flatline, SWE data from the snow pillow can be used to fill the snow plug. Figure 4.5 provides an example of the February 2019 ROS event that occurred between two snowfall events Hatchett et al. (2020). Each snowfall event caused the precipitation gauge to plug, The first plug was released by the

rainfall while the second plug took longer to release. Replacing the precipitation data with SWE data allows the precipitation data to be recuperated and this is verified by the daily SNOTEL data. However, a coefficient typically must be applied to the SWE data to account for the difference in catch efficiency between the 7.5 sq m snow pillow and 30 cm diameter precipitation gauge. It is best to check with your local NRCS Data Collection Office or use the daily data to identify the coefficient for the specific station.

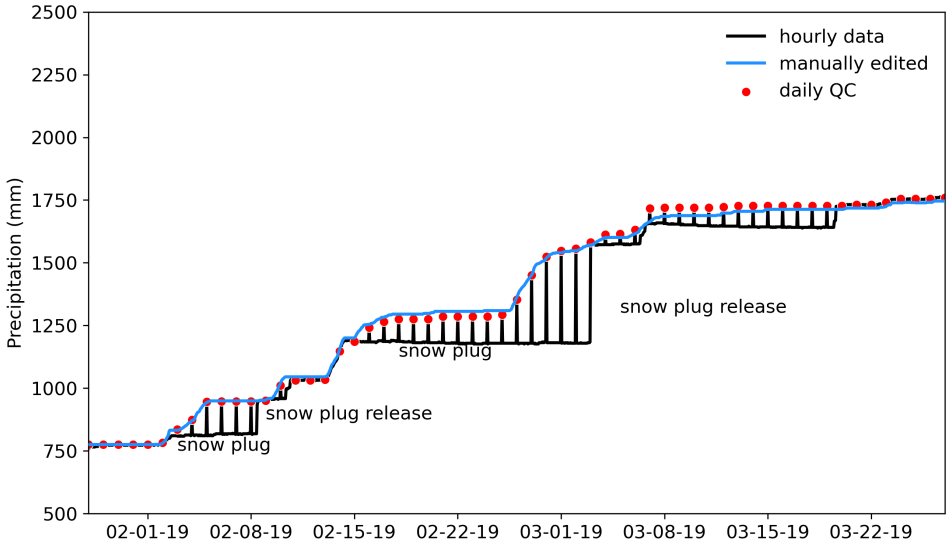

Figure 4.5: Example of cleaned precipitation data product after snow plug formation. SNOTEL hourly data (black), reviewed SNOTEL daily data (red), and cleaned hourly data using the methods outlined in the paper (blue).

There are two other anomalies with SWE data that are important to discuss. First, ROS events can cause a specific signature in snow pillow data. There are varying hypotheses as to why this signature occurs (Brandt et al., 2022b). It may simply be the transient storage and subsequent drainage of rainwater in the snowpack, excavation of snow from the snow pillow surface causing a temporary decrease in the applied weight of the snowpack until it is able to resettle after the event, or standing water impacting the applied weight through buoyancy. Regardless, it is important to retain this data as it is evidence of a significant ROS event. For example, between February 12-15, 2019 an exceptionally strong atmospheric river made landfall in California (Hatchett et al., 2020) and impacted the CSSL (Figure 4.6b). Abrupt increases in soil moisture validate the SWE data, which responded to the ROS event by

increasing 140 mm before decreases in SWE were observed. The snowpack began to release water approximately four hours after the precipitation occurred with temperatures above 0 °C but 11 hours before the decline in SWE. Another anomaly is a jump in SWE during the onset of the ablation period. These increases also correspond with an increase in soil moisture as the snowpack transitions from the midwinter accumulation and ripening period to the ablation period (Figure 4.6c). This data is not representative of the snowpack and should be edited.

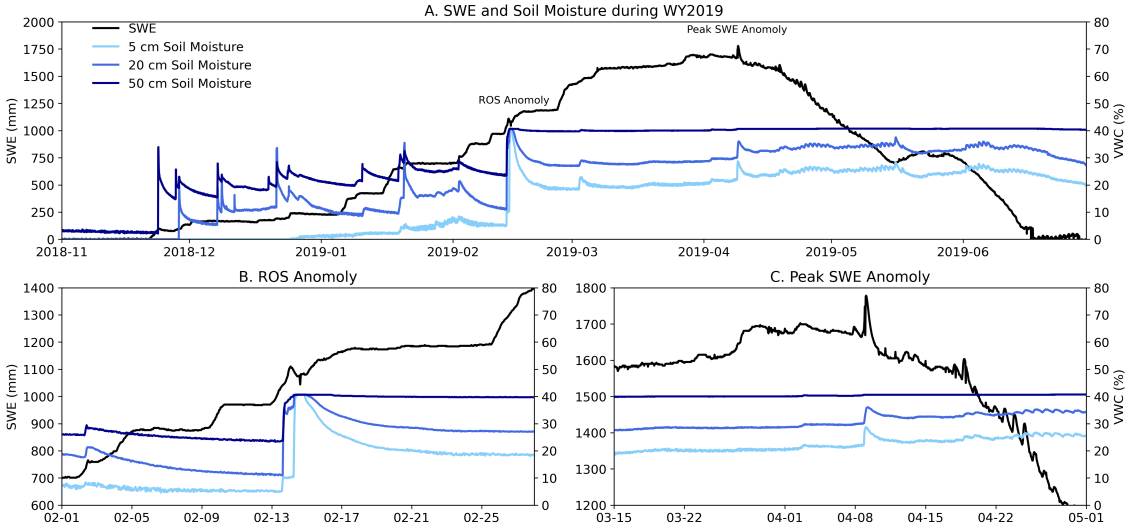

Figure 4.6: An example of SWE data anomalies and the value of soil moisture data for intersensor comparison. (A) SWE data (black) compared with soil moisture at 5 cm (blue), 20 cm (orange), and 50 cm (green). (B) Rapid increase and decrease of SWE during a rainfall event is validated by a rapid increase in soil moisture. (B) A jump in SWE observations corresponds with an increase in soil moisture.

4.7 Discussion

This first step towards improving the hourly SNOTEL data is more than simply methods to edit data. The application of these methods essentially creates a new data set opening up new applications in traditionally under-observed mountain regions. Daily SNOTEL data has been a bridge between operations and research. Increasing the reliability and usability of hourly data can provide insights into sub-daily snowpack processes at a larger scale due to the size of the SNOTEL network. In this section, we will discuss a few first-order findings

and applications for hourly SNOTEL data.

Figure 4.7 illustrates hourly changes in SWE (A), snow depth (B), and precipitation (C) for CSSL (1), Blue Lakes (2), and Spratt Creek (3). While admittedly simplistic, it has not yet been possible to explore sub-daily trends in the intensity and duration of precipitation, snow accumulation, or snow melt across the SNOTEL network. Both CSSL and Blue Lakes had decreases in SWE greater than 10mm/hr. CSSL only had three decreases in SWE greater than 10 mm/hr, all associated with the February 2017 ROS event. This is likely not a result of the snowpack melting, but the drainage of transiently stored rainwater. Blue Lakes, on the other hand, had 21 decreases in SWE with 16 hours of true snowmelt occurring on the days surrounding the summer solstice in water years 2011, 2017, and 2019. These three years were large snowpack years, meaning that there was still snow during the summer solstice when the duration of solar radiation is the greatest. The CSSL only had snow during the summer solstice in 2011 where maximum snowmelt rates were 8 mm/hr.

Beyond identifying the trends in hourly data for a single parameter, the SNOTEL data offers a unique opportunity to look at the intersection of parameters, which gives a more comprehensive understanding of what the weather and snowpack did hour by hour. For example, we can look at changes in the snowpack density (a function of SWE and snow depth) during precipitation events as a starting block to identify the precipitation phase. When precipitation falls between 0 °C and 3 °C, there is no way to know with certainty if the precipitation fell as rain, snow, or a mixed phase with direct observations (Jennings et al., 2023; Dai, 2008). However, changes in the snowpack density can help reduce the uncertainty since a decrease in density is typically caused by snowfall while an increase in density is typically caused by rain or higher-density mixed-phase precipitation. This is not always the case since ROS events can result in a decrease in density as transiently stored water can take several hours to drain from the snowpack. To verify if the decrease in density is caused by ROS, soil moisture data can be analyzed to see if there is evidence of the snowpack releasing water into the soil in well-draining soils that are not saturated.

Hourly soil moisture data can improve our understanding of how the snowpack responds to ROS events as illustrated in Chapter 2. CSSL, Blue Lakes, and Spratt Creek have well-

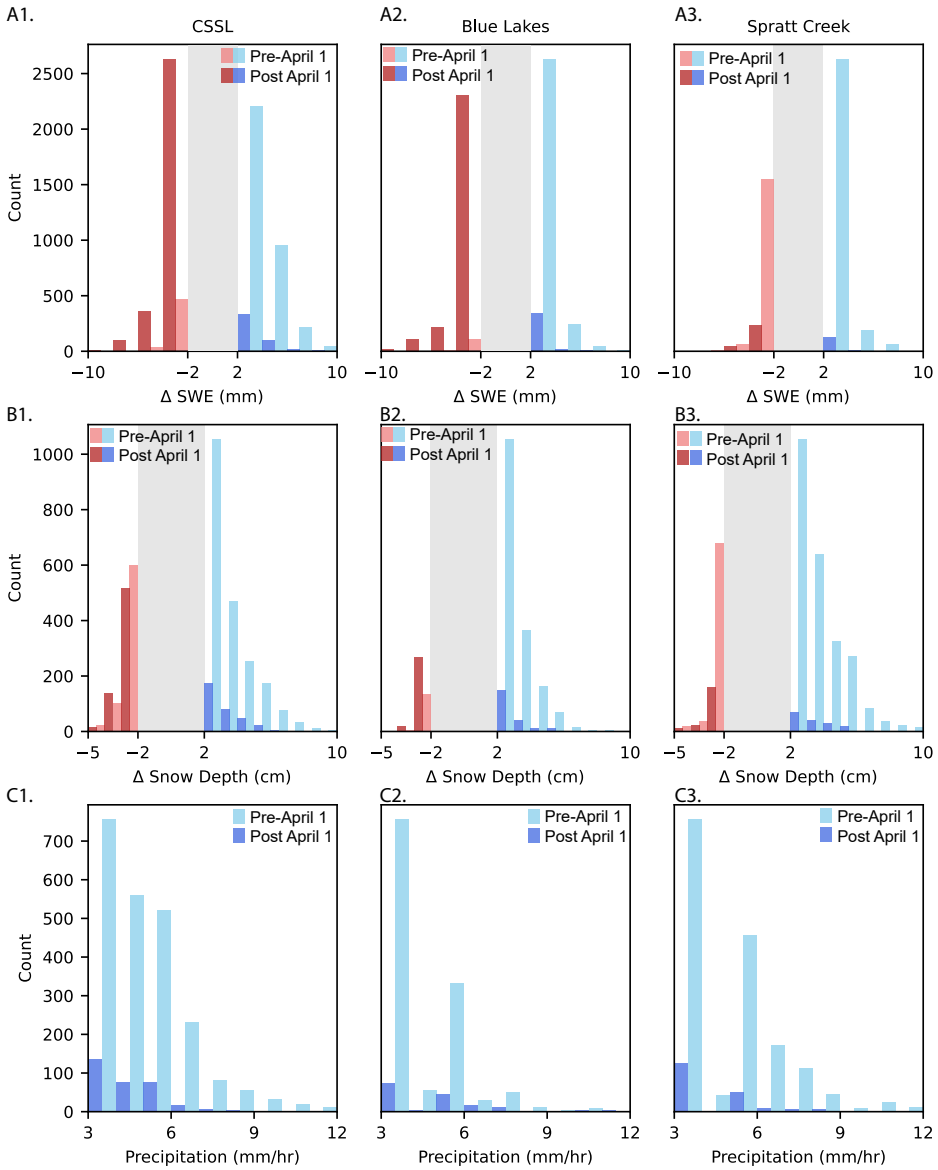

Figure 4.7: Hourly changes in SWE (A), snow depth (B), and precipitation (C) for CSSL (1), Blue Lakes (2), and Spratt Creek (3). Pre-April 1 decreases in light red and increases in light blue. Post April-1 decreases in red and increases in blue. The grey center bar represents the most common increases and decreases that were not included in this illustration.

draining soil, so it is possible to identify the initiation and duration of TWI. Using the methods established in (Heggli et al., 2022), we developed a TWI algorithm for Blue Lakes and Spratt Creek and classified the TWI as either deriving from ROS or warm day melt and discarded any changes that could not be verified as deriving from rain or a warm sunny day. In total, Blue Lakes experienced 665 hours of TWI with 43% from ROS while CSSL had 721

hours of TWI with 63% from ROS and Spratt Creek had 809 hours of TWI with 70% from ROS. We also found that warm day melt TWI typically occurs for 2-5 hours starting in the late afternoon. ROS TWI can occur for consecutive days as it did at the CSSL January 7–9, 2017 (Heggli et al., 2022). Looking at TWI initiation is not only helpful to understand how the snowpack responds to rainfall, but it also can be useful to understand the hydrologic impact of ROS events across a watershed, which will be discussed further in Chapter 4.

4.8 Summary

Across the Western US, there are at least 16 years (and counting) of hourly data have been collected but not yet used at the scale of SNOTEL daily data. Such high-quality operational networks can serve as the bridge between operations and research, providing researchers with an abundant dataset to explore or use to validate models from a network designed for operational decision-making. The presented quality control methods are intended to be a step towards increasing the usability and confidence of SNOTEL hourly data to push the understanding of watersheds across from looking at changes day-by-day to hour-by-hour. We can only learn so much from daily data and this is especially true for ROS or exceptional snowmelt events, which have secondary impacts on debris flows (Oakley et al., 2023), avalanches Hatchett et al. (2017b), and flooding (McCabe et al., 2007). While these methods can and should be improved upon, the Level 2 data product with automated flagging of suspect data can open the door for sub-daily data exploration. As more data is manually reviewed, more analysis can be done across the Western US.

Chapter 5

The Application of Snowpack Runoff Decision Support in the Upper Carson Watershed

5.1 Introduction

This chapter integrates the conceptual snowpack runoff decision support system (SR-DSS) developed in Chapter 2 with the quality-controlled data set from Chapter 4 and applies the guiding principles for visual communication of probabilistic hazard information identified in Chapter 3. The principal objective of this chapter is to test whether the approach developed in Chapter 2 can be applied at a basin scale in order to provide valuable and timely information to decision-makers like the Nevada Department of Transportation about potential road impacts as well as water managers to optimize water supply and emergency managers to mitigate flood risk at various local, state, and federal agencies. Typically, these agencies rely on information from the National Weather Service (NWS). Across the United States, the NWS works as a "force multiplier" by connecting hydrometeorological observations to forecasts and warnings to decision-making through providing Impact-Based Decision Support System (IDSS) information to decision-makers in their communities (Uccellini and Ten Hoeve, 2019). However, there is currently no tool available to communicate the potential for mid-winter snowpack runoff at an event scale.

There is an outstanding need to communicate real-time changes in the snowpack during rain-on-snow (ROS) events across the Western U.S. (McCabe et al., 2007). To meet this

need, we have developed a framework for SR-DSS, which is currently designed to provide situational awareness to communicate real-time changes in the snowpack at hourly timescales. Eventually, this tool will be expanded to integrate probabilistic forecast information to increase the lead time for decision-making during cascading hazards such as flooding (Oakley et al., 2023).

Designing an end-to-end operational solution requires forethought regarding spatial and temporal constraints. Effective decision support systems must be able to reliably ingest data and provide output at time scales relevant to decision-making (Uccellini and Ten Hoeve, 2019). Therefore, the Natural Resource Conservation Service (NRCS) SNOw TELemetry (SNOTEL) network, which collects and transmits data hourly from high-elevation stations across the West, is a useful tool to observe event-based snowpack changes. Moreover, the SNOTEL data is already integrated into the NWS operations.

In this chapter we calibrate the SR-DSS thresholds for terrestrial water input (TWI) by incorporating data from water year (WY) 2006–2022 at the Central Sierra Snow Laboratory (CSSL) and two stations in the Upper Carson watershed (Blue Lakes and Spratt Creek) with Level 3 data. We then apply the SR-DSS to two case studies on data that was not included in the training process using only the Level 2 product developed in Chapter 4 Section 4.4.3 to assess the feasibility and reliability of the SR-DSS in an operational setting. By identifying TWI drivers and antecedent conditions leading to the greatest hydrometeorological impacts at the sub-basin scale (8-digit Hydrologic Unit Code), this chapter focuses on furthering the development of a quasi-deterministic SR-DSS. The aim of SR-DSS is to improve forecast confidence at longer lead times to help protect life and property while also optimizing increasingly scarce water resources (Hatchett et al., 2020; Uccellini and Ten Hoeve, 2019).

5.2 Study Area

The regional study in this paper focuses on the Carson River watershed, which has two main forks feeding the Carson River and runs a total of 296 km (USGS, 2022). The East Fork (119 km) begins on the northern slopes of Sonora Peak at an elevation of 3,200 m

while the West Fork (64 km) begins near Lost Lakes at 2,700 m. Both forks flow from California eastward and join near Genoa, Nevada before flowing through Carson City, NV to the Carson Sink at an elevation of approximately 1,180 m.

This paper will focus on the Upper Carson sub-basin within the Carson River watershed, which is 2,482 km^2 and has 12 SNTOEL stations that are representative of the watershed. Six of those are within the watershed boundaries. There are four USGS streamgages in the Upper Carson that serve as CNRFC hydrologic forecast points (Figure 5.1). The Upper Carson reached flood stage at all streamgages during 1997, 2005, and 2017 rain-on-snow events. The 1997 event was the record flood event for all three locations, with $55 million in projected damages in Douglas County (Thomas and Williams, 1997) and over $450 million (unadjusted) in damages across Nevada (USACE, 2013).

5.3 Methods

5.3.1 Data Availability

SNOTEL data was downloaded and processed using methods outlined in Chapter 4. Hourly streamflow data was also downloaded from the USGS Water Data Dashboard (`dashboard.waterdata.usgs`) for gaging stations 10311000 (Carson City, NV), 10309000 (Gardnerville, NV), 10308200 (Markleeville, NV), and 10310000 (Woodfords, NV) for WY2006–202. Monitor and flood levels were extracted from the CNRFC graphical river forecast page for each of the forecast points (`https://www.cnrfc.noaa.gov/`).

5.3.2 Calibration of TWI Potential Thresholds by Station

The methods applied to this paper build off of the methods developed by Heggli et al. (2022) and continue the focus on mid-winter TWI before the ablation period begins though several additions were made. First, we updated the results from Chapter 2 by including data through WY2022 for CSSL. Second, we calibrated the TWI identification algorithm for Blue Lakes and Spratt Creek. Third, after TWI was identified, we filtered the data for periods when there was more than 100 mm of SWE as was done in Chapter 2. The

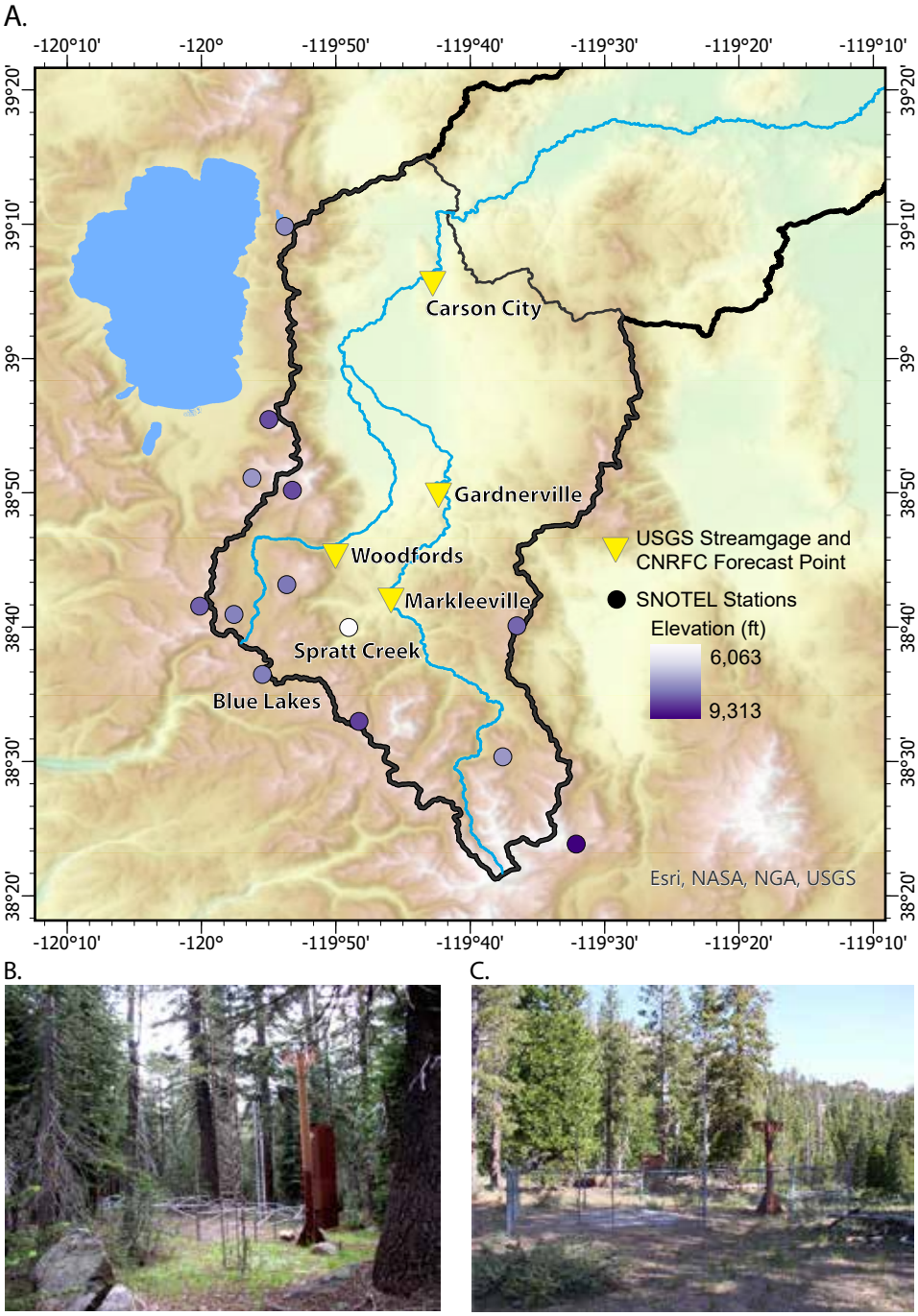

Figure 5.1: (A) Map of the Upper Carson sub-basin (thin black line) within the Carson watershed (thick black line) with SNOTEL stations (circle) color-coded by elevation and USGS gaging stations and CNRFC forecast points are marked in a yellow upside-down triangle. (B) Photo of the Blue Lakes SNOTEL station. (C) Photo of the Spratt Creek SNOTEL station.

100 mm SWE threshold applied to Spratt Creek eliminated entire water years of data as some years SWE never exceeded 100 mm at the lower elevation station, so we adjusted the threshold to examine TWI data when there was at least 50 mm of SWE. The classification for TWI type as ROS or warm/sunny day melt (W/SDM) was done manually to assure the highest quality of data is being applied. The Heggli et al. (2022) methods were simplified to only differentiate ROS and W/SDM and do not include the ROS + SWE loss. This simplification was necessary due to the limited number of observations for ROS and SWE loss at Blue Lakes and at Spratt Creek, which would not provide reliable statistics.

In addition to snowpack density 1 hour prior to TWI, 6 hour maximum air temperature, and 6 hour precipitation totals, we also included snowpack density 6 hour prior to TWI, 12 hour maximum air temperature, and 12 hour precipitation totals. These extended times account for the siting of the Blue Lakes station which is located within the forest canopy unlike Sprat Creek (Figure 5.1) or CSSL (Figure 2.2). Just above the Blue Lakes station is a south-facing slope and there were numerous times when the 20 cm soil moisture sensor registered an increase likely due to snowmelt on the south-facing aspect upslope from the station. It was important to capture the parameters that caused any increase in TWI at the stations, so the time period was increased from 6 to 12 hours to allow for sufficient travel time.

In order to identify the patterns of present weather and antecedent snowpack conditions with the potential to produce TWI mid-winter, we analyzed violin plots for density 1 and 6 hours prior to TWI, 6 hour and 12 hour maximum air temperature, and 6 and 12 hour precipitation totals for ROS and W/SDM. Following the methods in Heggli et al. (2022), we use the first quartile values as a more conservative threshold for TWI potential.

5.3.3 Visual Communication

Decision support tools benefit from, if not require, effective visual communication that capitalizes on the efficiency of the visual system to extract information and should make the effort to ensure accessibility to individuals with color vision deficiencies and neurodivergent characteristics (Chapter 3). Although the SR-DSS is not developed sufficiently to establish

the layout and content that will be provided in the tool, we can integrate color-blind safe color pallets that do not conflict with existing color scales that communicate hazard or impact (Gordon et al., 2022; National Weather Service Western Regional Headquarters, 2022) and sans-serif fonts like Helvetica and Arial that are not only effective for warning messages but also found to perform better than serif (embellished fonts) for all populations including individuals with dyslexia (Bernard et al., 2001; Chaparro et al., 2010; Rello and Baeza-Yates, 2013; Koskinas et al., 2023). We selected Arial for the visuals included in this chapter. Following the work of Crameri et al. (2020) regarding the use (and misuse) of colors in science communication, we selected two colors from the batlow color pallet that vary in lightness to communicate confidence in the potential for TWI Chapter 3 (Section 3.3.4).

5.4 Results and Discussion

5.4.1 TWI Potential Thresholds by Station

We examine the distribution of snowpack density 1 and 6 hours prior to TWI, 6 and 12 hour maximum air temperature, and 6 and 12 hour precipitation totals during ROS TWI and W/SDM TWI expanding the dataset for CSSL from Chapter 2 and including Level 3 data for Blue Lakes and Spratt Creek from Chapter 4 (Figure 5.2).

The differences between snowpack density 1 hour and 6 hours prior to TWI are minimal for each TWI threshold. However, the snowpack density threshold for ROS TWI at Blue Lakes is almost 5% higher than Spratt Creek and CSSL and more than 8% higher for W/SDM. The ROS snowpack density threshold provides evidence for the formation of preferential flow paths as a uniform wetting front would require the snowpack to evenly absorb all of the rainwater prior to releasing TWI. The lower elevation stations typically have a lower snowpack density during ROS TWI compared to the higher elevation Blue Lakes station. While one might initially think that the higher elevation station has deeper snow, and therefore will need to have a greater density for the water to make its way through the snowpack, Blue Lakes does not typically have a deeper snowpack than CSSL. In fact

the biggest snow years in the period of study (WY2011, WY2017, and WY2019) CSSL had a larger snowpack throughout the entire winter than Blue Lakes. A more plausible explanation of the increased snowpack density could be because precipitation more often falls close to 0 °C at the higher elevation Blue Lakes, and therefore the preferential flow path formation will progress more slowly than in a warmer snowpack, thereby increasing the bulk density of the snowpack (McGurk et al., 1988). While Blue Lakes W/SDM density threshold is more consistent with a "ripe" snowpack that has become isothermal with near 40% density values (Kattelmann and Dozier, 1999), CSSL and Spratt Creek also give evidence for the movement of snowmelt water through preferential flow paths. This is inferred from the observation that the first-quartile observed density values are 31.4% and 28.2% accordingly. Even the median values of 36.0% and 35.3% are below density values considered to be necessary for the initiation of daily snowmelt. This could be because the snowpack is not homogeneous and density values at the base of the snowpack may have satisfied the requirements to transmit water while surface densities remained slightly lower (Kattelmann and Dozier, 1999). While further analysis is needed, this data signals that the snowpack does not need to reach 40-50 % bulk densities in order to transmit snowmelt to the land surface and thus contribute to flooding.

The first-quartile 12 hour maximum air temperature thresholds for ROS TWI are consistent with the 6 hour thresholds, especially at Blue Lakes and CSSL. Between each station, the 6 and 12 hour maximum temperature thresholds for ROS TWI potential for each station follow a moist adiabatic lapse rate of 3.7 °C/km with a 2.3 °C difference for the 611 m of elevation difference between Blue Lakes and Spratt Creek. Whenever it is raining at Blue Lakes, the rainfall occurring at the lower elevation stations of CSSL and Spratt Creek will always be higher due to the moist adiabatic lapse rate. However, the observations at Blue Lakes show that even when the air temperature is 0.4 °C, there is the potential for ROS TWI. For W/SDM TWI potential the 12 hour maximum temperature threshold at Spratt Creek is 0.8 °C higher than the 6 hour threshold where Blue Lakes and CSSL are only 0.1 °C higher. The higher 12 hour maximum air temperature threshold could be influenced by non-precipitation temperatures, especially on the lee side of the mountain. However,

W/SDM 12 hour maximum air temperature threshold increased by 4.6 °C at Blue Lakes compared to the 6 hour maximum air temperature threshold. The increased time from 6 hours to 12 hours at Blue Lakes allows for the necessary lag time for the peak solar radiation, here identified using a temperature as a proxy (Painter et al., 2012), to melt the snow on the south-facing slope above the SNOTEL station and move through the soils to the soil moisture sensors.

The 6 hour precipitation thresholds for ROS TWI are relatively consistent across all stations at 4.5 mm, 5.0 mm, and 3.9 mm for Blue Lakes, CSSL, and Spratt Creek accordingly. The 12 hour precipitation thresholds are also consistent, though Spratt Creek requires less precipitation to produce TWI, which may be a reflection of the smaller snowpack at the lower elevation station. The violin plots in Figure 5.2 shows a higher snowpack density of ROS TWI around the first-quartile value, supporting the selection of first-quartile values for precipitation as an appropriate threshold. The consistency of the values across all stations and the high density of ROS TWI observations at this threshold increase the confidence that 3.9–5.0 mm of rain in six hours is sufficient to produce a soil moisture response.

5.4.2 Updated Thresholds for the SR-DSS

Figure 5.3 illustrates the distribution of present weather and antecedent snowpack conditions considered TWI potential for ROS and W/SDM for CSSL, Blue Lakes, and Spratt Creek for WY2006–2022. These values are consistent with the findings in Chapter 1 except that the W/SDM density values are higher (32.3% vs 27.6%). The increased snowpack density threshold is a result of the higher W/SDM densities at Blue Lakes, but also the addition of WY2020, WY2021, and WY2022 which all had extended mid-winter dry spells and mid-winter melt events prior to peak SWE (Hatchett et al., 2023). The W/SDM 6 hour maximum temperature is also substantially lower (3.3 °C vs 6.3°C) because of the location of the Blue Lakes station, which observes increased soil moisture due to the uphill south-facing slope exposed to increased solar radiation. A 12 hour maximum temperature threshold for W/SDM takes into account the added travel time for snowmelt to arrive at the soil moisture sensor at Blue Lakes. Therefore, the 12 hour maximum air temperature of 5.4

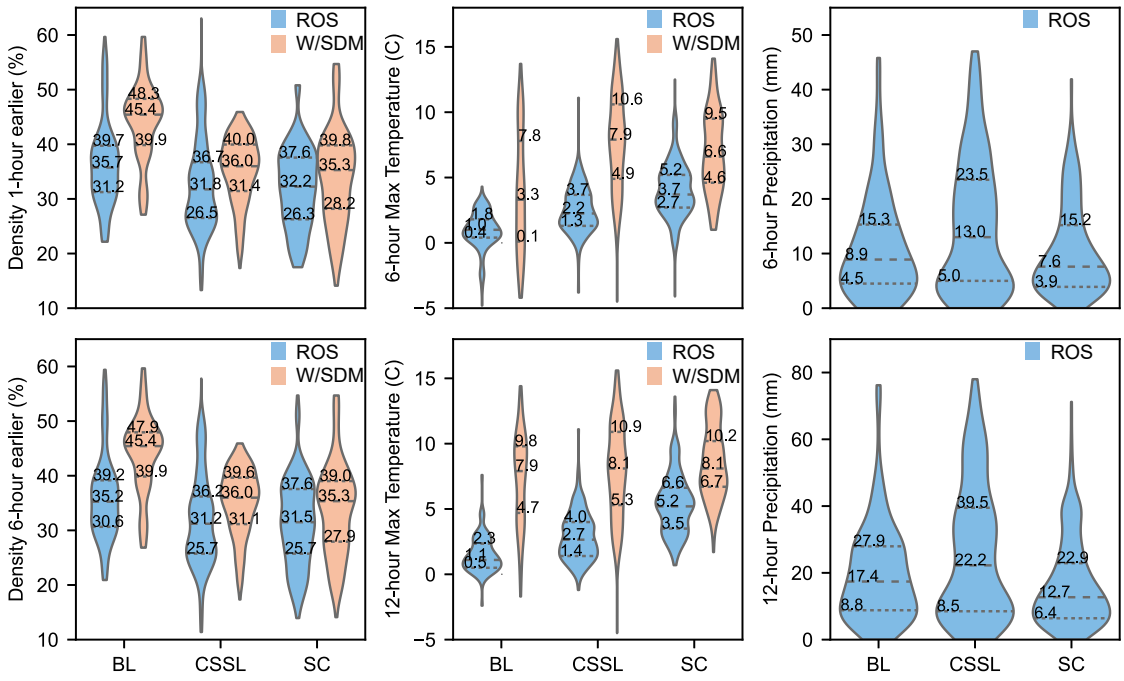

Figure 5.2: Violin plots of snowpack density 1 and 6 hours prior to TWI, 6 and 12 hour maximum air temperature, and 6 and 12 hour precipitation totals during ROS TWI (blue) and W/SDM TWI (orange) for Blue Lakes (BL), Central Sierra Snow Laboratory (CSSL), and Spratt Creek (SC).

°C for W/SDM was selected to be sure that any high temperatures and the necessary lag rates are accounted for. All other SR-DSS threshold parameters remain consistent with Chapter 1 but the following thresholds have been updated with the new data: density 1 hour prior for ROS (27.0%) and W/SDM (32.3%), 6 hour maximum temperature for ROS (1.3 °), and 6 hour precipitation totals for ROS (4.5 mm) and W/SDM (0 mm). Figure 5.4 provides a conceptual diagram and decision tree for ROS and W/SDM TWI potential with the addition of Low ROS and Low W/SDM thresholds. As a situational awareness tool, the SR-DSS is designed to indicate the potential for TWI ahead of initiation. ROS TWI could potentially occur when there is more than 0 mm of precipitation and air temperatures are above 0 °C, though this is a less-likely scenario based on historical data. Low W/SDM thresholds were set to the minimum snowpack density that W/SDM TWI occurred 14% and retained the 5.4 °C 6 hour maximum air temperature threshold.

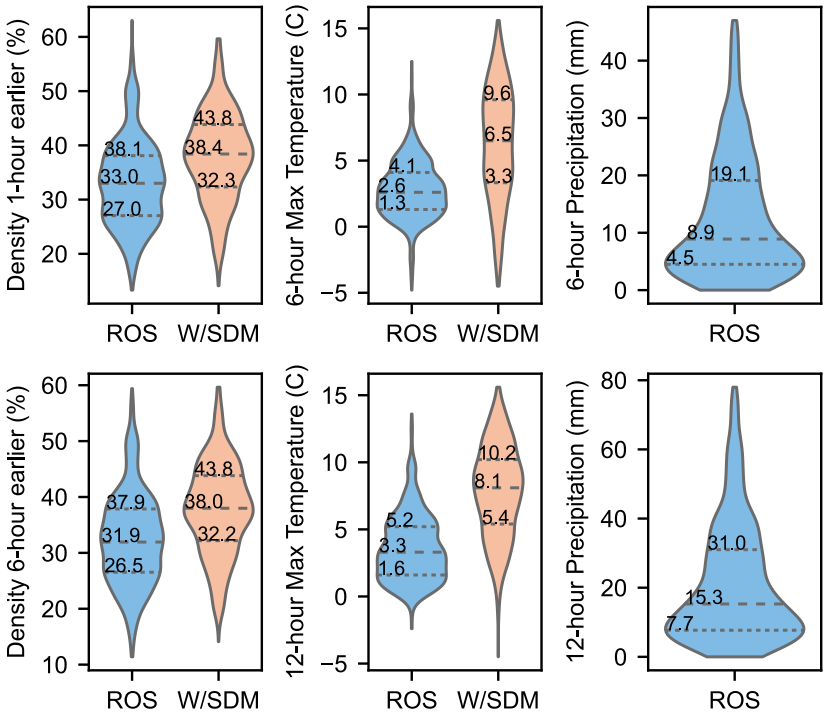

Figure 5.3: Violin plots of density 1 and 6 hours prior to TWI, 6 and 12 hour maximum air temperature, and 6 and 12 hour precipitation totals during ROS TWI (blue) and W/SDM TWI (orange) for combined observations at Blue Lakes, CSSL, and Spratt Creek.

5.4.3 Test Case Assessment of SR-DSS

The objective of SR-DSS is to run operationally in real-time. In order to assess the reliability of the tool in an operational environment, we apply only the automated QC methods from Section 4.4.3 and assess data from WY2023 that was not included in the development of the SR-DSS thresholds. In addition to the test case assessments, we applied the SR-DSS to seven events from WY2006–2022 in Appendix C.

The remaining portion of this section focuses on two ROS test cases in WY2023: 29 December 2022–1 January 2023 and 9–12 March 2023. To aid in the regional assessment of the SR-DSS, we developed a regional map that includes all of the SNOTEL stations in the Central Sierra Nevada and color code the TWI potential at each station using the updated SR-DSS thresholds with the Level 2 data. Blue Lakes and Spratt Creek are noted on the map and active TWI is indicated with a thick black outline of the SNOTEL station.

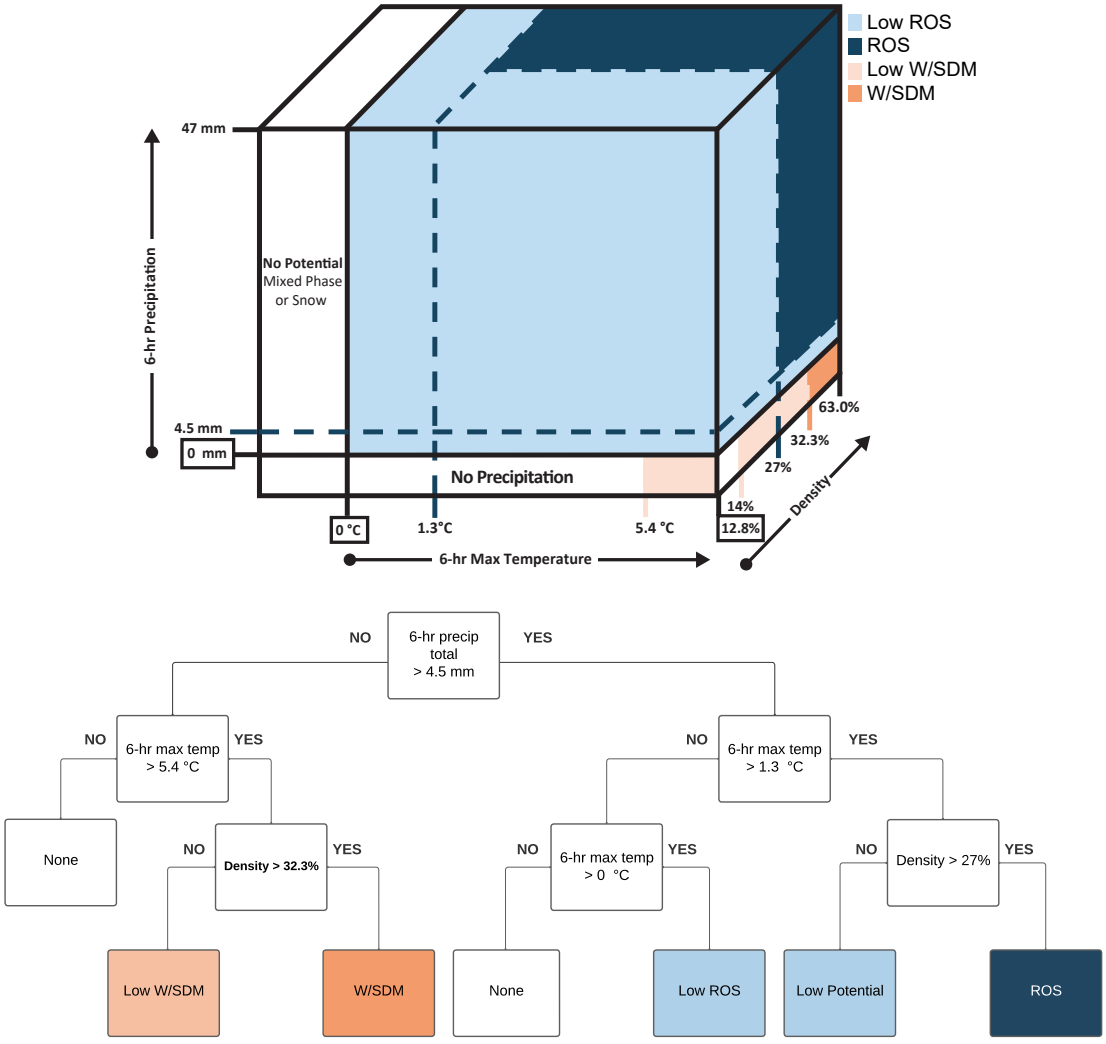

Figure 5.4: Snowpack runoff decision support conceptual framework developed through the application of first-quartile 6 hour precipitation, 6 hour maximum temperature, and snowpack density 1 hour earlier as indicators of low ROS (light blue), ROS (dark blue), low W/SDM (light orange), and W/SDM (orange) with associated decision tree.

The regional map also includes the four CNRFC forecast points that are color coded for monitor and flood stage. Each event will be discussed in detail in the following sections with figures that include three regional maps of TWI potential and streamflow response in the top panel (1A, B, and C) for selected times indicated with a pink vertical line in the lower panel (2A and B). The lower panel (2) shows the time series data from the Blue Lakes (2A) and Spratt Creek (2B) leading up to the streamflow response. The time series plots include 1 hour and 6 hour precipitation totals and 1 hour and 6 hour maximum air temperature in

the top panel. The second panel shows bulk snowpack density and SWE overlayed with the SR-DSS TWI potential is below that. The next panel shows soil moisture at 5 cm, 20 cm, and 50 cm depths with periods of active TWI highlighted in pink, and finally the maximum hourly stream flow at the four CNRFC forecast points in the Upper Carson River. This figure is provided for each test case and the events included in Appendix C.

5.4.3.1 29 December 2022–1 January 2023

From December 2022 and January 2023, the Sierra Nevada experienced nine back-to-back storms that predominately produced snowfall at the SNOTEL station elevations. Two of these events (29 December 2022 and 10 January 2023) were ROS events, but only the 29 December 2022 event resulted in flooding on the Carson River and will be the focus of the first test case (Figure 5.5). The snowpack at Blue Lakes (396 mm of SWE) and Spratt Creek (122 mm of SWE) was well above normal for the time of year. Ahead of this event, the depth-averaged soil moisture at Blue Lakes was below the period of record median and was about average at Spratt Creek. Prior to the ROS event, the region experienced anomalously high temperatures 24–26 December 2025 with maximum air temperatures at Blue Lakes ranging from 8.2–10.1 °C. A system moved into the region around midnight on December 26th that brought snowfall to Blue Lakes keeping the snowpack density relatively low at 29% and rain to Spratt Creek that increased the density to 33% (Figure 5.5.2A and B).

The air temperature at Blue Lakes was below freezing when the precipitation first started on 29 December 2023 but by 11:00 PST the following day the temperature threshold was met for Low ROS potential and at 17:00 PST the air temperature was 0.5 °C for the second consecutive hour and TWI had initiated at 20 cm and 50 cm depths (Figure 5.5.1B). The ROS TWI air temperature threshold was not met for another three hours. This is evidence that the air temperature threshold should be adjusted for elevation and the 0.4 °C 6 hour maximum threshold for Blue Lakes may be more effective at predicting ROS TWI (Figure 5.2). As the air temperature increased to meet the ROS TWI potential threshold, Blue Lakes continued to produce TWI until ROS TWI potential thresholds were no longer met and downgraded to low ROS TWI potential. At 10:00 PST on 31 December 2023 the

air temperature at Blue Lakes had dropped to 0 °C and TWI potential transitioned from low ROS to none after multiple hours of the air temperature being below the ROS TWI threshold (Figure 5.5.1C). TWI occurred for a total of 12 continuous hours at Blue Lakes though there is no evidence of snowmelt since SWE continuously increased throughout the storm.

On 30 December 2023 at 05:00 PST the ROS TWI thresholds were met at Spratt Creek and TWI initiated two hours later as SWE began to decline (Figure 5.5.1A). SWE continued to decline as soil moisture continued to register TWI until 10:00 on 31 December 2023 when air temperature dropped to 0.2 °C and SWE began to increase as density started to decrease indicating precipitation had transitioned from rain to snow. However, the 6 hour maximum air temperature threshold was still above 1.3 °C for another two hours before downgrading to Low ROS and then to no potential. TWI was active for a total of 20 hours at Spratt Creek and there is strong evidence of snow melt since the already dense snowpack lost SWE as soon as rain started. There is evidence that the rain was warm enough to melt the snowpack since the air temperature during precipitation on 30 December 2023 ranged from 3.6-6.8 °C.

Lower in the watershed, streamflow on the East Carson at Markleeville and Gardnerville began to slowly increase at the same time precipitation started at Spratt Creek. By the afternoon on 31 December 2022 the Garnerville station reached monitor stage and continued to steadily rise until hitting flood stage 5 hours later. The peak coincided with the drop in air temperature and the transition from rain to snow at both Blue Lakes and Spratt Creek around 10:00 on 31 December 2022 (Figure 5.5.1C). Despite Gardnerville reaching flood stage, Markleeville and Carson City were just shy of monitor stage.

5.4.3.2 9–12 March 2023

The 2023 winter resulted in a record-breaking snowpack at 19 of the 28 SNOTEL stations in the Central Sierra Nevada including Blue Lakes and Spratt Creek. By the beginning of March, Blue Lakes, had a record 1404 mm of SWE, which was 2.4 times larger than normal for the time of year. Spratt Creek had 574 mm of SWE, which not only was 6.7 times more

than normal for the time of year but exceeded the record peak SWE at the station. A series of storms moved through the region on March 4th and brought snow to Blue Lakes and Spratt Creek. A warmer system that moved into the region on 9 March 2023 raised snow levels to near 8000 feet (NWS, 2023). This warmer event brought a lot of media attention with concerns about collapsed roofs from added water to snow-covered roofs (Baker, 2023) and flooding in the region citing the potential for rapid snowmelt at low elevationsLeonard (2023). Our assessment of the SR-DSS covers this warmer event for March 9–12.

Precipitation began at Blue Lakes at 15:00 PST on 9 March 2023 (Figure 5.6.A2). The air temperature at Blue Lakes did not exceed 0 °C during the entire event, but snowpack density values continue to increase indicating that the precipitation might be mixed phase or at least a wet snow. By 12:00 PST on 10 March 2023, the precipitation measurements appear to end, but SWE continues to climb (Figure 59.1A). It is at this point that a snow plug formed that persisted until 9 April 2023. Since the precipitation observations were no longer reliable, SWE values could be used to assess accumulated precipitation. However, there is no TWI potential for the duration of the storm as the air temperature does not exceed the required thresholds. The soil moisture sensors also do not register any TWI which verifies that the SR-DSS accurately predicted the potential for TWI.

At the lower elevation Spratt Creek, precipitation started five hours before Blue Lakes and by 9 March 2023 at 16:00 PST the TWI potential increased from Low ROS to ROS at the same time SWE starts to increase (Figure 5.6.1A). However, soil moisture never responds throughout the entire event despite having registered TWI during the 29 December 2023 event. Upon reviewing data earlier in the winter, we find evidence for the potential formation of a crust layer or ice lens around 13 February 2023 after several days of warm temperatures reaching a maximum of 14.2 before a cold front brought a daytime high of -1.2 °C on 14 March 2023. After this point, the SWE data begins to show erratic behavior and starts to increase without any new precipitation. The hourly SWE data stabilized on 26 February 2023 when observations are back in line with the daily SNOTEL data. The formation of an ice lens can promote the lateral flow of water in the snowpack, routing water away from the array of soil moisture sensors. SWE and snowpack density continue

to increase, and SWE actually increased to 688 mm in the raw data, but the peak was slightly muted because of the 6 hour rolling median. The trade-off for automated QC is that some peaks may be lost, but unprocessed data could be available as a quick reference by decision-makers as is demonstrated in Figure 5.6.2B. Despite the shortcomings of the automated QC process and the soil moisture sensors are unable to register TWI, we can verify that the SR-DSS accurately predicts the potential for ROS TWI. The decrease in SWE occurring simultaneously with rainfall means that water had to move through the snowpack. The water would have moved laterally until a weakness in the snowpack layers would allow rainwater to begin to move vertically down the snowpack and eventually reach the soil or a stream (Marsh and Woo, 1984a; Eiriksson et al., 2013). The potential for ROS TWI continued for the remainder of the event as precipitation continued to fall at lower intensities but above the Low ROS and ROS air temperature threshold. However, there is no clear evidence of snowmelt in this event as in there was in the 29–31 December 2022 event (Figure 5.5). There was 604 mm of SWE prior to the event and after the rainwater had drained from the snowpack, there was 609 mm of SWE. These findings agree with Chapter 2 that snowmelt is not a primary source of runoff during ROS events in deep snow (SWE >100 mm) despite maximum air temperatures during rainfall reaching 5.7 °C.

Despite the media's concern for flooding caused by rapid snowmelt, there was no flooding at Gardnerville or Markleeville. Carson City did hit monitor stage on 11 March 2023 as water moved through the watershed and rainfall continued intermittently after the main wave of the storm had passed. The air temperature was also warm and overnight lows at Spratt Creek did not drop below 0 °C until 15 March 2023. It is possible that the combination of the ROS event followed by above-freezing temperatures and intermittent rain at lower elevations helped to increase flows at Carson City to reach monitor stage. However, the high-elevation Blue Lakes station was not producing TWI as it did not receive any rain as it did during the 29 December 2023 event. If the near 0 °C temperatures were just 0.5 °C warmer, there is evidence based on past ROS events at Blue Lakes that the precipitation would have fallen as rain and TWI would have occurred. The 9–12 March 2023 event highlights the importance of accurately forecasting the snow level, and the SR-

DSS can provide real-time validation of the snow level forecast.

5.4.3.3 SR-DSS Assessment

To assess the reliability of the SR-DSS for real-time communication, these two case studies demonstrate that the automated Level 2 data can perform sufficiently for this event. However, neither precipitation event experienced a snow plug. January 4th the Blue Lakes precipitation gauge did plug and inhibited the gauge to record new precipitation for 16 days. One advantage of using the Level 2 data for ROS events is that most major sensor issues occur during snowfall. Snow depth sensors struggle to measure during heavy snowfall (Anderson and Wirt, 2008), snow plugs only occur with snow or mixed-phase precipitation that sticks and accumulates to the side of the precipitation gauge, and bridging of the snow pillow will not register new snowfall. If a snow plug has not released prior to a ROS event, sufficient rain can release the snow plug and regain accurate and timely precipitation observations (Chapter 4 Figure 4.5). Complex structures like melt-freeze crusts that cause bridging over a snow pillow can also be released by rainfall (Chapter 4 Figure 4.3). Because the Level 2 QC integrates automated flagging of suspect data, the formation of snow plugs and bridges can be tracked to notify potential data users that the data may not be reliable.

For the purpose of testing the reliability of Level 2 data to establish SR-DSS thresholds, we performed the pattern recognition on Level 2 data for CSSL, Blue Lakes, and Spratt Creek (Figure 5.7). The Level 2 derived SR-DSS thresholds only have slight changes from the Level 3 derived thresholds: snowpack density 1 hour prior for ROS of 25.4% vs 27.0% and 32.8% vs 32.3% for W/SDM, 6 hour maximum temperature for ROS of 1.5 °C vs 1.3 °C, 12 hour maximum temperature for W/SDM of 5.2 °C vs 5.2 °C, and 6 hour precipitation totals for ROS of 3.7 mm vs 4.5 mm. Although more stations should be developed manually to confirm the reliability of the Level 2 data for automated threshold analysis, this first assessment demonstrates the utility of the Level 2 data to provide situational awareness for mid-winter snowpack runoff.

5.5 Limitations and Future work

The SR-DSS demonstrates improved situational awareness for ROS flood events. However, in order to better assess the reliability of the SR-DSS at a basin scale, more SNOTEL stations need to be integrated into the framework. While the automated QA/QC methods overcome one major hurdle, TWI cannot yet be classified as ROS or W/SDM automatically. The classification of TWI as ROS and W/SDM is essential for the pattern recognition of present weather and antecedent snowpack conditions during TWI. In Chapter 2, we developed a decision tree model to automate the TWI classification and upon testing that model on Blue Lakes and Spratt Creek we discovered that a classification model may need to be built for each station. Since TWI needs to manually be classified in order to build the decision tree classification model, it may not be necessary to invest in a TWI classification model unless one can be built that is effective at all SNOTEL stations. Furthermore, the TWI identification algorithm approach only works on stations with well-draining soil that can register the input of additional water.

Once TWI is classified as ROS and W/SDM, the SR-DSS thresholds would benefit from further refinement with the addition of new stations. For example, our study shows that the air temperature threshold at higher elevation stations like Blue Lakes should be lowered since at least two events (Section 6 and 5.4.3) events had TWI initiate with 6 hour maximum air temperatures of 0.5 °C. Including more SNOTEL stations outside of the Sierra Nevada will further enhance the understanding of present weather and antecedent snowpack conditions that produce TWI across the western U.S.

Future developments would also benefit from the statistical classification of the SR-DSS to over and under-predict the onset of TWI (e.g., how many times does the SR-DSS predict TWI that does not occur and how many times does TWI occur that was not predicted). Trust can be lost between the decision-makers and a decision support tool when the prediction is unreliable either by over or under-predicting the outcome (Ripberger et al., 2022). The confidence in the tool needs to be quantified and made transparent with decision-makers in order to earn trust in the SR-DSS.

Beyond increasing the confidence and reliability of the SR-DSS, our next step will attempt to integrate probabilistic forecast information to increase lead time. Products like the NWS National Blend of Models provide the range of expected precipitation and air temperatures with their associated confidence. By integrating this information into the SR-DSS thresholds we aim to provide high and low scenarios that communicate what percentage of the watershed is expected to experience ROS and produce TWI with the associated uncertainty.

5.6 Summary

We expanded on the work of Heggli et al. (2022) and integrate the data methods in Chapter 4 to asses and further calibrate the present weather and antecedent snowpack conditions that produce TWI and connect the data to CNRFC hydrologic forecast points in the Upper Carson River Watershed. We applied the updated SR-DSS thresholds to asses four historical floods. We also assessed an operational approach for the SR-DSS by applying data subjected only to automated quality control routines and apply the SR-DSS to an event that was not included in the development of thresholds. The case studies highlight how complicated the snowpack runoff process is as each event brings a different combination of antecedent conditions and present weather impacts. However, our research found that precipitation at 0.5 °C can produce TWI within two hours and further prove that the snowpack does not need to reach a certain density to be able to produce TWI. This paper not only advances the development of SR-DSS to serve an unmet need but also improves the understanding of ROS runoff process. Integrating hourly SNOTEL data provides insight into lag-rates on rainwater moving through the snowpack, snowmelt during ROS, and the total duration of TWI during ROS. Observing patterns of ROS events and connecting those patterns to streamflow provides valuable insights for flood forecasting and management in the Upper Carson watershed.

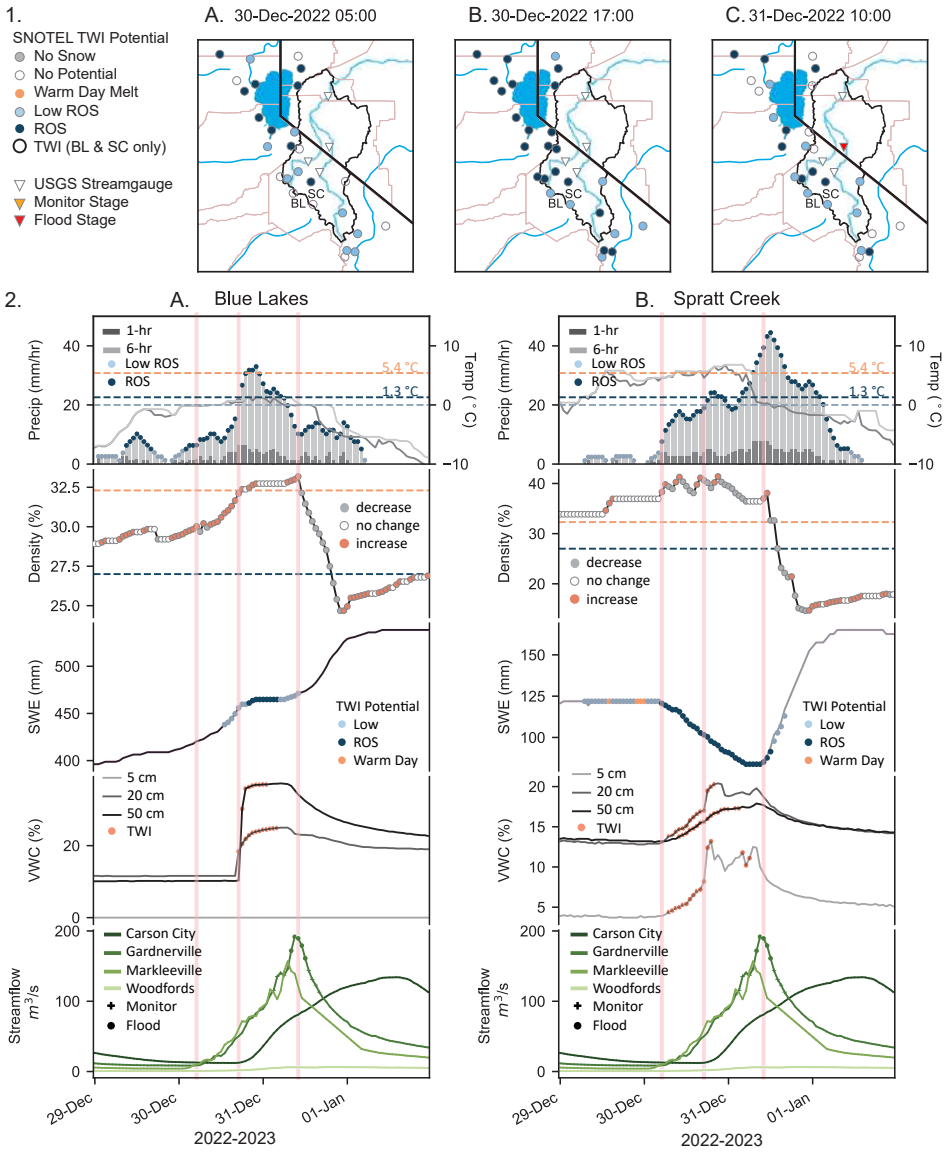

Figure 5.5: 29 December 2022–1 January 2023: Regional maps of TWI potential and streamflow response (1A, B, and C) for selected times indicated with a pink vertical line (2A and B). Time series data from the Blue Lakes (2A) and Spratt Creek (2B) leading up to the streamflow response. There are four panels: 1 hour (dark grey) and 6 hour (light grey) precipitation totals and 1 hour (dark grey) and 6 hour (light grey) maximum air temperature in the top panel; shows bulk snowpack density color coded to communicate increases (pink), decreases (grey), and no change (white) in density values each hour; SWE (black) overlayed with the SR-DSS TWI potential (low ROS in light blue, ROS in dark blue, low W/SDM in light orange, and W/SDM in orange); soil moisture ranging from light to dark grey at 5 cm, 20 cm, and 50 cm depths accordingly with periods of active TWI highlighted in pink; maximum hourly stream flow in green ranging from dark to light green in the following order: Carson City, Gardnerville, Markleeville, and Woodfords.

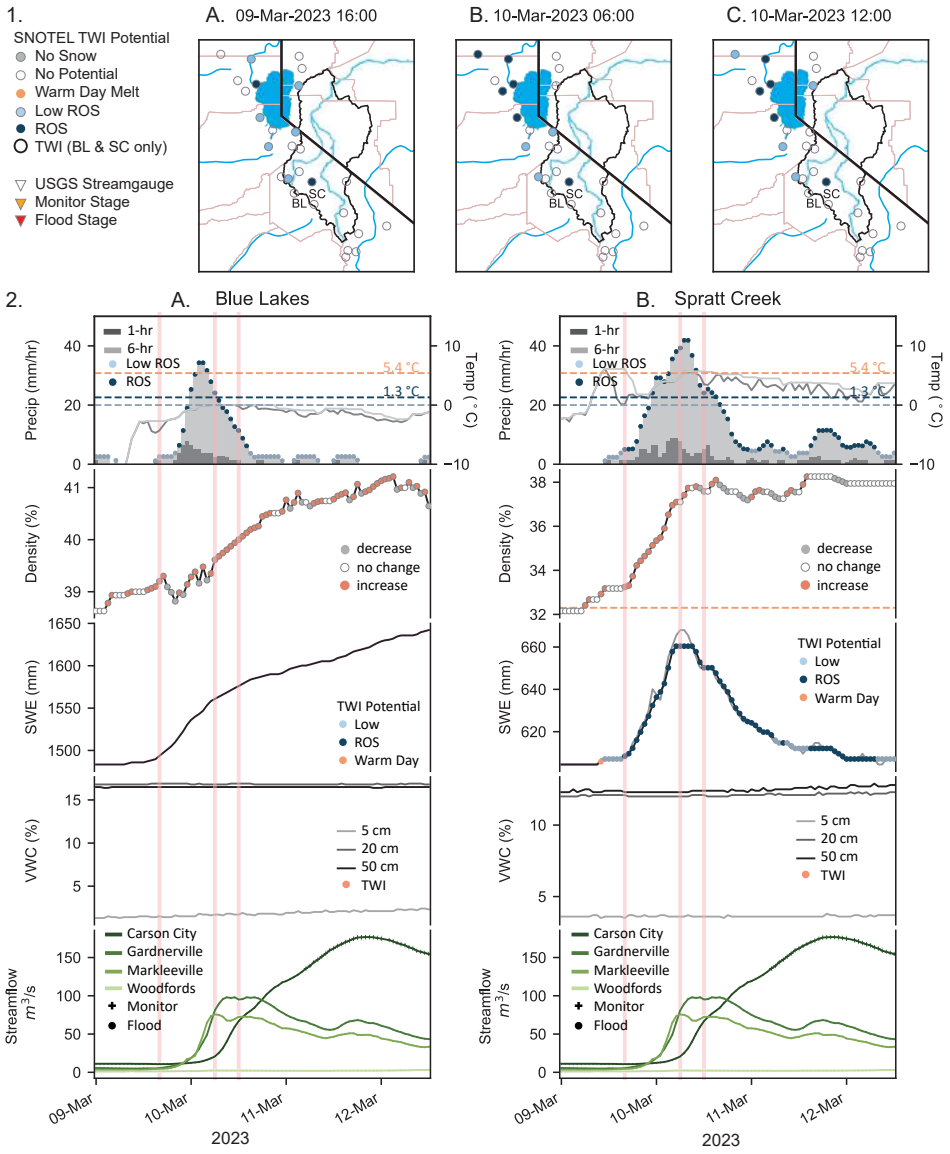

Figure 5.6: 9-12 March 2023 case study: Regional maps of TWI potential and streamflow response (1A, B, and C) for selected times indicated with a pink vertical line (2A and B). Time series data from the Blue Lakes (2A) and Spratt Creek (2B) with four panels: 1 hour (dark grey) and 6 hour (light grey) precipitation totals and 1 hour (dark grey) and 6 hour (light grey) maximum air temperature; bulk snowpack density color coded to communicate increases (pink), decreases (grey), and no change (white) in density values; SWE (black) with the addition of unprocessed SWE data (light grey) overlayed with the SR-DSS TWI potential (low ROS in light blue, ROS in dark blue, low W/SDM in light orange, and W/SDM in orange); soil moisture ranging from light to dark grey at 5 cm, 20 cm, and 50 cm depths accordingly with active TWI highlighted in pink; maximum hourly stream flow in green ranging from dark to light green in the following order: Carson City, Gardnerville, Markleeville, and Woodfords.

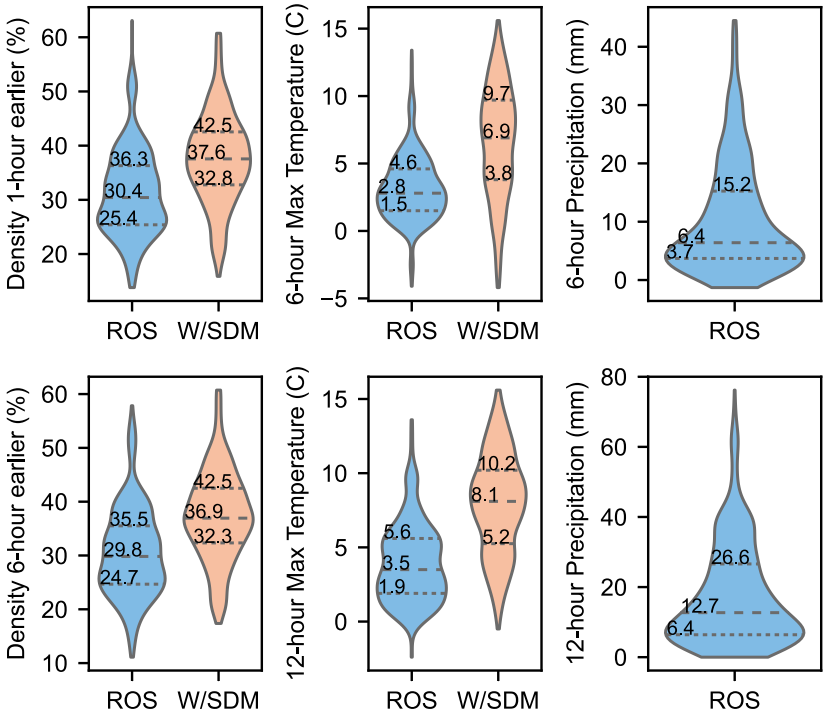

Figure 5.7: Violin plots of snowpack density 1 and 6 hours prior to TWI, 6 and 12 hour maximum air temperature, and 6 and 12 hour precipitation totals during ROS TWI (blue) and W/SDM TWI (orange) for Blue Lakes (BL), Central Sierra Snow Laboratory (CSSL), and Spratt Creek (SC) using Level 2 automated QA/QC process from Chapter 4.

Chapter 6

Summary

The four dissertation chapters (Chapters 2–5) establish the foundation for a novel snowpack runoff decision support system (SR-DSS) and identify necessary visual communication principles to connect decision-relevant data with decision-makers (Uccellini and Ten Hoeve, 2019). Throughout the development of this research, the four chapters were developed with a customer service approach that included consistent communication and guidance from the agencies they were developed for: NDOT, NWS, NRCS, and hydropower agencies. Developing this work and these relationships through the research process has highlighted the value of end-to-end solutions as work with each agency will continue beyond this dissertation.

This work identified key thresholds for present weather and antecedent snowpack conditions with the potential to produce TWI. Beyond identifying TWI potential thresholds that were integrated into the SR-DSS, the hourly SNOTEL data demonstrated that the snowpack can absorb rainwater through the slower progressions of the uniform wetting front while simultaneously releasing water through the rapid formation of preferential flow paths that route water through the snowpack. This work also found that snowmelt is not a primary source of runoff and the snowpack does not need to become ripe in order to produce TWI. Furthermore, we found that it is possible for TWI to begin within one hour of rainfall, even in deeper snowpacks. Further enhancements to the semi-automated QA/QC process for hourly SNOTEL data will improve the reliability of the hourly SNOTEL data while also reducing the human review time, making the widespread application of the methods more feasible. A reliable hourly SNOTEL data product will multiply the value of the investment in the network for both operational applications and new research developments.

Currently, the SR-DSS has only integrated three stations into the development of the

thresholds for a small region of the Sierra Nevada. Not only must the SR-DSS be fully developed to assess the utility of the tool at the watershed scale by integrating the remaining SNOTEL stations in the Upper Carson, but the SR-DSS must also be calibrated and assessed for different snow climates. Furthermore, the SR-DSS is only useful for real-time situational awareness. The future integration of probabilistic forecast information would increase lead time for decision-making to communicate high and low scenarios ahead of the event in order to optimize water resource management. Furthermore, the reliability of the tool must also be quantified and made transparent with decision-makers in order to earn trust in the SR-DSS.

Coupling the data integration into the SR-DSS with the findings for effective visual communication, we can continue to fully assess the utility of the tool from the reliability of the TWI potential to effective visual communication. The templates from Chapter 3 will be integrated into surveys disseminated by NWS offices in Portland, OR, Pocatello, ID, Reno, NV, San Diego, CA, and Pheonix, AZ to core partners and public audiences as a part of the NOAA-funded project "Employing Rhetoric to Improve Probabilistic Forecast Communication". However, the visual communication of the SR-DSS has not yet been assessed by the intended stakeholders. The visualization for the SR-DSS has improved with each iteration, but further development must receive feedback and guidance from the intended users to align the research with operational decision-making.

The continued development of the SR-DSS will require many steps to operationalize the system. It will also require continued cooperation from NWS offices. While this work will continue in regions of Nevada funded by NDOT, the SR-DSS will need to be scaled up to cover the entire Sierra Nevada and eventually the entire SNOTEL network. Collaboration from NRCS staff to improve the quality of hourly SNOTEL data not only historically, but in real-time to be ingested into the SR-DSS would optimize this outcome. In order to expand the SR-DSS to cover the entire Sierra Nevada, stations in California that are not a part of the SNOTEL network will need to be integrated. To address this, we are applying for grants in collaboration with East Bay Municipal Utility District and Pacific Gas and Electric to translate the work from the Upper Carson to the Mokelumne. Future research

will also focus on evaluating the effectiveness of the system in supporting decision-making and optimizing water resource management in different hydrological contexts.

We aim to continue to develop the SR-DSS in a way that could sit at the CNRFC to have the greatest reach to decision-makers and potentially impacted communities. The future iterations of the SR-DSS focus on the benefit for NWS hydrologic forecasters with an emphasis on supporting hydropower agencies and the Nevada Department of Transportation (NDOT). NDOT is just one of many stakeholders potentially impacted by ROS flooding in this area. Collaboration with stakeholders and end-users is crucial throughout the entire process of developing end-to-end solutions from assistance in installing new sensors to the visual communication of the integrated data. Stakeholder engagement ensures the usability and relevance of the SR-DSS, and will continue to be central to the progress of this applied research.

Bibliography

Ambrose, G., Harris, P., Ball, N., 2019. The Fundamentals of Graphic Design. Fundamentals, Bloomsbury Publishing. URL: https://books.google.com/books?id=QaKxDwAAQBAJ.

Anderson, E., 2006. Snow Accumulation and Ablation Model-SNOW-17. Technical Report. National Weather Service. URL: https://www.nrcs.usda.gov/wps/PA_NRCSConsumption/download?cid=nrcseprd1805290&ext=pdf.

Anderson, J., Wirt, J., 2008. Ultrasonic snow depth sensor accuracy, reliability, and performance, Hood River, OR. URL: sites/westernsnowconference.org/PDFs/2008Anderson.pdf.

Andry, T., Hurter, C., Lambotte, F., Fastrez, P., Telea, A., 2021. Interpreting the effect of embellishment on chart visualizations, in: Proceedings of the 2021 CHI Conference on Human Factors in Computing Systems, ACM. URL: https://doi.org/10.1145/3411764.3445739, doi:10.1145/3411764.3445739.

Arienzo, M.M., Collins, M., Jennings, K.S., 2021. Enhancing engagement of citizen scientists to monitor precipitation phase. Frontiers in Earth Science 9, 68. doi:10.3389/feart.2021.617594.

Ash, K.D., Schumann, R.L., Bowser, G.C., 2014. Tornado warning trade-offs: Evaluating choices for visually communicating risk. Weather, Climate, and Society 6, 104–118. URL: https://doi.org/10.1175/wcas-d-13-00021.1, doi:10.1175/wcas-d-13-00021.1.

Authority, E.F.S., Hart, A., Maxim, L., Siegrist, M., Goetz, N.V., da Cruz, C., Merten, C., Mosbach-Schulz, O., Lahaniatis, M., Smith, A., Hardy, A., 2019. Guidance on communication of uncertainty in scientific assessments. EFSA Journal 17. URL: https://data.europa.eu/doi/10.2903/j.efsa.2019.5520, doi:10.2903/j.efsa.2019.5520.

Avanzi, F., Michele, C.D., Ghezzi, A., Jommi, C., Pepe, M., 2014. A processing–modeling routine to use SNOTEL hourly data in snowpack dynamic models. Advances in Water Resources 73, 16–29. URL: https://doi.org/10.1016/j.advwatres.2014.06.011, doi:10.1016/j.advwatres.2014.06.011.

Bai, Q., Dan, Q., Mu, Z., Yang, M., 2019. A systematic review of emoji: Current research and future perspectives. Frontiers in Psychology 10. URL: https://doi.org/10.3389/fpsyg.2019.02221, doi:10.3389/fpsyg.2019.02221.

Baker, L., 2023. City of south lake tahoe urges residents to prepare for impacts of rain-on-snow event - sierra nevada alliance. https://sierranevadaalliance.org/city-of-south-lake-tahoe-urges-residents-to-prepare-for-impacts-of-rain-on-snow-event/. (Accessed on 07/17/2023).

Bakker, A., Biehler, R., Konold, C., 2004. Should young students learn about box plots. Curricular development in statistics education: International Association for Statistical Education , 163–173.

Bales, R.C., Hopmans, J.W., O'Geen, A.T., Meadows, M., Hartsough, P.C., Kirchner, P., Hunsaker, C.T., Beaudette, D., 2011. Soil moisture response to snowmelt and rainfall in a sierra nevada mixed-conifer forest. Vadose Zone Journal 10, 786–799. URL: https://doi.org/10.2136/vzj2011.0001, doi:10.2136/vzj2011.0001.

Bartles, M., Brauer, T., David Ho, M.F., Karlovits, G., Pak, J., Van, N., Willis, J., 2021. Hydrologic Modeling System HEC-HMS User's Manual. Technical Report. URL: https://www.hec.usace.army.mil/confluence/hmsdocs/hmsum/4.9.

Basak, A., Roy, S.T., 2022. Visual ergonomics for colourblindness: Applying universal design principles in graphical user interface to provide affordance to the colourblind users. Proceedings of the Design Society 2, 2055–2066. URL: https://doi.org/10.1017/pds.2022.208, doi:10.1017/pds.2022.208.

Bateman, S., Mandryk, R.L., Gutwin, C., Genest, A., McDine, D., Brooks, C., 2010. Useful junk? the effects of visual embellishment on comprehension and memorability of charts, in: Proceedings of the SIGCHI conference on human factors in computing systems, pp. 2573–2582.

Bean, H., Sutton, J., Liu, B.F., Madden, S., Wood, M.M., Mileti, D.S., 2015. The study of mobile public warning messages: A research review and agenda. Review of Communication 15, 60–80. URL: https://doi.org/10.1080/15358593.2015.1014402, doi:10.1080/15358593.2015.1014402.

Berman, E.S.F., Gupta, M., Gabrielli, C., Garland, T., McDonnell, J.J., 2009. High-frequency field-deployable isotope analyzer for hydrological applications. Water Resources Research 45. URL: https://doi.org/10.1029/2009wr008265, doi:10.1029/2009wr008265.

Bernard, M., Liao, C.H., Mills, M., 2001. The effects of font type and size on the legibility and reading time of online text by older adults, in: CHI '01 Extended Abstracts on Human Factors in Computing Systems, ACM. URL: https://doi.org/10.1145/634067.634173, doi:10.1145/634067.634173.

Berris, S.N., Harr, R.D., 1987. Comparative snow accumulation and melt during rainfall in forested and clear-cut plots in the western cascades of oregon. Water Resources Research 23, 135–142. URL: https://doi.org/10.1029/wr023i001p00135, doi:10.1029/wr023i001p00135.

van der Bles, A.M., van der Linden, S., Freeman, A.L.J., Spiegelhalter, D.J., 2020. The effects of communicating uncertainty on public trust in facts and numbers. Proceedings

of the National Academy of Sciences 117, 7672–7683. URL: https://doi.org/10.1073/pnas.1913678117, doi:10.1073/pnas.1913678117.

Borland, D., Ii, R.M.T., 2007. Rainbow color map (still) considered harmful. IEEE Computer Graphics and Applications 27, 14–17. URL: https://doi.org/10.1109/mcg.2007.323435, doi:10.1109/mcg.2007.323435.

Brandt, W.T., Cannon, F., Cooper, A., Monache, L.D., Haleakala, K., Hatchett, B.J., McGurk, B., Pan, M., Ralph, F.M., 2022a. Complementary observations aid identification of the mountain rain-snow transition elevation URL: https://doi.org/10.1002/essoar.10510466.1, doi:10.1002/essoar.10510466.1.

Brandt, W.T., Haleakala, K., Hatchett, B.J., Pan, M., 2022b. A review of the hydrologic response mechanisms during mountain rain-on-snow. Frontiers in Earth Science doi:10.3389/feart.2022.791760.

Breznitz, S., 2013. Cry wolf: The psychology of false alarms. Psychology Press.

Broad, K., Leiserowitz, A., Weinkle, J., Steketee, M., 2007. Misinterpretations of the "cone of uncertainty" in florida during the 2004 hurricane season. Bulletin of the American Meteorological Society 88, 651–668. URL: https://doi.org/10.1175/bams-88-5-651, doi:10.1175/bams-88-5-651.

Brown, C.R., Domonkos, B., Brosten, T., DeMarco, T., Rebentisch, A., 2019. Transformation of the snotel temperature record - methodology and implications, in: 87th Annual Western Snow Conference, pp. 37–44.

Bunn, P.T., Wood, A.W., Newman, A.J., Chang, H.I., Castro, C.L., Clark, M.P., Arnold, J.R., 2022. Improving station-based ensemble surface meteorological analyses using numerical weather prediction: A case study of the oroville dam crisis precipitation event. Journal of Hydrometeorology URL: https://doi.org/10.1175/jhm-d-21-0193.1, doi:10.1175/jhm-d-21-0193.1.

Cardell-Oliver, R., Kranz, M., Smettem, K., Mayer, K., 2005. A reactive soil moisture sensor network: Design and field evaluation. International Journal of Distributed Sensor Networks 1, 149–162. URL: https://doi.org/10.1080/15501320590966422, doi:10.1080/15501320590966422.

Carr, R.H., Montz, B., Maxfield, K., Hoekstra, S., Semmens, K., Goldman, E., 2016. Effectively communicating risk and uncertainty to the public: Assessing the national weather service's flood forecast and warning tools. Bulletin of the American Meteorological Society 97, 1649–1665. URL: https://journals.ametsoc.org/view/journals/bams/97/9/bams-d-14-00248.1.xml, doi:10.1175/BAMS-D-14-00248.1.

Carr, R.H., Semmens, K., Montz, B., Maxfield, K., 2021. Improving the use of hydrologic probabilistic and deterministic information in decision-making. Bulletin of the American Meteorological Society 102, E1878–E1896. URL: https://doi.org/10.1175/bams-d-21-0019.1, doi:10.1175/bams-d-21-0019.1.

Cayan, D.R., Georgakakos, K.P., 1995. Hydroclimatology of continental watersheds: 2. spatial analyses. Water Resources Research 31, 677–697. URL: https://doi.org/10.1029/94wr02376, doi:10.1029/94wr02376.

Chang, E.K.M., Zheng, C., Lanigan, P., Yau, A.M.W., Neelin, J.D., 2015. Significant modulation of variability and projected change in california winter precipitation by extratropical cyclone activity. Geophysical Research Letters 42, 5983–5991. URL: https://doi.org/10.1002/2015gl064424, doi:10.1002/2015gl064424.

Changnon, S.A., 2001. Thunderstorm rainfall in the conterminous united states. Bulletin of the American Meteorological Society 82, 1925–1940. URL: https://doi.org/10.1175/1520-0477(2001)082<1925:tritcu>2.3.co;2, doi:10.1175/1520-0477(2001)082<1925:tritcu>2.3.co;2.

Chaparro, B.S., Shaikh, A.D., Chaparro, A., Merkle, E.C., 2010. Comparing the legibility of six ClearType typefaces to verdana and times new roman. Information Design Journal 18, 36–49. URL: https://doi.org/10.1075/idj.18.1.04cha, doi:10.1075/idj.18.1.04cha.

Chiarella, D., Yarbrough, J., Jackson, C.A.L., 2020. Using alt text to make science twitter more accessible for people with visual impairments. Nature Communications 11. URL: https://doi.org/10.1038/s41467-020-19640-w, doi:10.1038/s41467-020-19640-w.

Cho, E., Jacobs, J.M., 2020. Extreme value snow water equivalent and snowmelt for infrastructure design over the contiguous united states. Water Resources Research 56. URL: https://doi.org/10.1029/2020wr028126, doi:10.1029/2020wr028126.

Church, J., 1948. The evolution of snow-melt by dyes and drip-pan. International Association of Hydrological Sciences, General Assembly of Oslo 2, 115–117.

Church, J.E., 1933. The biography of snow surveying. URL: https://westernsnowconference.org/node/107.

Clark, M.P., Nijssen, B., Luce, C.H., 2017. An analytical test case for snow models. Water Resources Research 53, 909–922. URL: https://doi.org/10.1002/2016wr019672, doi:10.1002/2016wr019672.

CNRFC, 2006. Heavy Precipitation Event Southwest Oregon, Northern California, and Western Nevada December 24, 2005 - January 3, 2006. Technical Report. National Weather Service. URL: https://www.cnrfc.noaa.gov/storm_summaries/dec2005storms.php.

CNRFC, 2017. Heavy Precipitation Events California and Northern Nevada January and February 2017. Technical Report. National Weather Service. URL: https://www.cnrfc.noaa.gov/storm_summaries/janfeb2017storms.php.

Colbeck, S.C., 1972. A theory of water percolation in snow. Journal of Glaciology 11, 369–385. URL: https://doi.org/10.3189/s0022143000022346, doi:10.3189/s0022143000022346.

Colbeck, S.C., 1976. An analysis of water flow in dry snow. Water Resources Research 12, 523–527. URL: https://doi.org/10.1029/wr012i003p00523, doi:10.1029/wr012i003p00523.

Congress, U.S., 1973. Section 508 of the rehabilitation act of 1973. 29 U.S.C. section 794d.

National Research Council, on Earth, D., Studies, L., on Atmospheric Sciences, B., Climate, on Estimating, C., in Weather, C.U., Forecasts, C., 2006. Completing the Forecast.

Crameri, F., Shephard, G.E., Heron, P.J., 2020. The misuse of colour in science communication. Nature Communications 11. URL: https://doi.org/10.1038/s41467-020-19160-7, doi:10.1038/s41467-020-19160-7.

Craven, J.P., Rudack, D.E., Shafer, P.E., 2020. National blend of models: a statistically post-processed multi-model ensemble. Journal of Operational Meteorology 8.

Dacre, H.F., Clark, P.A., Martinez-Alvarado, O., Stringer, M.A., Lavers, D.A., 2015. How do atmospheric rivers form? Bulletin of the American Meteorological Society 96, 1243–1255. doi:10.1175/BAMS-D-14-00031.1.

Dai, A., 2008. Temperature and pressure dependence of the rain-snow phase transition over land and ocean. Geophysical Research Letters 35, n/a–n/a. URL: https://doi.org/10.1029/2008gl033295, doi:10.1029/2008gl033295.

Dallo, I., Stauffacher, M., Marti, M., 2020. What defines the success of maps and additional information on a multi-hazard platform? International Journal of Disaster Risk Reduction 49, 101761. URL: https://www.sciencedirect.com/science/article/pii/S2212420920312632, doi:https://doi.org/10.1016/j.ijdrr.2020.101761.

Dasgupta, A., Poco, J., Rogowitz, B., Han, K., Bertini, E., Silva, C.T., 2020. The effect of color scales on climate scientists' objective and subjective performance in spatial data analysis tasks. IEEE Transactions on Visualization and Computer Graphics 26, 1577–1591. URL: https://doi.org/10.1109/tvcg.2018.2876539, doi:10.1109/tvcg.2018.2876539.

Deeb, S., 2005. The molecular basis of variation in human color vision. Clinical Genetics 67, 369–377. URL: https://doi.org/10.1111/j.1399-0004.2004.00343.x, doi:10.1111/j.1399-0004.2004.00343.x.

Delaney, C.J., Hartman, R.K., Mendoza, J., Dettinger, M., Monache, L.D., Jasperse, J., Ralph, F.M., Talbot, C., Brown, J., Reynolds, D., Evett, S., 2020. Forecast informed reservoir operations using ensemble streamflow predictions for a multipurpose reservoir in northern california. Water Resources Research 56. URL: https://doi.org/10.1029/2019wr026604, doi:10.1029/2019wr026604.

Dettinger, M.D., , and, M.L.A., 2015. Storage in california's reservois and snowpack in this time of drought. San Francisco Estuary and Watershed Science 13. URL: https://doi.org/10.15447/sfews.2015v13iss2art1, doi:10.15447/sfews.2015v13iss2art1.

Dettinger, M.D., Cayan, D.R., 1995. Large-scale atmospheric forcing of recent trends toward early snowmelt runoff in california. Journal of Climate 8, 606–623. URL: https://doi.org/10.1175/1520-0442(1995)008<0606:lsafor>2.0.co;2, doi:10.1175/1520-0442(1995)008<0606:lsafor>2.0.co;2.

Doswell, C.A., Brooks, H.E., Maddox, R.A., 1996. Flash flood forecasting: An ingredients-based methodology. Weather and Forecasting 11, 560–581. URL: https://doi.org/10.1175/1520-0434(1996)011<0560:fffaib>2.0.co;2, doi:10.1175/1520-0434(1996)011<0560:fffaib>2.0.co;2.

Eden, G.F., Moats, L., 2002. The role of neuroscience in the remediation of students with dyslexia. Nature Neuroscience 5, 1080–1084. URL: https://doi.org/10.1038/nn946, doi:10.1038/nn946.

Edwards, T.G., Özgün Koca, A., Barr, J., 2017. Interpretations of boxplots: Helping middle school students to think outside the box. Journal of Statistics Education 25, 21–28. URL: https://doi.org/10.1080/10691898.2017.1288556, doi:10.1080/10691898.2017.1288556, arXiv:https://doi.org/10.1080/10691898.2017.1288556.

Eiriksson, D., Whitson, M., Luce, C.H., Marshall, H.P., Bradford, J., Benner, S.G., Black, T., Hetrick, H., McNamara, J.P., 2013. An evaluation of the hydrologic relevance of lateral flow in snow at hillslope and catchment scales. Hydrological Processes 27, 640–654. URL: https://doi.org/10.1002/hyp.9666, doi:10.1002/hyp.9666.

Elder, A.M., 2018. What words can't say. Journal of Information, Communication and Ethics in Society 16, 2–15. URL: https://doi.org/10.1108/jices-08-2017-0050, doi:10.1108/jices-08-2017-0050.

Environmental Protection Agency, E., 1999. 40 cfr part 58 air quality index reporting; final rule. Federal Register 64. URL: https://www.airnow.gov/sites/default/files/2018-06/air-quality-index-reporting-final-rule.pdf.

Eraslan, S., Yesilada, Y., Yaneva, V., Ha, L.A., 2020. "keep it simple!": an eye-tracking study for exploring complexity and distinguishability of web pages for people with autism. Universal Access in the Information Society 20, 69–84. URL: https://doi.org/10.1007/s10209-020-00708-9, doi:10.1007/s10209-020-00708-9.

Essen, D.C.V., Anderson, C.H., Felleman, D.J., 1992. Information processing in the primate visual system: An integrated systems perspective. Science 255, 419–423. URL: https://doi.org/10.1126/science.1734518, doi:10.1126/science.1734518.

Fassnacht, S.R., Records, R.M., 2015. Large snowmelt versus rainfall events in the mountains. Journal of Geophysical Research: Atmospheres 120, 2375–2381. URL: https://doi.org/10.1002/2014jd022753, doi:10.1002/2014jd022753.

Fleischhut, N., Herzog, S.M., Hertwig, R., 2020. Weather literacy in times of climate change. Weather, Climate, and Society 12, 435–452. URL: https://doi.org/10.1175/wcas-d-19-0043.1, doi:10.1175/wcas-d-19-0043.1.

Fleming, S.W., Zukiewicz, L., Strobel, M.L., Hofman, H., Goodbody, A.G., 2023. SNOTEL, the soil climate analysis network, and water supply forecasting at the natural resources conservation service: Past, present, and future. JAWRA Journal of the American Water Resources Association URL: https://doi.org/10.1111/1752-1688.13104, doi:10.1111/1752-1688.13104.

Fletcher, J.M., Lyon, G.R., Fuchs, L.S., Barnes, M.A., 2018. Learning disabilities: From identification to intervention. Guilford Publications.

Flint, A.L., Flint, L.E., Dettinger, M.D., 2008. Modeling soil moisture processes and recharge under a melting snowpack. Vadose Zone Journal 7, 350–357. URL: https://doi.org/10.2136/vzj2006.0135, doi:10.2136/vzj2006.0135.

Flynn, F.J., Lide, C.R., 2022. Communication miscalibration: The price leaders pay for not sharing enough. Academy of Management Journal URL: https://doi.org/10.5465/amj.2021.0245, doi:10.5465/amj.2021.0245.

Force, N.U.D.F.T., 2005. NOAA-USGS Debris-Flow Warning System–final report. U.S. Dept. of the Interior, U.S. Geological Survey, Reston, Va.

Franconeri, S.L., Padilla, L.M., Shah, P., Zacks, J.M., Hullman, J., 2021. The science of visual data communication: What works. Psychological Science in the Public Interest 22, 110–161. URL: https://doi.org/10.1177/15291006211051956, doi:10.1177/15291006211051956.

Frigge, M., Hoaglin, D.C., Iglewicz, B., 1989. Some implementations of the boxplot. The American Statistician 43, 50–54. doi:10.1080/00031305.1989.10475612.

Fundel, V.J., Fleischhut, N., Herzog, S.M., Göber, M., Hagedorn, R., 2019. Promoting the use of probabilistic weather forecasts through a dialogue between scientists, developers and end-users. Quarterly Journal of the Royal Meteorological Society 145, 210–231. URL: https://doi.org/10.1002/qj.3482, doi:10.1002/qj.3482.

Georgakakos, K.P., 2006. Analytical results for operational flash flood guidance. Journal of Hydrology 317, 81–103. URL: https://doi.org/10.1016/j.jhydrol.2005.05.009, doi:10.1016/j.jhydrol.2005.05.009.

Godsey, S.E., Kirchner, J.W., Tague, C.L., 2014. Effects of changes in winter snowpacks on summer low flows: case studies in the sierra nevada, california, usa. Hydrological Processes 28, 5048–5064. URL: https://onlinelibrary.wiley.com/doi/abs/10.1002/hyp.9943, doi:https://doi.org/10.1002/hyp.9943, arXiv:https://onlinelibrary.wiley.com/doi/pdf/10.1002/hyp.9943.

Goodison, B.E., Louie, P.Y., Yang, D., 1998. Wmo solid precipitation measurement intercomparison .

Gordon, A., Chimenti, E., Amirazizi, R., Busalacchi, S., Buhler, M., Goedderz, P., Grevin, C., Kashani, S., 2022. Crafting effective public safety messages for wildfire and subsequent debris flow risks. URL: https://www.weather.gov/mlb/seasonal_wind_threat#:~:text=%22An%20Extreme%20Threat%20to%20Life,with%20a%20high%20wind%20warning.

van Gorp, T., Adams, E., 2012. Design for Emotion. Design for Emotion, Elsevier Science. URL: https://books.google.com/books?id=8lgSs1GoPN8C.

Grounds, M.A., Joslyn, S., Otsuka, K., 2017. Probabilistic interval forecasts: An individual differences approach to understanding forecast communication. Advances in Meteorology 2017, 1–18. URL: https://doi.org/10.1155/2017/3932565, doi:10.1155/2017/3932565.

Grounds, M.A., Joslyn, S.L., 2018. Communicating weather forecast uncertainty: Do individual differences matter? Journal of Experimental Psychology: Applied 24, 18–33. URL: https://doi.org/10.1037/xap0000165, doi:10.1037/xap0000165.

Guan, B., Waliser, D.E., Ralph, F.M., Fetzer, E.J., Neiman, P.J., 2016. Hydrometeorological characteristics of rain-on-snow events associated with atmospheric rivers. Geophysical Research Letters 43, 2964–2973. URL: https://doi.org/10.1002/2016gl067978, doi:10.1002/2016gl067978.

Haleakala, K., Brandt, W.T., Hatchett, B.J., Li, D., Lettenmaier, D.P., Gebremichael, M., 2022. Watershed memory amplified the oroville rain-on-snow flood of february 2017. PNAS Nexus 2. URL: https://doi.org/10.1093/pnasnexus/pgac295, doi:10.1093/pnasnexus/pgac295.

Harr, R., 1981. Some characteristics and consequences of snowmelt during rainfall in western oregon. Journal of Hydrology 53, 277–304. URL: https://doi.org/10.1016/0022-1694(81)90006-8, doi:10.1016/0022-1694(81)90006-8.

Harrison, D.R., Elliott, M.S., Jirak, I.L., Marsh, P.T., 2022. Utilizing the high-resolution ensemble forecast system to produce calibrated probabilistic thunderstorm guidance. Weather and Forecasting 37, 1103–1115. URL: https://doi.org/10.1175/waf-d-22-0001.1, doi:10.1175/waf-d-22-0001.1.

Harrower, M., Brewer, C., 2003. Colorbrewer.org: An online tool for selecting color schemes for maps. The Cartographic Journal 40(1), 27–37. URL: https://colorbrewer2.org/.

Hatchett, B., Daudert, B., Garner, C., Oakley, N., Putnam, A., White, A., 2017a. Winter snow level rise in the northern sierra nevada from 2008 to 2017. Water 9, 899. URL: https://doi.org/10.3390/w9110899, doi:10.3390/w9110899.

Hatchett, B.J., Benmarhnia, T., Guirguis, K., VanderMolen, K., Gershunov, A., Kerwin, H., Khlystov, A., Lambrecht, K.M., Samburova, V., 2021. Mobility data to aid assessment of human responses to extreme environmental conditions. The Lancet Planetary Health 5, e665–e667. URL: https://doi.org/10.1016/s2542-5196(21)00261-8, doi:10.1016/s2542-5196(21)00261-8.

Hatchett, B.J., Burak, S., Rutz, J.J., Oakley, N.S., Bair, E.H., Kaplan, M.L., 2017b. Avalanche fatalities during atmospheric river events in the western united states. Journal of Hydrometeorology 18, 1359–1374. URL: https://doi.org/10.1175/jhm-d-16-0219.1, doi:10.1175/jhm-d-16-0219.1.

Hatchett, B.J., Cao, Q., Dawson, P.B., Ellis, C.J., Hecht, C.W., Kawzenuk, B., Lancaster, J.T., Osborne, T.C., Wilson, A.M., Anderson, M.L., Dettinger, M.D., Kalansky, J.F., Kaplan, M.L., Lettenmaier, D.P., Oakley, N.S., Ralph, F.M., Reynolds, D.W., White, A.B., Sierks, M., Sumargo, E., 2020. Observations of an extreme atmospheric river storm with a diverse sensor network. Earth and Space Science 7. URL: https://doi.org/10.1029/2020ea001129, doi:10.1029/2020ea001129.

Hatchett, B.J., Kaplan, M.L., Burak, S., 2016. Some characteristics of upside-down storms in the northern sierra nevada, california-nevada, usa, in: Proceedings of the International Snow Science Workshop, Breckenridge, CO, USA, Colorado State University. pp. 1165–1172. URL: https://arc.lib.montana.edu/snow-science/item/2436.

Hatchett, B.J., Koshkin, A.L., Guirguis, K., Rittger, K., Nolin, A.W., Heggli, A., Rhoades, A.M., East, A.E., Siirila-Woodburn, E.R., Brandt, W.T., Gershunov, A., Haleakala, K., 2023. Midwinter dry spells amplify post-fire snowpack decline. Geophysical Research Letters 50. URL: https://doi.org/10.1029/2022gl101235, doi:10.1029/2022gl101235.

Hatchett, B.J., McEvoy, D.J., 2018. Exploring the origins of snow drought in the northern sierra nevada, california. Earth Interactions 22, 1–13. URL: https://doi.org/10.1175/ei-d-17-0027.1, doi:10.1175/ei-d-17-0027.1.

Hauptmann, P., Hoppe, N., Püttmer, A., 2002. Application of ultrasonic sensors in the process industry. Measurement Science and Technology 13, R73–R83. URL: https://doi.org/10.1088/0957-0233/13/8/201, doi:10.1088/0957-0233/13/8/201.

Hawkins, M.D., Brown, V., Ferrell, J., 2017. Assessment of noaa national weather service methods to warn for extreme heat events. Weather, Climate, and Society 9, 5–13. URL: https://journals.ametsoc.org/view/journals/wcas/9/1/wcas-d-15-0037_1.xml, doi:10.1175/WCAS-D-15-0037.1.

He, M., Whitin, B., Hartman, R., Henkel, A., Fickenschers, P., Staggs, S., Morin, A., Imgarten, M., Haynes, A., Russo, M., 2016. Verification of ensemble water supply forecasts for sierra nevada watersheds. Hydrology 3, 35. URL: https://doi.org/10.3390/hydrology3040035, doi:10.3390/hydrology3040035.

National Weather Service Western Regional Headquarters, 2022. Risky Business - Supplement for Advancing IDSS through Probabilities. Technical Report.

Heggli, A., 2023. Hourly snotel data. URL: https://zenodo.org/record/7820055, doi:10.5281/ZENODO.7820055.

Heggli, A., Hatchett, B., Schwartz, A., Bardsley, T., Hand, E., 2022. Toward snowpack runoff decision support. iScience 25, 104240. URL: https://doi.org/10.1016/j.isci.2022.104240, doi:10.1016/j.isci.2022.104240.

Heggli, A., Hatchett, B., Tolby, Z., Lambrecht, K., Collins, M., Olman, L., Jeglum, M., 2023. Visual communication of probabilistic information to enhance decision support. URL: https://zenodo.org/record/7600486, doi:10.5281/ZENODO.7600486.

Henn, B., Musselman, K.N., Lestak, L., Ralph, F.M., Molotch, N.P., 2020. Extreme runoff generation from atmospheric river driven snowmelt during the 2017 oroville dam spillways incident. Geophysical Research Letters 47. URL: https://doi.org/10.1029/2020gl088189, doi:10.1029/2020gl088189.

Hilligoss, S., Howard, T., 2002. Visual communication: A writer's guide. Longman Publishers.

Hirashima, H., Yamaguchi, S., Sato, A., Lehning, M., 2010. Numerical modeling of liquid water movement through layered snow based on new measurements of the water retention curve. Cold Regions Science and Technology 64, 94–103. URL: https://doi.org/10.1016/j.coldregions.2010.09.003, doi:10.1016/j.coldregions.2010.09.003.

Hirschberg, P.A., Abrams, E., Bleistein, A., Bua, W., Monache, L.D., Dulong, T.W., Gaynor, J.E., Glahn, B., Hamill, T.M., Hansen, J.A., Hilderbrand, D.C., Hoffman, R.N., Morrow, B.H., Philips, B., Sokich, J., Stuart, N., 2011. A weather and climate enterprise strategic implementation plan for generating and communicating forecast uncertainty information. Bulletin of the American Meteorological Society 92, 1651–1666. URL: https://doi.org/10.1175/bams-d-11-00073.1, doi:10.1175/bams-d-11-00073.1.

Holle, R.L., 2014. Some aspects of global lightning impacts, in: 2014 International Conference on Lightning Protection (ICLP), IEEE. URL: https://doi.org/10.1109/iclp.2014.6973348, doi:10.1109/iclp.2014.6973348.

Hollins, L., Eisenberg, D., Seager, T., 2018. Risk and resilience at the oroville dam. Infrastructures 3, 49. URL: https://doi.org/10.3390/infrastructures3040049, doi:10.3390/infrastructures3040049.

Howe, L.C., MacInnis, B., Krosnick, J.A., Markowitz, E.M., Socolow, R., 2019. Acknowledging uncertainty impacts public acceptance of climate scientists' predictions. Nature Climate Change 9, 863–867. URL: https://doi.org/10.1038/s41558-019-0587-5, doi:10.1038/s41558-019-0587-5.

Huntsman, S., 2022. An image for all: The rhetoric for writing alt-text, in: 2022 IEEE International Professional Communication Conference (ProComm), IEEE. URL: https://doi.org/10.1109/procomm53155.2022.00012, doi:10.1109/procomm53155.2022.00012.

Hyndman, S., 2016. Why fonts matter. Virgin books London.

Jasechko, S., Birks, S.J., Gleeson, T., Wada, Y., Fawcett, P.J., Sharp, Z.D., McDonnell, J.J., Welker, J.M., 2014. The pronounced seasonality of global groundwater recharge. Water Resources Research 50, 8845–8867. URL: https://doi.org/10.1002/2014wr015809, doi:10.1002/2014wr015809.

Jenkins, S.C., Harris, A.J., Lark, R., 2018. Understanding 'unlikely (20% likelihood)' or '20% likelihood (unlikely)' outcomes: The robustness of the extremity effect. Journal of Behavioral Decision Making 31, 572–586. URL: https://doi.org/10.1002%2Fbdm.2072, doi:10.1002/bdm.2072.

Jenkins, S.C., Harris, A.J.L., Lark, R.M., 2019. When unlikely outcomes occur: the role of communication format in maintaining communicator credibility. Journal of Risk Research 22, 537–554. URL: https://doi.org/10.1080/13669877.2018.1440415, doi:10.1080/13669877.2018.1440415.

Jennings, K., Jones, J.A., 2015. Precipitation-snowmelt timing and snowmelt augmentation of large peak flow events, western cascades, oregon. Water Resources Research 51, 7649–7661. URL: https://doi.org/10.1002/2014wr016877, doi:10.1002/2014wr016877.

Jennings, K.S., Arienzo, M.M., Collins, M., Hatchett, B.J., Nolin, A.W., Aggett, G., 2023. Crowdsourced data highlight precipitation phase partitioning variability in rain-snow transition zone. Earth and Space Science 10. URL: https://doi.org/10.1029/2022ea002714, doi:10.1029/2022ea002714.

Joel Atwood, J., Domonkos, B., Hill, K., Brosten, T., DeMarco, T., Hultstrand, M., Tappa, D., Austin, L., Buckman, A., 2023. Evaluation of ysi temperature correction equations for bias-reducing snotel network temperature data, Flag Staff, AZ. URL: https://www.nrcs.usda.gov/sites/default/files/2023-05/Final_Temperature_Correction_Study05262023.pd.

Johnson, J.B., 2004. A theory of pressure sensor performance in snow. Hydrological Processes 18, 53–64. URL: https://doi.org/10.1002/hyp.1310, doi:10.1002/hyp.1310.

Johnson, J.B., Marks, D., 2004. The detection and correction of snow water equivalent pressure sensor errors. Hydrological Processes 18, 3513–3525. URL: https://doi.org/10.1002/hyp.5795, doi:10.1002/hyp.5795.

Johnson, J.B., Schaefer, G.L., 2002. The influence of thermal, hydrologic, and snow deformation mechanisms on snow water equivalent pressure sensor accuracy. Hydrological Processes 16, 3529–3542. URL: https://doi.org/10.1002/hyp.1236, doi:10.1002/hyp.1236.

Joslyn, S., Demnitz, R., 2019. Communicating climate change: Probabilistic expressions and concrete events. Weather, Climate, and Society 11, 651–664. URL: https://doi.org/10.1175/wcas-d-18-0126.1, doi:10.1175/wcas-d-18-0126.1.

Joslyn, S., LeClerc, J., 2013. Decisions with uncertainty: The glass half full. Current Directions in Psychological Science 22, 308–315. URL: https://doi.org/10.1177/0963721413481473, doi:10.1177/0963721413481473.

Joslyn, S., Savelli, S., 2010. Communicating forecast uncertainty: public perception of weather forecast uncertainty. Meteorological Applications 17, 180–195. URL: https://doi.org/10.1002/met.190, doi:10.1002/met.190.

Joslyn, S., Savelli, S., 2021. Visualizing uncertainty for non-expert end users: The challenge of the deterministic construal error. Frontiers in Computer Science 2. URL: https://doi.org/10.3389/fcomp.2020.590232, doi:10.3389/fcomp.2020.590232.

Joslyn, S.L., Grounds, M.A., 2015. The use of uncertainty forecasts in complex decision tasks and various weather conditions. Journal of Experimental Psychology: Applied 21, 407–417. URL: https://doi.org/10.1037/xap0000064, doi:10.1037/xap0000064.

Joslyn, S.L., LeClerc, J.E., 2012. Uncertainty forecasts improve weather-related decisions and attenuate the effects of forecast error. Journal of Experimental Psychology: Applied 18, 126–140. URL: https://doi.org/10.1037/a0025185, doi:10.1037/a0025185.

Juanchich, M., Sirota, M., 2018. Not as gloomy as we thought: reassessing how the public understands probability of precipitation forecasts. Journal of Cognitive Psychology 31, 116–129. URL: https://doi.org/10.1080/20445911.2018.1553884, doi:10.1080/20445911.2018.1553884.

Julander, R.P., 2007. Soil surface temperature difference between steel and hypalon pillows. URL: sites/westernsnowconference.org/PDFs/2007Julander.pdf.

Julander, R.P., Holcombe, J., 2005. Soil type and site location impacts on soil moisture data collection at high-elevation snotel sites, in: Proceedings of the Western Snow Conference, Colorado State University. p. 65.

Kaplan, M.L., Adaniya, C.S., Marzette, P.J., King, K.C., Underwood, S.J., Lewis, J.M., 2009. The role of upstream midtropospheric circulations in the sierra nevada enabling leeside (spillover) precipitation. part ii: A secondary atmospheric river accompanying a midlevel jet. Journal of Hydrometeorology 10, 1327–1354. doi:10.1175/2009JHM1106.1.

Katsushima, T., Yamaguchi, S., Kumakura, T., Sato, A., 2013. Experimental analysis of preferential flow in dry snowpack. Cold Regions Science and Technology 85, 206–216. URL: https://doi.org/10.1016/j.coldregions.2012.09.012, doi:10.1016/j.coldregions.2012.09.012.

Kattelmann, R., 1985. Macropores in snowpacks of sierra nevada. Annals of Glaciology 6, 272–273. URL: https://doi.org/10.3189/1985aog6-1-272-273, doi:10.3189/1985aog6-1-272-273.

Kattelmann, R., Dozier, J., 1999. Observations of snowpack ripening in the sierra nevada, california, u.s.a. Journal of Glaciology 45, 409–416. URL: https://doi.org/10.3189/s002214300000126x, doi:10.3189/s002214300000126x.

Kattlemann, R., 1997. Flooding from rain-on-snow in the sierra nevada, in: Destructive Water: Water-Caused Natural Disasters, Their Abatement and Control, Anaheim, California. p. 412. URL: https://books.google.com/books?hl=en{&}lr={&}id=8nbLGQw5fckC{&}oi=fnd{&}pg=PA59{&}dq=Kattelmann,+R.+(1997).+Flooding+from+rain-on-snow+events+in+the+Sierra+Nevada.{&}ots=Niz1IdG8Lg{&}sig=l1D6YcmTdNn5WlZJDJqjK6ZuUVE{#}v=onepage{&}q=Kattelmann{%}2CR.(1997).Floodingfromrai.

Kinar, N.J., Pomeroy, J.W., 2015. Measurement of the physical properties of the snowpack. Reviews of Geophysics 53, 481–544. URL: https://doi.org/10.1002/2015rg000481, doi:10.1002/2015rg000481.

Kondragunta, C.R., Shrestha, K., 2006. Automated real-time operational rain gauge quality-control tools in nws hydrologic operations , 2–4.

Koskinas, A., Tegos, A., Tsira, P., Dimitriadis, P., Iliopoulou, T., Papanicolaou, P., Koutsoyiannis, D., Williamson, T., 2019. Insights into the oroville dam 2017 spillway incident. Geosciences 9, 37. URL: https://doi.org/10.3390/geosciences9010037, doi:10.3390/geosciences9010037.

Koskinas, A., Tegos, A., Tsira, P., Dimitriadis, P., Iliopoulou, T., Papanicolaou, P., Koutsoyiannis, D., Williamson, T., 2023. Insights into the oroville dam 2017 spillway incident. Geosciences 9, 37. URL: https://www.nrcs.usda.gov/sites/default/files/2023-05/Final_Temperature_Correction_Study05262023.pdf.

Kuller, M., Schoenholzer, K., Lienert, J., 2021. Creating effective flood warnings: A framework from a critical review. Journal of Hydrology 602, 126708. URL: https://doi.org/10.1016/j.jhydrol.2021.126708, doi:10.1016/j.jhydrol.2021.126708.

Lambrecht, K., Hatchett, B.J., VanderMolen, K., Feldkircher, B., 2021. Identifying community values related to heat: recommendations for forecast and health risk communication. Geoscience Communication 4, 517–525. URL: https://doi.org/10.5194/gc-4-517-2021, doi:10.5194/gc-4-517-2021.

Lambrecht, K.M., Hatchett, B.J., Walsh, L.C., Collins, M., Tolby, Z., 2019. Improving visual communication of weather forecasts with rhetoric. Bulletin of the American Meteorological Society 100, 557–563. URL: https://doi.org/10.1175/bams-d-18-0186.1, doi:10.1175/bams-d-18-0186.1.

LeClerc, J., Joslyn, S., 2012. Odds ratio forecasts increase precautionary action for extreme weather events. Weather, Climate, and Society 4, 263–270. URL: https://doi.org/10.1175/wcas-d-12-00013.1, doi:10.1175/wcas-d-12-00013.1.

LeClerc, J., Joslyn, S., 2015. The cry wolf effect and weather-related decision making. Risk Analysis 35, 385–395. URL: https://doi.org/10.1111/risa.12336, doi:10.1111/risa.12336.

Lenhardt, E.D., Cross, R.N., Krocak, M.J., Ripberger, J.T., Ernst, S.R., Silva, C.L., Jenkins, H.C., 2020. How likely is that chance of thunderstorms? a study of how national weather service forecast offices use words of estimative probability and what they mean to the public. Journal of Operational Meteorology , 64–78URL: https://doi.org/10.15191/nwajom.2020.0805, doi:10.15191/nwajom.2020.0805.

Leonard, D., 2023. Heavy rains to hit snow-covered california, fueling worries of flooding - the washington post. https://www.washingtonpost.com/weather/2023/03/09/california-snow-rain-floods-atmospheric-river/. (Accessed on 07/17/2023).

Ligare, S.T., Viers, J.H., Null, S.E., Rheinheimer, D.E., Mount, J.F., 2011. NON-UNIFORM CHANGES TO WHITEWATER RECREATION IN CALIFORNIA's SIERRA NEVADA FROM REGIONAL CLIMATE WARMING. River Research and Applications 28, 1299–1311. URL: https://doi.org/10.1002/rra.1522, doi:10.1002/rra.1522.

Lipkus, I.M., Hollands, J.G., 1999. The Visual Communication of Risk . JNCI Monographs 1999, 149–163. URL: https://doi.org/10.1093/oxfordjournals.jncimonographs.a024191, doi:10.1093/oxfordjournals.jncimonographs.a024191.

Losee, J.E., Joslyn, S., 2018. The need to trust: How features of the forecasted weather influence forecast trust. International Journal of Disaster Risk Reduction 30, 95–104. URL: https://doi.org/10.1016/j.ijdrr.2018.02.032, doi:10.1016/j.ijdrr.2018.02.032.

Lowry, D.A., Glahn, H.R., 1976. An operational model for forecasting probability of precipitation—PEATMOS PoP. Monthly Weather Review 104, 221–232. URL: https://doi.org/10.1175/1520-0493(1976)104<0221:aomffp>2.0.co;2, doi:10.1175/1520-0493(1976)104<0221:aomffp>2.0.co;2.

Lynn, E., Cuthbertson, A., He, M., Vasquez, J.P., Anderson, M.L., Coombe, P., Abatzoglou, J.T., Hatchett, B.J., 2020. Technical note: Precipitation-phase partitioning at landscape scales to regional scales. Hydrology and Earth System Sciences 24, 5317–5328. URL: https://doi.org/10.5194/hess-24-5317-2020, doi:10.5194/hess-24-5317-2020.

Malamed, C., 2015. Visual design solutions: Principles and creative inspiration for learning professionals. John Wiley & Sons.

Marks, D., Kimball, J., Tingey, D., Link, T., 1998. The sensitivity of snowmelt processes to climate conditions and forest cover during rain-on-snow: a case study of the 1996 pacific northwest flood. Hydrological Processes 12, 1569–1587. URL: https://doi.org/10.1002/(sici)1099-1085(199808/09)12:10/11<1569::aid-hyp682>3.0.co;2-l, doi:10.1002/(sici)1099-1085(199808/09)12:10/11<1569::aid-hyp682>3.0.co;2-l.

Marks, D., Link, T., Winstral, A., Garen, D., 2001. Simulating snowmelt processes during rain-on-snow over a semi-arid mountain basin. Annals of Glaciology 32, 195–202. URL: https://doi.org/10.3189/172756401781819751, doi:10.3189/172756401781819751.

Marsh, P., 1987. Grain growth in a wet arctic snow cover. Cold Regions Science and Technology 14, 23–31. URL: https://doi.org/10.1016/0165-232x(87)90041-3, doi:10.1016/0165-232x(87)90041-3.

Marsh, P., 1999. Snowcover formation and melt: recent advances and future prospects. Hydrological Processes 13, 2117–2134. URL: https://doi.org/10.1002/(sici)1099-1085(199910)13:14/15<2117::aid-hyp869>3.0.co;2-9, doi:10.1002/(sici)1099-1085(199910)13:14/15<2117::aid-hyp869>3.0.co;2-9.

Marsh, P., Woo, M.K., 1984a. Wetting front advance and freezing of meltwater within a snow cover: 1. observations in the canadian arctic. Water Resources Research 20, 1853–1864. URL: https://doi.org/10.1029/wr020i012p01853, doi:10.1029/wr020i012p01853.

Marsh, P., Woo, M.K., 1984b. Wetting front advance and freezing of meltwater within a snow cover: 2. a simulation model. Water Resources Research 20, 1865–1874. URL: https://doi.org/10.1029/wr020i012p01865, doi:10.1029/wr020i012p01865.

Mazurkiewicz, A.B., Callery, D.G., McDonnell, J.J., 2008. Assessing the controls of the snow energy balance and water available for runoff in a rain-on-snow environment. Journal of Hydrology 354, 1–14. URL: https://doi.org/10.1016/j.jhydrol.2007.12.027, doi:10.1016/j.jhydrol.2007.12.027.

McCabe, G.J., Clark, M.P., Hay, L.E., 2007. Rain-on-snow events in the western united states. Bulletin of the American Meteorological Society 88, 319–328. URL: https://doi.org/10.1175/bams-88-3-319, doi:10.1175/bams-88-3-319.

Mcgee, M., 2012. Neurodiversity. Contexts 11, 12–13. URL: https://doi.org/10.1177/1536504212456175, doi:10.1177/1536504212456175.

McGurk, B., Azuma, D., Kattelmann, R., 1988. Density of new snow in the central sierra nevada, in: Proceedings 56th Western Snow Conference, pp. 71–80.

McGurk, B.J., 1986. Precipitation and snow water equivalent sensors: an evaluation URL: sites/westernsnowconference.org/PDFs/1986McGurk.pdf.

Mesinger, F., DiMego, G., Kalnay, E., Mitchell, K., Shafran, P.C., Ebisuzaki, W., Jović, D., Woollen, J., Rogers, E., Berbery, E.H., Ek, M.B., Fan, Y., Grumbine, R., Higgins, W., Li, H., Lin, Y., Manikin, G., Parrish, D., Shi, W., 2006. North american regional reanalysis. Bulletin of the American Meteorological Society 87, 343–360. URL: https://journals.ametsoc.org/view/journals/bams/87/3/bams-87-3-343.xml, doi:10.1175/BAMS-87-3-343.

Miran, S.M., Ling, C., Gerard, A., Rothfusz, L., 2019. Effect of providing the uncertainty information about a tornado occurrence on the weather recipients' cognition and protective action: Probabilistic hazard information versus deterministic warnings. Risk Analysis URL: https://doi.org/10.1111/risa.13289, doi:10.1111/risa.13289.

Morss, R.E., Demuth, J.L., Lazo, J.K., 2008. Communicating uncertainty in weather forecasts: A survey of the u.s. public. Weather and Forecasting 23, 974–991. URL: https://doi.org/10.1175/2008waf2007088.1, doi:10.1175/2008waf2007088.1.

Morss, R.E., Lazo, J.K., Demuth, J.L., 2010. Examining the use of weather forecasts in decision scenarios: results from a US survey with implications for uncertainty communication. Meteorological Applications 17, 149–162. URL: https://doi.org/10.1002/met.196, doi:10.1002/met.196.

Motulsky, A., Deeb, S., 2001. Color vision and its genetic defects. The metabolic and molecular bases of inherited disease 4, 5955–5976.

Murchie, K.J., Diomede, D., 2020. Fundamentals of graphic design—essential tools for effective visual science communication. FACETS 5, 409–422. URL: https://doi.org/10.1139/facets-2018-0049, doi:10.1139/facets-2018-0049.

Murphy, A.H., 1993. What is a good forecast? an essay on the nature of goodness in weather forecasting. Weather and Forecasting 8, 281–293. URL: https://doi.org/10.1175/1520-0434(1993)008<0281:wiagfa>2.0.co;2, doi:10.1175/1520-0434(1993)008<0281:wiagfa>2.0.co;2.

Musselman, K.N., Addor, N., Vano, J.A., Molotch, N.P., 2021. Winter melt trends portend widespread declines in snow water resources. Nature Climate Change 11, 418–424. URL: https://doi.org/10.1038/s41558-021-01014-9, doi:10.1038/s41558-021-01014-9.

Musselman, K.N., Clark, M.P., Liu, C., Ikeda, K., Rasmussen, R., 2017. Slower snowmelt in a warmer world. Nature Climate Change 7, 214–219. URL: https://doi.org/10.1038/nclimate3225, doi:10.1038/nclimate3225.

Musselman, K.N., Lehner, F., Ikeda, K., Clark, M.P., Prein, A.F., Liu, C., Barlage, M., Rasmussen, R., 2018. Projected increases and shifts in rain-on-snow flood risk over western north america. Nature Climate Change 8, 808–812. URL: https://doi.org/10.1038/s41558-018-0236-4, doi:10.1038/s41558-018-0236-4.

Nadav-Greenberg, L., Joslyn, S.L., 2009. Uncertainty forecasts improve decision making among nonexperts. Journal of Cognitive Engineering and Decision Making 3, 209–227. URL: https://doi.org/10.1518/155534309x474460, doi:10.1518/155534309x474460.

National Weather Service, N., 2022. Advancing IDSS Through Probabilities: FY22 Western Region Goals & Guidance. Technical Report. National Weather Service Western Regional Headquarters.

Nauslar, N.J., Hatchett, B.J., 2018. Dry thunderstorms, in: Encyclopedia of Wildfires and Wildland-Urban Interface (WUI) Fires. Springer International Publishing, pp. 1–10. URL: https://doi.org/10.1007/978-3-319-51727-8_176-1, doi:10.1007/978-3-319-51727-8_176-1.

Nersesian, S., Vitkin, N., Grantham, S., Bourgaize, S., 2020. Illustrating your research: design basics for junior clinicians and scientists. bmj 370.

NOAA, 2020. NOAA Research and Develoment Vision Areas: 2020-2026. Technical Report. URL: https://www.weather.gov/media/wrn/NWS_Weather-Ready-Nation_Strategic_Plan_2019-2022.pdf.

Norbiato, D., Borga, M., Degli Esposti, S., Gaume, E., Anquetin, S., 2008. Flash flood warning based on rainfall thresholds and soil moisture conditions: An assessment for gauged and ungauged basins. Journal of Hydrology 362, 274–290. doi:10.1016/j.jhydrol.2008.08.023.

Novak, D.R., Perfater, S.E., Demuth, J.L., Bieda, S.W., Carbin, G., Craven, J., Erickson, M.J., Jeglum, M.E., Kastman, J., Nelson, J.A., Rudack, D.E., Staudenmaier, M.J., Waldstreicher, J.S., 2023. Innovations in winter storm forecasting and decision support services. Bulletin of the American Meteorological Society 104, E715–E735. URL: https://doi.org/10.1175/bams-d-22-0065.1, doi:10.1175/bams-d-22-0065.1.

NRCS, 2014. Part 622 snow survey and water supply forecasting. National Engineering Handbook 210–VI–NEH. URL: https://directives.sc.egov.usda.gov/viewerFS.aspx?hid=32040.

NRCS, 2023. Snowpack telemetry network (snotel). URL: https://www.nrcs.usda.gov/wps/portal/wcc/home/quicklinks/imap#version=167&elements=&networks=!&states=!&counties=!&hucs=&minElevation=&maxElevation=&elementSelectType=any&activeOnly=true&activeForecastPointsOnly=false&hucLabels=false&hucIdLabels=false&hucParameterLabels=true&stationLabels=&overlays=&hucOverlays=2&basinOpacity=75&basinNoDataOpacity=25&basemapOpacity=100&maskOpacity=0&mode=data&openSections=dataElement,parameter,date,basin,options,elements,location,networks&controlsOpen=true&popup=&popupMulti=&popupBasin=&base=esriNgwm&displayType=station&basinType=6&dataElement=WTEQ&depth=-8&param

eter=PCTMED&frequency=DAILY&duration=I&customDuration=&dayPart=E&year=2023&month=5&day=29&monthPart=E&forecastPubMonth=5&forecastPubDay=1&forecastExceedance=50&useMixedPast=true&seqColor=1&divColor=7&scaleType=D&scaleMin=&scaleMax=&referencePeriodType=POR&referenceBegin=1991&referenceEnd=2020&minimumYears=20&hucAssociations=true&lat=40.00&lon=-99.00&zoom=4.0.

NWS, 2023. Mar23_nws_renoclimatereport. https://www.weather.gov/media/rev/Hydro/NWS_Reno_ClimateReportMar23.pdf. (Accessed on 07/17/2023).

Oakley, N.S., Lancaster, J.T., Hatchett, B.J., Stock, J., Ralph, F.M., Roj, S., Lukashov, S., 2018. A 22-year climatology of cool season hourly precipitation thresholds conducive to shallow landslides in california. Earth Interactions 22, 1–35. URL: https://journals.ametsoc.org/view/journals/eint/22/14/ei-d-17-0029.1.xml, doi:10.1175/EI-D-17-0029.1.

Oakley, N.S., Lancaster, J.T., Kaplan, M.L., Ralph, F.M., 2017. Synoptic conditions associated with cool season post-fire debris flows in the transverse ranges of southern california. Natural Hazards 88, 327–354. URL: https://doi.org/10.1007/s11069-017-2867-6, doi:10.1007/s11069-017-2867-6.

Oakley, N.S., Liu, T., McGuire, L.A., Simpson, M., Hatchett, B.J., Tardy, A., Kean, J.W., Castellano, C., Laber, J.L., Steinhoff, D., 2023. Toward probabilistic post-fire debris-flow hazard decision support. Bulletin of the American Meteorological Society URL: https://doi.org/10.1175/bams-d-22-0188.1, doi:10.1175/bams-d-22-0188.1.

National Oceanic, Atmospheric Administration, 2022. NOAA Weather, Water, and Climate Strategy FY 2023-2027. Technical Report. URL: https://www.noaa.gov/sites/default/files/2022-12/NOAA-FY23-27-Weather-Water-and-Climate-Strategy-12092022.pdf.

OECD, 2012. OECD Environmental Outlook to 2050. URL: https://www.oecd-ilibrary.org/content/publication/9789264122246-en, doi:https://doi.org/https://doi.org/10.1787/9789264122246-en.

O'Hara, B.F., Kaplan, M.L., Underwood, S.J., 2009. Synoptic climatological analyses of extreme snowfalls in the sierra nevada. Weather and Forecasting 24, 1610–1624. doi:10.1175/2009WAF2222249.1.

Osterhuber, R., 2009. URL: https://www.sierracollege.edu/ejournals/jscnhm/v2n1/climatesummary.html.

Osterhuber, R., Schwartz, A., 2021. Snowpack, precipitation, and temperature measurements at the central sierra snow laboratory for water years 1971 to 2019. URL: http://datadryad.org/stash/dataset/doi:10.6078/D1941T, doi:10.6078/D1941T.

Padilla, L., Dryhurst, S., Hosseinpour, H., Kruczkiewicz, A., 2021. Multiple hazard uncertainty visualization challenges and paths forward. Frontiers in Psychology 12. URL: https://doi.org/10.3389/fpsyg.2021.579207, doi:10.3389/fpsyg.2021.579207.

Painter, T.H., Skiles, S.M., Deems, J.S., Bryant, A.C., Landry, C.C., 2012. Dust radiative forcing in snow of the upper colorado river basin: 1. a 6 year record of energy balance, radiation, and dust concentrations. Water Resources Research 48. URL: https://doi.org/10.1029/2012wr011985, doi:10.1029/2012wr011985.

Palmer, T.N., 2002. The economic value of ensemble forecasts as a tool for risk assessment: From days to decades. Quarterly Journal of the Royal Meteorological Society 128, 747–774. URL: https://doi.org/10.1256/0035900021643593, doi:10.1256/0035900021643593.

Pappenberger, F., Stephens, E., Thielen, J., Salamon, P., Demeritt, D., van Andel, S.J., Wetterhall, F., Alfieri, L., 2012. Visualizing probabilistic flood forecast information: expert preferences and perceptions of best practice in uncertainty communication. Hydrological Processes 27, 132–146. URL: https://doi.org/10.1002/hyp.9253, doi:10.1002/hyp.9253.

Pedregosa, F., Varoquaux, G., Gramfort, A., Michel, V., Thirion, B., Grisel, O., Blondel, M., Prettenhofer, P., Weiss, R., Dubourg, V., Vanderplas, J., Passos, A., Cournapeau, D., Brucher, M., Perrot, M., Duchesnay, E., 2011. Scikit-learn: Machine learning in Python. Journal of Machine Learning Research 12, 2825–2830.

Peterson, C.J., 2000. Catastrophic wind damage to north american forests and the potential impact of climate change. Science of The Total Environment 262, 287–311. URL: https://doi.org/10.1016/s0048-9697(00)00529-5, doi:10.1016/s0048-9697(00)00529-5.

Poulin, R., 2017. Design school: Type. Design School, Rockport, Beverly, MA.

Poulin, R., 2018. Design school: Layout. Rockport, Beverly, MA.

Prince, H.D., Gibson, P.B., DeFlorio, M.J., Corringham, T.W., Cobb, A., Guan, B., Ralph, F.M., Waliser, D.E., 2021. Genesis locations of the costliest atmospheric rivers impacting the western united states. Geophysical Research Letters 48, e2021GL093947. doi:https://doi.org/10.1029/2021GL093947.

Ralph, F.F., Dettinger, M., White, A., Reynolds, D., Cayan, D., Schneider, T., Cifelli, R., Redmond, K., Anderson, M., Gherke, F., Jones, J., Mahoney, K., Johnson, L., Gutman, S., Chandrasekar, V., Lundquist, J., Molotch, N., Brekke, L., Pulwarty, R., Horel, J., Schick, L., Edman, A., Mote, P., Abatzoglou, J., Pierce, R., Wick, G., Diego, S., 2014. A vision for future observations for western u.s. extreme precipitation and flooding. Journal of Contemporary Water Research & Education 153, 16–32. doi:10.1111/j.1936-704x.2014.03176.x.

Ralph, F.M., Coleman, T., Neiman, P.J., Zamora, R.J., Dettinger, M.D., 2013. Observed impacts of duration and seasonality of atmospheric-river landfalls on soil moisture and runoff in coastal northern california. Journal of Hydrometeorology 14, 443–459. URL: https://journals.ametsoc.org/view/journals/hydr/14/2/jhm-d-12-076_1.xml, doi:10.1175/JHM-D-12-076.1.

Ralph, F.M., Rutz, J.J., Cordeira, J.M., Dettinger, M., Anderson, M., Reynolds, D., Schick, L.J., Smallcomb, C., 2019. A scale to characterize the strength and impacts of atmospheric

rivers. Bulletin of the American Meteorological Society 100, 269–289. doi:10.1175/bams-d-18-0023.1.

Rello, L., Baeza-Yates, R., 2013. Good fonts for dyslexia, in: Proceedings of the 15th International ACM SIGACCESS Conference on Computers and Accessibility, ACM. URL: https://doi.org/10.1145/2513383.2513447, doi:10.1145/2513383.2513447.

Rello, L., Pielot, M., Marcos, M.C., 2016. Make it big!, in: Proceedings of the 2016 CHI Conference on Human Factors in Computing Systems, ACM. URL: https://doi.org/10.1145/2858036.2858204, doi:10.1145/2858036.2858204.

Ripberger, J., Bell, A., Fox, A., Forney, A., Livingston, W., Gaddie, C., Silva, C., Jenkins-Smith, H., 2022. Communicating probability information in weather forecasts: Findings and recommendations from a living systematic review of the research literature. Weather, Climate, and Society 14, 481–498. URL: https://doi.org/10.1175/wcas-d-21-0034.1, doi:10.1175/wcas-d-21-0034.1.

Rogowitz, B., Treinish, L., 1998. Data visualization: the end of the rainbow. IEEE Spectrum 35, 52–59. URL: https://doi.org/10.1109/6.736450, doi:10.1109/6.736450.

Rosen, Z., Henery, G., Slater, K.D., Sablan, O., Ford, B., Pierce, J.R., Fischer, E.V., Magzamen, S.L., 2023. A culture of fire: Identifying community risk perceptions surrounding prescribed burning in the flint hills, kansas. Journal of Applied Communications 106. URL: https://doi.org/10.4148/1051-0834.2455, doi:10.4148/1051-0834.2455.

Rosen, Z., Krocak, M.J., Ripberger, J.T., Cross, R., Lenhardt, E., Silva, C.L., Jenkins-Smith, H.C., 2021. Communicating probability information in hurricane forecasts: Assessing statements that forecasters use on social media and implications for public assessments of reliability. Journal of Operational Meteorology , 89–101URL: https://doi.org/10.15191/nwajom.2021.0907, doi:10.15191/nwajom.2021.0907.

Rössler, O., Froidevaux, P., Börst, U., Rickli, R., Martius, O., Weingartner, R., 2014. Retrospective analysis of a nonforecasted rain-on-snow flood in the alps-a matter of model limitations or unpredictable nature? Hydrology and Earth System Sciences 18, 2265–2285. URL: https://www.hydrol-earth-syst-sci.net/18/2265/2014/, doi:10.5194/hess-18-2265-2014.

Rothfusz, L.P., Karstens, C., Hilderband, D., 2014. Next-generation severe weather forecasting and communication. Eos, Transactions American Geophysical Union 95, 325–326. URL: https://agupubs.onlinelibrary.wiley.com/doi/abs/10.1002/2014EO360001, doi:https://doi.org/10.1002/2014EO360001, arXiv:https://agupubs.onlinelibrary.wiley.com/doi/pdf/10.1002/2014EO360001.

Samara, T., 2020. Design Elements: Understanding the rules and knowing when to break them-A Visual Communication Manual. Rockport publishers.

Sattler, B., Lippy, B., Jordan, T., 1997. Hazard communication: A review of the science underpinning the art of communication for health and safety .

Savelli, S., Joslyn, S., 2012. Boater safety: Communicating weather forecast information to high-stakes end users. Weather, Climate, and Society 4, 7–19. URL: https://doi.org/10.1175/wcas-d-11-00025.1, doi:10.1175/wcas-d-11-00025.1.

Savelli, S., Joslyn, S., 2013. The advantages of predictive interval forecasts for non-expert users and the impact of visualizations. Applied Cognitive Psychology 27, 527–541. URL: https://doi.org/10.1002/acp.2932, doi:10.1002/acp.2932.

Schneebeli, M., 1995. Development and stability of preferential flow paths in a layered snowpack. IAHS Publications-Series of Proceedings and Reports-Intern Assoc Hydrological Sciences 228, 89–96.

Schumacher, P.N., Deitsch, K., Demuth, J.L., Fowle, M., Gagan, J., Graham, R.A., Greif, C., Just, A., Nutter, P., Serr, K., et al., 2022. Using ensembles and probabilities to message winter weather hazards. URL: https://ams.confex.com/ams/102ANNUAL/meetingapp.cgi/Paper/394274.

Schumacher, P.N., Demuth, J.L., Foster, A., Fowle, M., Gagan, J., Graham, R.A., Greif, C., Just, A., Nutter, P., Smith, B., et al., 2021. Incorporating probabilistic information into winter storm services. URL: https://ams.confex.com/ams/101ANNUAL/meetingapp.cgi/Paper/381654.

Serreze, M.C., Clark, M.P., Armstrong, R.L., McGinnis, D.A., Pulwarty, R.S., 1999. Characteristics of the western united states snowpack from snowpack telemetry (snotel) data. Water Resources Research 35, 2145–2160. URL: https://agupubs.onlinelibrary.wiley.com/doi/abs/10.1029/1999WR900090, doi:10.1029/1999WR900090.

National Weather Service, 2017. How the national weather service leverages social media for severe weather. URL: https://www.weather.gov/wrn/summer-article-how-the-NWS-leverages-social-media.

National Weather Service, 2019a. Building a Weather-Ready Nation: 2019-2022 strategic plan. Technical Report. URL: https://www.weather.gov/media/wrn/NWS_Weather-Ready-Nation_Strategic_Plan_2019-2022.pdf.

National Weather Service, 2019b. NWS Directives 10-515 WFO Non-Precipitation Weather Products Specification. Technical Report. National Oceanic and Atmospheric Administration National Weather Service.

National Weather Service, 2022. National blend of models - mdl - virtual lab. URL: https://vlab.noaa.gov/web/mdl/nbm.

Sharpe, L.T., Stockman, A., Jägle, H., Nathans, J., 1999. Opsin genes, cone photopigments, color vision, and color blindness. Color vision: From genes to perception 351.

Siirila-Woodburn, E., Rhoades, A.M., Hatchett, B.J., Huning, L., Szinai, J., Tague, C., Nico, P.S., Feldman, D., Jones, A.D., Collins, W.D., Kaatz, L., 2021. A low-to-no snow future and its impacts on water resources in the western united states. Nature Reviews Earth and Environment 2, 800–819. doi:http://dx.doi.org/10.1038/s43017-021-00219-y.

Singh, P., Spitzbart, G., Hübl, H., Weinmeister, H.W., 1997. Hydrological response of snowpack under rain-on-snow events: A field study. Journal of Hydrology 202, 1–20. doi:10.1016/S0022-1694(97)00004-8.

Sivle, A.D., Kolstø, S.D., Hansen, P.J.K., Kristiansen, J., 2014. How do laypeople evaluate the degree of certainty in a weather report? a case study of the use of the web service yr.no. Weather, Climate, and Society 6, 399–412. URL: https://doi.org/10.1175/wcas-d-12-00054.1, doi:10.1175/wcas-d-12-00054.1.

Statham, G., Haegeli, P., Birkeland, K.W., Greene, E., Israelson, C., Tremper, B., Stethem, C., McMahon, B., White, B., Kelly, J., 2010. The north american public avalanche danger scale, in: 2010 International Snow Science Workshop, pp. 117–123.

Stauffer, R., Mayr, G.J., Dabernig, M., Zeileis, A., 2015. Somewhere over the rainbow: How to make effective use of colors in meteorological visualizations. Bulletin of the American Meteorological Society 96, 203–216. URL: https://doi.org/10.1175/bams-d-13-00155.1, doi:10.1175/bams-d-13-00155.1.

Steinschneider, S., Brown, C., 2012. Dynamic reservoir management with real-option risk hedging as a robust adaptation to nonstationary climate. Water Resources Research 48. URL: https://agupubs.onlinelibrary.wiley.com/doi/abs/10.1029/2011WR011540, doi:https://doi.org/10.1029/2011WR011540, arXiv:https://agupubs.onlinelibrary.wiley.com/doi/pdf/10.1029/2011WR011540.

Sterle, K., Hatchett, B.J., Singletary, L., Pohll, G., 2019. Hydroclimate variability in snow-fed river systems: Local water managers' perspectives on adapting to the new normal. Bulletin of the American Meteorological Society 100, 1031–1048. URL: http://journals.ametsoc.org/bams/article-pdf/100/6/1031/4834798/bams-d-18-0031{_}1.pdf, doi:10.1175/BAMS-D-18-0031.1.

Stone, T., AdamsMorioka, Adams, S., Morioka, N., 2008. Color Design Workbook: A Real World Guide to Using Color in Graphic Design. Rockport Publishers. URL: https://books.google.com/books?id=CjuLl_bNO9UC.

Sumargo, E., Wilson, A.M., Ralph, F.M., Weihs, R., White, A., Jasperse, J., Asgari-Lamjiri, M., Turnbull, S., Downer, C., Monache, L.D., 2020. The hydrometeorological observation network in california's russian river watershed: Development, characteristics, and key findings from 1997 to 2019. Bulletin of the American Meteorological Society 101, E1781 – E1800. URL: https://journals.ametsoc.org/view/journals/bams/101/10/bamsD190253.xml, doi:10.1175/BAMS-D-19-0253.1.

Sutcliffe, K., 2014. Soil moisture dynamics during snowmelt. URL: sites/westernsnowconference.org/PDFs/2014Sutcliffe.pdf.

Sutcliffe, K., Clayton, J., 2021. Editing soil moisture and soil temperature data at SNOTEL and SCAN sites. Technical Report.

Sutton, J., Kuligowski, E.D., 2019. Alerts and warnings on short messaging channels: Guidance from an expert panel process. Natural Hazards Review 20. URL: https://doi.org/10.1061/(asce)nh.1527-6996.0000324, doi:10.1061/(asce)nh.1527-6996.0000324.

Sweller, J., 2011. Cognitive load theory, in: Psychology of learning and motivation. Elsevier. volume 55, pp. 37–76.

Thomas, K.A., Williams, R.P., 1997. Flood of january 1997 in the carson river basin, california and nevada. URL: https://doi.org/10.3133/fs18397, doi:10.3133/fs18397.

Todhunter, P.E., 2011. Caveant admonitus ("let the forewarned beware"): The 1997 grand forks (usa) flood disaster. Disaster Prevention and Management: An International Journal 20, 125–139. URL: https://doi.org/10.1108/09653561111126076, doi:10.1108/09653561111126076.

Tondreau, B., 2019. Layout essentials revised and updated. Rockport, Beverly, MA.

Tripp, D.D., Trujillo-Falcón, J.E., Klockow-McClain, K.E., Reeves, H.D., Berry, K.L., Waldstreicher, J.S., Nelson, J.A., 2023. Foundational needs of forecasters for probabilistic winter forecasting. Weather and Forecasting 38, 3–15. URL: https://doi.org/10.1175/waf-d-22-0116.1, doi:10.1175/waf-d-22-0116.1.

Tufte, E., 1997. The visual display of quantitative information (1983). Graphics Press, Cheshire, Connecticut.

Uccellini, L.W., Ten Hoeve, J.E., 2019. Evolving the national weather service to build a weather-ready nation. Bulletin of the American Meteorological Society 100, 1923–1942. URL: http://journals.ametsoc.org/bams/article-pdf/100/10/1923/4871556/bams-d-18-0159{_}1.pdf, doi:10.1175/BAMS-D-18-0159.1.

Underwood, S.J., Kaplan, M.L., King, K.C., 2009. The role of upstream midtropospheric circulations in the sierra nevada enabling leeside (spillover) precipitation. part i: A synoptic-scale analysis of spillover precipitation and flooding in a leeside basin. Journal of Hydrometeorology 10, 1309–1326. URL: https://doi.org/10.1175/2009jhm1105.1, doi:10.1175/2009jhm1105.1.

USACE, U.A.C.o.E.S., 2013. Truckee meadows flood control project, nevada URL: https://www.spk.usace.army.mil/Portals/12/documents/civil_works/Truckee/Truckee_Meadows_Final_GRR_Dec2013.pdf.

USGS, U.G.S., 2022. National hydrography dataset (ver. usgs national hydrography dataset best resolution (nhd) for hydrologic unit (hu) 4 - 2001 (published 20191002). URL: https://www.usgs.gov/national-hydrography/access-national-hydrography-products.

VanderMolen, K., Kimutis, N., Hatchett, B.J., 2022. Recommendations for increasing the reach and effectiveness of heat risk education and warning messaging. International Journal of Disaster Risk Reduction 82, 103288. URL: https://doi.org/10.1016/j.ijdrr.2022.103288, doi:10.1016/j.ijdrr.2022.103288.

Vicuna, S., Leonardson, R., Hanemann, M.W., Dale, L.L., Dracup, J.A., 2008. Climate change impacts on high elevation hydropower generation in california's sierra nevada: a case study in the upper american river. Climatic Change 87, 123–137. URL: https://doi.org/10.1007/s10584-007-9365-x, doi:10.1007/s10584-007-9365-x.

Wernstedt, K., Roberts, P.S., Arvai, J., Redmond, K., 2018. How emergency managers (mis?)interpret forecasts. Disasters 43, 88–109. URL: https://doi.org/10.1111/disa.12293, doi:10.1111/disa.12293.

Wever, N., Fierz, C., Mitterer, C., Hirashima, H., Lehning, M., 2014a. Solving richards equation for snow improves snowpack meltwater runoff estimations in detailed multi-layer snowpack model. The Cryosphere 8, 257–274.

Wever, N., Jonas, T., Fierz, C., Lehning, M., 2014b. Model simulations of the modulating effect of the snow cover in a rain-on-snow event. Hydrology and Earth System Sciences 18, 4657–4669. URL: www.hydrol-earth-syst-sci.net/18/4657/2014/, doi:10.5194/hess-18-4657-2014.

Whitaker, A.C., Sugiyama, H., 2005. Seasonal snowpack dynamics and runoff in a cool temperate forest: lysimeter experiment in niigata, japan. Hydrological Processes 19, 4179–4200. URL: https://doi.org/10.1002/hyp.6059, doi:10.1002/hyp.6059.

White, A.B., Anderson, M.L., Dettinger, M.D., Ralph, F.M., Hinojosa, A., Cayan, D.R., Hartman, R.K., Reynolds, D.W., Johnson, L.E., Schneider, T.L., Cifelli, R., Toth, Z., Gutman, S.I., King, C.W., Gehrke, F., Johnston, P.E., Walls, C., Mann, D., Gottas, D.J., Coleman, T., 2013. A twenty-first-century california observing network for monitoring extreme weather events. Journal of Atmospheric and Oceanic Technology 30, 1585–1603. URL: https://journals.ametsoc.org/view/journals/atot/30/8/jtech-d-12-00217_1.xml, doi:10.1175/JTECH-D-12-00217.1.

White, A.B., Moore, B.J., Gottas, D.J., Neiman, P.J., 2019. Winter storm conditions leading to excessive runoff above california's oroville dam during january and february 2017. Bulletin of the American Meteorological Society 100, 55–70. URL: https://journals.ametsoc.org/view/journals/bams/100/1/bams-d-18-0091.1.xml, doi:10.1175/BAMS-D-18-0091.1.

Wilms, L., Oberfeld, D., 2017. Color and emotion: effects of hue, saturation, and brightness. Psychological Research 82, 896–914. URL: https://doi.org/10.1007/s00426-017-0880-8, doi:10.1007/s00426-017-0880-8.

Windschitl, P.D., Smith, A.R., Scherer, A.M., Suls, J., 2017. Risk it? direct and collateral impacts of peers' verbal expressions about hazard likelihoods. Thinking & Reasoning 23, 259–291. URL: https://doi.org/10.1080/13546783.2017.1307785, doi:10.1080/13546783.2017.1307785.

WMO, 2021. WMO Guidelines on Multi-hazard Impact-based Forecast and Warning Services Part II: Putting Multi-hazard into Practice. World Meteorological Organization, Geneva, Switzerland.

Wong, B., 2010. Points of view: Color coding. nature methods 7, 573.

Wong, B., 2011. Color blindness. nature methods 8, 441.

Yan, H., Sun, N., Wigmosta, M., Skaggs, R., Hou, Z., Leung, R., 2018. Next-generation intensity-duration-frequency curves for hydrologic design in snow-dominated environments. Water Resources Research 54, 1093–1108. doi:10.1002/2017WR021290.

Zabini, F., Grasso, V., Magno, R., Meneguzzo, F., Gozzini, B., 2014. Communication and interpretation of regional weather forecasts: a survey of the italian public. Meteorological Applications 22, 495–504. URL: https://doi.org/10.1002/met.1480, doi:10.1002/met.1480.

Zacks, J.M., Franconeri, S.L., 2020. Designing graphs for decision-makers. Policy Insights from the Behavioral and Brain Sciences 7, 52–63. URL: https://doi.org/10.1177/2372732219893712, doi:10.1177/2372732219893712.

Zhongming, Z., Linong, L., Xiaona, Y., Wangqiang, Z., Wei, L., et al., 2021. Wmo guidelines on multi-hazard impact-based forecast and warning services part ii putting multi-hazard ibfws into practice .

Appendix A

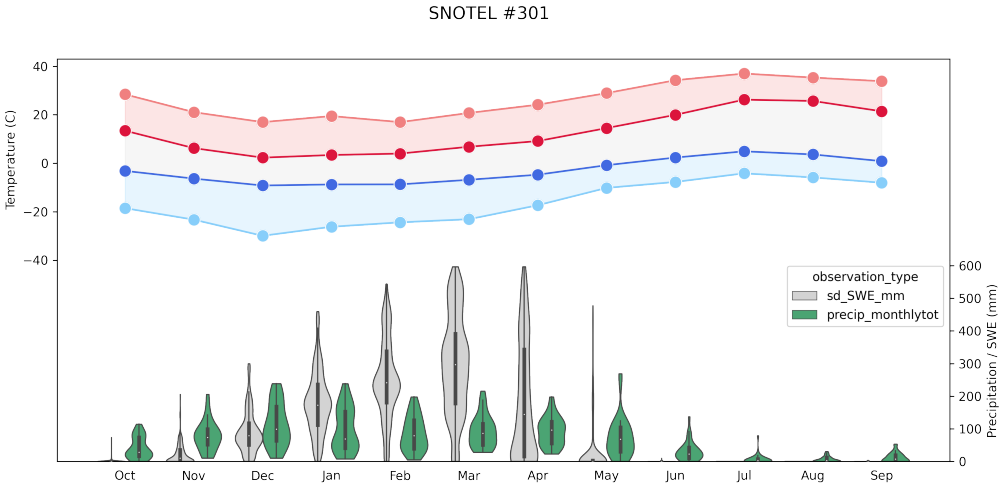

Figure 1: SNOTEL #301 Climatology.

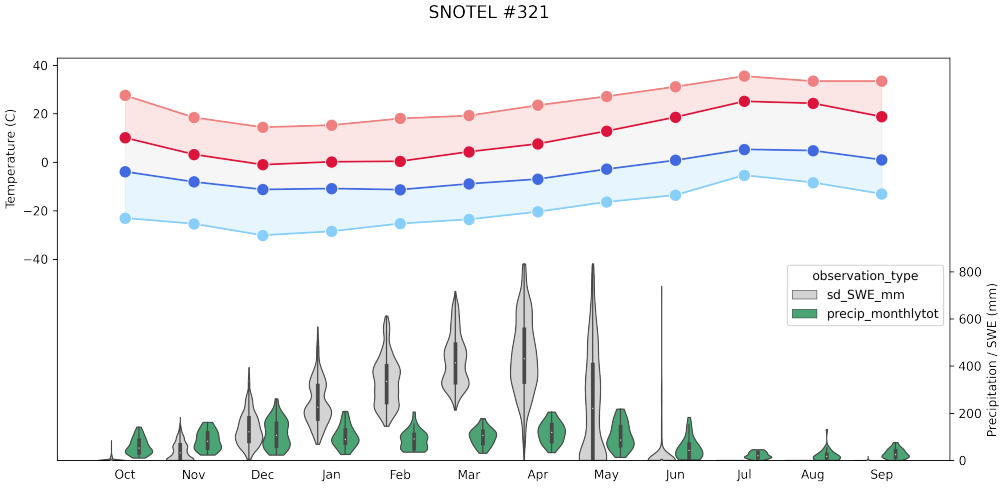

Figure 2: SNOTEL #321 Climatology.

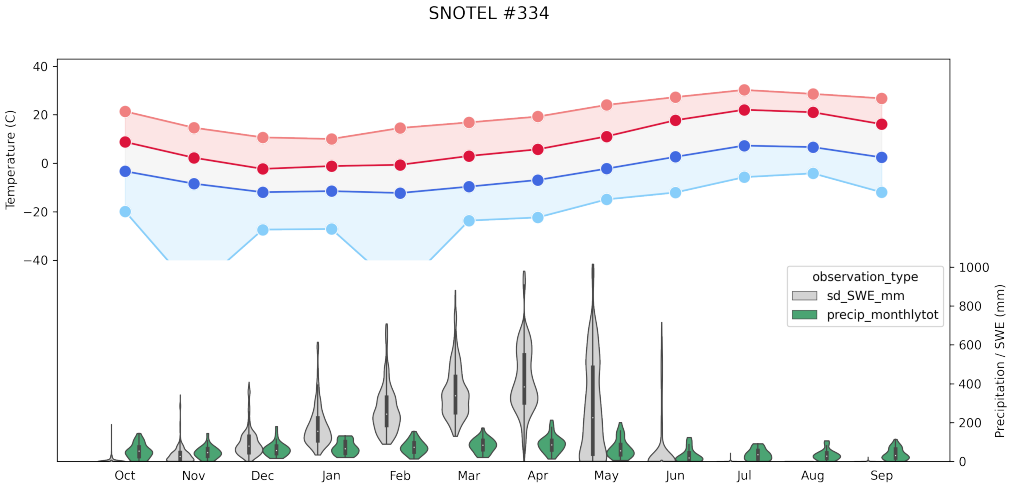

Figure 3: SNOTEL #334 Climatology.

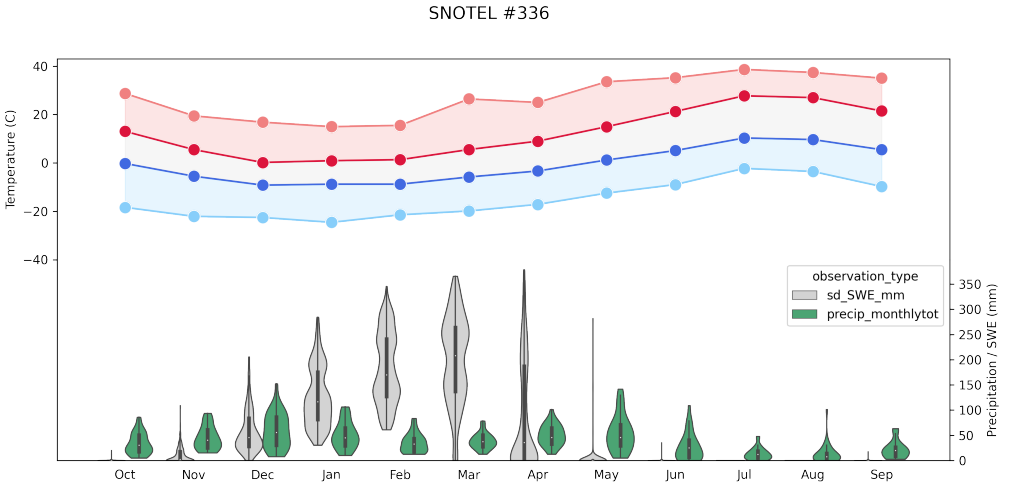

Figure 4: SNOTEL #336 Climatology.

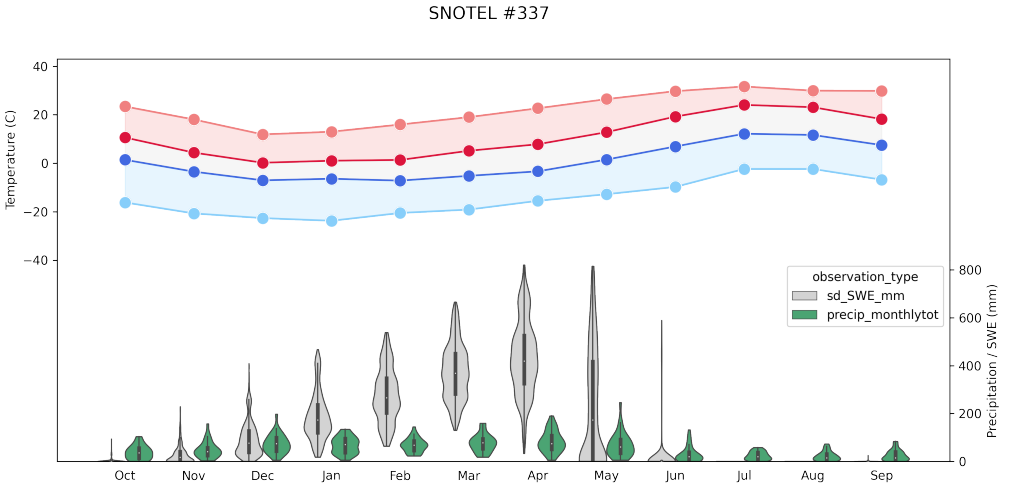

Figure 5: SNOTEL #337 Climatology.

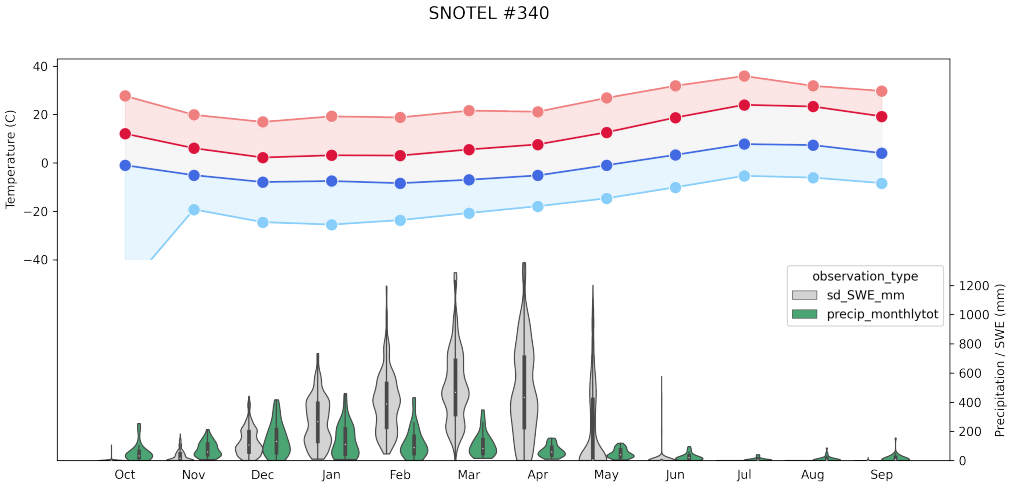

Figure 6: SNOTEL #340 Climatology.

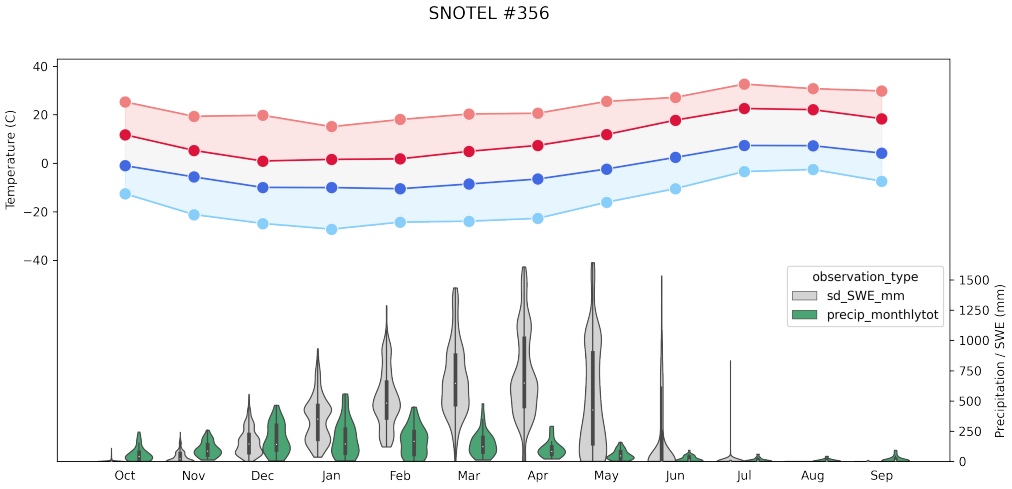

Figure 7: SNOTEL #356 Climatology.

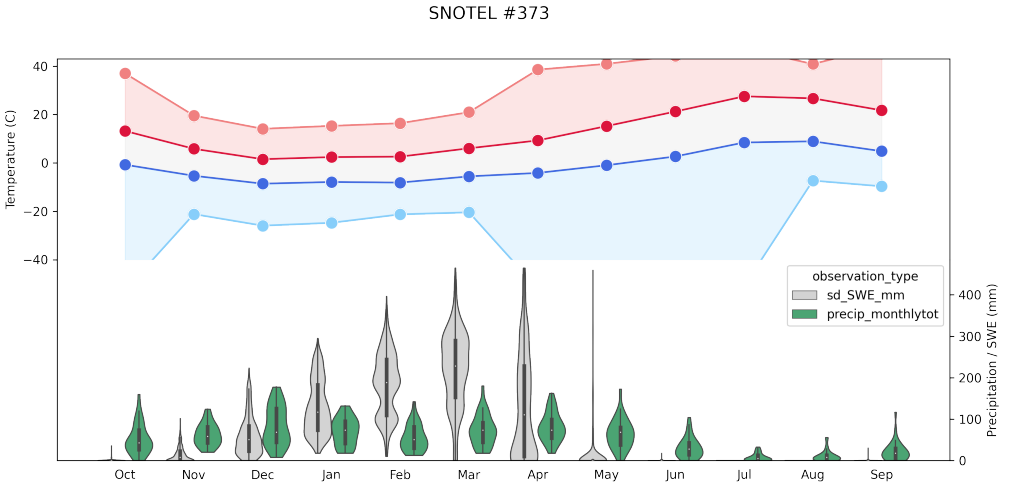

Figure 8: SNOTEL #373 Climatology.

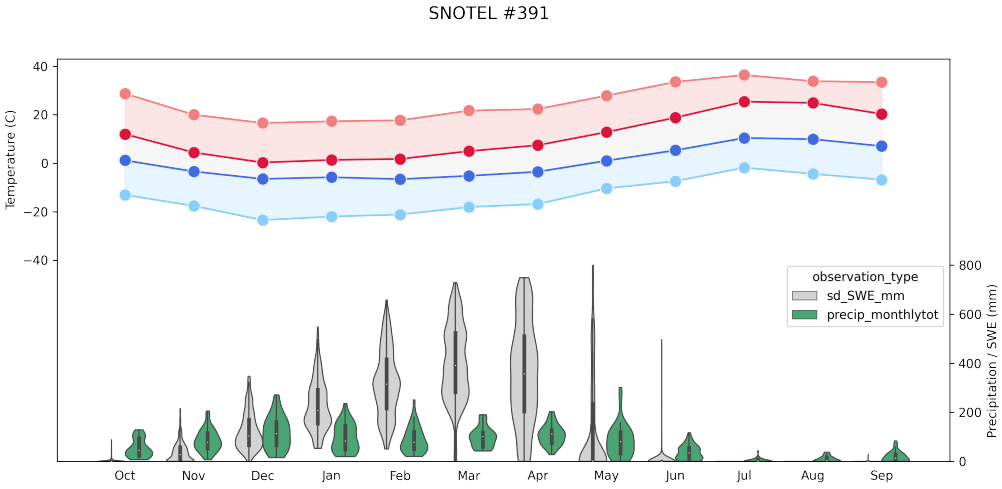

Figure 9: SNOTEL #391 Climatology.

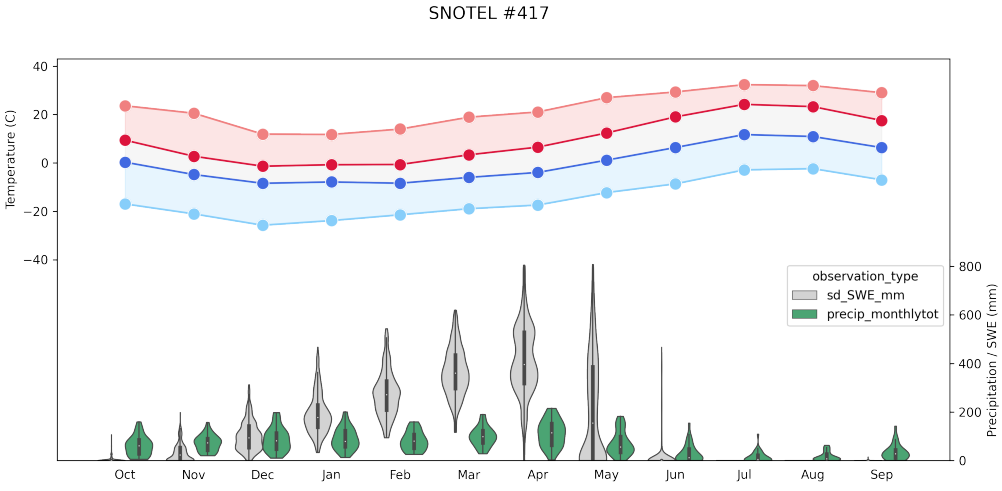

Figure 10: SNOTEL #417 Climatology.

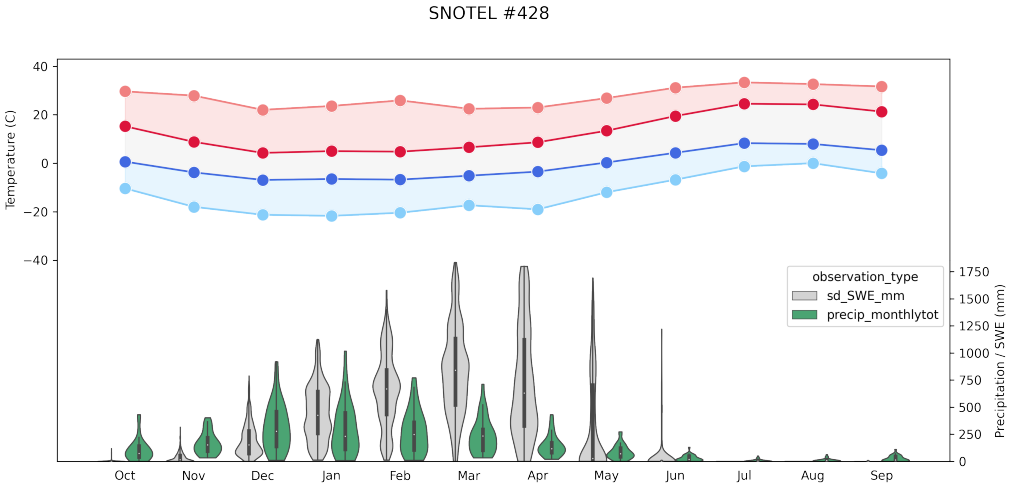

Figure 11: SNOTEL #428 Climatology.

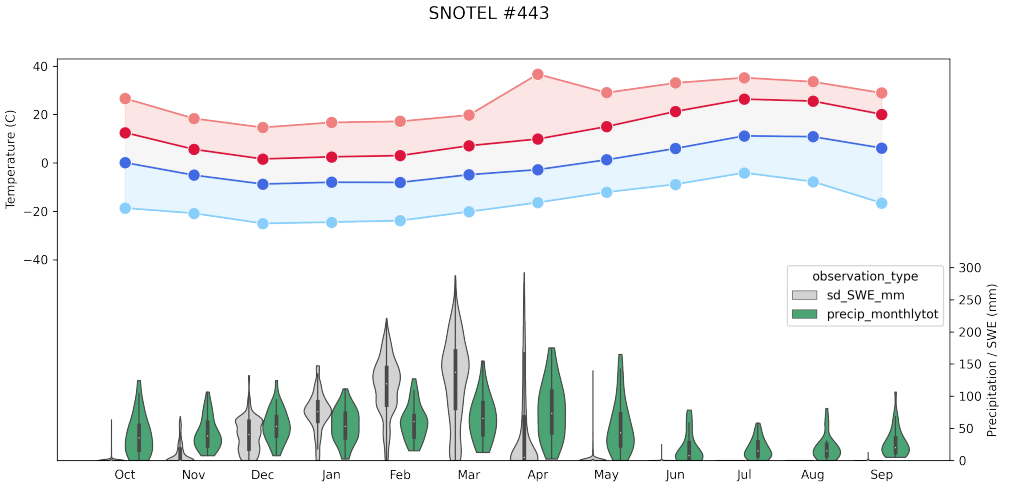

Figure 12: SNOTEL #443 Climatology.

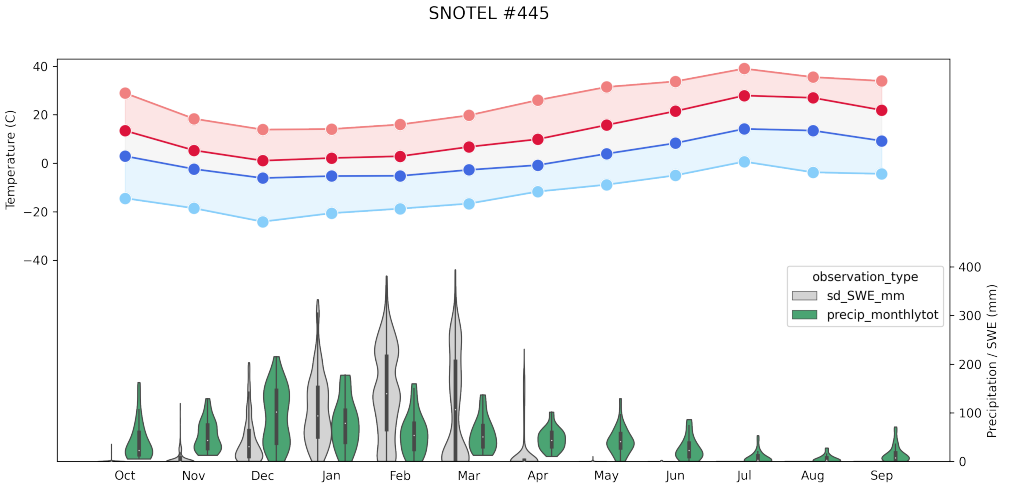

Figure 13: SNOTEL #445 Climatology.

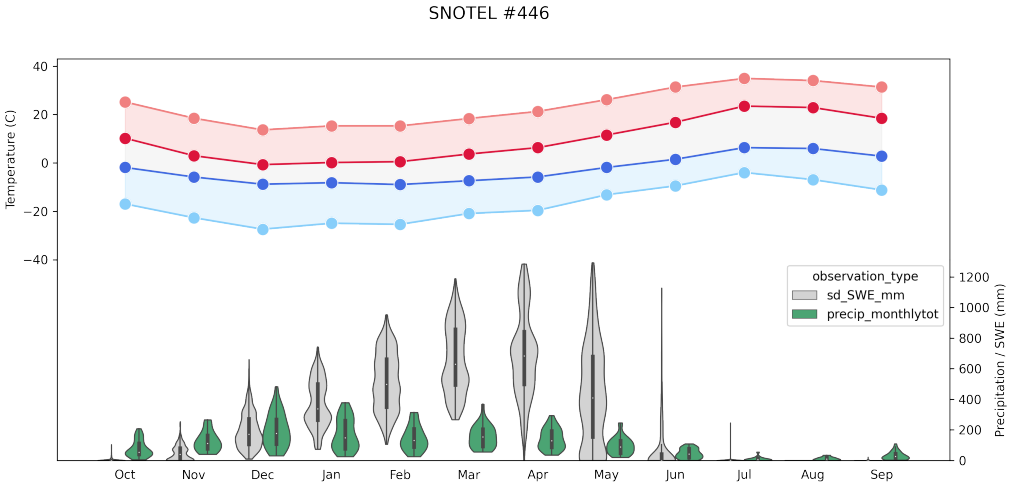

Figure 14: SNOTEL #446 Climatology.

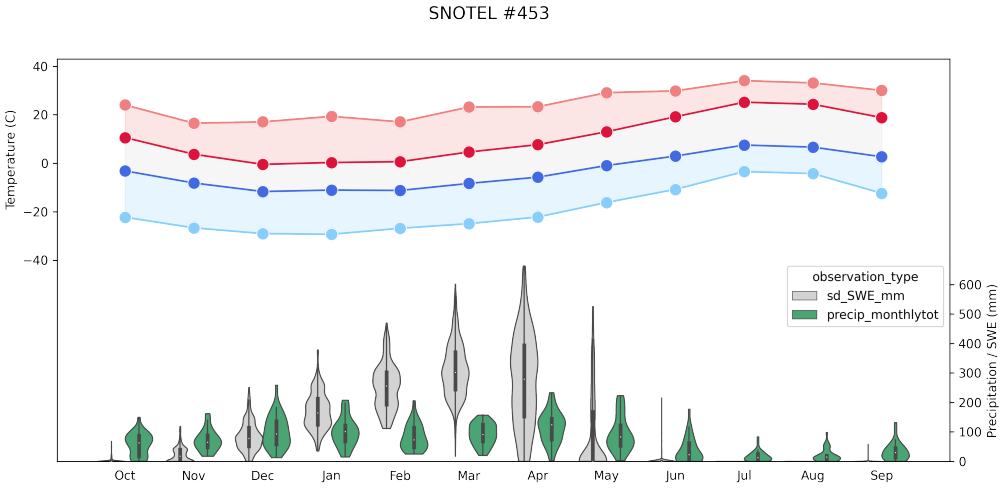

Figure 15: SNOTEL #453 Climatology.

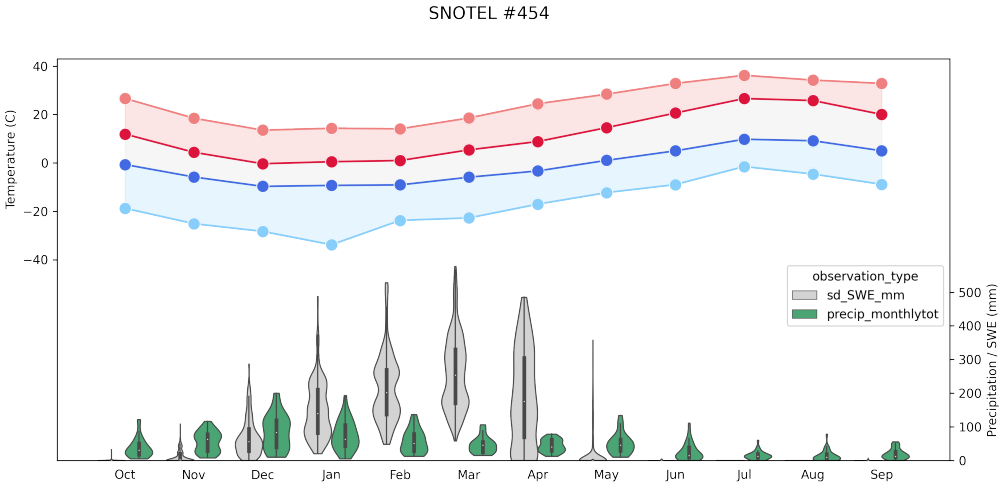

Figure 16: SNOTEL #454 Climatology.

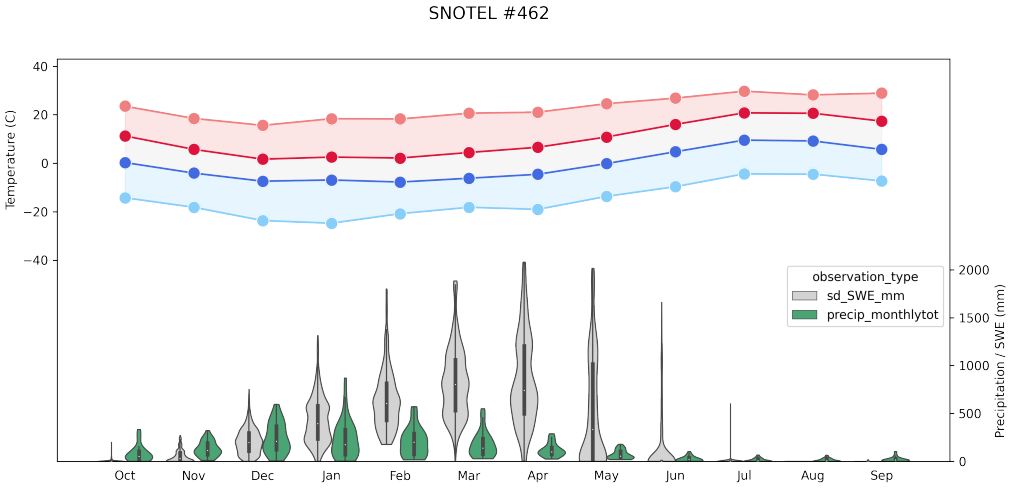

Figure 17: SNOTEL #462 Climatology.

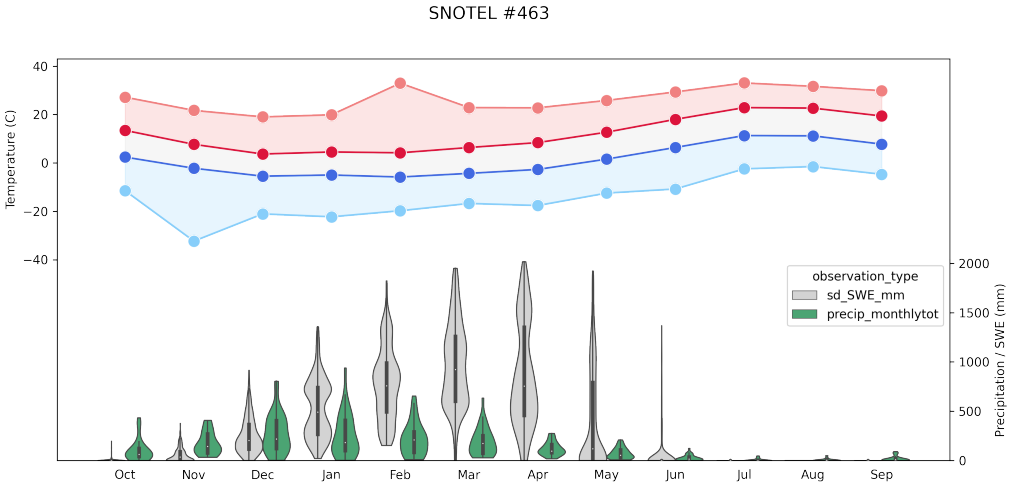

Figure 18: SNOTEL #463 Climatology.

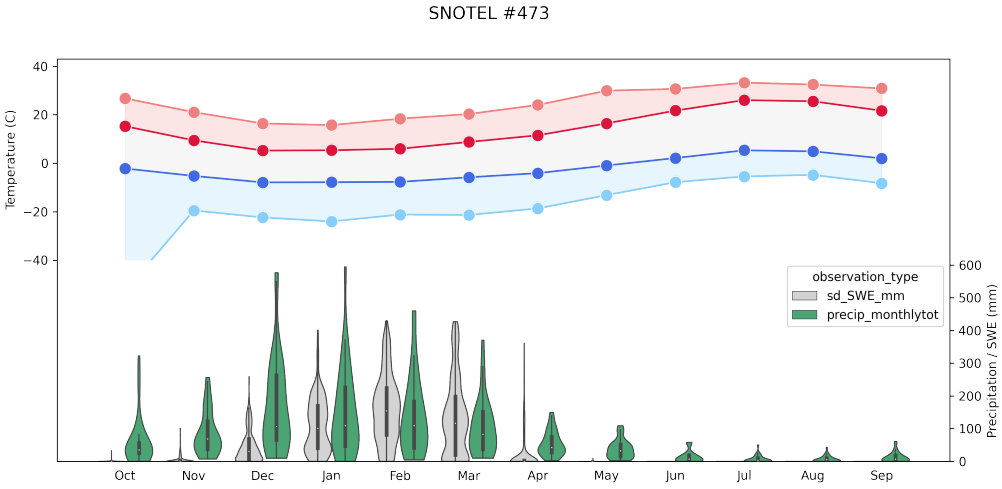

Figure 19: SNOTEL #473 Climatology.

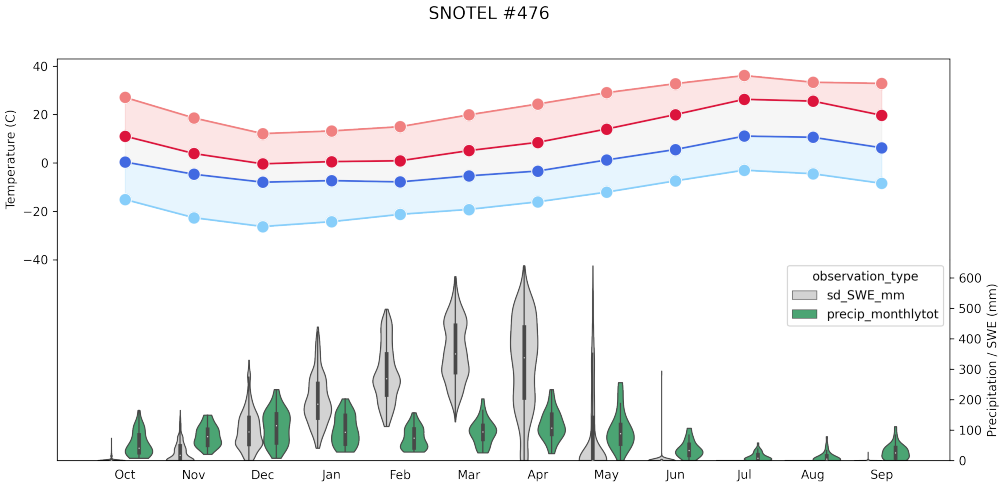

Figure 20: SNOTEL #476 Climatology.

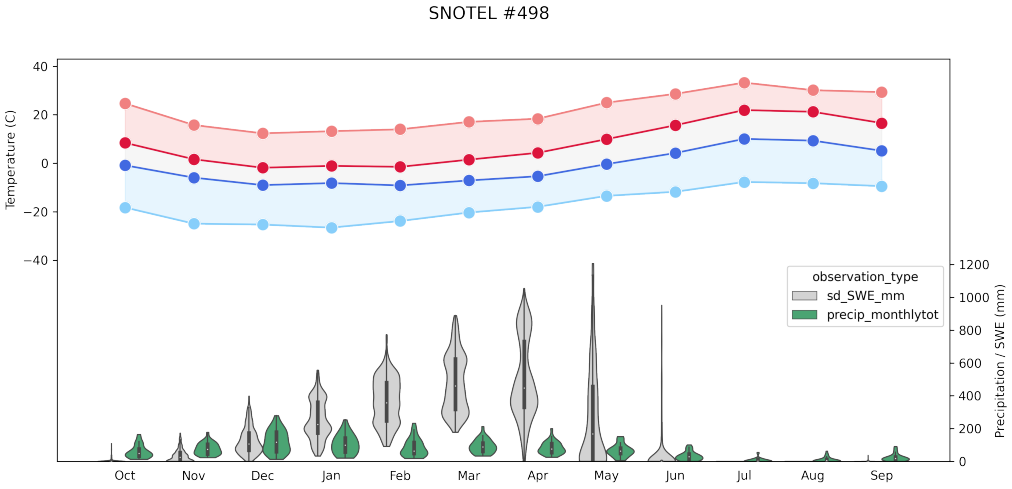

Figure 21: SNOTEL #498 Climatology.

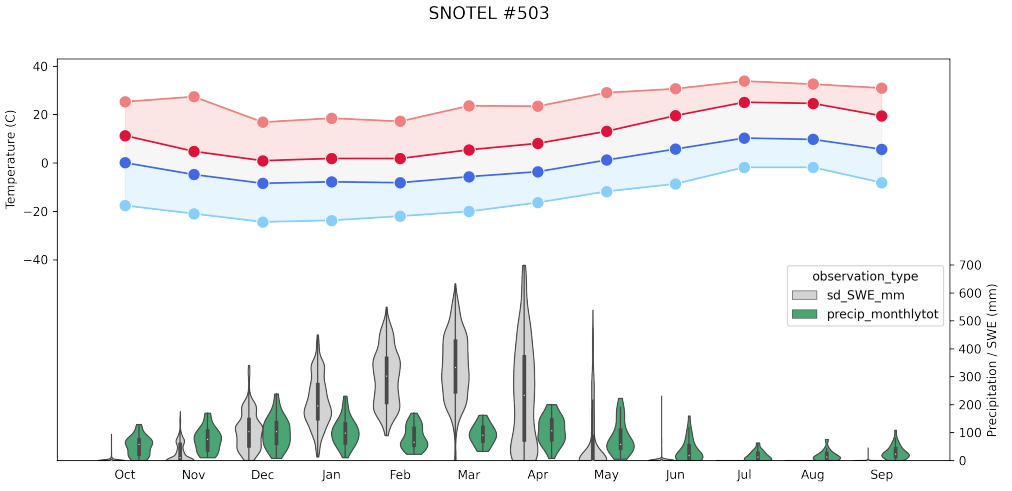

Figure 22: SNOTEL #503 Climatology.

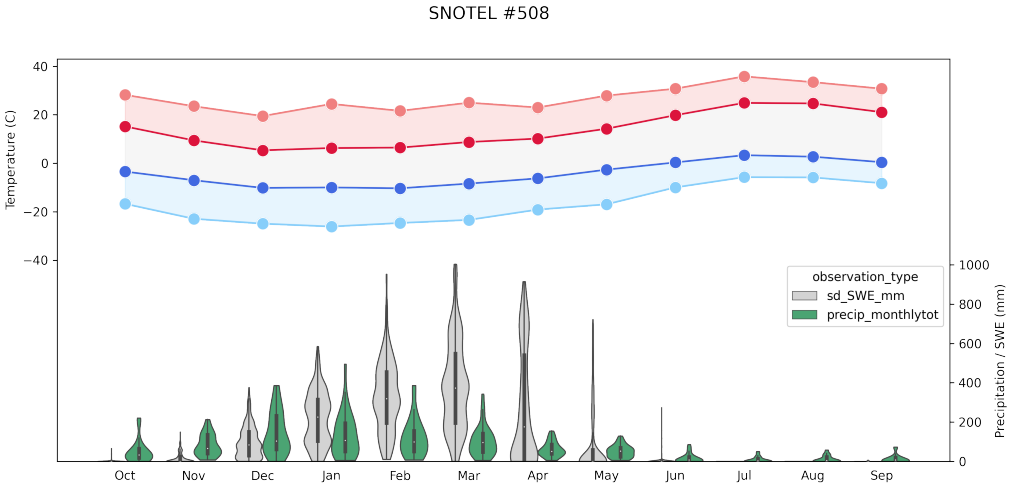

Figure 23: SNOTEL #508 Climatology.

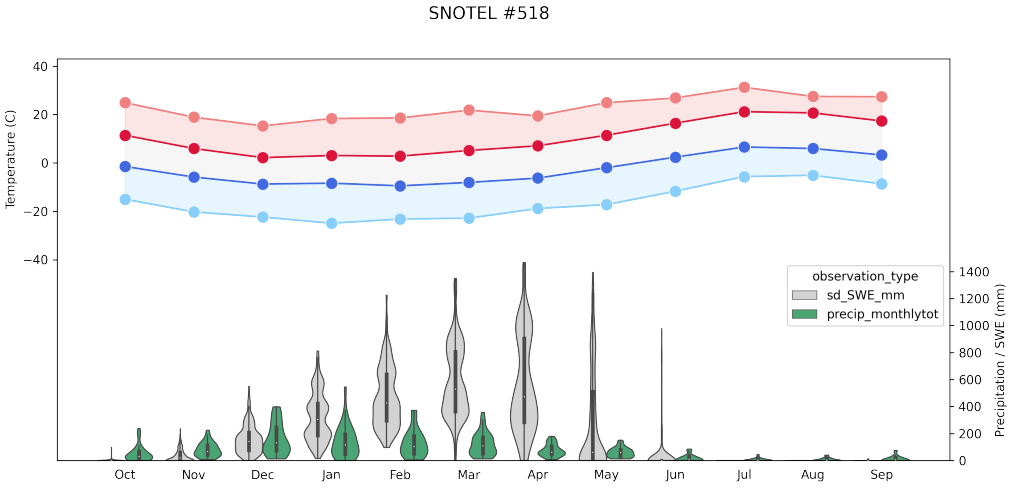

Figure 24: SNOTEL #518 Climatology.

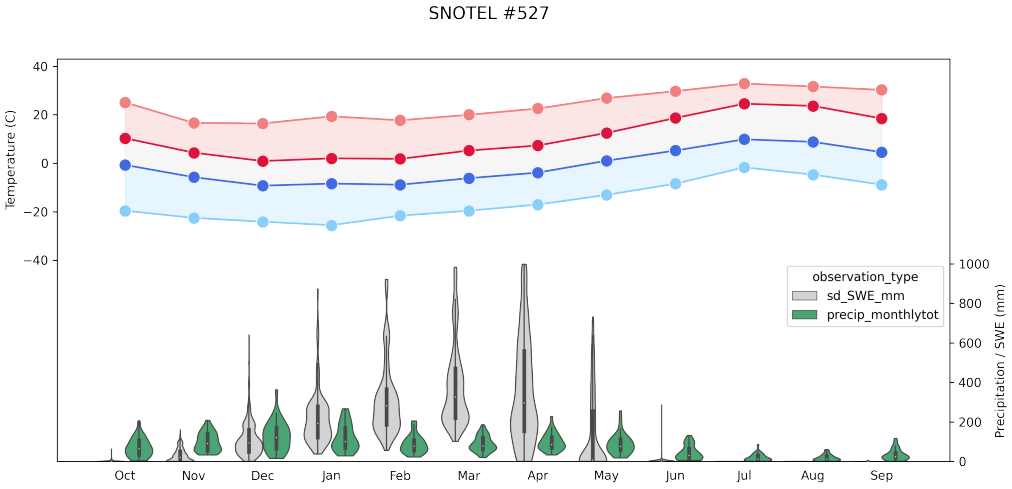

Figure 25: SNOTEL #527 Climatology.

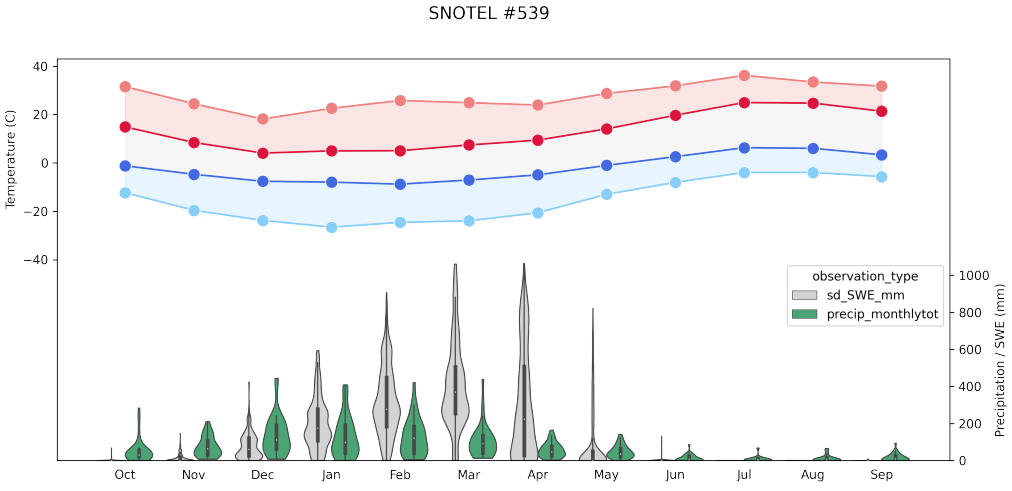

Figure 26: SNOTEL #539 Climatology.

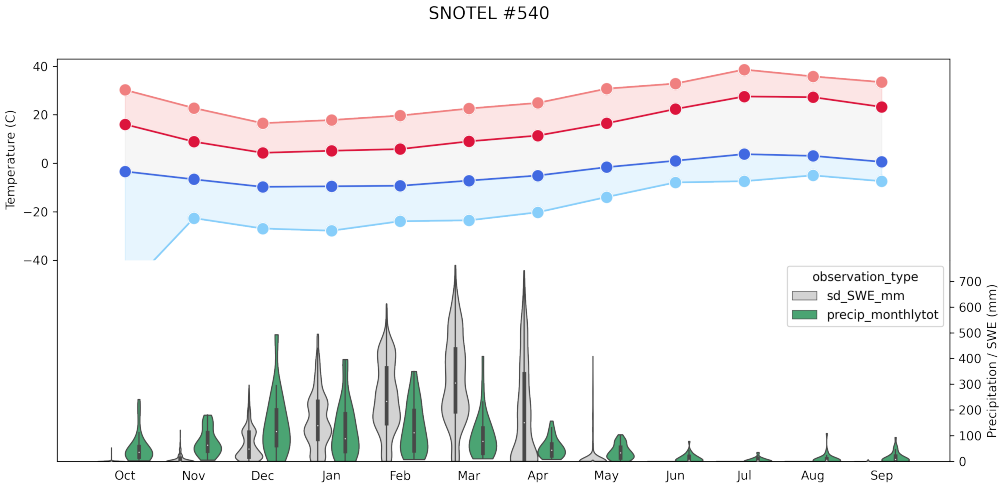

Figure 27: SNOTEL #540 Climatology.

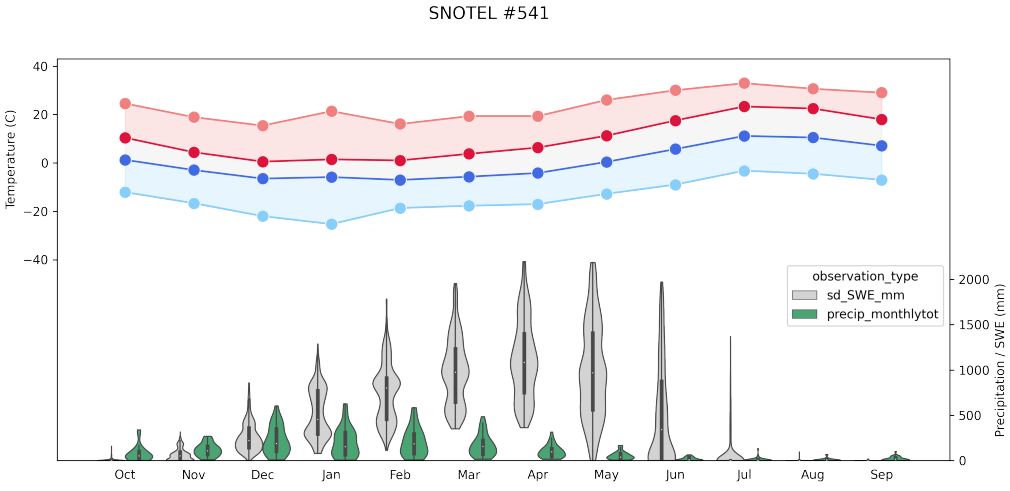

Figure 28: SNOTEL #541 Climatology.

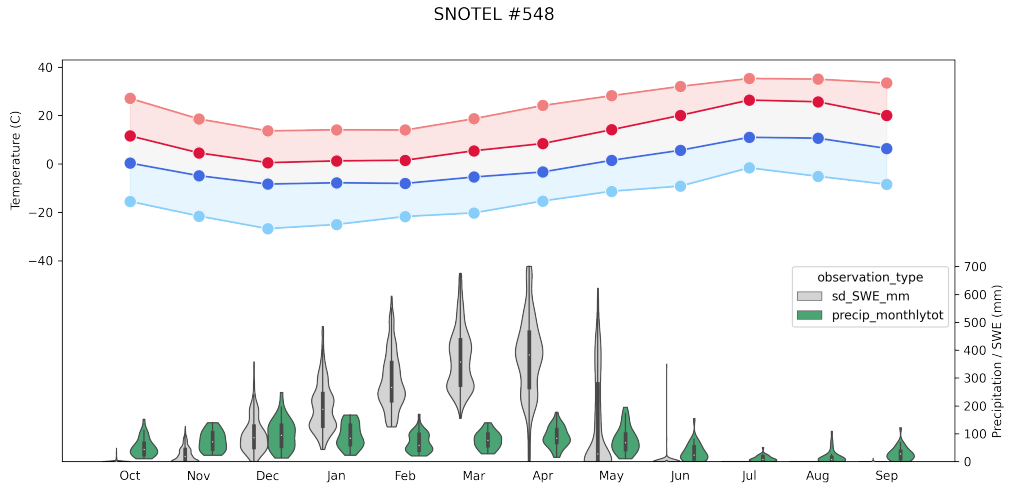

Figure 29: SNOTEL #548 Climatology.

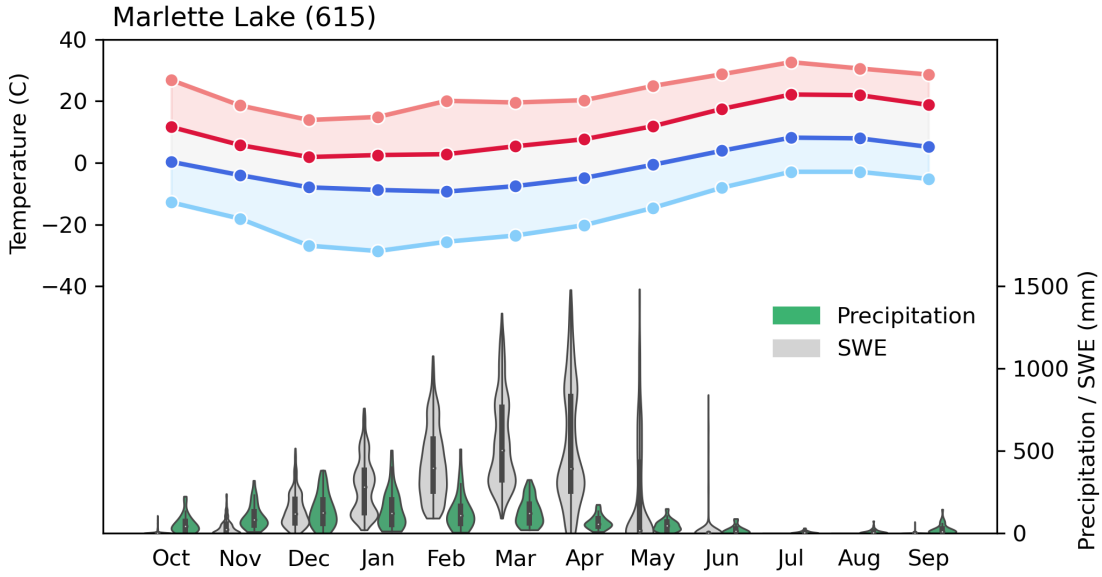

Figure 30: SNOTEL #615 Climatology.

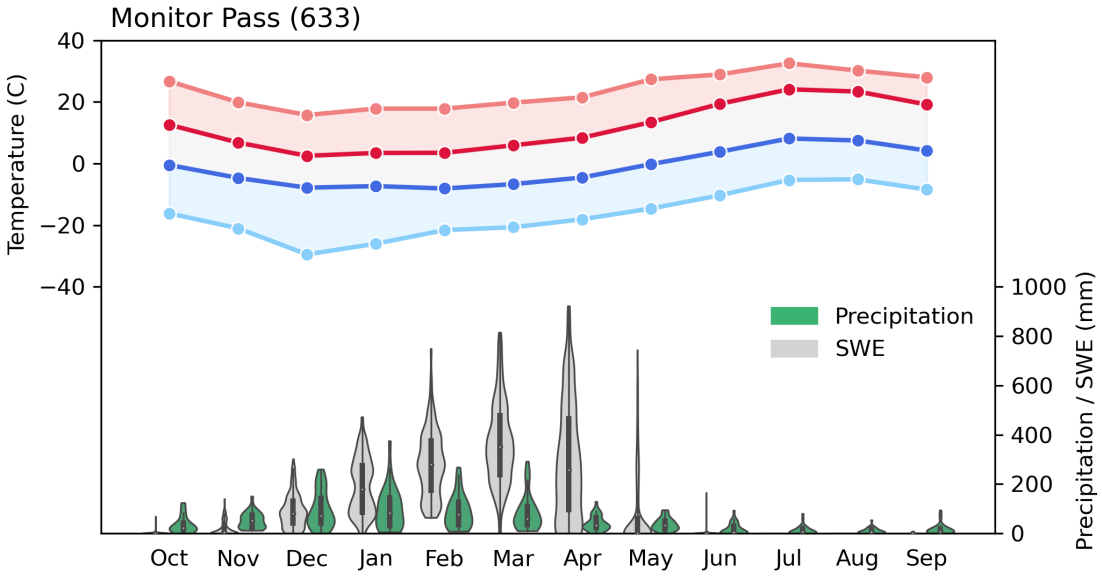

Figure 31: SNOTEL #633 Climatology.

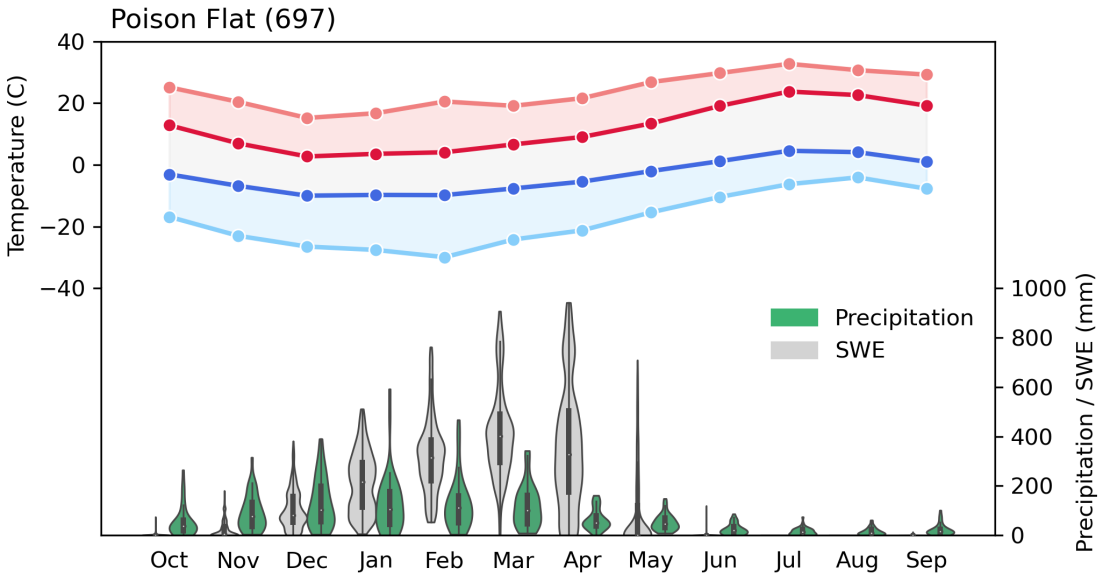

Figure 32: SNOTEL #967 Climatology.

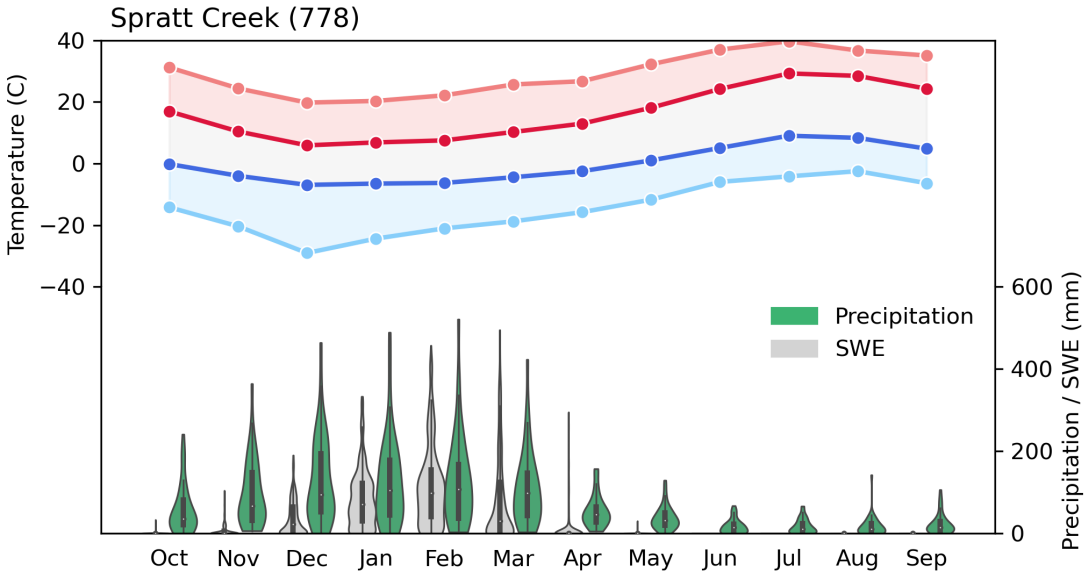

Figure 33: SNOTEL #778 Climatology.

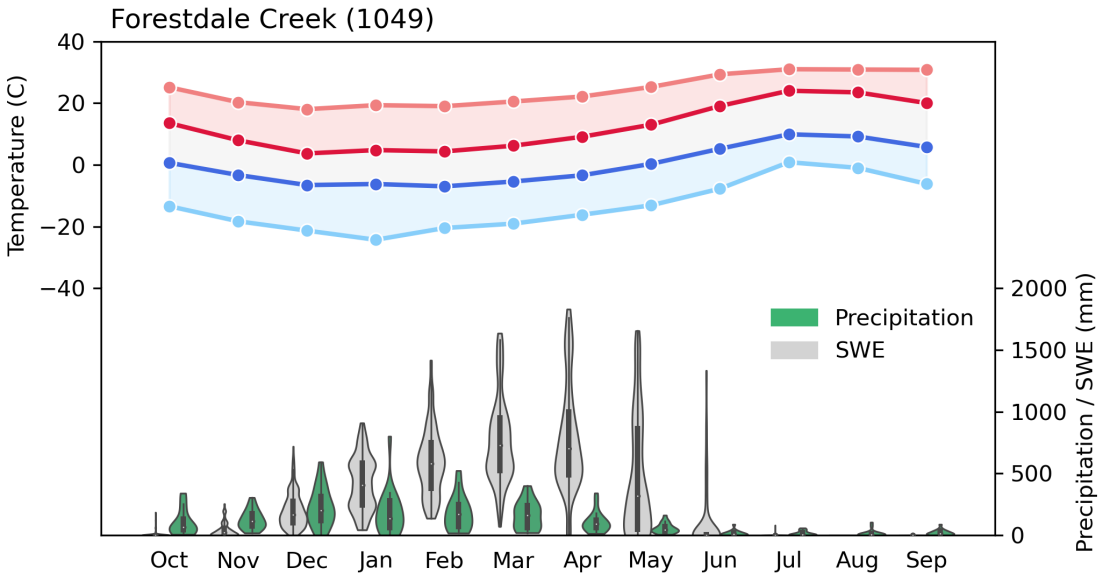

Figure 34: SNOTEL #1049 Climatology.

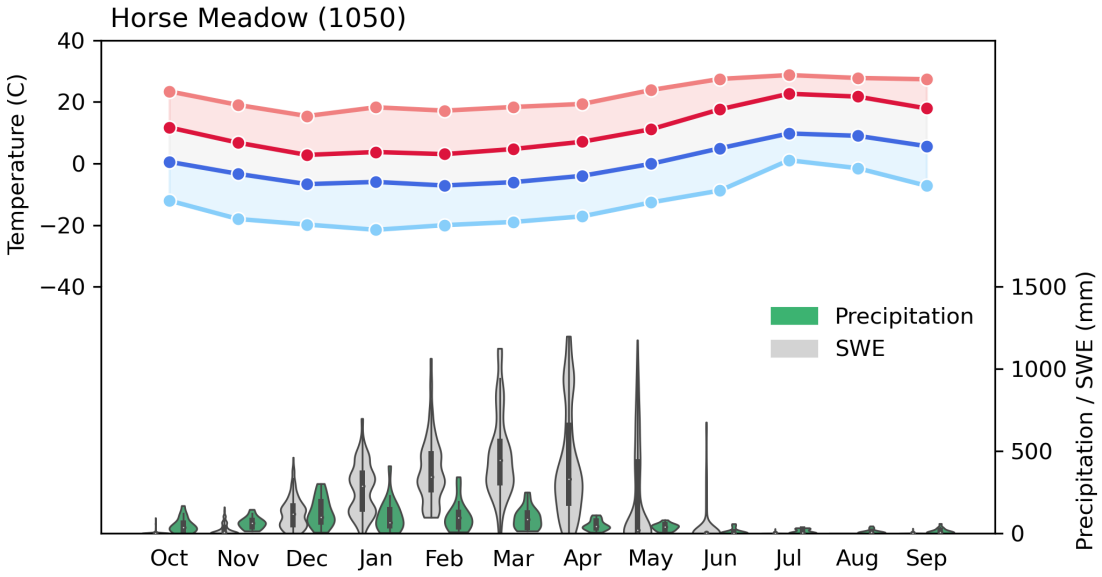

Figure 35: SNOTEL #1050 Climatology.

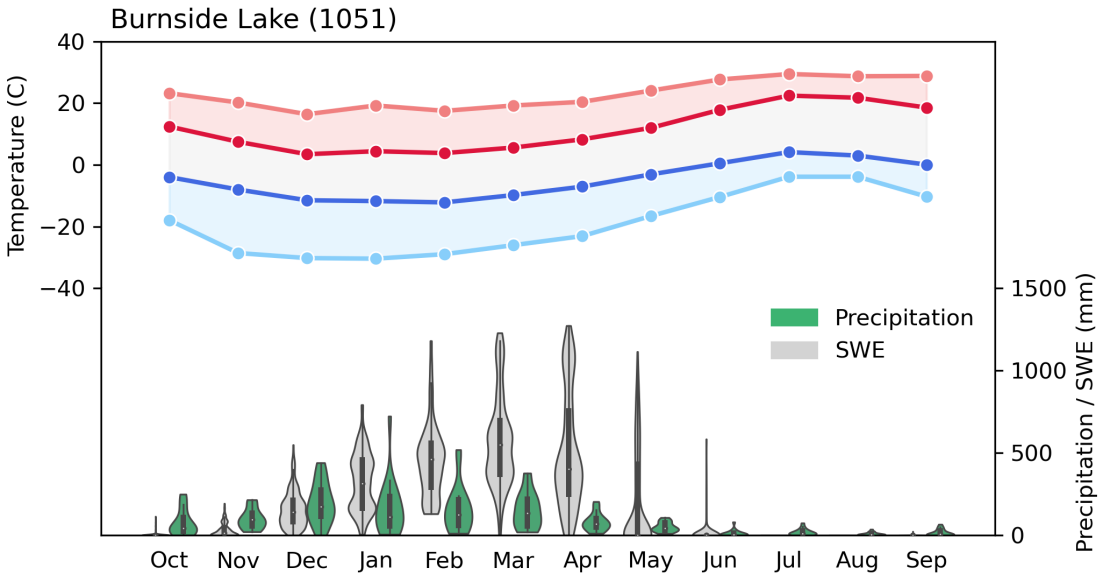

Figure 36: SNOTEL #1051 Climatology.

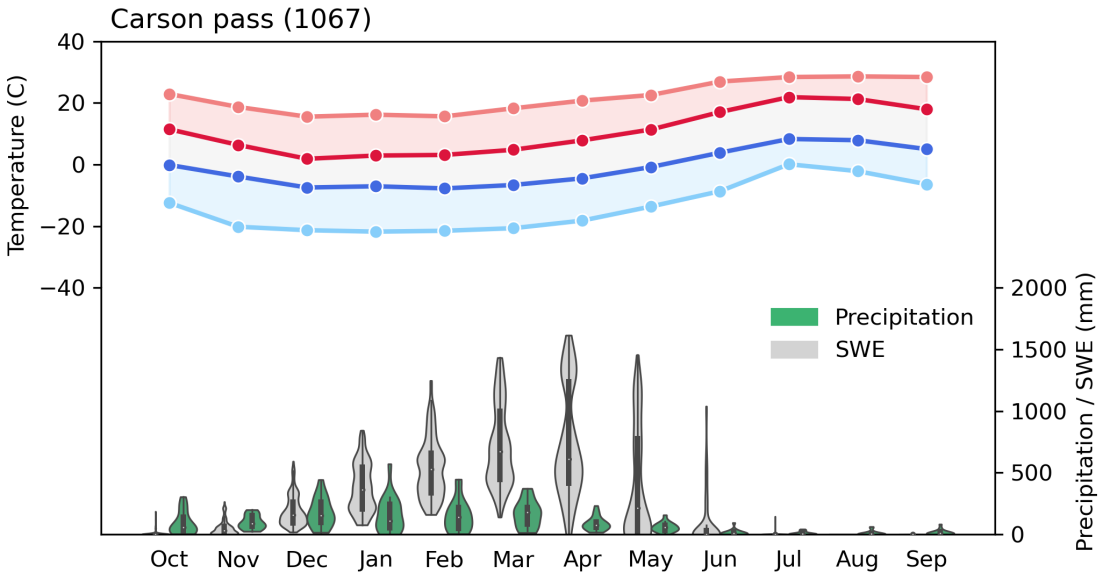

Figure 37: SNOTEL #1067 Climatology.

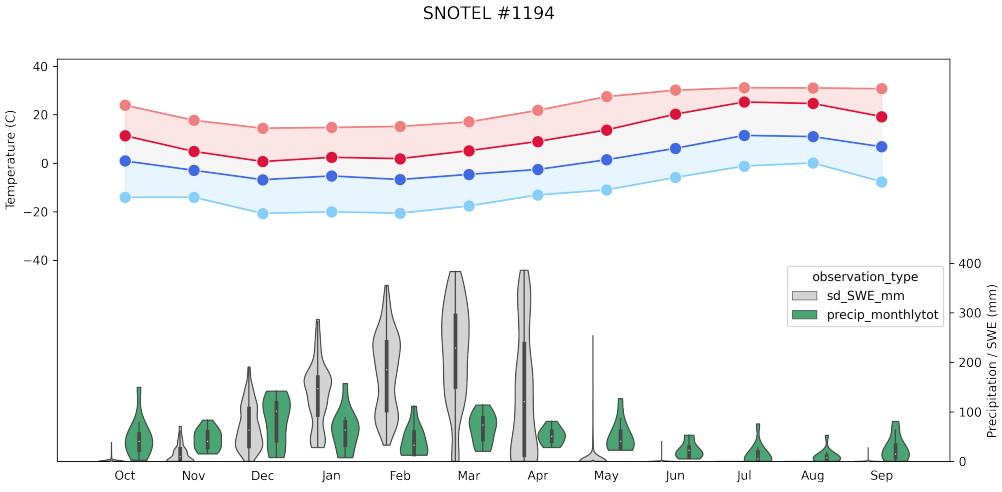

Figure 38: SNOTEL #1194 Climatology.

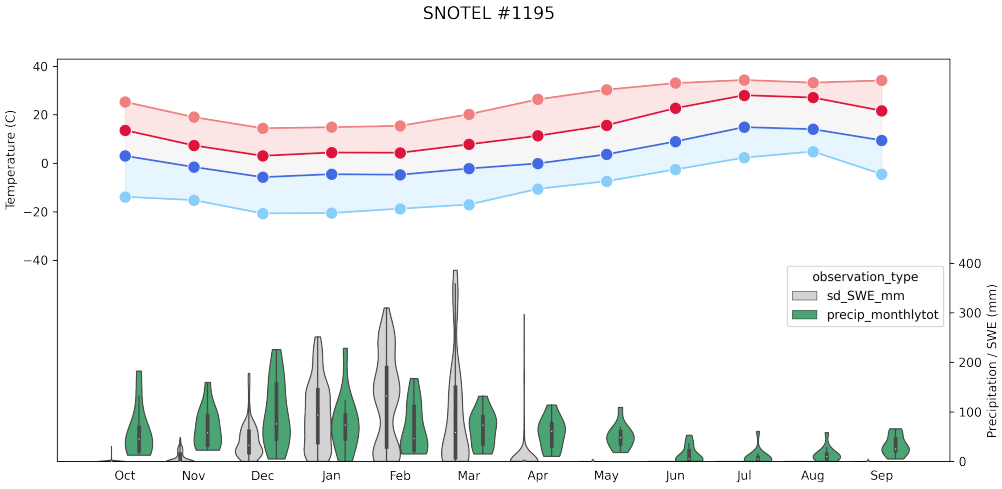

Figure 39: SNOTEL #1195 Climatology.

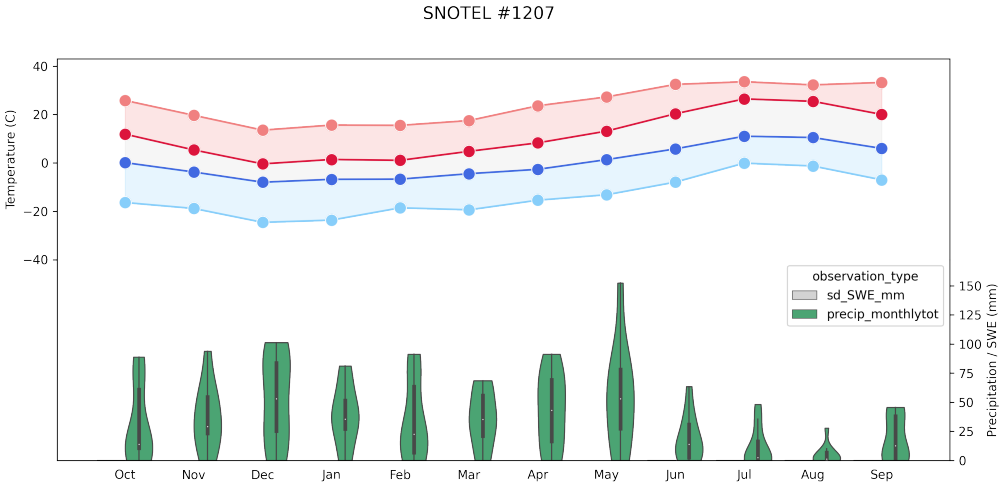

Figure 40: SNOTEL #1207 Climatology.

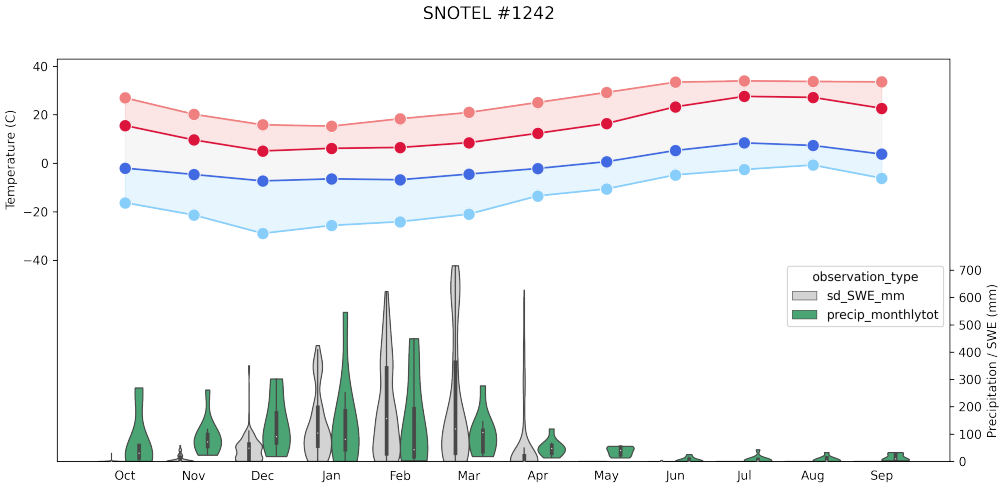

Figure 41: SNOTEL #1242 Climatology.

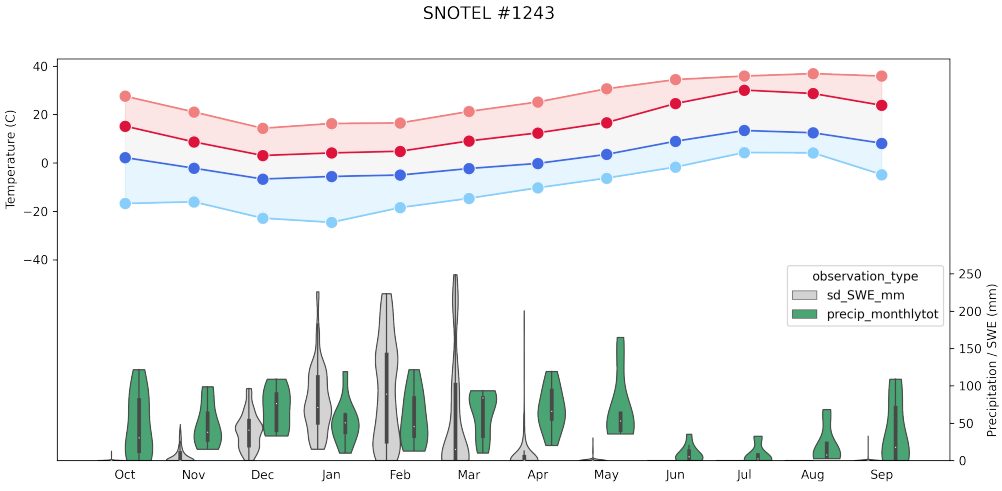

Figure 42: SNOTEL #1243 Climatology.

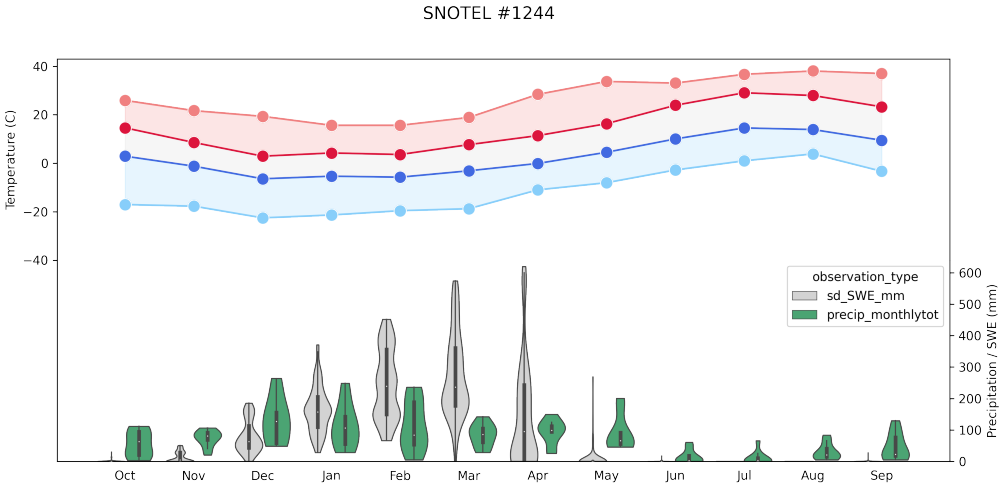

Figure 43: SNOTEL #1244 Climatology.

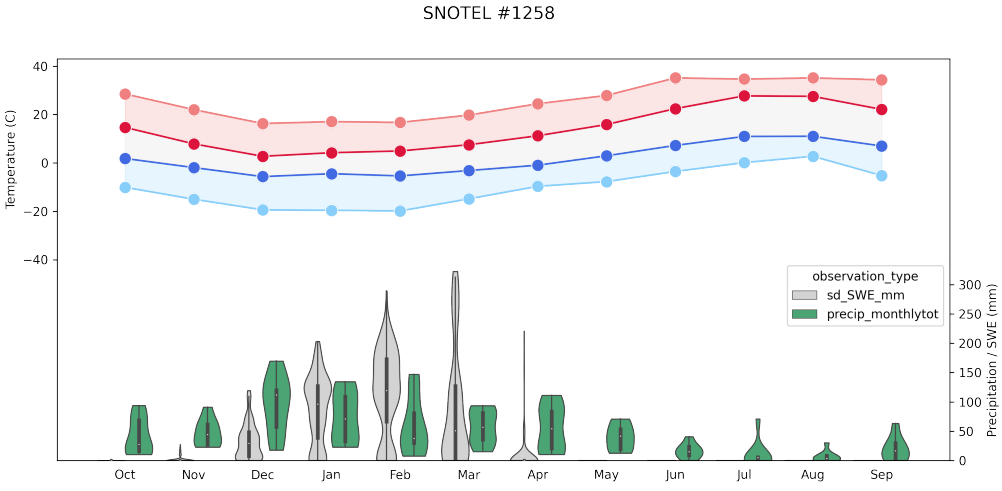

Figure 44: SNOTEL #1258 Climatology.

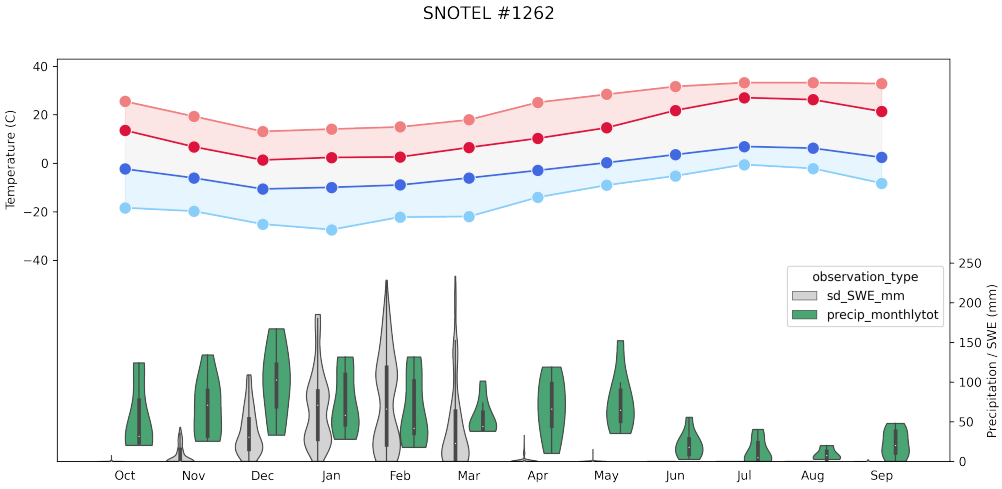

Figure 45: SNOTEL #1262 Climatology.

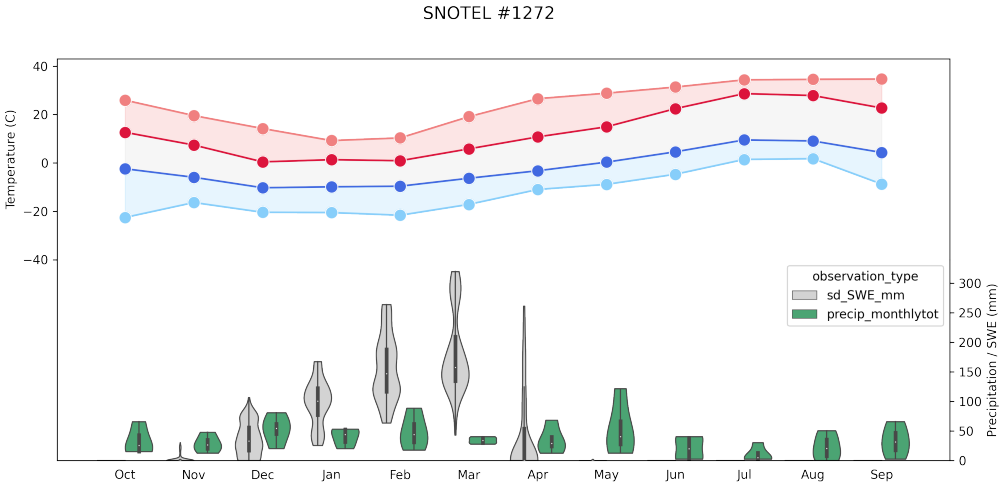

Figure 46: SNOTEL #1272 Climatology.

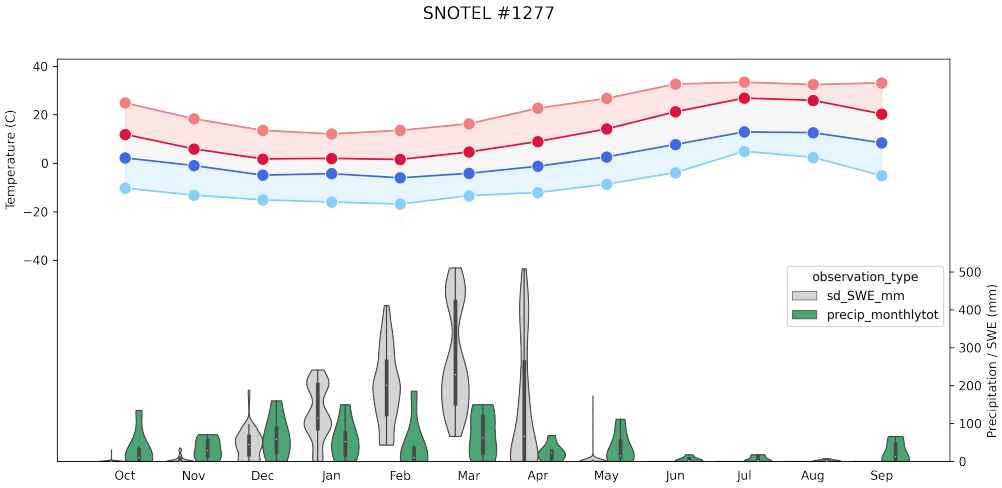

Figure 47: SNOTEL #1277 Climatology.

Apprendix B

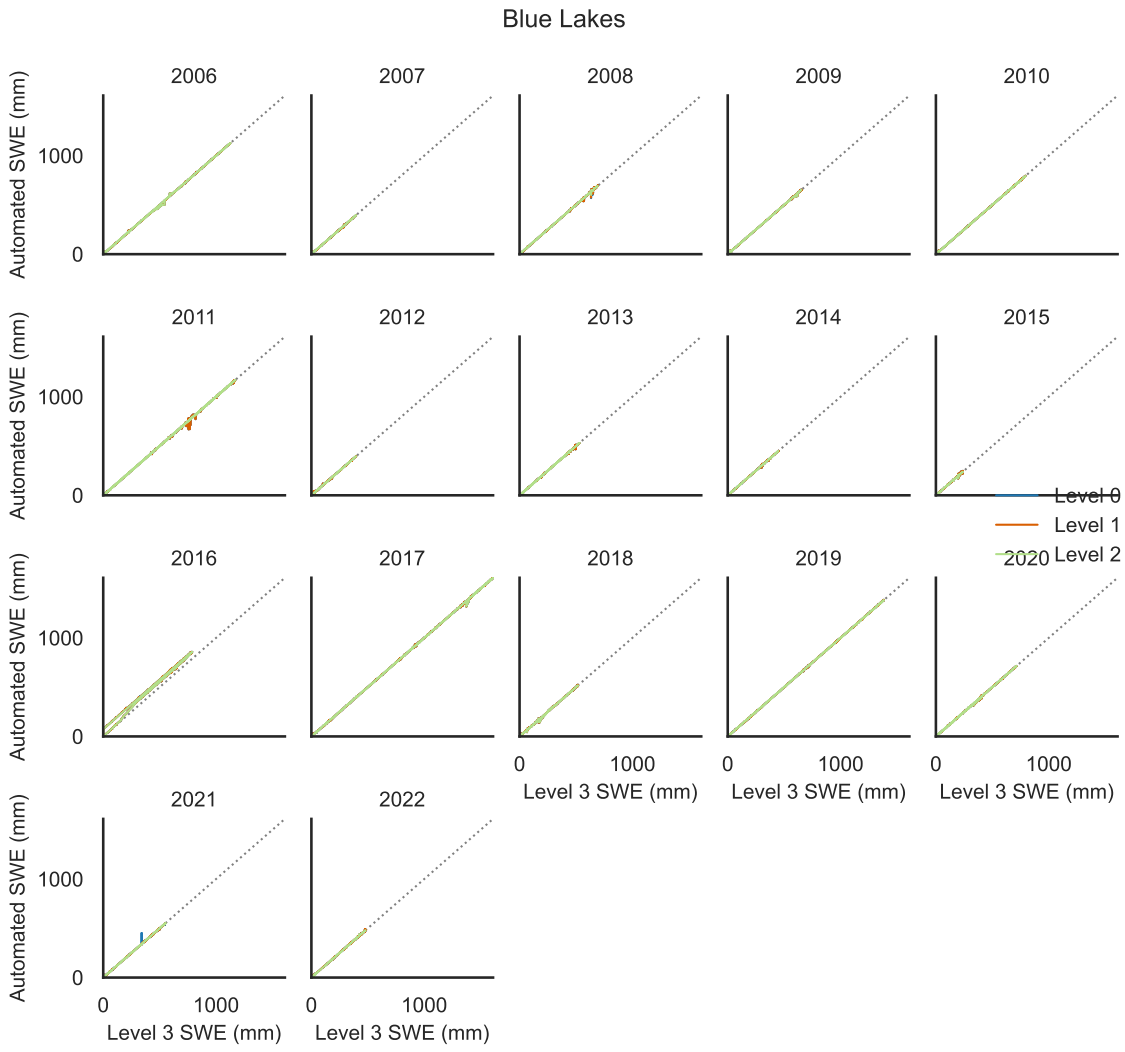

Figure 48: Comparison of Level 0 (blue), Level 1 (orange), Level 2 (green) vs Level 3 SWE data for Blue Lakes.

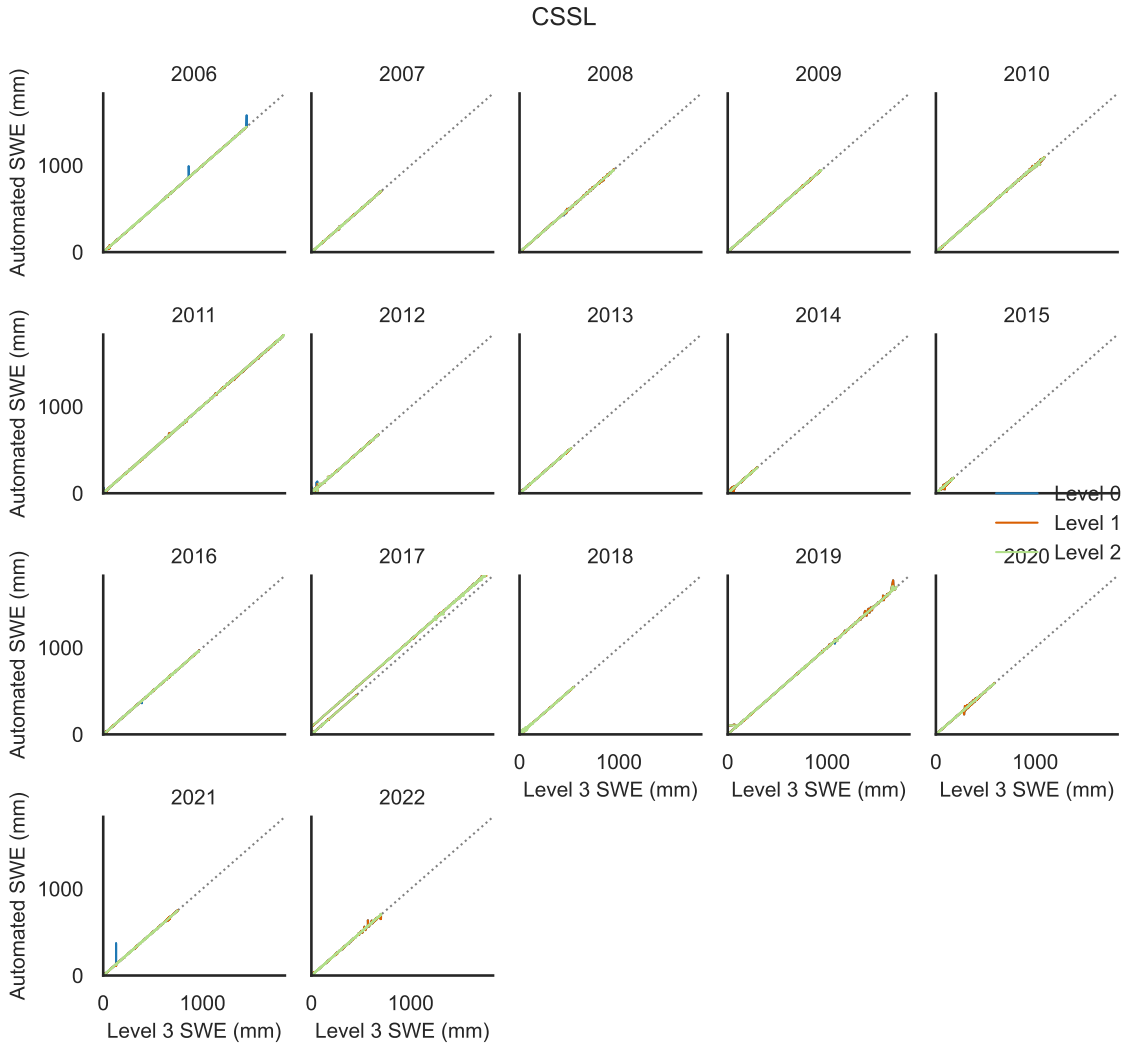

Figure 49: Comparison of Level 0 (blue), Level 1 (orange), Level 2 (green) vs Level 3 SWE data for CSSL.

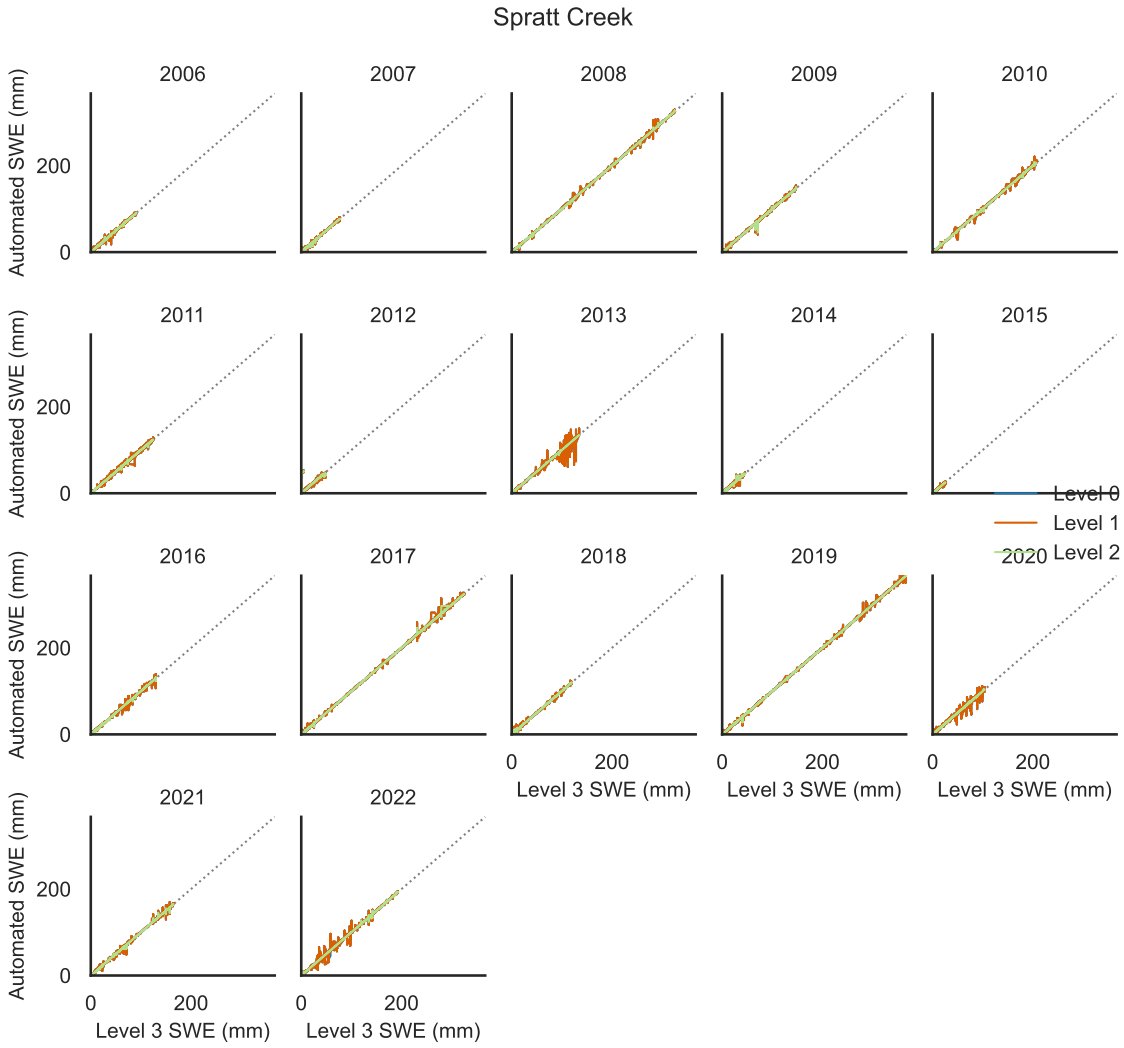

Figure 50: Comparison of Level 0 (blue), Level 1 (orange), Level 2 (green) vs Level 3 SWE data for Spratt Creek.

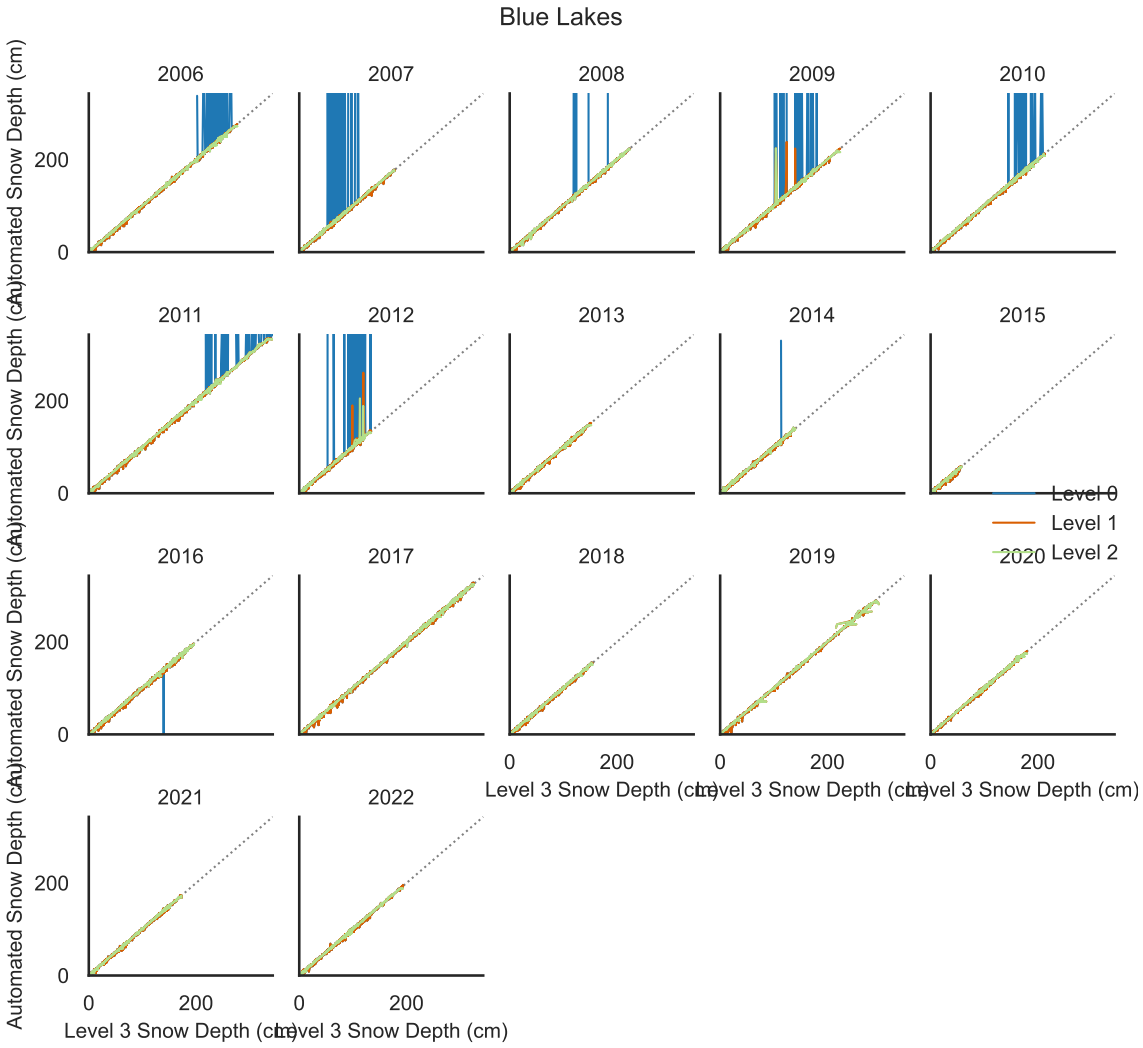

Figure 51: Comparison of Level 0 (blue), Level 1 (orange), Level 2 (green) vs Level 3 snow depth data for Blue Lakes.

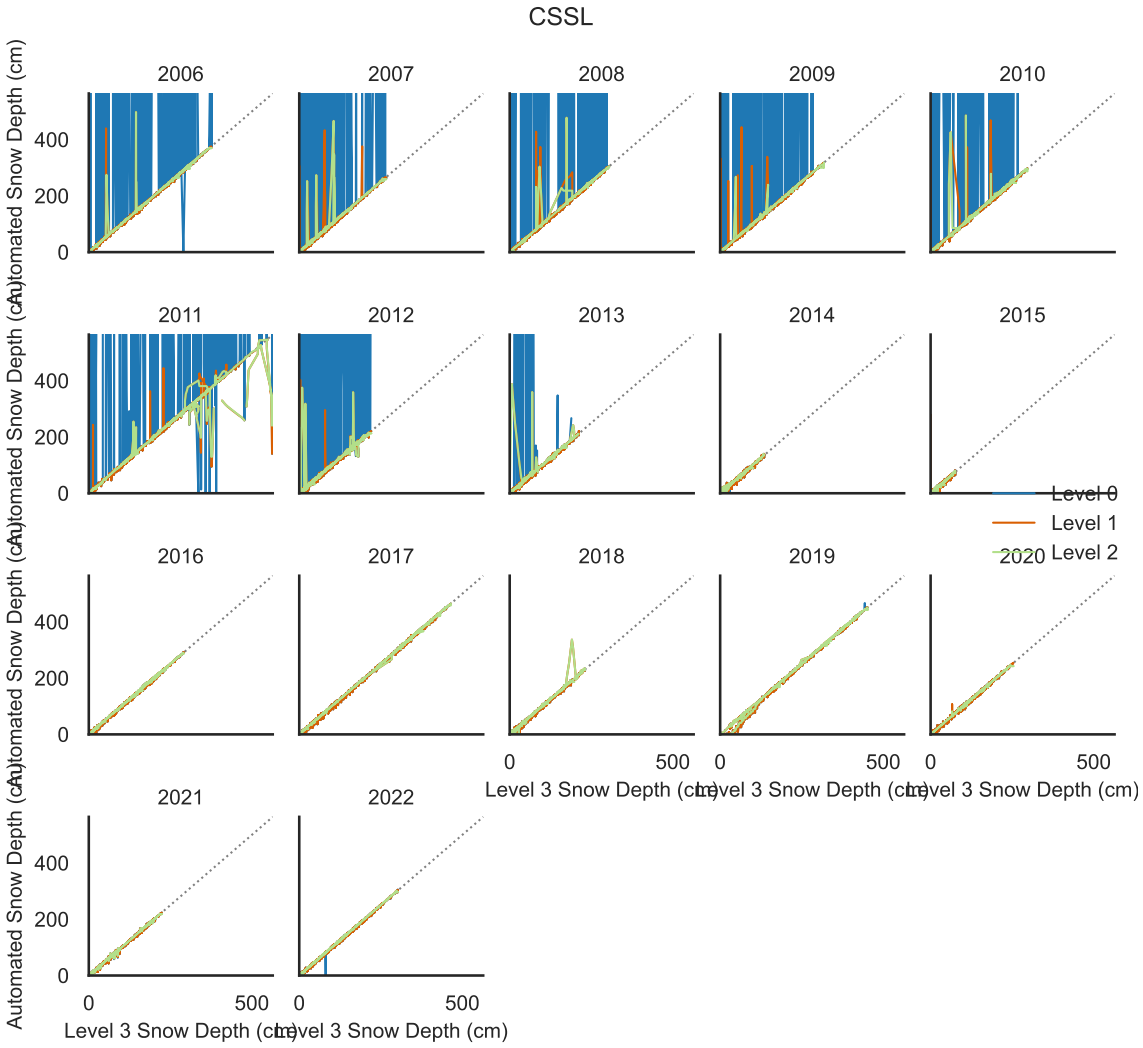

Figure 52: Comparison of Level 0 (blue), Level 1 (orange), Level 2 (green) vs Level 3 snow depth data for CSSL.

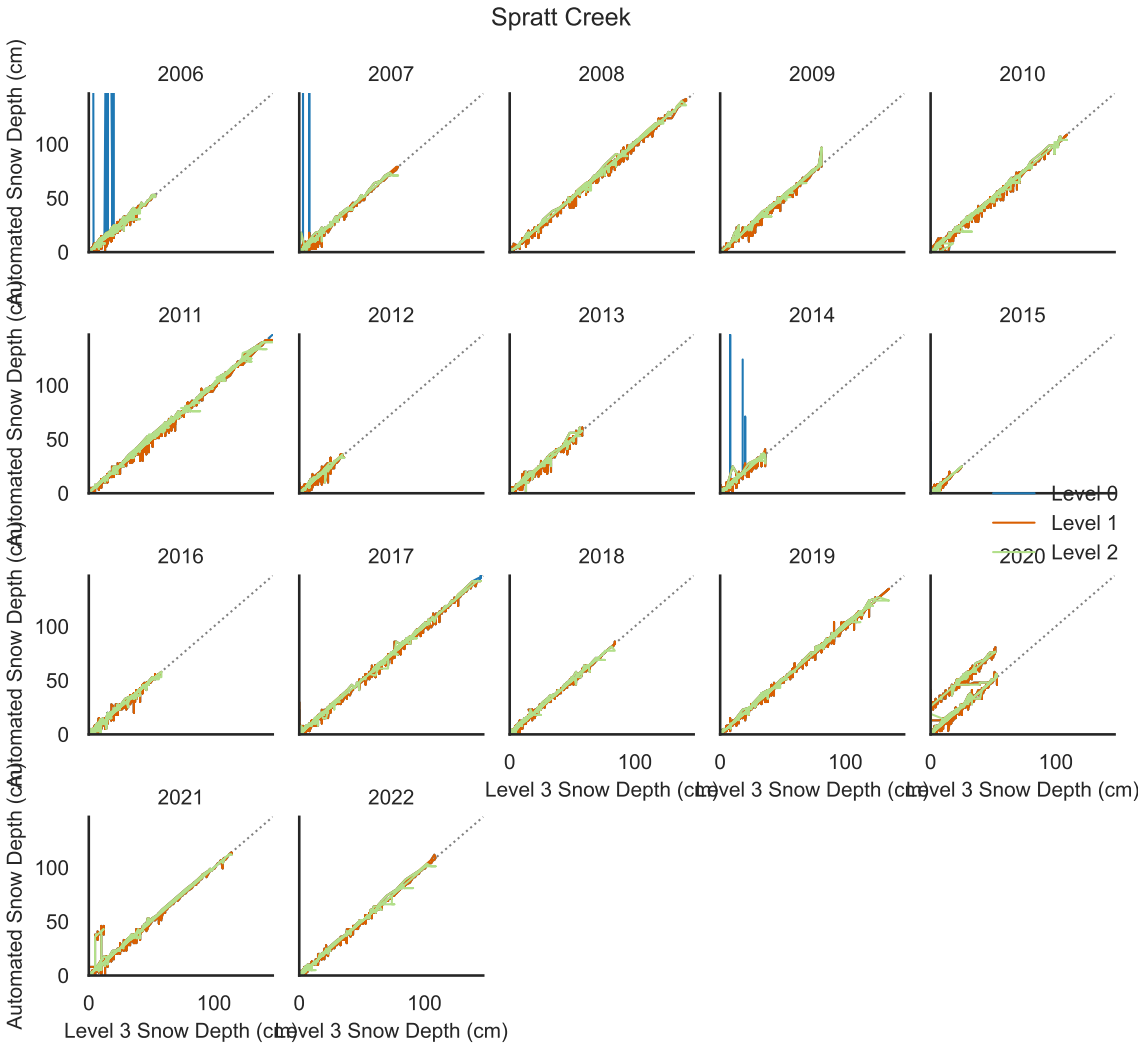

Figure 53: Comparison of Level 0 (blue), Level 1 (orange), Level 2 (green) vs Level 3 snow depth data for Spratt Creek.

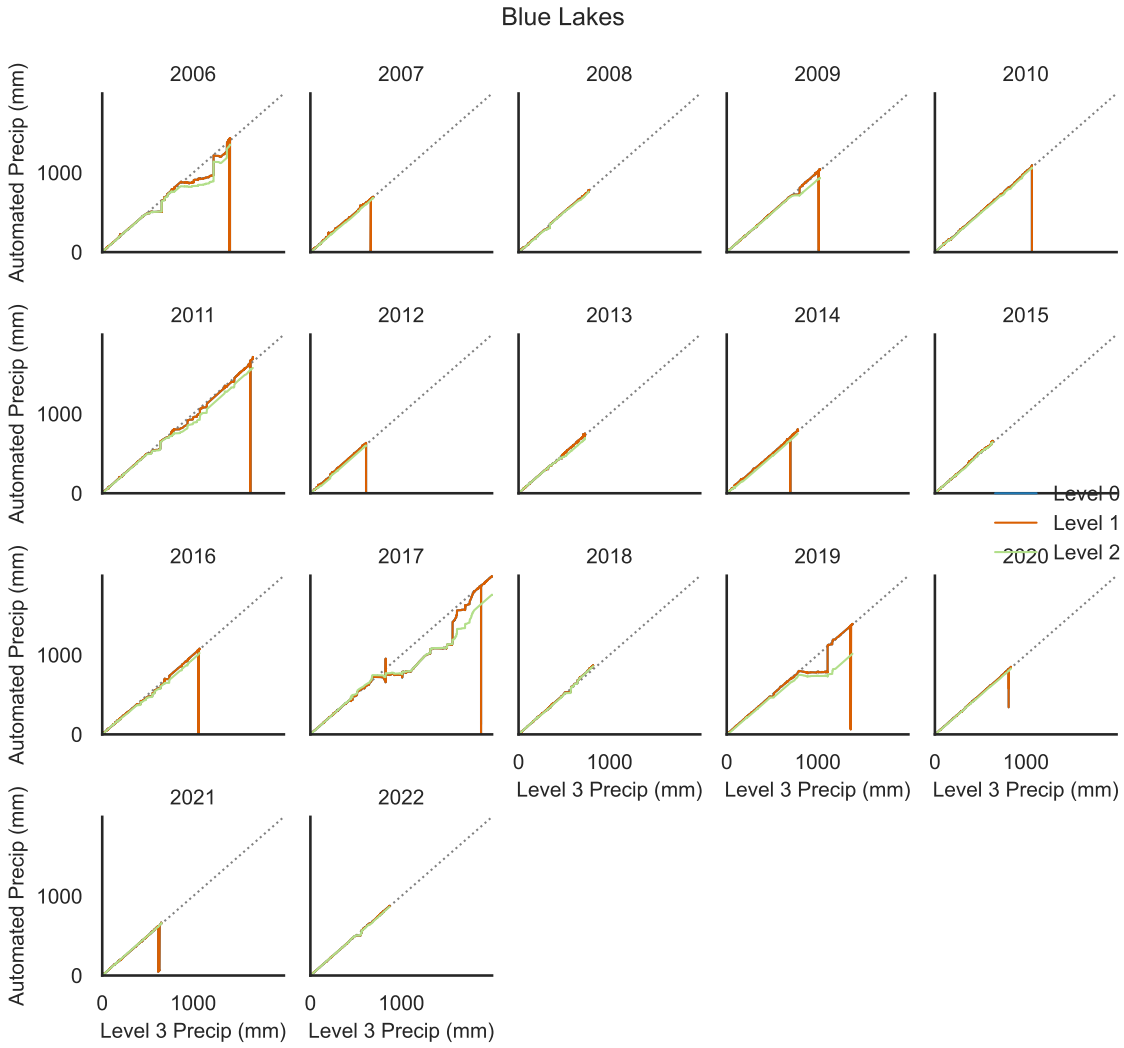

Figure 54: Comparison of Level 0 (blue), Level 1 (orange), Level 2 (green) vs Level 3 SWE precipitation for Blue Lakes.

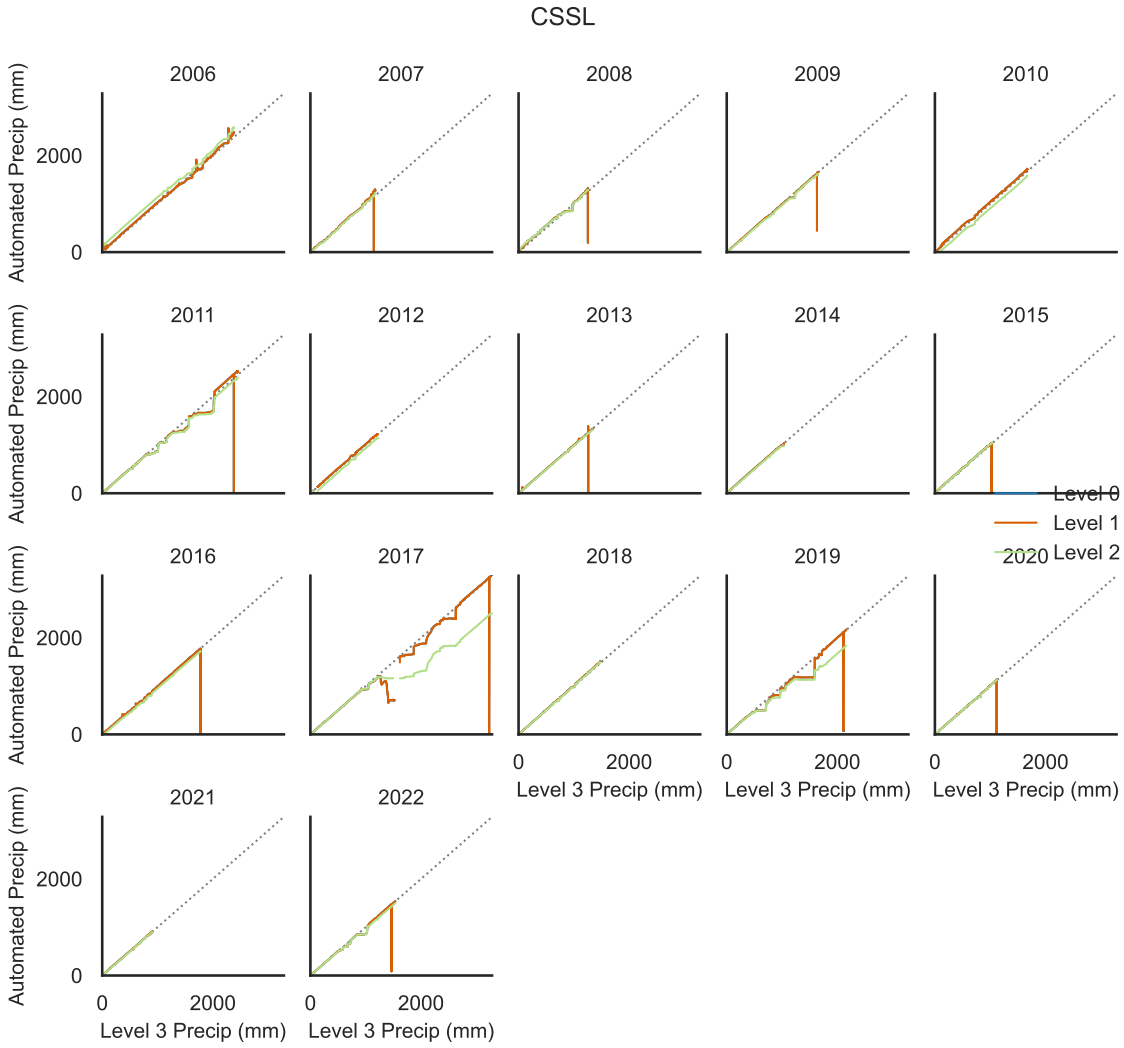

Figure 55: Comparison of Level 0 (blue), Level 1 (orange), Level 2 (green) vs Level 3 precipitation data for CSSL.

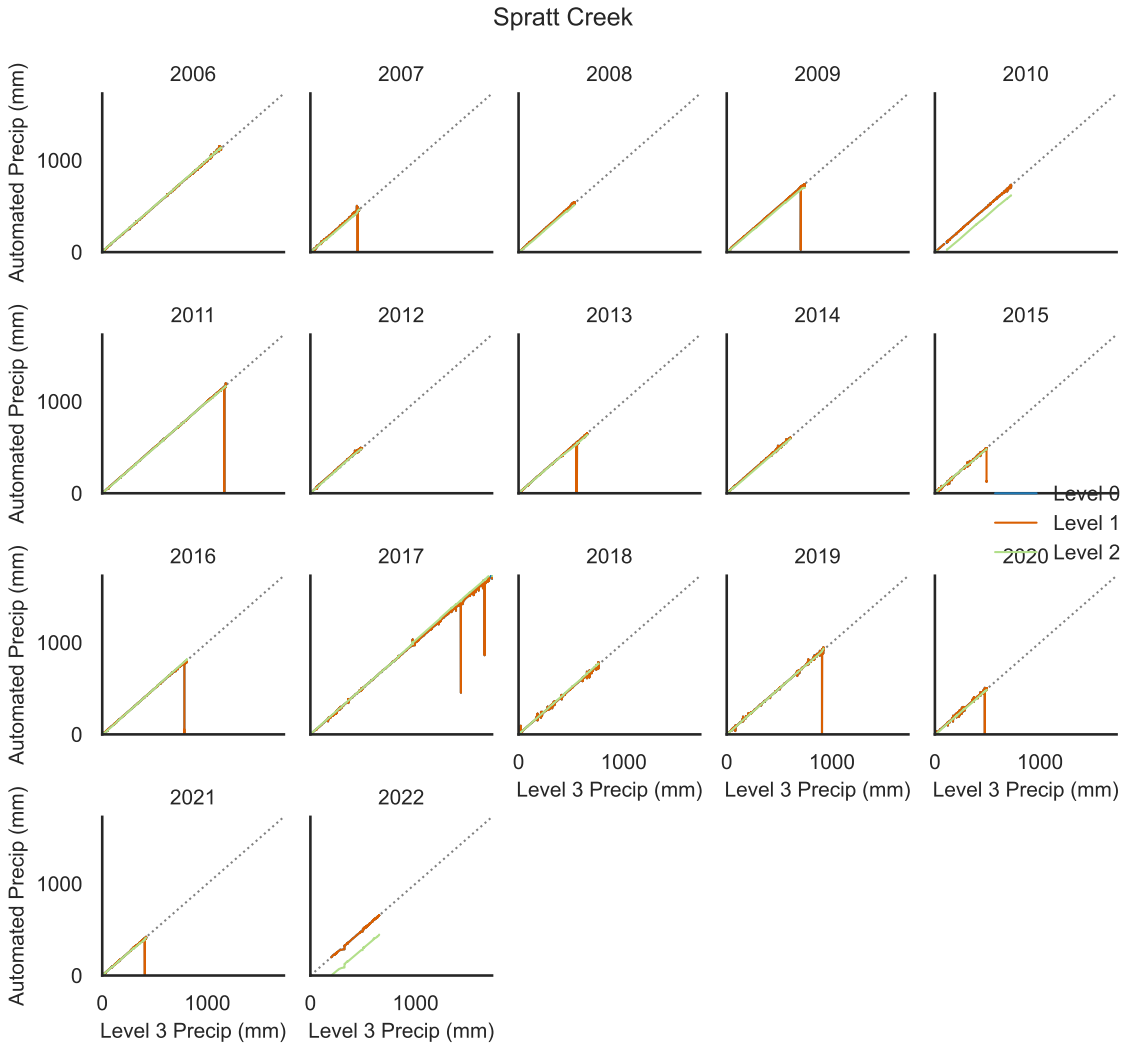

Figure 56: Comparison of Level 0 (blue), Level 1 (orange), Level 2 (green) vs Level 3 precipitation data for Spratt Creek.

Appendix C

Case Study 1: 30 December 2005–1 January 2006 Flood

This first example expands upon the test case in Chapter 2. A series of storms from December 25 through January 1 brought widespread precipitation that spilled over the crest of the Sierra Nevada with the greatest 48-hour precipitation rates occurring December 30 through January 1 (CNRFC, 2006). Figure 57.A shows the TWI potential for December 30 at 12:00 PST PST, December 30 at 21:00 PST, and December 31 at 11:00 PST also represented by light blue vertical lines in Figure 57.B. Spratt Creek did not have a snowpack during this event but two prior systems (December 18-19 and December 26-27) brought produced snow at Spratt Creek which melted out between each event, temporarily elevating soil moisture at the station. Blue Lakes had a relatively small snowpack with just 280 mm of SWE and 91 cm of snow depth. Precipitation can still be validated at Spratt Creek with the precipitation observations but also the increase in soil moisture. Changes in snowpack density indicate that precipitation is a mixed phase or rainfall since the snowpack density starts at 30% and consistently increases until air temperature drops after the 31st at 11:00 PST. Therefore, the density of the precipitation must be greater than the density of the existing snowpack. As the air temperature increase, the SR-DSS identifies a low ROS potential at Blue Lakes as air temperature crosses the 0 °C threshold and just four hours later the 20 cm soil moisture sensor registers TWI. TWI initiated at Blue Lakes during this event with a 6-hour maximum air temperature of 0.5 °C, consistent with the station-specific threshold of 0.4 °C. While it is not possible to validate the initiation of rainfall, observing soil moisture response narrows the window for rainfall onset to just four hours; therefore the lag rate for the rainwater to penetrate the snowpack and produce TWI was within four hours. Spratt Creek had a total of 150 mm of precipitation with hourly precipitation rates up to 9 mm/hr (Figure 57.B2).

Prior to the event, the depth averaged soil moisture was about average for Blue Lakes for the time of year but it was near the historical maximum at Spratt Creek. The low-elevation rainfall confirmed coupled with elevated soil moisture values at Spratt Creek resulted a quicker streamflow response at Markleeville and Gardnerville, while the Woodfords gage takes a little longer to respond in this event. The morning of December 31st, Gardnerville reaches monitor stage and within four hours it reaches flood stage peaking on December 31 at 11:00 PST am (Figure 57 A3). As Gardnerville begins to recede, the station at Carson City hits the monitor stage and continues to increase to flood stage well after the ROS event has ended, connecting the recession of the soil moisture sensors to the travel time for water to move through the soils into the Carson River.

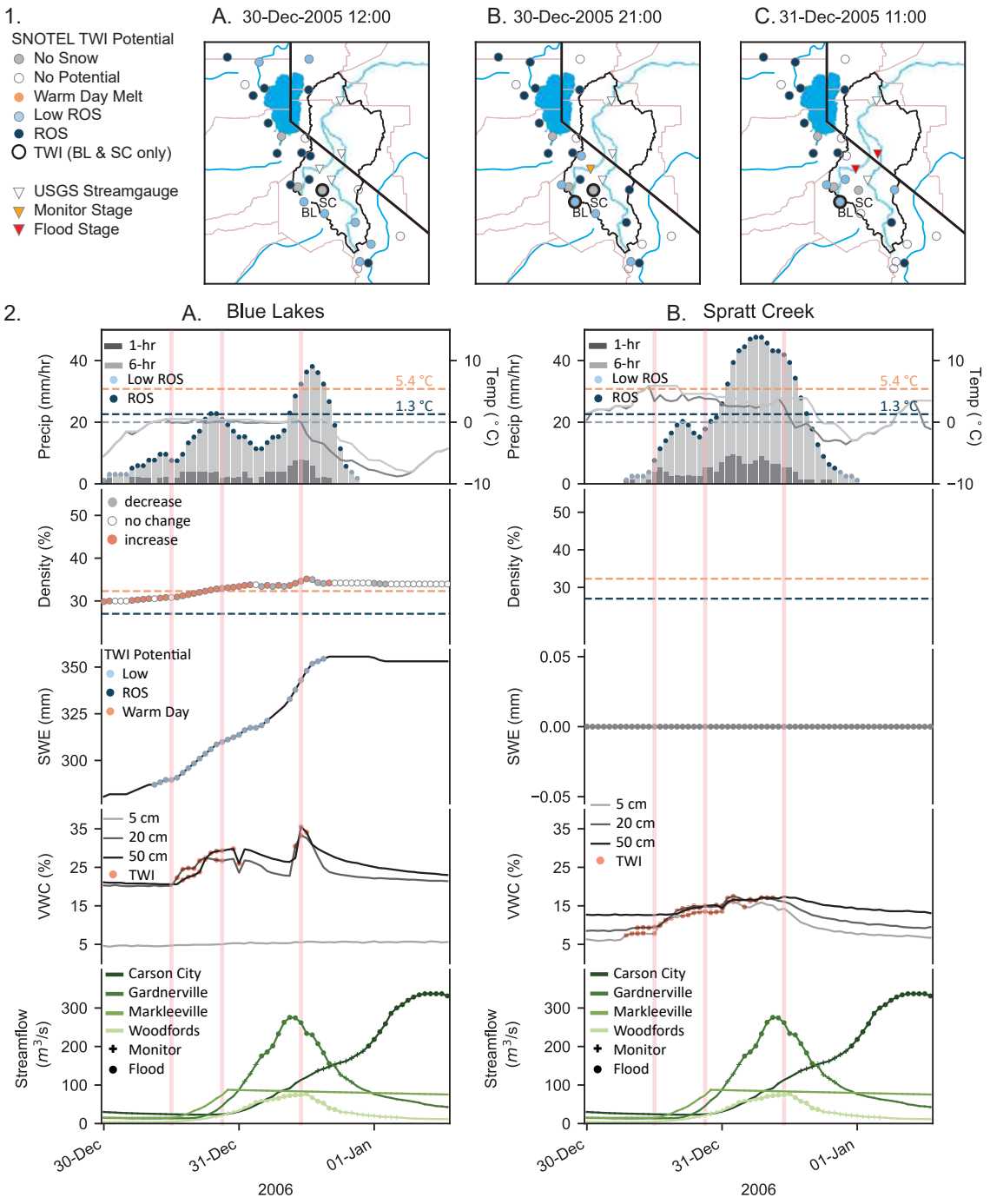

Figure 57: Historical event assessment: 30 December 2005–1 January 2006.

Case Study 2: 7–10 January 2017 Flood

While much focus on 2017 has been given to the February event and will be discussed further as the next case study, the January ROS event primed the snowpack and soil moisture the way for greater hydrologic impact in February (Haleakala et al., 2022). Leading to the event, a high pressure set up in the Gulf of Alaska, and a cut-off low moved southeast along the California coast, helping to direct a plume of moisture into California with precipitation beginning on the 6th ahead of a warm frontal boundary (CNRFC, 2017). We examine the performance of the SR-DSS starting on January 7th (Figure 58) as the snow level begins to rise and precipitation transitions from snow to rain. The snowpack was about average for the time of year for both stations and the snowpack density was just below the ROS threshold. On January 7 at 20:00 PST (Figure 58.1A) Blue Lakes registered TWI even though there was a low potential for ROS TWI as air temperature had been hovering around 0 °C for six hours. TWI continued for six more hours until there was a break in precipitation. The next wave of the storm was warmer and by 07:00 PST on the 8th (Figure 58.1B), the air temperature and precipitation rates signal the potential for ROS TWI. During that next hour soil moisture increased at 20 cm and 50 cm depth by 6.2% and 11% in a single hour as SWE continued to increase. The storm weakens at Blue Lakes by 14:00 PST on the 8th as SWE and density plateau though TWI continues with less than 2 mm of additional precipitation. At Spratt Creek, precipitation began the morning of the 7th as rain and within a couple of hours the 6-hour precipitation rate threshold was crossed even though TWI started just one hour after rainfall has started. These observations agree with those of Kattlemann (1997) that state rain can move through a snowpack in as little as one hour. Our analysis provides further evidence of the formation of preferential flow paths to route rainwater ahead of a uniform wetting front (Marsh and Woo, 1984b). The snowpack density during the event starts by increasing as the rainwater is transiently stored in the snowpack prior to little to no increase in the snowpack as soil moisture values continue to increase. This is further evidence of the snowpack simultaneously absorbing and releasing water. SWE values begin to decrease, indicating that the snowpack is beginning to either drain the transiently stored water or actually beginning to melt. By 18:00 PST on the 8th (Figure 58.1C), density and soil moisture at Spratt Creek and streamflow at Gardnerville and Markleeville all reach a peak and begin to recede and all stations except Carson City have exceeded the flood stage though the Carson City gage does reach flood stage as the water in the soils moves through the watershed. Prior to the event, the depth average soil moisture at Spratt Creek was about average for the time of year but Blue Lakes had record high soil moisture. The higher-intensity rainfall events and elevated soil moisture levels are likely key contributors to why this event was the largest flood event in the period of this study to impact the Carson City gage.

Case Study 3: 6–11 February 2017 Flood

The February 2017 series of storms spanning from the 2nd through the 10th has been well studied in the Feather River watershed as these events coincided with the failure of the Orville Dam principal spillway (Henn et al., 2020; Haleakala et al., 2022; Bunn et al., 2022; Hollins et al., 2018; White et al., 2019; Koskinas et al., 2019). It is worth noting that the failure of the spillway was not due to unprecedented flows being released over the

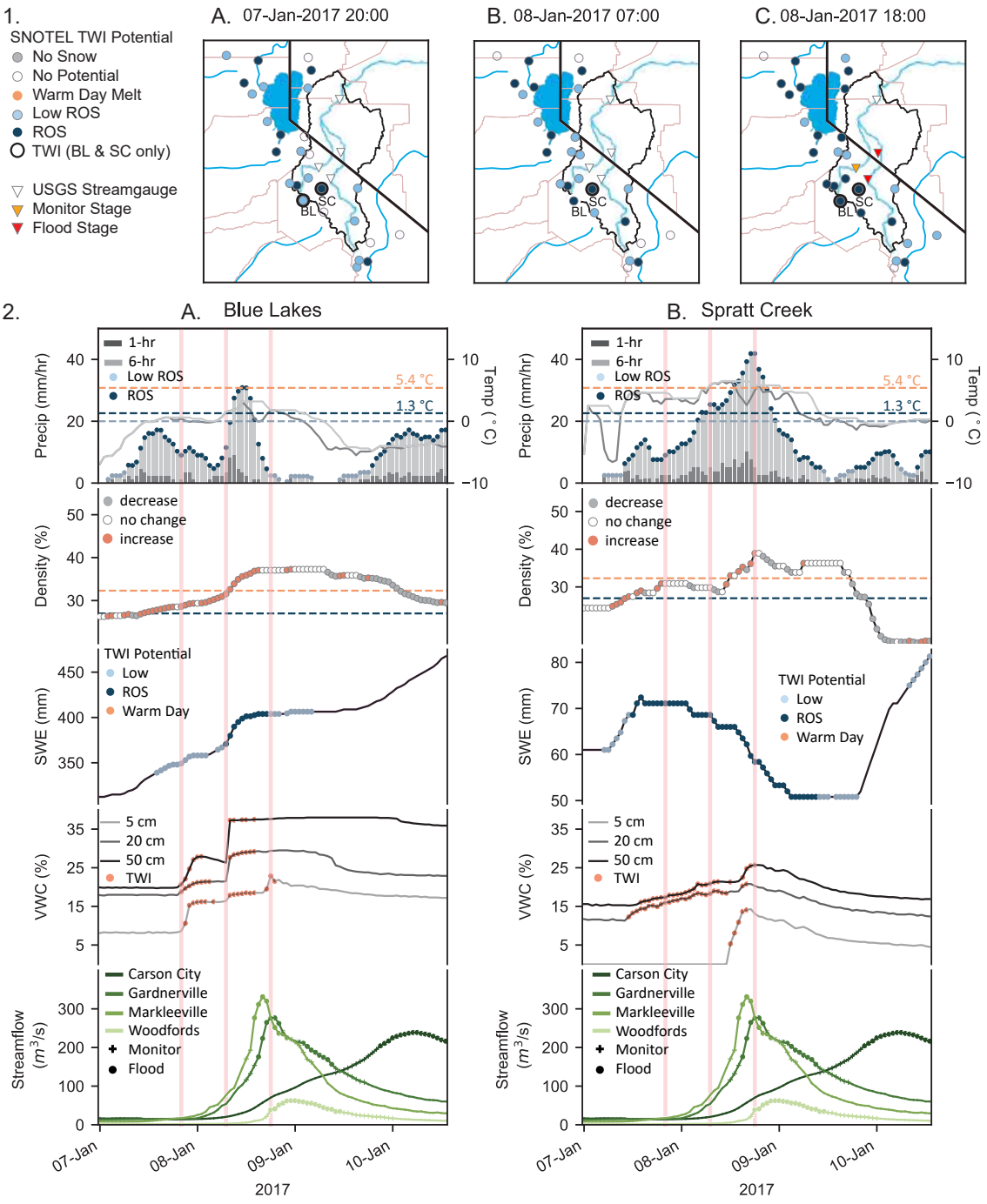

Figure 58: Historical event assessment: 7–10 January 2017.

spillway, but was an infrastructure failure of the spillway on February 7th during the first wave of precipitation that compromised the safety of the dam as more water was entering the reservoir and eventually required the use of the emergency spillway to save the dam and downstream communities (CNRFC, 2017). According to the CNRFC storm summary

report(CNRFC, 2017), this event consisted of a series of four waves within the storm event. A cold front moved through bringing snow to the mountains starting late afternoon on the 5th into the afternoon of the 6th. There was a slight break in the storm before the nest system brought precipitable water values up to 34.4 mm and an increase in snow levels that were between 2438 m and 3048 m from the 8th through the 10th.

The analysis begins on February 6th and goes through February 11th at 12:00 PST. Blue Lakes (Figure 59.2A) and Spratt Creek (Figure 59.2B) both registered precipitation that was though Blue Lakes was experiencing snowfall while Spratt Creek was likely experiencing snowfall that transitioned to rain during the morning of the 6th. The SR-DSS TWI potential changed from Low ROS to ROS as TWI initiated at 07:00 PST on the 6th at Spratt Creek though it was still snowing at Blue Lakes (Figure 591.A). By 13:00 PST on the 7th, the TWI potential transitioned from Low ROS to ROS as the air temperature crossed the 1.3 °C threshold and soil moisture increased at all three depths indicating TWI while precipitation rates begin to decrease at Spratt Creek and over the next few hours TWI potential is downgraded from ROS to Low ROS and TWI is no longer active. By the onset of the fourth system (Figure 59.1C), Spratt Creek had met the conditions for warm day melt during the break between systems with air temperatures reaching 10 °C while Blue Lakes had experienced a decrease in SWE equivalent to the increase it had over the last 48 hours as SWE begins to increase as air temperature being to drop, downgrading TWI potential from ROS to Low ROS to none as precipitation transitioned to snow. During this last system, SWE continues to decrease after draining the excess water from the snowpack from the prior system which was a combination of rainfall and snowmelt as SWE values were 38.1 mm lower than the antecedent SWE values. The snowpack again reaches 40% density (a "ripe" snowpack where it can be assumed that the snowpack is now isothermal) before consistently decreasing as the snowpack continues to decrease and soil moisture values plateau before receding as precipitation ends. Streamflow at Markleeville and Woodfords increase with each of the last three systems that produced rainfall rates over 5 mm/hr at the low-elevation Spratt Creek station, each event amplifying the streamflow response for the next event pushing the river into flood stage in the third and fourth systems. Carson City streamflow gradually continued to increase and reached flood stage around 12:00 PST on the 10th. The February 2017 event fell onto a snowpack that had already experienced one significant ROS event that had increased the soil moisture, increased the snowpack density, and likely established preferential flow paths allowing conditions to be primed for increased runoff efficiency, emphasizing the importance of tracking all parameters throughout the entire winter.

Case Study 4: 6–9 April 2018 Flood

The fourth flood event in the Upper Carson occurred in the spring after peak SWE at Blue Lakes and Spratt Creek had already melted out entirely during a rain event in between days with maximum air temperatures ranging from 7.5-14.9 °C at Blue Lakes and up to 18.3 °C the day before the snowpack melted out at Spratt Creek on March 31st. We examine the effectiveness of the SR-DSS starting on April 5th at 12:00 PST through April 9th at 08:00 PST (Figure 60.2). Since Spratt Creek had melted out, there is no TWI potential from the snowpack and the station would be adhering to a direct rainfall runoff regime. Blue Lakes had 510 mm of SWE and 99 cm of snow depth with peak SWE occurring on March 30th,

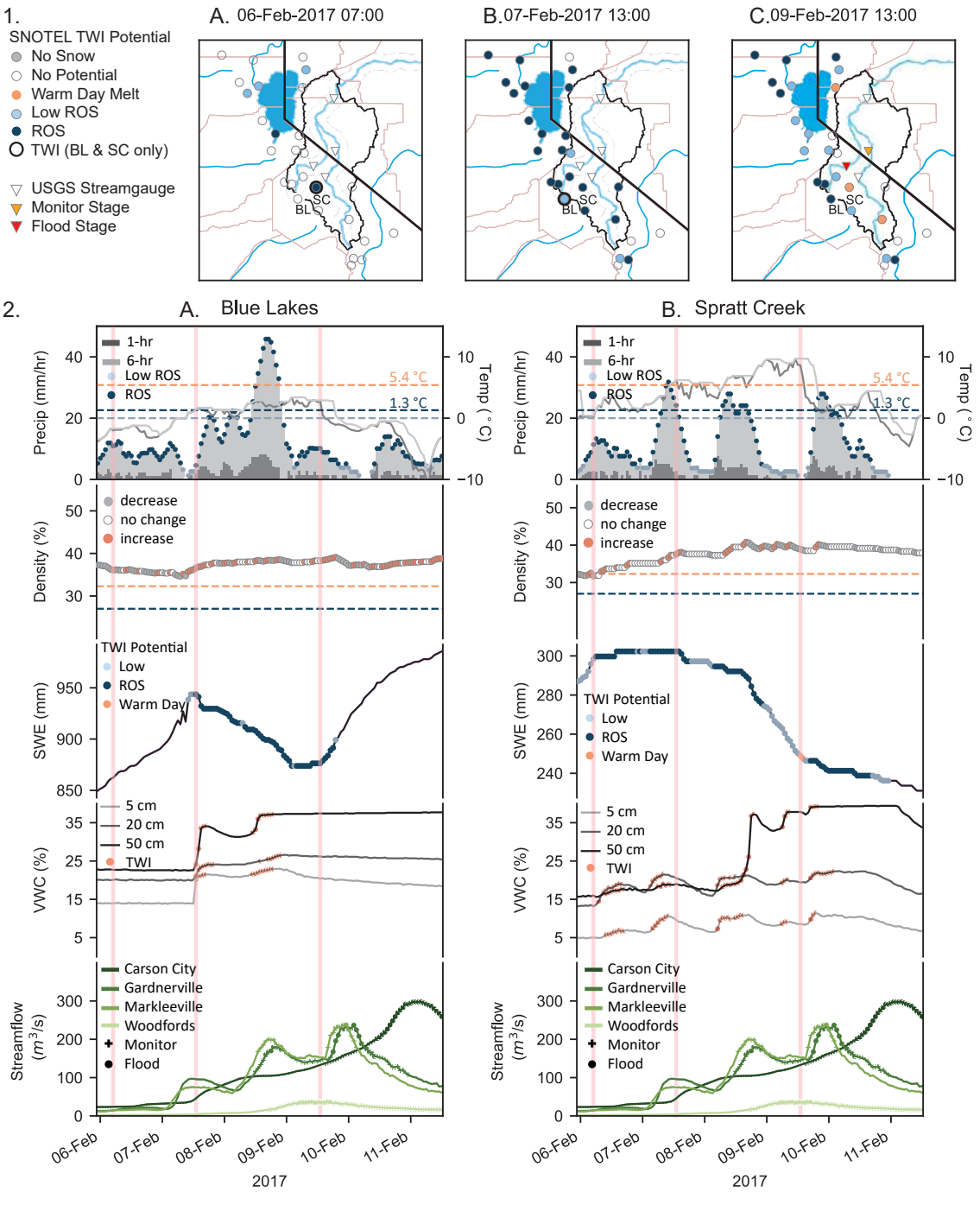

Figure 59: Historical event assessment: 6–11 February 2017.

the ablation period had just begun and it can be assumed that the snowpack is nearly ripe. Precipitation began at 03:00 PST on the 6th at Blue Lakes though there was no change in SWE or density until 06:00 PST when air temperature and 6-hour precipitation values crossed the threshold to indicate ROS potential at the same SWE began to increase (Figure

60.1A). The density of the snow continued to increase thought SWE began to decline and by 03:00 PST on April 7th (Figure 60.1B), the density of the snowpack reaches a maximum and begins to decline as the snowpack starts to melt from rain falling at 5.5 °C on an isothermal snowpack. SWE continued to decline after the rain ended as transiently stored rainwater continues to drain from the snowpack leading into a warm sunny day on the 8th where warm day melt potential was seen throughout the region (Figure 60.1C).

While the soil moisture responded to the rain at Spratt Creek, Blue Lakes did not have any soil moisture response despite clear evidence that the snowpack was losing water. This could be that soil moisture sensors were experiencing an error, though examining the soil moisture data later in the ablation period shows that the sensors were operating correctly. Another explanation for there not being a soil moisture response could be an ice layer that moves the water laterally rather than allowing the water to penetrate vertically. Upon reviewing the evolution of the snowpack, there is evidence for the formation of an ice lens in early February after 13 days of maximum air temperatures reaching 10 °C and diurnal soil moisture response indicating the release of snowmelt followed by an abrupt cold where the maximum temperature on February 12 was -6.6°C. While there is no way to prove that there was an ice lens, the data indicates that it is a likely hypothesis that there was lateral flow. Lateral flow would increase the runoff efficiency of the ROS event since the water can travel overland and not through the soil. Flows at the USGS stream gages increase more slowly while precipitation rates are below 5 mm/hr but begin to rise more rapidly into the flood stage as precipitation rates hit and exceed 5 mm/hr. While only 71.1 mm and 39 mm of precipitation fell at Blue Lakes and Spratt Creek accordingly, the ripe snowpack and warm rainfall on soils with elevated soil moisture that had already begun to increase baseflow downstream provided the ingredients for the spring flooding.

Case Study 5: 28–31 January 2016 No Flooding

By the end of January 2016, Blue Lakes and Spratt Creek had a slightly above-average snowpack for the time of year though Spratt Creek had reached peak SWE approximately one month ahead of average in part due to the snowmelt caused by the ROS event. The morning of January 29th through the morning a 24-hour ROS event impacted the region after four days of maximum air temperatures ranging from 2.7 °C to 5.8 °C at Blue Lakes and 5.5 °C to 13.7 °C at Spratt Creek crossing the WDM threshold for both stations on the 28th (Figure 61.1A). The ROS event started at 03:00 PST at Blue Lakes and by 08:00 PST air temperature and precipitation thresholds were met to change the TWI potential from Low ROS to ROS though he 5 cm soil moisture sensor had registered TWI since 04:00 PST, just one hour after precipitation began (Figure 61.1B). Precipitation started 07:00 PST at very low intensities though the air temperature was warm enough to ensure that all precipitation was falling as rain (Figure 61.2B). However, TWI initiated nine hours earlier at 22:00 PST when the air temperature was 6.7 °C, indicating a snowpack that is readily transmitting water despite snowpack density values of 35% which quickly climb to 40% under the warm air temperatures since only 2.5 mm of precipitation had fallen. At 18:00 PST on the 29th, enough precipitation had fallen at Spratt Creek to upgrade the TWI potential to ROS and the snowpack density begins to climb as the snowpack simultaneously took on and released water (Figure 61.1C). By the end of the storm, Blue Lakes had a net increase of 35.5 mm and Spratt Creek lost a total of 38.1 mm of SWE. Despite the active

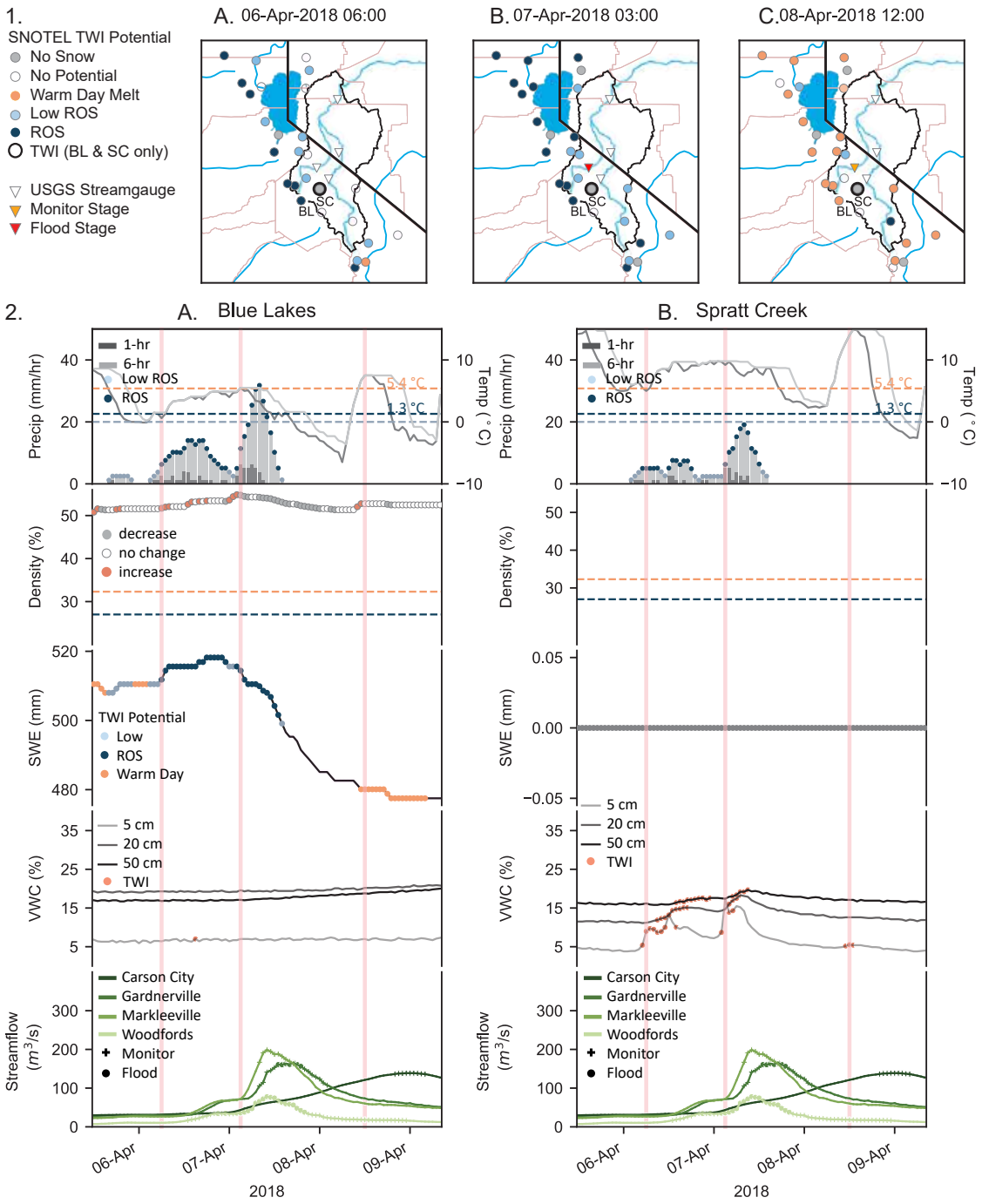

Figure 60: Historical event assessment: 6–9 April 2018.

snowmelt at Spratt Creek and 19 hours of TWI at Blue Lakes, this event did not produce flooding at the gauging stations. Both stations were around the climatological median for depth-averaged soil moisture (NRCS, 2023). However, baseflow was measurably lower than the flood events that had at least doubled and even up to ten times the volume of water in

the river prior to the event.

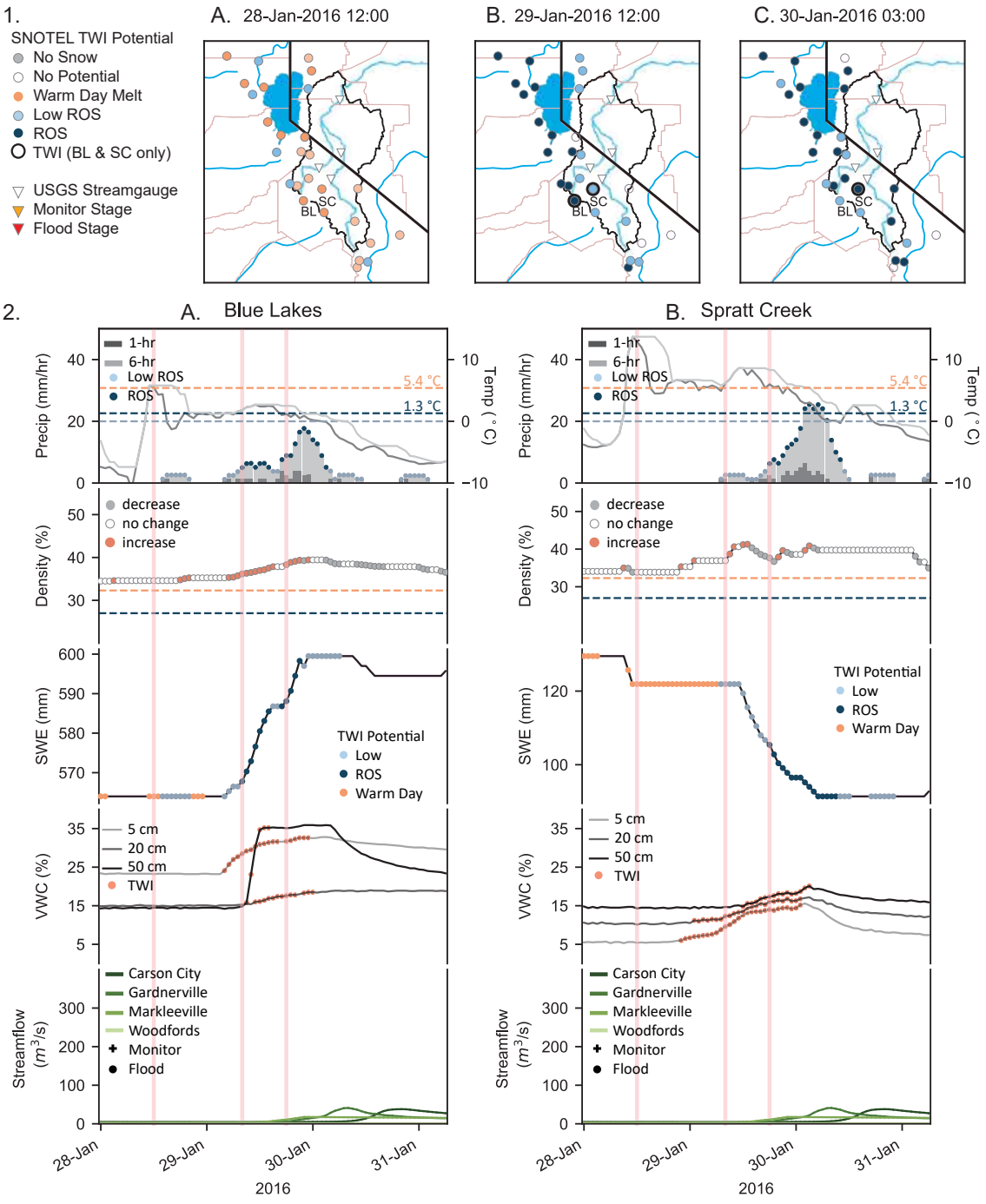

Figure 61: Historical event assessment: 28–31 January 2016.

Case Study 6: 13–15 February 2019 No Flooding

In 2019 an atmospheric river with integrated water vapor values exceeding 1000 kg m^{-1} s^{-1} brought heavy precipitation to the region 13–15 February 2019 (Hatchett et al., 2020). Prior to the event, the snowpack at each location was well above average for the time of year and Blue Lakes had slightly higher snowpack density than Spratt Creek (Figure 62.2A & B). Precipitation began at both stations on the morning of the 13th though air temperatures at Blue Lakes were below 0 °C until 13:00 PST. The Spratt Creek station crossed the precipitation threshold by 07:00 PST and the air temperature threshold by 10:00 PST but it wasn't until 12:00 PST that the snowpack density reached the ROS threshold (Figure 62.1A). However, TWI was initiated at Spratt Creek at 10:00 PST indicating the formation of preferential flow paths that only increased the snowpack density enough to move through the snowpack until it reached the base and TWI initiated within the same hour. It wasn't until 01:00 PST on the 14th that Blue Lakes registered TWI after 12 hours of Low ROS potential with air temperatures between 0.1 °C and 0.7 °C (Figure 62.1B). TWI at Blue Lakes continues for a total of 12 hours despite temperatures reaching 0 °C before receding as precipitation changes from rain to snow as temperatures drop 2.6 °C in a single hour. TWI at Spratt Creek lasts a total of 18 hours with a slight recession during a pause in precipitation. Soil moisture peaks at 07:00 PST on the 14th at Sprat Creek as precipitation rates begin to decline and TWI continues for another two hours (Figure 62.1C). The event results in a net increase in the snowpacks water content for both stations, again demonstrating that the snowpack can simultaneously take on and release water and does not wet uniformly prior to releasing water. The depth-averaged soil moisture for both locations was above normal. However, the baseflow leading up to the event was only slightly higher than the January 2016 event, and at least half of the lowest baseflow leading into one of the flood events.

Case Study 7: 22–24 December 2021 No Flooding

December 2021 brought record snowfall totals for the month across the SNOTEL stations in the Sierra Nevada. The snowpack was around average for the time of year at Blue Lakes but was in the 10th percentile for Spratt Creek. Since the snowpack began to accumulate at the beginning of December with just one large snow-dominated storm prior to this event, the snowpack had not yet crossed the ROS density threshold. This second December storm started on December 22 and had a brief lull on the evening of the 24th before another snow-dominated system started (Figure 63.2A & B). Precipitation started at 05:00 PST on the 22nd at Blue Lakes and two hours later at Spratt Creek. The air temperature at Blue Lakes was well below 0 °C when precipitation started but the snowpack density was increasing, indicating that the precipitation was more dense than the antecedent snowpack density and likely mixed phase. By 12:00 PST on the 22nd, Sprat Creek registered TWI two hours after the ROS potential was indicated after only 6.3 mm of precipitation (Figure 63.1A). At Blue Lakes, the snowpack reached a peak in snow density at 23:00 PST on the 22nd as air temperature dropped slightly below 0 °C, downgrading the Low ROS potential to no potential (Figure 63.1B.). During this same time, the snowpack density at Spratt Creek plateaued though TWI continued until the hourly air temperature dropped below the ROS threshold and snowpack density started to increase, indicating that the precipitation phase changed to snow (Figure 63.1C). The soil moisture at Blue Lakes did not respond,

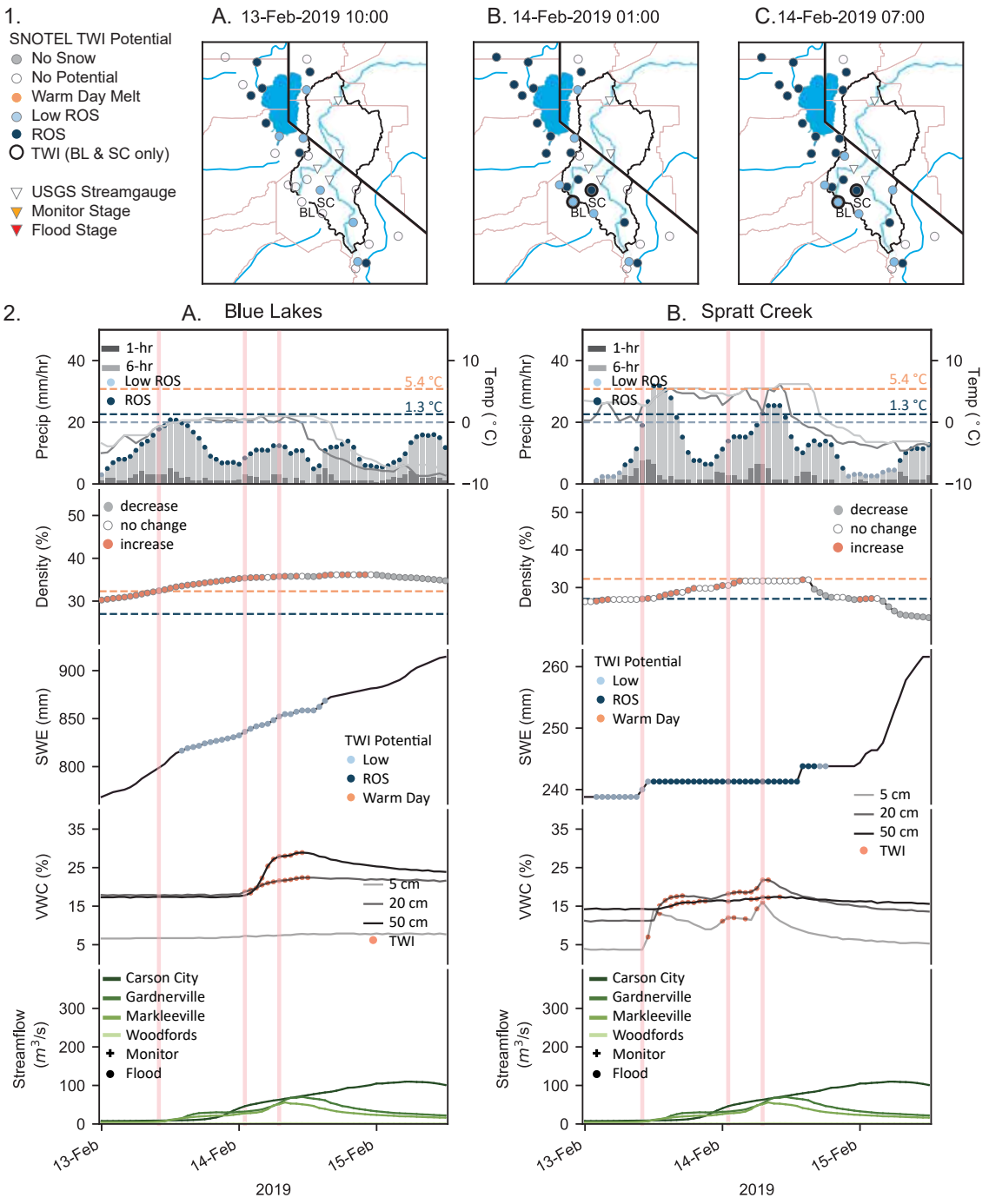

Figure 62: Historical event assessment: 13–15 February 2019.

which indicates that the precipitation was mostly mixed phase or the snowpack was cold enough that it was able to slow the progression of preferential flow paths for the low-intensity precipitation rates (Marsh and Woo, 1984b; McGurk et al., 1988). This event did produce a streamflow response, but the combination of low precipitation rates, near 0 °C

temperatures at Blue Lakes, and low baseflow prior did not produce flooding at any of the gauging stations.

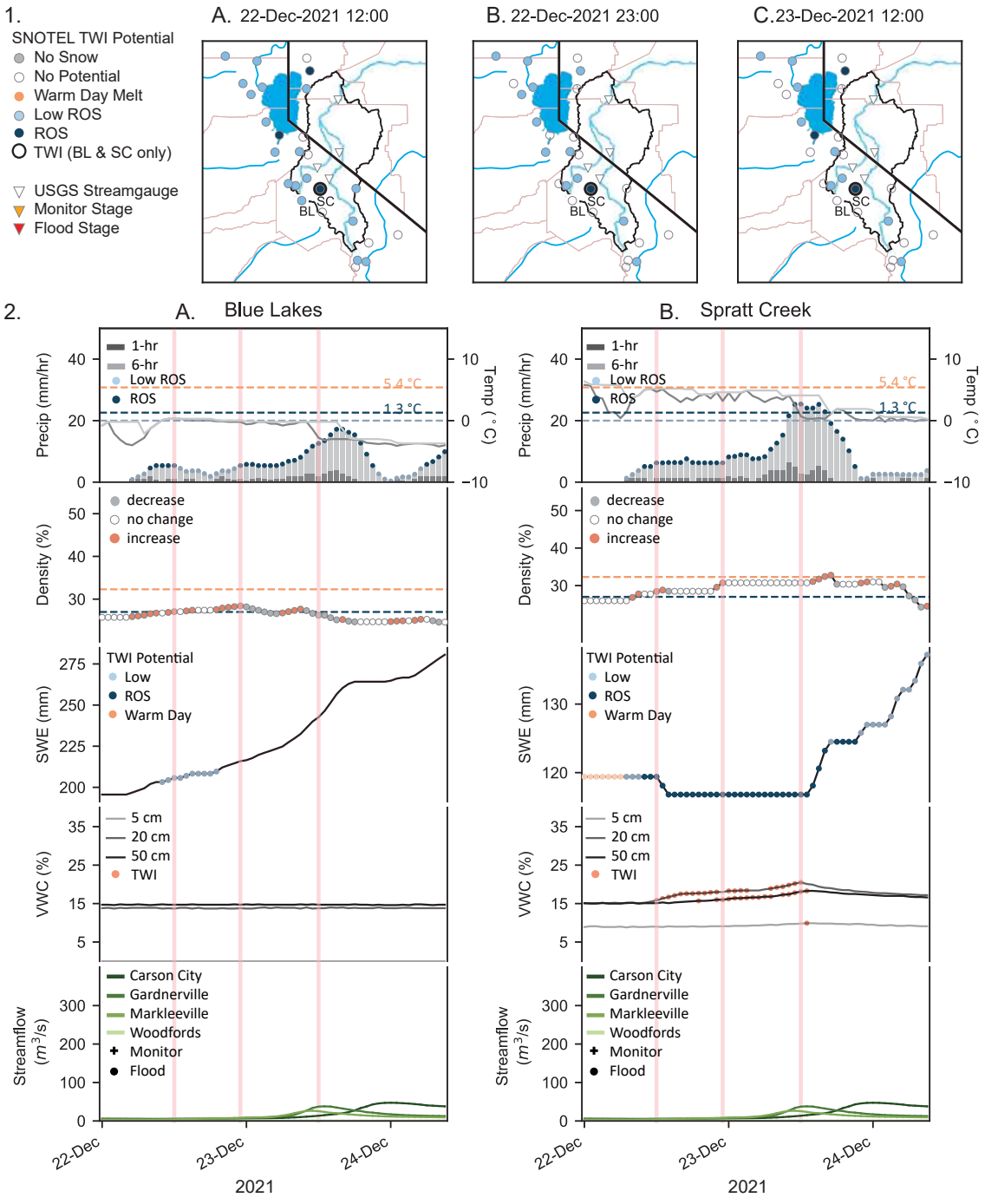

Figure 63: Historical event assessment: 22–24 December 2021.